Novel Luminescent Lanthanide Complexes as Reporters of Cellular Oxidative Stress

Thesis

Novel luminescent lanthanide complexes as reporters of cellular oxidative stress

A thesis submitted for the Degree of Doctor of Philosophy in Chemistry

Bianca Vitiello

July 2017

Department of Life, Health and Chemical Science

The Open University, Walton Hall, Milton Keynes, MK7 6AA, UK

Author's Declaration

I declare that the work outlined in this thesis was carried out by the author between February 2013 and July 2017 under the supervision of Dr James Bruce, Dr Jon Golding at the Open University, Milton Keynes, Dr James Phillips at UCL, London, and Dr Andrew Nicholls and Jim Armitage from GSK pharmaceutical company.

This thesis is the work of the author except where acknowledged by reference, and contains material that has been submitted for any other degree.

Bianca Vitiello

Dedication

This thesis is dedicated to my daughter Francesca, you provided the inspiration necessary for me to complete this research project.

Acknowledgement

I would like to express my special thanks to my supervisor, Doctor James Bruce, to whom I am exceptionally grateful for the guidance and encouragement he has given me throughout the whole of my Ph.D.

My sincere gratitude goes to my supervisors Doctor Jon Golding, Doctor James Phillips, Doctor Andrew Nicholls and Jim Armitage for their continuous guidance and encouragement throughout.

A very special thanks also goes to Professor Peter Taylor, Professor Alan Bassindale and Doctor Sergei Bylikin for their continuous guidance and support.

I particularly want to thank my husband Antonio for having always supported and encouraged me throughout. I thank to my family too especially my mother, my father, my brothers Christian and Mirko, my parents-in-law, my aunt Mariarosaria, and my sisters-in-law Gabriella and Sandra.

I would also like to thank Matthew Kershaw for his help with the NMR and Mass Spectrometry facilities and my colleagues Alexandra, Laura, Delphine, Elizabeth, Radka, Sophie, Nadia and Roy for their help and support.

I equally thank The Open University and GSK pharmaceutical company to financially support me throughout my research.

Abstract

A series of lanthanide complexes based on asymmetrically substituted cyclen ligands were designed and synthesised in this project in order to develop ROS-responsive luminescent molecular sensors. A synthetic strategy involving the synthesis of an intermediate ligand was applied to the asymmetrically functionalisation of the cyclen ring. The intermediate ligand was called “the generic ligand” since it possesses a generic chemical structure that could be modified in many ways in order to produce different types of ligands. The generic ligand was designed and synthesised by exploiting an orthogonal protection strategy. The synthetic strategy involving the synthesis of the intermediate generic ligand proved to be very versatile and successfully applicable to the synthesis of different asymmetrically substituted cyclen-based ligands. Seven types of ligands (**L1**-**L7**) were synthesised in this project exploiting the synthetic strategy mentioned above. The ligands were complexed with trivalent lanthanide ions giving arise to eleven lanthanide complexes **EuL1**-**EuL7**.

The photophysical properties of the lanthanide complexes were measured using absorption and emission spectroscopy. The photophysical properties of two Eu(III) based complexes were measured in presence of ROS species generated in situ by H_2O_2 and Fe(II) perchlorate. The ROS response of these Eu(III)-based complexes was also measured in vitro by using a cellular ROS assay. In this assay H_2O_2 and tBHP were used to increase the ROS production within the cells.

A mitochondrial stress test (MST) was performed on **EuL1**-**TbL4** with the aim to identify compounds that exhibit a potential mitochondrial and/or cellular toxicity. A calcium loading capacity assay was performed on the same lanthanide complexes tested with the MST with the aim of investigating their effect on the mitochondrial capability to uptake and internalize Ca^{2+}.

Abbreviations and Symbols

A - absorbance

OAc - acetoxy

ADP - adenosine diphosphate

ATP - adenosine triphosphate

Boc - tert-butyloxycarbonyl

BPS - 4,7-diphenyl-1,10-phenanthroline-disulfonate

c - molar concentration

CAT - catalase

CLC - calcium loading capacity

^{13}C NMR - carbon nuclear magnetic resonance spectroscopy

CPL - circularly polarized luminescence

CRC - calcium retention capacity

d - doublet (multiplicity of NMR splitting)

δ - chemical shift

DABC - 1-N-Boc ethylamine-4,7-diallyl acetate-1,4,7,10-tetraazacyclododecane

DABBC - 1-N-Boc ethylamine-4,7-diallyl acetate-10-benzyl acetate-1,4,7,10-tetraazacyclododecane

DABnC - 1-ethylamine-4,7-diallyl acetate-10-benzyl acetate-1,4,7,10-tetraazacyclododecane

DAABBC - 1-N-Boc ethylamine-4,7-diacetic acid-10-benzyl acetate-1,4,7,10 tetraazacyclododecane

DCM - dichloromethane

DMAP - 4-dimethylaminopyridine

DMF - dimethylformamide

DMSO - dimethyl sulfoxide

DNA - deoxyribonucleic acid

DO3A - 1,4,7-tris(carboxymethyl)-1,4,7,10- tetraazacyclododecane

DPA - bis(2-picolyl)aniline

dpp - diphenylphosphinamide

DTPPBC - 1-ethylamine-4,7-di-(triphenylphosphonium bromide ethyl)acetamide-10-benzyl acetate-1,4,7,10-tetraazacyclododecane

DTPPBBC - 1-N-Boc-ethylamine-4,7-di-(triphenylphosphonium bromide ethyl)acetamide-10-benzyl acetate-1,4,7,10-tetraazacyclododecane

ε - molar absorption coefficient

E'_0 - reduction potential

ECAR - rxtracellular acidification rate

EDCI*HCl - 1-(3-dimethylaminopropyl)-3-ethylcarbodiimide hydrochloride

eq. - equivalent

ESI-MS - electrospray Ionization-mass spectrometry

ET- energy transfer

EtAc - ethyl acetate

ETC – mitochondrial electron transport chain

EtOH - ethanol

$FADH_2$ - flavin adenine dinucleotide

FBS - fetal bovine serum

FCCP - carbonyl cyanide-4 (trifluoromethoxy) phenylhydrazone

FMN - flavin mononucleotide

FRET - fluorescence resonance energy transfer

GPX - glutathione peroxidase

GRX - glutaredoxin

GSH - glutathione

h - hour

h - Planck's constant

HSA - fixed human serum albumin solution.

HBSS - Hanks' balanced salt solution

HepG2 - liver cancer cell line

HOBt - hydroxybenzotriazole

^{1}H NMR - proton nuclear magnetic resonance spectroscopy

HSC-3 - human squamous cell carcinoma cell line

I – intensity of light

IC – internal conversion

ISC - intersystem crossing

$^{i}PrNH_2$ – isopropylamine

LETM1 - leucine zipper-EF-hand containing transmembrane protein 1

M - molar (mol dm^{-3})

m - multiplet (multiplicity of NMR splitting)

MALDI-MS - matrix-assisted laser desorption/ionization-mass spectrometry

MCU - mitochondrial calcium uniporter

MeCN - acetonitrile

MeOH - methanol

MLCT - metal-ligand charge transfer

MPTP - mitochondria permeability transition pore

MS - mass spectrometry

MST- mitochondria Stress Test

ν - frequency

NADH - nicotinamide adenine dinucleotide

NADPH - nicotinamide adenine dinucleotide phosphate

NMR - nuclear magnetic resonance

$^{1}O_2$ - singlet oxygen

O_2^{-}• - superoxide radical

OCR - oxygen consumption rate

OH• - hydroxyl radical

O-P-Ser – O-phosphorylated serine

O-P-Thr – O-phosphorylated threonine

O-P-Tyr – O-phosphorylated tyrosine

$Pd(OAc)_2$ - palladium acetate

PET - photo-induced electron transfer

PRX - peroxiredoxin

QH_2 - ubiquinol

ROS - reactive oxygen species

s - singlet (multiplicity of NMR splitting)

S_1 S_2 - electronic singlet excited states

S_0 - electronic ground state

SOD - superoxide dismutase

t - triplet (multiplicity of NMR splitting)

T_1 - electronic triplet exited state

TABC – 1-N-Boc-ethylamine-4,7,10-triallyl acetate-1,4,7,10-tetraazacyclododecane

TAC - 1-ethylamine-4,7,10-triallyl acetate-1,4,7,10-tetraazacyclododecane

tBHP - tert-butyl hydroperoxide

TEA - triethylamine

TFA - trifluoroacetic acid

TLC - thin layer chromatography

TPP - triphenylphosphine

TPPTS - triphenylphosphinotrisulfonate

TRX - thioredoxin

UV-Vis - ultraviolet-visible spectroscopy

Table of content

1. Introduction

Luminescence is defined as the emission of light by a substance following excitation that in most cases is represented by the absorption of light [1]. Luminescence is a highly sensitive tool that can be applied for the detection of single molecules in complex biological systems, since it allows a real time detection of a target biomolecule in living cells [1]. For this reason it has received a great importance as a diagnostic tool in medical and biological fields. Over the last decades many research studies have focused their attention on the development of ever more efficient luminescent molecular probes [1], [2]. A molecular probe, also known as molecular sensor or chemosensor, is a molecular or supramolecular system that is able to transform probe-analyte interactions into a signal which allows analyte sensing [3]. In the case of luminescent molecular probes, an analyte can be detected through the changes of the photophysical properties of the probe, such as increasing or decreasing of the emission intensity, as consequence of analyte-probe interaction [4]. The use of lanthanide complexes for the detection of biological analytes such as anions, pH and metal ions has grown significantly over the last decade [5], [6]. Lanthanide ions-based complexes possess unique photophysical properties, such as large Stokes shift, narrow emission bands and long luminescence decay time, which make them ideal luminescent probes for biological systems [5], [6]. For example, their long luminescence lifetimes, ranging from microsecond to millisecond, contrarily to that of biological (i.e., organic) species that possess lifetimes in the order of nanoseconds, make lanthanide-based complexes particularly useful for the application in living cells [7]. In fact, using time-gating techniques it is possible to separate the signals coming from the lanthanide ions from the short-lived fluorescence of molecular background (autofluorescence), which is due to certain fluorescent molecules present within the cells, such as proteins [7]. The aim of this project is to develop novel luminescent lanthanide complexes capable of producing detectable changes of their

photophysical properties following the interaction with biological analytes, thus allowing analyte detection. The biological analytes that were analysed in this project are ROS (reactive oxygen species), such as hydrogen peroxide (H_2O_2) and the hydroxyl radical ($OH\bullet$). ROS are a group of chemically reactive molecules and radicals containing oxygen, which are mainly produced within the mitochondria [8]. ROS play a key role in many physiological processes, such as signal transduction and inflammation, and for this reason ROS are very important for the cell survival [9]. However, increased concentrations of ROS may lead to oxidative damage to lipid, DNA and proteins that can be the cause of many cellular and/or cellular organelles dysfunctions [10]. Cells are continuously exposed to basal oxidative damage as consequence of an increased ROS production, such as that caused by the immune system response to the pathogens' invasion [11], however, cells possess enzymatic and non-enzymatic antioxidants able to regulate ROS levels and prevent or repair oxidative damage [12]. When the overproduction of ROS is not balanced by the ability of the cellular antioxidants to neutralize the excess of ROS and repair the oxidative damage, there could be serious consequences for the cells and/or cellular organelles [10]. For example, mitochondrial dysfunction can be caused by increased production of superoxide radical ($O_2^{-}\bullet$), which represents another type of ROS, occurring when the DNA lesions, previously caused by high ROS levels, are not repaired [9]. Moreover, increased ROS production is also observed following the administration of certain drugs, such as doxorubicin [13]. Because of the ROS involvement in many physiological and pathological processes, over the last decades many research studies were focused on the development of ever more sensitive probes to selectively monitor ROS in living cells [14]. This would help to further elucidate their biological roles. The lanthanide complexes synthetized in this project should be able to signal the presence of ROS species, such as H_2O_2 and $OH\bullet$, and for this reason, they may represent new tools finalized to measure the level of oxidative stress and studying the effects on mitochondrial function. They can be also applied to the screening of drug candidates during the drug development phase, where they can be employed to measure

the drug induced oxidative stress via ROS detection. This may allow to identify potential toxic drugs. Drug-induced oxidative stress is involved as a mechanism of toxicity in many tissues and organ systems, such as liver, kidney, cardiovascular and nervous systems [15]. For example doxorubicin, which is an anthracycline antibiotic used in numerous chemotherapy protocols, is well known to cause a dose-dependent cardiotoxicity that is associated with an increase of ROS production [15].

1.1 Photophysical Overview

In this section, some concepts of general photophysics and lanthanide photophysics will be described before introducing the concept of luminescent molecular sensors. In particular, the absorption process, fluorescence and phosphorescence, and the photophysical properties of trivalent lanthanide ions will be described in the following sections. This aids in the description of the systems studied in this work and understanding their photophysical behaviour.

1.1.1 Absorption Process

According to the quantum theory, molecules can only take discrete energy values [1], [16]. These discrete values are called “energy levels”. There are three types of energy levels: rotational, vibrational and electronic. The electrons in atoms or molecules can change their energy level by absorbing or emitting a photon, whose energy must be equal to the difference between the two energy levels. This phenomenon is called electronic transition [1], [16]. Molecules can also undergo to rotational and vibrational transitions. Rotational transitions occur after the absorption of radiations with wavelengths falling in the microwave region of the electromagnetic spectrum. Vibrational transitions take place in the near infra-red region, while electronic transitions of the bonding electrons occur after the absorption of a molecule in the UV and in the visible region [1], [16] (Figure 1).

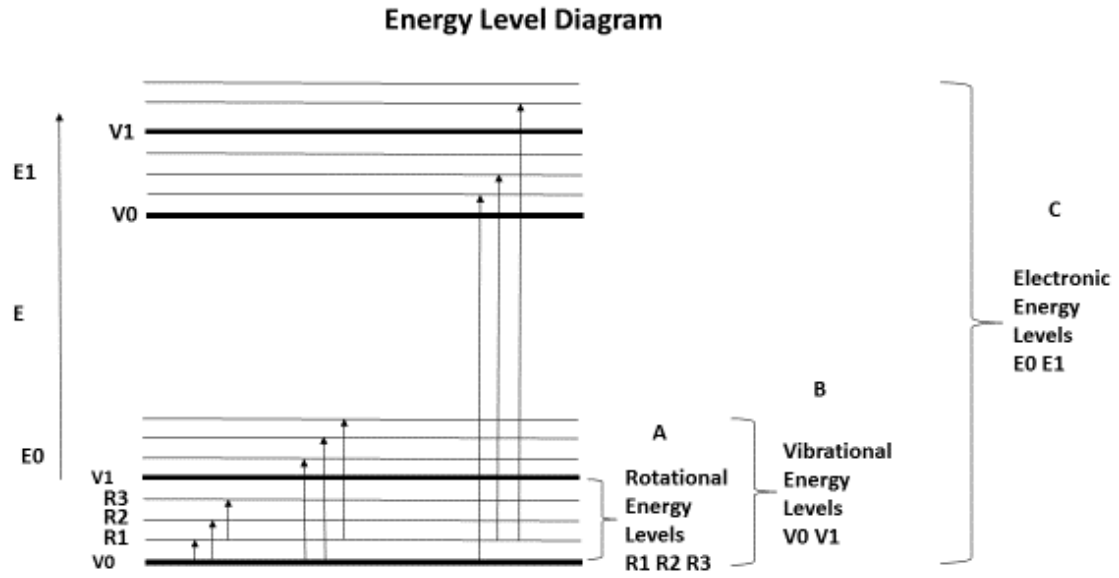

Figure 1. Energy level diagram describing A - the rotational changes, B – the vibrational changes and C - the electronic changes of the molecules energy.

When the bonding electrons of organic molecules are in the ground state, they occupy the lowest energy orbitals according to Pauli's Exclusion Principle [1], [16]. Therefore, the bonding orbitals σ, π (for unsaturated molecules) and n (non-bonding orbital for molecules containing heteroatoms such as N and O) are fully occupied, while the antibonding orbitals of type σ* and π* are empty. An electronic transition consists of the passage of an electron from a lower energy molecular orbital to a higher energy molecular orbital. For this reason electronic transitions in organic molecules can occur mainly in three ways: from an orbital σ to an orbital σ* (σ→σ* transition), from an orbital of type π to an orbital of type π* (π→π* transition) and from an orbital n to an orbital π* (n→π* transition) (Figure 2) [1], [16].

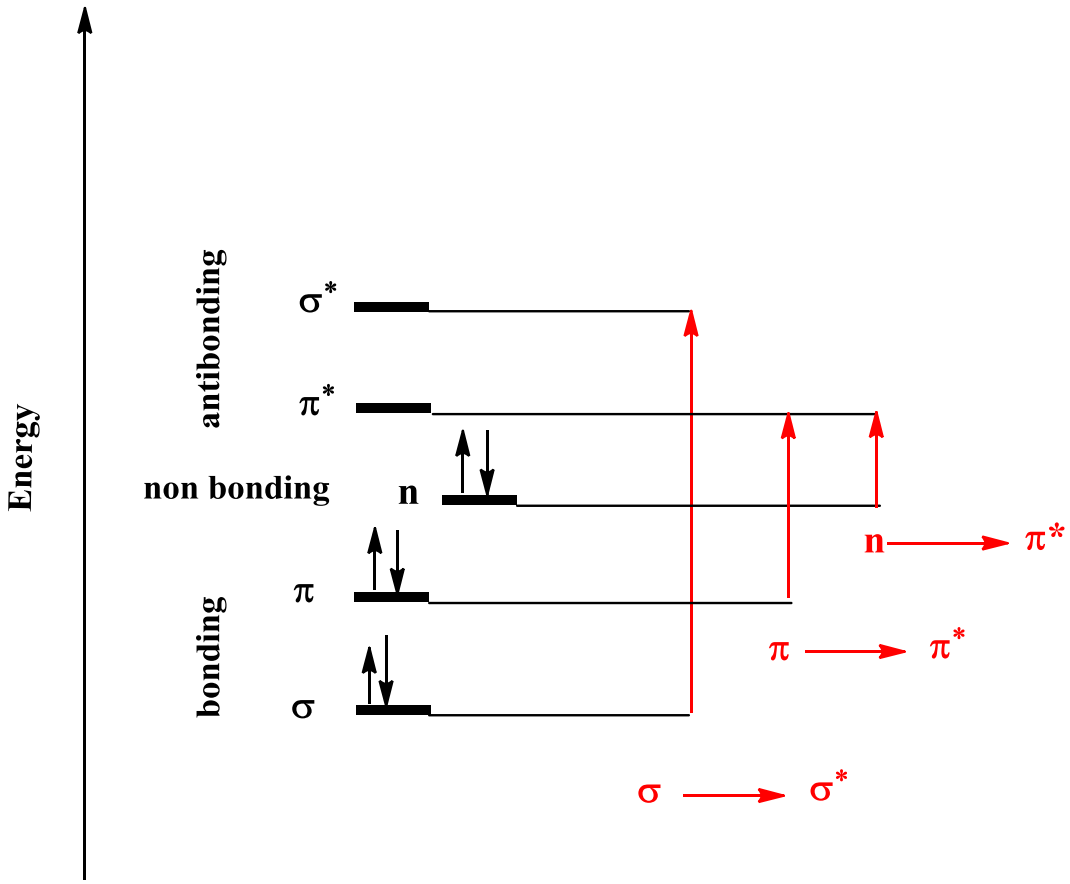

Figure 2. Diagram of electronic transitions.

For organic molecules transitions involving σ bonds (σ→σ* transitions) occur after the absorption of electromagnetic radiations with wavelengths falling in the region of the far UV, below 190 nm, because the energy difference between the two levels is quite high. π→π* and n→π* transitions take place in molecules containing double bonds and/or heteroatoms [1], [16]. These types of transitions occur after the absorption of electromagnetic radiations with wavelengths falling in the region of UV-visible. In order for absorption to occur it is necessary that the energy of the absorbed photon is equal to or greater than the energy difference between the ground state and the excited state. When a photon is absorbed, its energy is transferred to the electron which is promoted to a higher energy electronic orbital, thus leading the molecule to the excited state [1], [16]. The molar absorption coefficient (ε) (also called molar extinction coefficient or molar

absorptivity) is a measure of how strongly a substance absorbs light at a certain wavelength and is usually measured in $M^{-1}cm^{-1}$. The relationship between the molar absorption coefficient and the absorbance of a chemical species is governed by Beer-Lambert's law [1], [16]:

$$A = \varepsilon.l.c$$

Where A represents the absorbance value, ε is the molar absorption coefficient, l is the path length and c is the molar concentration of the chemical species [1], [16].

1.1.2 Fluorescence and Phosphorescence

Luminescence is defined as the radiation emitted by a molecule, or an atom, after it had absorbed energy to go to an exited state [1], [16]. The main types of luminescence are the fluorescence and phosphorescence. Electronic states of organic molecules can be grouped into two main categories, singlet states and triplet states. In a singlet state all of the electrons of the molecule have their spins paired. In a triplet states one set of electron spin have become unpaired [1], [16]. A triplet state has always a lower energy than its corresponding singlet state [1], [16]. Figure 3 shows a partial energy diagram for a photoluminescence system.

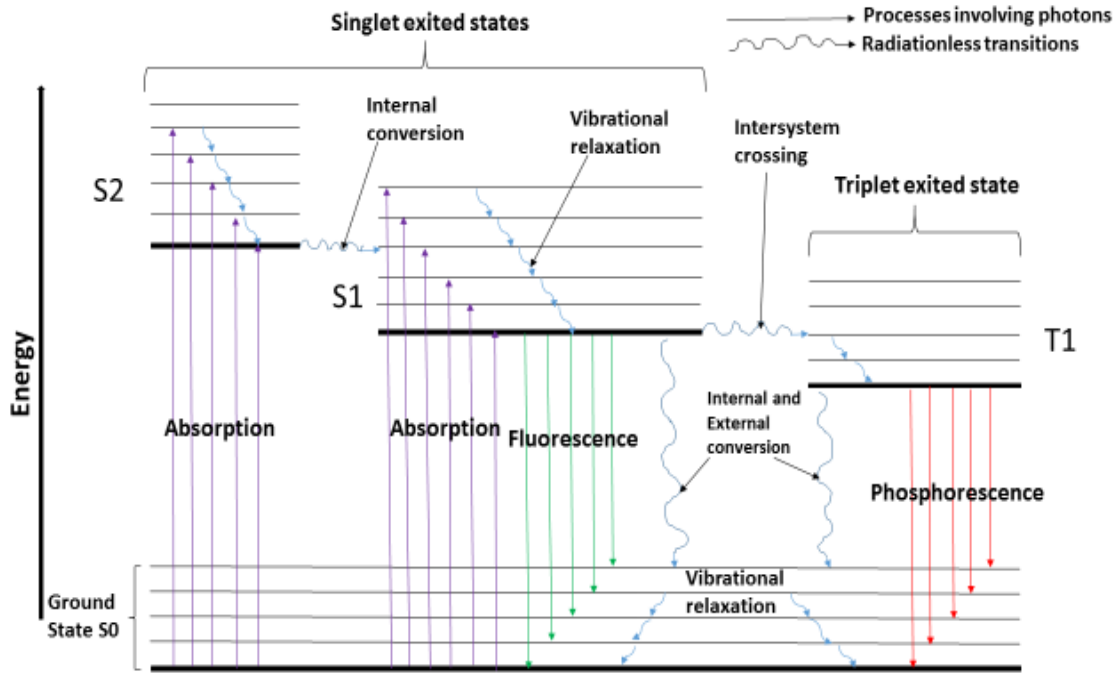

Figure 3. The Jablonski diagram provides a representation of ground and excited electronic states of a molecule and the processes related to the absorption and emission (radiative and nonradiative) of energy.

S_0 represents the electronic ground state, S_1 and S_2 are the two electronic excited singlet states, and T_1 is the excited triplet state. When an electron in a molecule is excited to the singlet state after the absorption of electromagnetic radiation, it returns to the ground state through both radiative and non-radiative processes. An example of non-radiative process is the vibrational relaxation, which is indicated on the Jablonski diagram (Figure 3) as a curved arrow between vibrational levels. Vibrational relaxation is a non-radiative process because the energy transferred to the electron by a photon is then converted into kinetic energy [1], [16]. The vibrational relaxation takes place between the vibrational levels of the same excited state; therefore the electrons do not change their electronic level through this pathway. In fact through this pathway a molecule, which has been previously excited to one of the many vibrational levels of a singlet state, is conducted to the lowest vibrational level of the same singlet excited state. This means that photon emission always occurs from the lowest vibrational level of an excited state. If a molecule is excited to a singlet state S_2 and if the lowest vibrational level of S_2 overlaps with the

higher vibrational levels of the S_1 state, a transition of the molecule from the lowest vibrational level of the S_2 state to a higher vibrational level of the S_1 singlet state can occur through another non-radiative process called internal conversion. During this process part of the molecular energy is converted into heat [1], [16] Once the molecule has reached a higher vibrational levels of the S_1 state, vibrational relaxation leads the molecule to the lowest vibrational level of this state. At this stage the molecule returns to the ground state S_0 through two pathways. One of these pathways is represented by the non-radiative process of internal conversion, which causes the conversion of all energy into heat as mentioned above. The other pathway is a radiative pathway involving the emission of a photon from the lowest vibrational level of S_1. This process is called fluorescence and occurs in 10^{-9} to 10^{-7} seconds [1], [16]. The energy of the photon emitted is equal to the difference of energy between the lowest vibrational level of the exited singlet state (S_1) and the ground state (S_0). This means that the energy of fluorescent photons is in most cases lower than that of the exciting photons. Since the energy of an electromagnetic radiation (or a photon) is given by the product of the Planck's constant (h) and the frequency (ν) (which is the inverse of the wavelength), generally the radiation emitted during the fluorescence occurs at wavelength longer than the one absorbed. The difference in energy (or wavelength) between the absorbed photon (or absorbed radiation) and the emitted photon (or emitted radiation) is known as the Stokes shift [1], [16]. (Figure 4).

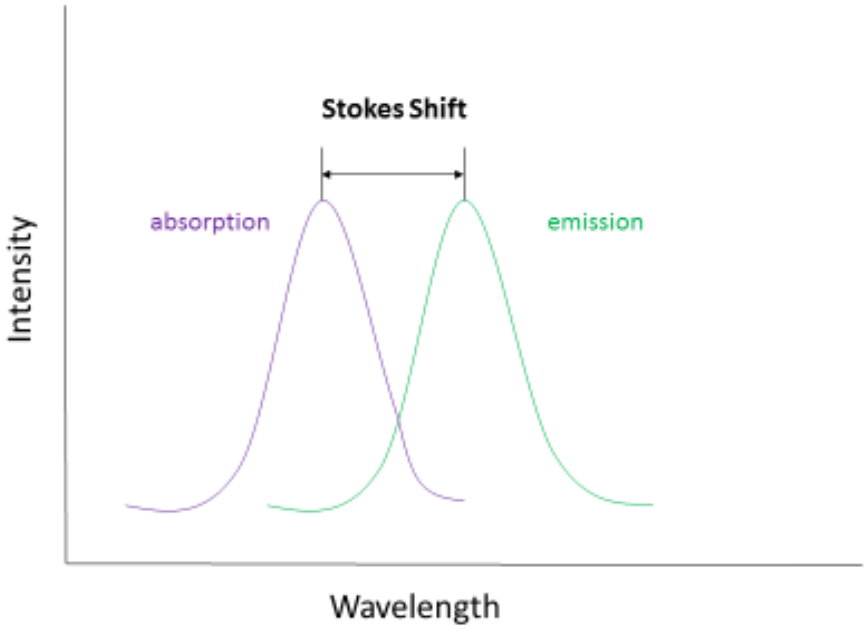

Figure 4. **The absorption and emission bands of a molecule.** The difference in wavelength between the peaks is known as the Stokes shift.

The average time a molecule stays in its excited state before emitting a photon is known as lifetime. Although the direct absorption of photon from the ground state to the triplet states is not an efficient process, in some molecules a more efficient process allows the population of triplet states from the lowest excited singlet state. This process is known as intersystem crossing. This is a spin-dependent internal conversion process because it involves the change in the electron spin and is usually indicated by a horizontal, curved arrow from one column to another. The mechanism for intersystem crossing involves vibrational coupling between the excited singlet state and a triplet state [1], [16]. Once the intersystem crossing has occurred, the molecule undergoes the usual vibrational relaxation process and reaches the lowest vibrational level of the triplet state. Once a molecule reaches this state, a radiative transition can occur leading the molecule in the ground state. This radiative process is called phosphorescence and occurs in 10^{-4} - 10^{-1} seconds [1], [16]. Now that some basic concepts of photophysics have been introduced, it is possible to introduce the photophysical properties of the lanthanide ions, which will

be described in details in the following section. This will help to understand the photophysical behaviour of the systems studied in this project.

1.1.3 Photophysical properties of Lanthanide ions

The lanthanides are the group of 15 elements ranging from lanthanum (atomic number 57) to lutetium (atomic number 71). All lanthanides, with the exception of lanthanum, are called f-block elements because of the gradual filling of last electrons in f-orbitals. When moving from cerium to lutetium, the 4f orbitals are gradually filled. The electronic configuration of lanthanide atoms is usually reported as $[Xe]4f^n6s^2$, where [Xe] represents the electronic configuration of the noble gas xenon, and n represents the number of electrons from 0 to 14 (0 for La to 14 for Lu). In aqueous solutions the majority of the lanthanides exist in the oxidation state +3 (Ln^{3+} where Ln is referred to any lanthanide). The electronic configuration of all trivalent lanthanide ions is $[Xe]4f^{n-1}$, indicating that the 6s electrons and one 4f electron are lost. These f orbitals are shielded by the filled $5s^2$ and $5p^6$ sub-shells. Although these sub-shells are lower in energy, they are spatially extended outside the 4f orbitals causing their shielding. The shielding of the 4f orbitals by the filled $5p^6$ and $5s^2$ sub-shells results in the characteristic spectroscopic properties of lanthanide ions. According to the Laporte's parity selection rule the 4f-4f transitions are forbidden. It states that the electronic transitions between states with the same parity are forbidden [17], [18], [19]. The 4f-5d transitions are parity allowed but require high energy to occur, their intensity is quite weak and their emission bands are very broad. As consequence direct excitation of lanthanide ions only produces low level of luminescence (for 4f-4f transitions the molar absorption coefficient is of the order of 1 M^{-1} cm^{-1}) [17], [18], [19]. Some lanthanide ions are luminescent and the luminescence of some of them is easier to observe. The efficiency of a lanthanide ion emission depends on two main factors. The first factor affecting the efficiency of lanthanides emission is the ease with which the non-radiative deactivation pathways are minimized. Lanthanides emission is highly influenced by interaction with molecular vibrational modes. Stretching

of O-H bonds represents the most efficient quenching process, but N-H, C-H and C=O stretching vibrations may also have a significant contribute [20]. The efficiency of luminescence quenching is inversely proportional to the energy gap between the excited emissive state and ground state. Therefore lanthanide ions having a relatively bigger energy gap between their lowest energy excited states (emissive states) and ground states are less efficiently quenched by the surrounding molecular environment (Figure 5).

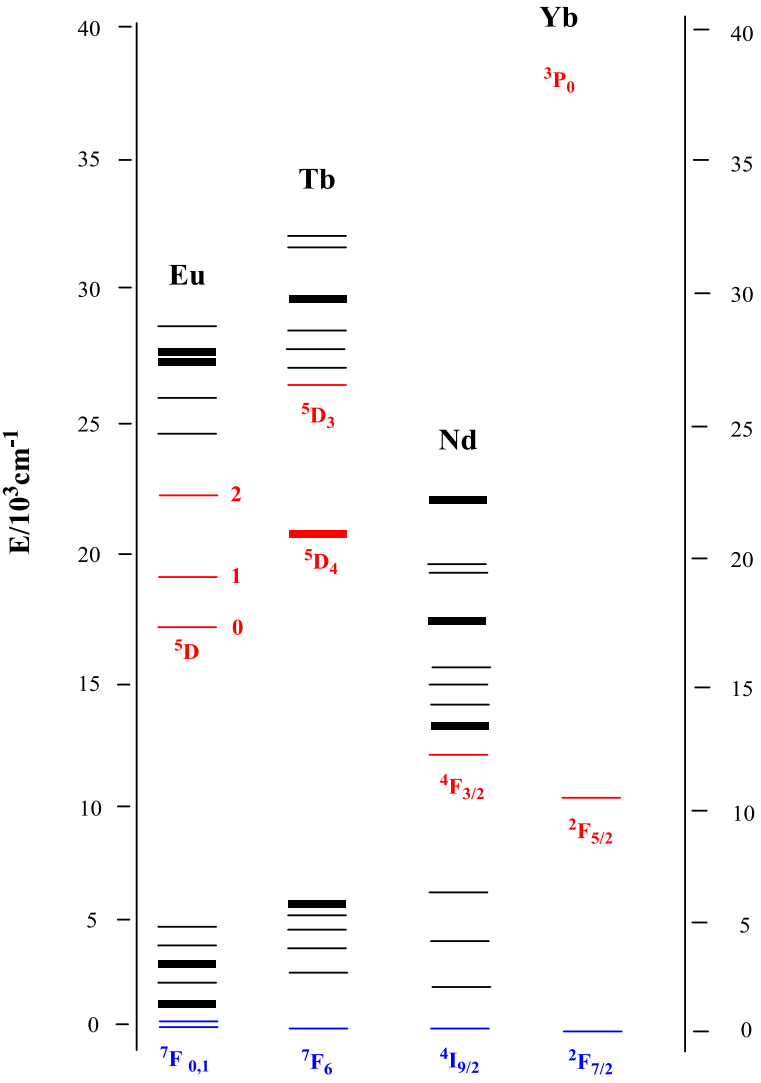

Figure 5. **This figure shows the partial energy diagrams of some lanthanide ions.** The main luminescent levels are drawn in red, while the fundamental levels are indicated in blue.

Another important factor influencing the efficiency of lanthanides emission is the facility with which their exited states can be populated. Ln ions are photochemically inert because direct photoexcitation is difficult due to their low molar absorption coefficient, associated with 4f–4f transitions of lanthanide ions. For effective excitation of Ln ions, they must be sensitized using an organic chromophore, so-called "antenna" [20]. In these systems, the photoexcited antenna successfully transfers its energy to the Ln ion (energy transfer (ET) process), producing the metal ion excited state thus allowing the lanthanide ion to luminesce (Figure 6).

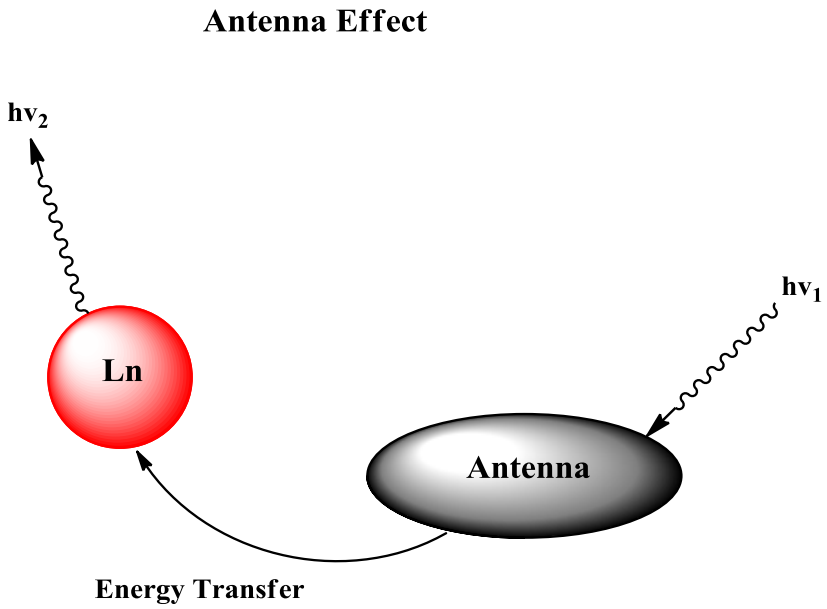

Figure 6. Schematic representation of the antenna effect.

1.1.4 Sensitized lanthanide emission

In the lanthanide complexes bearing an organic chromophore as sensitizer antenna, the absorption of a photon by the antenna promotes it to a high vibrational level of its excited singlet state S_1. From this level the vibrational relaxation takes place leading the chromophore to the lowest vibrational level of its excited singlet state. If an intersystem crossing takes place the organic chromophore passes from the lowest level of its S_1 to

the triplet state T_1. From the triplet state, three competing processes can occur: back energy transfer through intersystem crossing to the singlet state, chromophore phosphorescence or energy transfer process to the excited state of lanthanide ion. If the sensitizer has a high molar absorption coefficient and the intersystem crossing and the energy transfer processes occur efficiently, the excited states of lanthanide ion can be populated leading to an intense emission from lanthanide ion after the irradiation with conventional light sources (Figure 7). For an energy transfer process to occur it is necessary that the energy level of the lowest vibrational level of the sensitizer triplet state is higher (> 1700 cm^{-1}) than the energy level of the lanthanide ion excited state. This prevents the back energy transfer from the lanthanide ion excited state to the sensitizer triplet state [21].

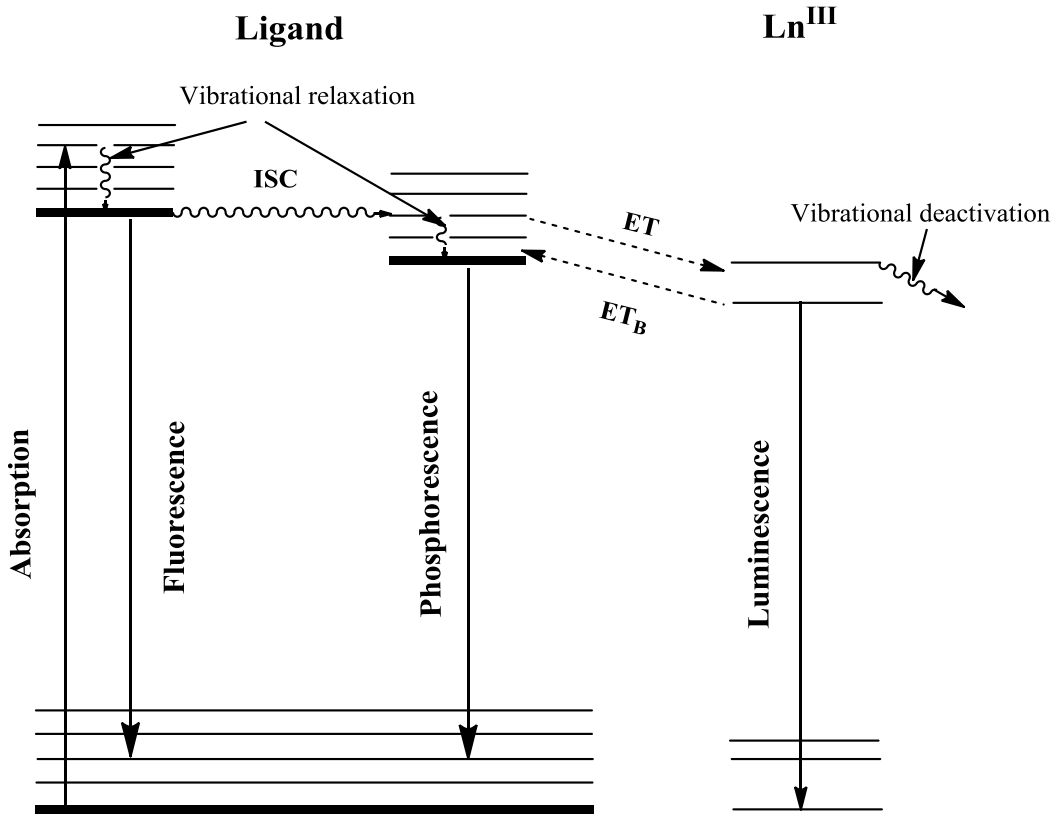

Figure 7. Jablonski diagram showing the indirect excitation of a lanthanide ion via an organic chromophore.

Despite the good overlap between the chromophore antenna and lanthanide ion energy levels, for a sensitised lanthanide emission a radiative energy transfer is unlikely to occur because of the low molar absorption coefficient of Ln(III). The energy transfer process therefore takes place by a non-radiative mechanism [22]. The energy transfer process from the sensitizer antenna to the lanthanide (III) can occur through one of the two non-radiative energy transfer mechanisms; the Dexter (exchange) mechanism and the Förster (dipole-dipole) mechanism [22]. The emission spectra of lanthanide ions and their complexes consist of very narrow bands because they arise from inner-shell electronic transitions that are unaffected by the environment and occur at well-defined wavelengths [20]. For europium complexes, five emission bands are observed, which arise from electronic transitions from the lowest excited state, $^5D_0$, to the ground state, ^7F_J, *(ΔJ* = 0 to 4), with a maximum emission peak at about 616 nm, corresponding to Δ*J* = 2 emission band (Figure 8). For terbium complexes, four intense bands are observed, originating from transitions from the emissive $^5D_4$ level to the $^7F_6$, $^7F_5$, $^7F_4$ and $^7F_3$ levels of the ground levels, with a maximum emission peak at 545 nm, corresponding to the *ΔJ* = 1 band [20], [23], [24].

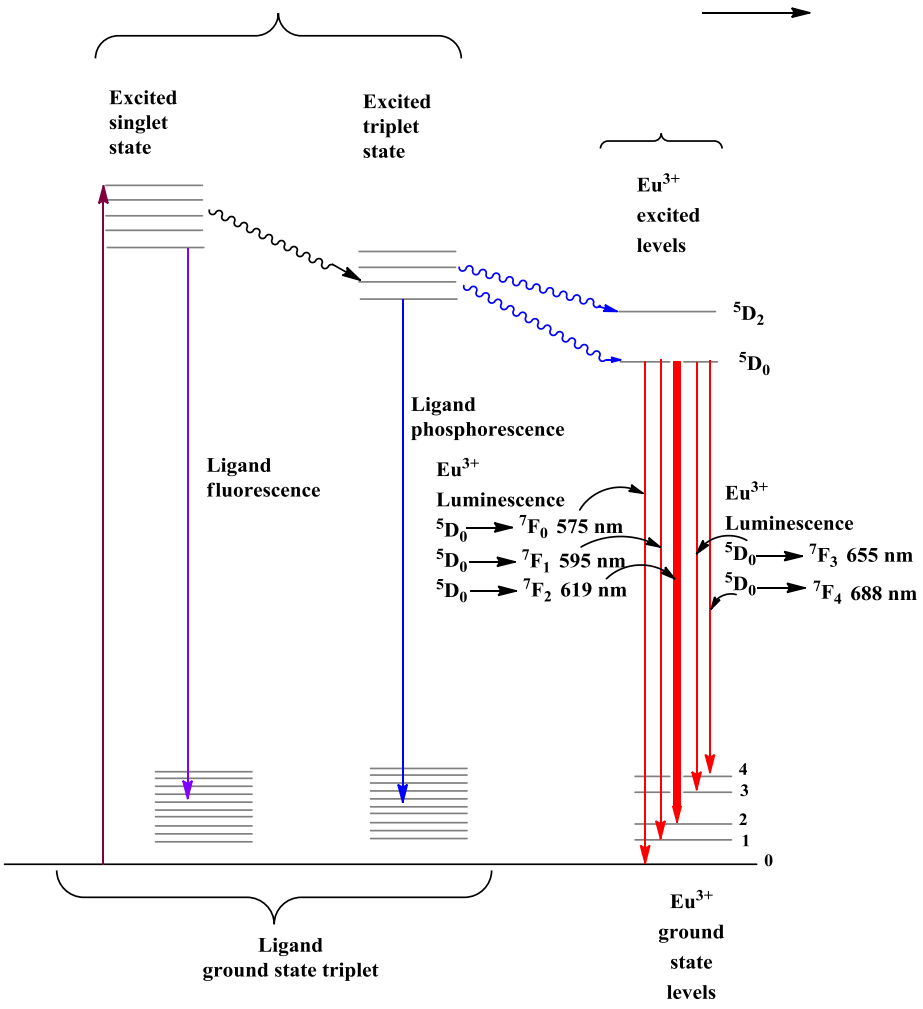

Figure 8. Jablonski diagram showing the energy transfer process involved in the luminescence of Eu^{3+} complexes of organic ligands.

Since the general photophysics concepts and the photophysical properties of the trivalent lanthanide ions have been described so far, it is now possible to introduce the concept of a molecular sensor. In the following sections, a brief introduction of the concept of molecular sensors is provided, followed by a more detailed description of luminescent molecular sensors. In particular, the attention will be focused on the luminescent molecular sensors based on luminescent lanthanide complexes, since they represent the object of study of this project.

1.2 Molecular sensor

A molecular sensor, also known as a chemosensor or probe, is a molecular system that is able to interact with a molecule or ion (analytes) and transform this interaction into a detectable signal that allows analyte sensing [25]. The signalling can take place for example by a change in the electrochemical, luminescence or NMR properties. Although there are many variable properties to choose from, photoluminescence is particularly attractive since it allows high sensitivity, real-time detection and relatively low cost [25].

1.2.1 Luminescent molecular sensors

A luminescent molecular sensor can be defined as a molecular system able to signal the presence of a specific analyte (such as an anion, a cation or a molecule) via changes in its photophysical properties, such as absorbance profile or an enhancement or quenching of the emission profile [25]. Although there are many types of luminescent molecular sensors based on different sensing mechanisms, such as photo-induced electron transfer (PET), metal-ligand charge transfer (MLCT) and fluorescence resonance energy transfer (FRET), in this chapter the attention will be focused on the luminescent lanthanide-based molecular sensors since they represent the type of molecular sensor studied in this project. In the following sections, several examples of molecular sensors based on luminescent lanthanide-complexes will be described to provide a clear evidence of how their unique photophysical properties can be exploited for analyte sensing. The following examples of luminescent lanthanide-complexes also show how the luminescence of the lanthanide ions can be controlled by opportunely modulating the chemical structure of the ligand used for the complexation. This may help to understand the rational design behind and the mechanism of action of the molecular systems that are the object of study of this project.

1.2.1.1 pH Responsive lanthanide complexes

In lanthanide-based chemosensors, the lanthanide usually represents the signalling unit, while the ligand contains the receptor unit able to bind the analyte. In some cases the signalling unit may also act as receptor unit. The interaction of the analyte with the receptor or signalling unit can be transduced into a luminescent response form the lanthanide, allowing the analyte detection. McMahon and co-workers developed a bright pH-responsive europium luminescent probe that localises selectively in the endoplasmic reticulum of living cells [26]. The chemical structure of this complex is reported in Figure 9.

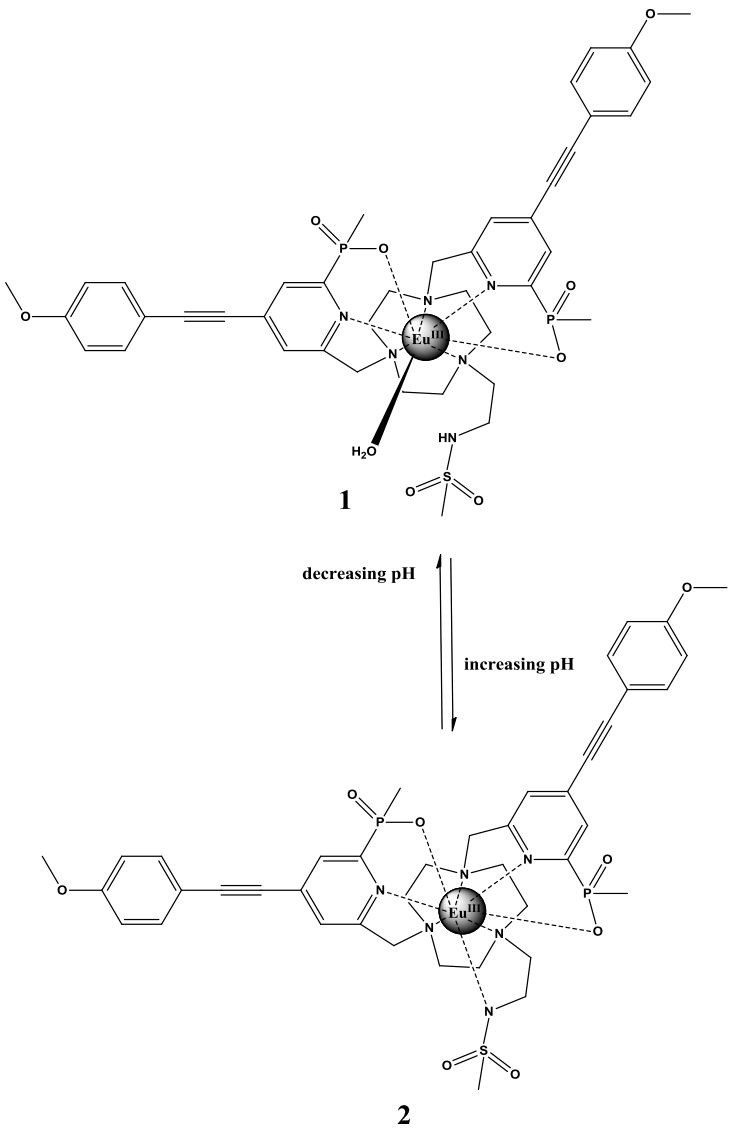

Figure 9. Representation of pH dependent sulphonamide ligation.

High quantum yields of 50% were achieved by using multiple aryl-alkynyl groups as sensitizer antennae compared to the azaxanthone used by the authors in previous studies [26], which exhibited quantum yields of 6%. The aryl-alkynyl groups in combination with the pyridyl groups selectively localise the complex within the endoplasmic reticulum. The sulfonamide moiety confers pH-sensitivity to the probe: in acidic conditions the sulfonamide is protonated and cannot take part in the Eu(III) coordination thus opening a coordination site for one molecule of water **(1)** (Figure 9). At higher pH the sulfonamide is deprotonated and can participate in the Eu(Ill) coordination through the nitrogen and displacement of the water molecule **(2)** (Figure 9). The Eu(III)

emission spectra of the europium complex as a function of pH (0.1 M NaCl, 298 K) showed substantial changes in the splitting of the $\Delta J = 1$ transition and also in the form of the $\Delta J = 2$ and $\Delta J = 4$ spectral bands. In particular, an 80% increase of $\Delta J = 2/[\Delta J = 0 + \Delta J = 1]$ emission intensity over the pH range 4-10 was observed, consistent with a change in the Eu(III) coordination environment. Other examples of pH responsive Eu(III)-based complexes was reported by Mark P. Lowe *et al* [27]. The luminescent properties of two Eu(III)-based complexes of two ligands formed by DO3A (1,4,7-tris(carboxymethyl)-1,4,7,10-tetraazacyclododecane), containing a pendant arm of diphenylphosphinamide moiety (dpp), were studied. The dpp moiety was used as chromophore antenna to sensitise the Eu(III) emission. The europium(III)-based emission of these complexes was recorded at pH 5.5, 8.4 and 10.0 upon excitation of the antenna at 270 nm. An overall increase in the intensity of the Eu(III) spectra as the pH moved toward more basic media was observed and the most significant change was the increase of the hypersensitive $\Delta J = 2$ band at around 617 nm [27]. The increased europium emission intensity observed in basic media could be attributed to the closer proximity of the chromophore to the Eu(III) center, which made the energy transfer more efficient and the fact that the Eu(III) coordination by the dpp moiety in basic media displaced a quenching water molecule, which further increased the Eu(III) emission intensity [27].

1.2.1.2 Modulation of lanthanide(III) sensitization by altering the antenna-lanthanide(III) distance

As discussed in the section 1.1.4, the sensitization of lanthanide complexes occurs via energy transfer from the triplet excited state of the antenna to the lanthanide(III) ion. Researchers have exploited the distance-dependence of the energy transfer process to modulate luminescence through altering the distance between the sensitizer antenna and the lanthanide(III) ion. While an obvious way to do this is to increase the number of bonds between the antenna and the Ln^{3+} [28], it has also been achieved reversibly

through complexation. Pierre *et al.* designed a water soluble Eu(III)-based probe **(3)** to signal the presence of K^+ [29]. The chemical structure and mode of action of this complex **(3)** are reported in Figure 10.

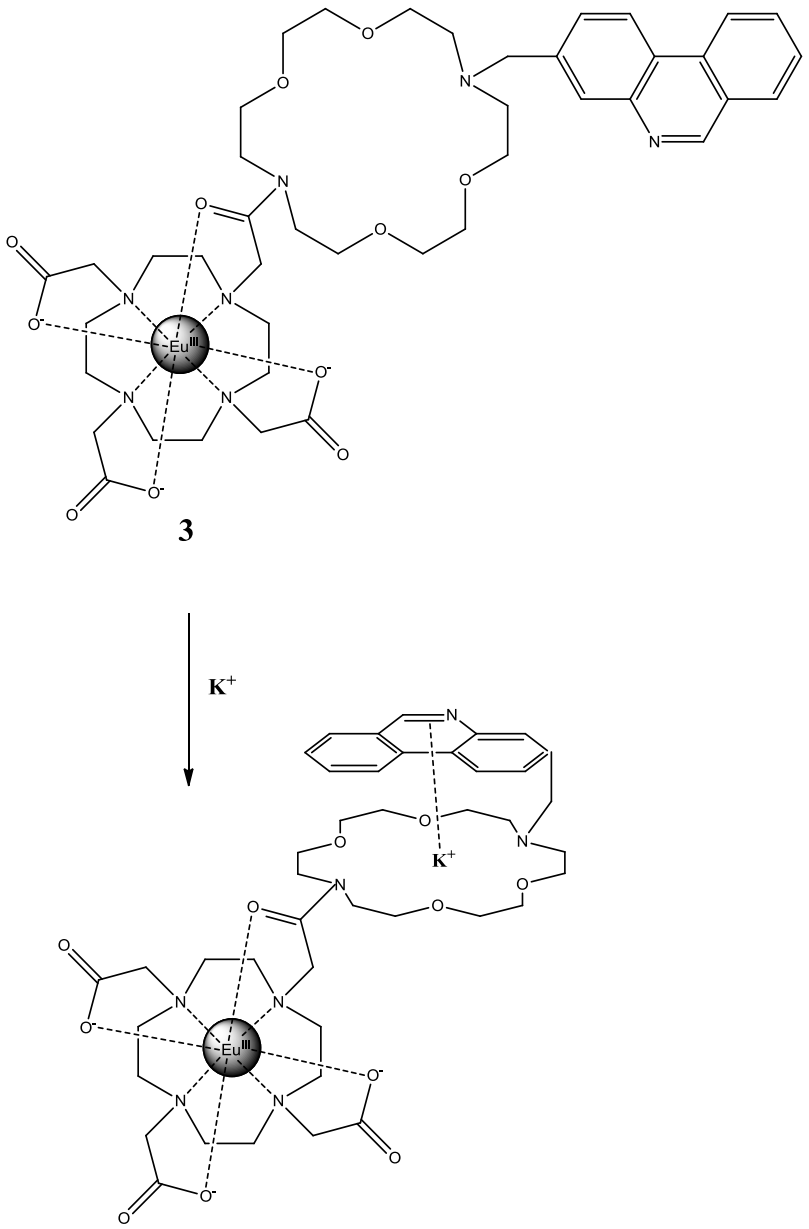

Figure 10. Structure and mode of action of the Eu(III)-probe **(3)**.

Complex **(3)** contains a phenanthridine group that acts as Eu(III) sensitizer antenna and, together with the crown ether, as K^+ complexing group. The complexation of K^+ by the crown ether and the phenanthridine group (via a cation-π interaction) caused a decrease

of the distance between the antenna and the Eu(III), which in turn caused an increase of the Eu(III)-based luminescence as consequence of an improved energy transfer process from the phenanthridine antenna to the lanthanide ion [29].

Switch-off probes have been designed exploiting the reverse strategy where the analyte of interest causes the dissociation of a coordinating antenna thus preventing it to act as sensitizer [29]. Gunnlaugsson and co-workers have used the coordinating water soluble antenna 4,7-diphenyl-1,10-phenanthroline-disulfonate (BPS) to signal the presence of dicationic transition metals, such as Fe(II) [30]. The chemical structure and the mode of action of the Eu(III)-based luminescent probe **(4)** are reported in Figure 11.

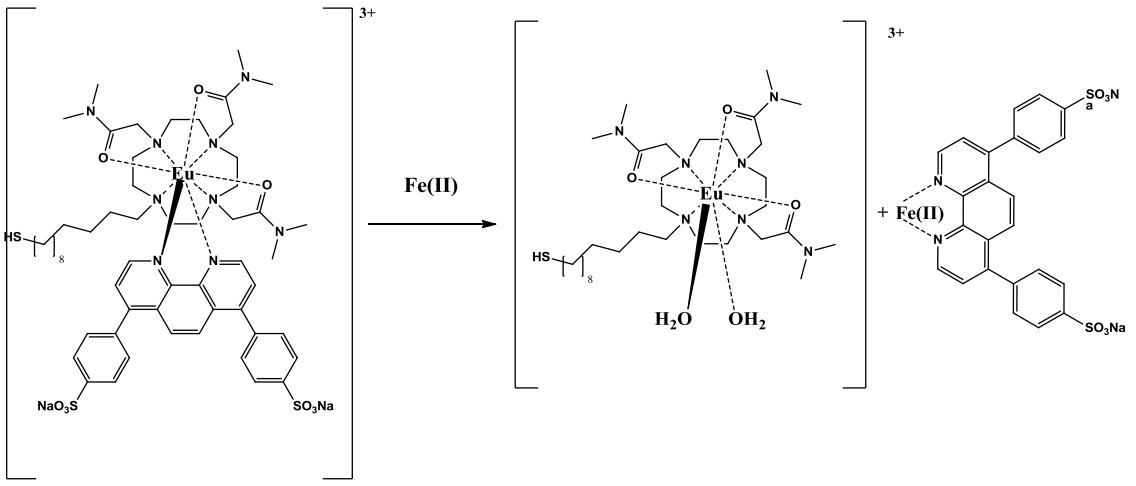

4

Figure 11. Structure and mode of action of the Eu(III)-probe **(4)**.

In absence of Fe(II), the BPS antenna coordinated the Eu(III) and sensitized its luminescence. In the presence of Fe(II), the BPS antenna, which has a high affinity for Fe(II), coordinated the Fe(II) forming a Fe(II)-BPS_3 complex. The displacement of the BPS antenna on the Eu(III) complex induced by the Fe(II) prevented the antenna to act efficiently as sensitizer and consequently a very low Eu(III) emission was observed [30].

1.2.1.3 Lanthanide complexes based on analyte-triggered antenna formation.

This section describes an example of luminescent lanthanide complexes containing pro-antennae masked by reactive cages. Pershagen and co-workers reported examples of lanthanide complexes based on caged coumarin antennae [31]. The general chemical structure **(5)** and the mode of action of these complexes in illustrated in Figure 12.

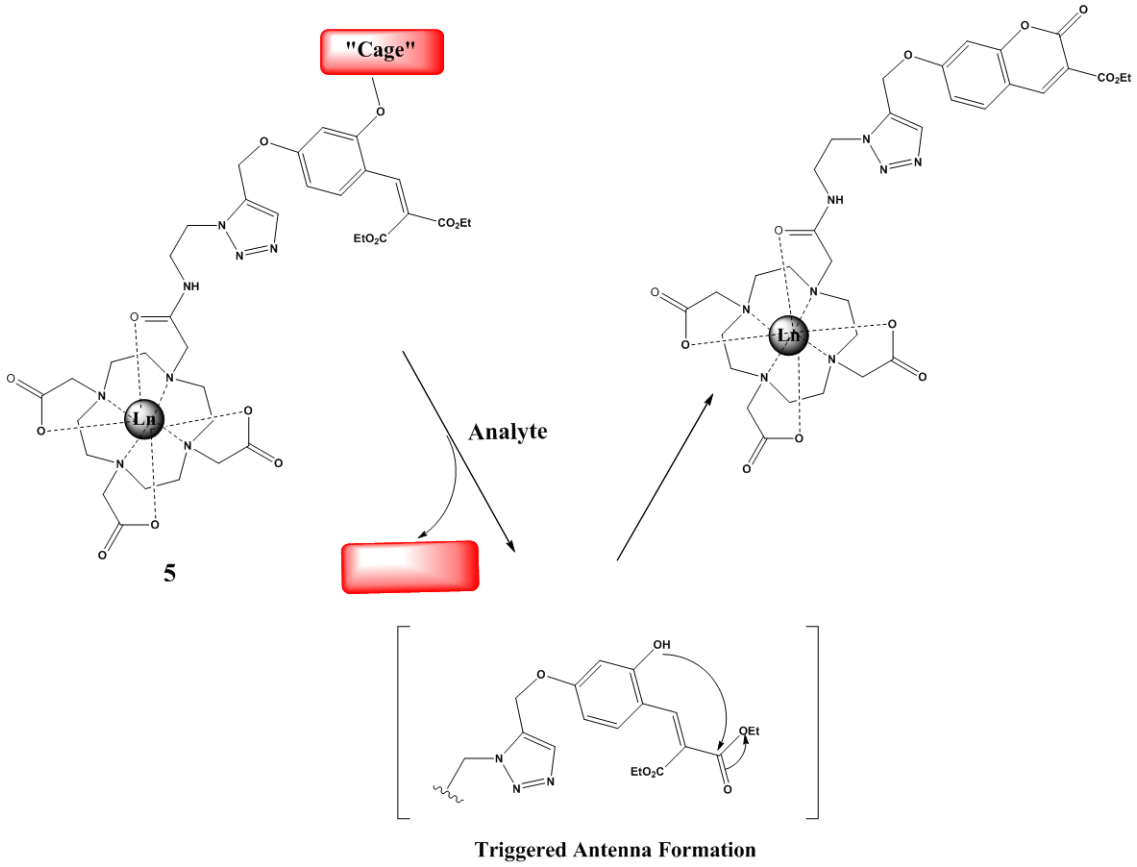

Figure 12. General chemical structure and mode of action of lanthanide complexes based on caged coumarin antennae.

In these complexes, the pro-antenna was derivatised (caged) with either phenylboronic acid, triisopropylsilane, allyl, or galactose cages for the detection of hydrogen peroxide, fluoride, palladium, or *β*-galactosidase, respectively. In the presence of the analyte, the

cage was removed as consequence of the reaction with the analyte, triggering the formation of the coumarin antenna, which was then able to sensitize the Ln(III) luminescence. While selectivity for hydrogen peroxide, fluoride, and β-galactosidase was not tested, the palladium probe was selective over other transition metals [31]. Moreover the authors demonstrated that the hydrogen peroxide and fluoride probes were able to signal the presence of their respective analytes with no detectable cross interference [31].

1.2.1.4 Other examples of luminescent molecular sensors based on lanthanide-complexes

An example of how the photophysical properties of luminescent lanthanide complexes can be exploited to selectively signal the presence of analytes, even in a complex biological environment, was reported by Bruce *et al*. [32]. In this study, the synthesis and the anion binding behaviour of a series of Eu(III) and Tb(III) complexes were reported. The chemical structure of one of the lanthanide complexes synthesised and tested in this study **(6)** is shown in Figure 13. Compound **(6)** is the triflate salt of an Eu(III)-based complex, whose ligand is formed by a trisubstituted cyclen containing three identical moieties of phenyl ethyl amine derivatives.

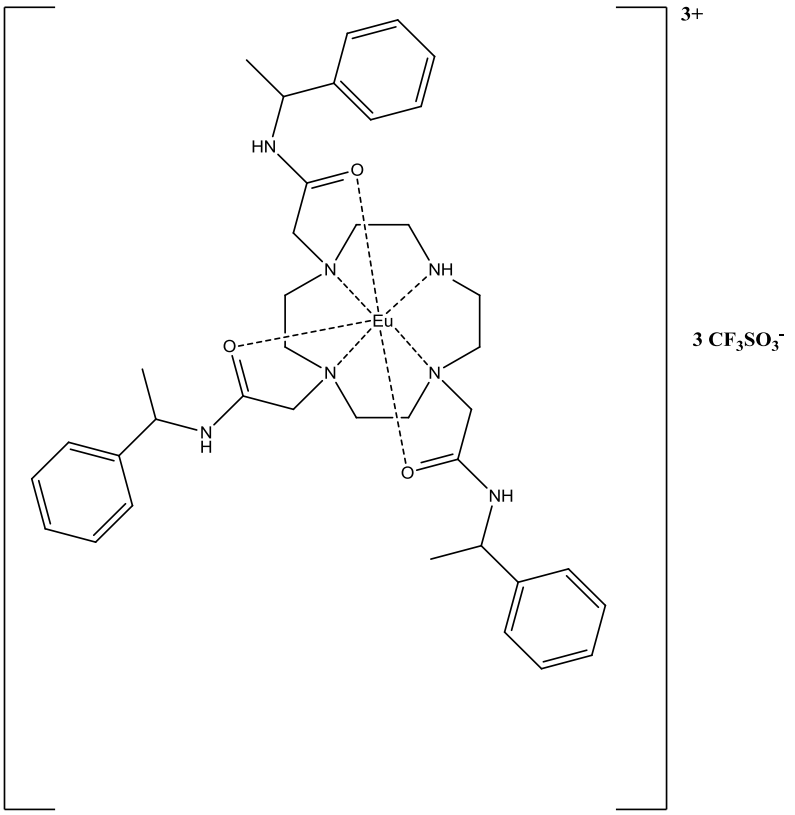

6

Figure 13. Chemical structure of the Eu(III)-based complex **(6)**.

The emission of **(6)** was recorded in presence of several anions, such as $NaHCO_3$, Na_2HPO_4, sodium lactate and disodium malonate, and the related emission profiles were compared with the emission profile recorded in absence of added anions. Significant changes of the emission profile of the Eu(III) complex **(6)** were observed upon addition of each anion. These changes were particularly significant upon the addition of the $NaHCO_3$, indicating that **(6)** was able to selectively sense HCO_3^- among a broad range of anions. This selectivity was particularly useful when the complex **(6)** was going to be tested in a complex biological environment. The comparison between the emission spectra of **(6)** recorded in absence and presence of HCO_3^- showed that in the latter case $\Delta J = 0$ emission band reduced in intensity by a factor of 4 and the $\Delta J = 2/\Delta J = 1$ ratio doubled. The changes of emission profiles observed with the complex **(6)** following the

addition of the anions were due to the changes of the coordination environment of Eu(III). These changes in turn were due to the replacement of two molecules of H_2O, involved in the Eu(III) coordination, with the anion. The reversible replacement of two molecules of H_2O with HCO_3^- anion is depicted is shown in Figure 14.

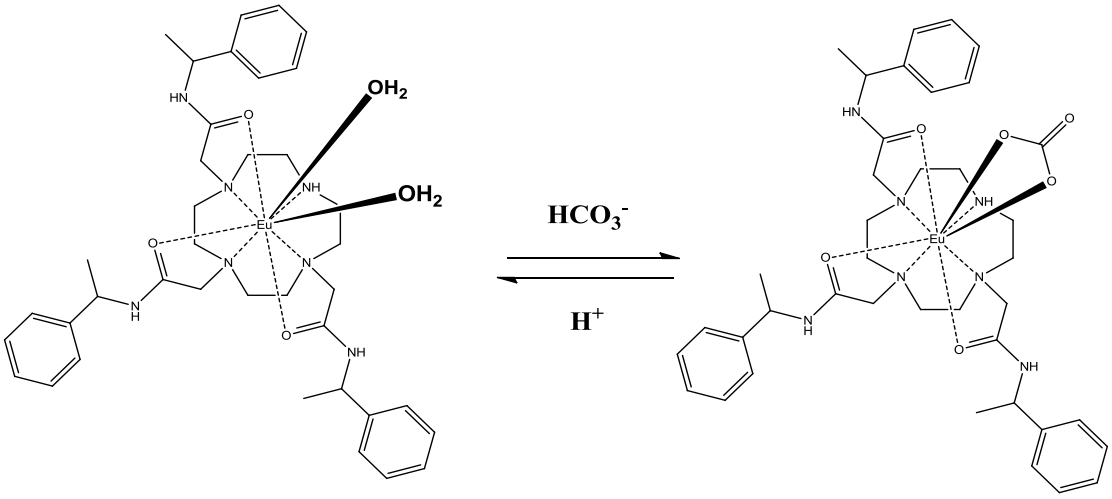

Figure 14. Reversible HCO_3^- binding to the Eu(III) core of complex **6**.

The bicarbonate signalling by luminescent lanthanide-based complexes was further investigated by Parker *et al.* [33]. In this study, a series of Eu and Tb complexes of four different ligands containing an azaxanthone as sensitizer antenna were evaluated as probes for the bicarbonate anion. The four ligands were complexed with Eu(III) and Tb(III), giving rise to two series of complexes: one including four Eu(III) complexes and the other comprising the Tb(III) complexes. Since similar results were obtained along the Eu(III)-series, and since the results were also similar for the complexes belonging to the Tb(III) series, in this section the photophysical behaviour of one Eu(III) and one Tb(III) complexes of the same ligand will be discussed as representative of the Eu(III) and Tb(III) series respectively. The structures of the Eu(III) and Tb(III) complexes (complexes

(7) and **(8)** respectively), whose photophysical properties are descried in this section, are shown in Figure 15.

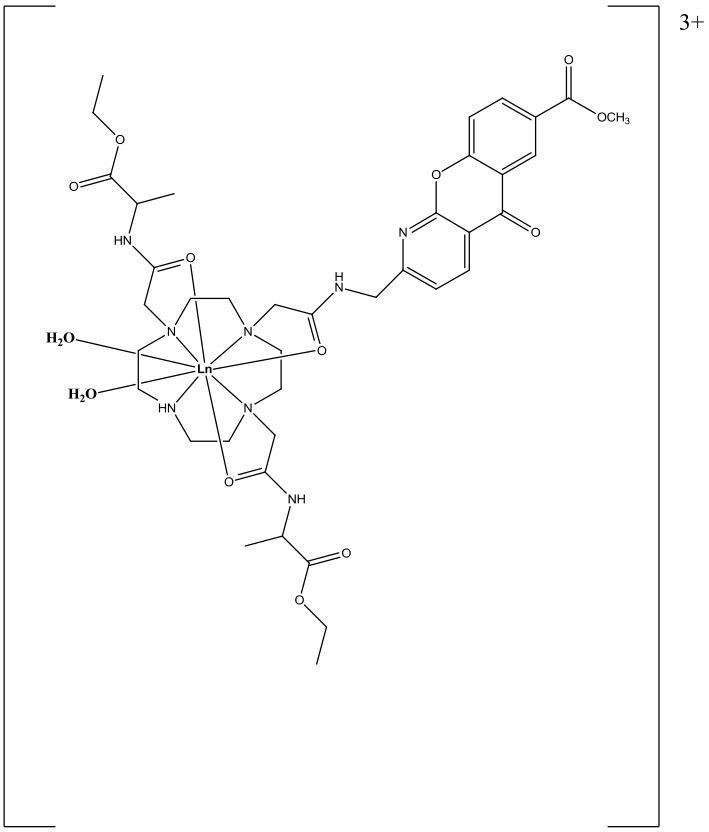

7 Ln = Eu
8 Ln = Tb

Figure 15. Chemical structures of two lanthanide complexes synthetized and tested by Parker et al. **(7)** is the Eu(III) complex, while **(8)** is the Tb(III) complex and both were obtained starting from the same ligand bearing an azaxanthone as sensitizer.

The emission of **(7)** was recorded during the titration with sodium bicarbonate up to a final concentration of 30 mm. A large increase in emission intensity was observed across the Eu(III) emission spectrum, particularly with the $\Delta J = 2$ emissive band. The maximum of the $\Delta J = 2$ band shifted slightly upon bicarbonate binding from 614 to 616 nm and changes to the overall form of emission were observed, mainly within the $\Delta J = 1$ band. The emission of **(8)** was recorded upon incremental addition of sodium bicarbonate

solutions. Although the presence of bicarbonate induced an increase of the relative intensity of Tb(III) emission, this increase was less intense compared to the large increase observed with **(7)** upon bicarbonate addition. The effect of a protein background upon bicarbonate binding was also examined in this study. In this case, the emission of Eu(III) of **(7)** was monitored upon incremental additions of sodium bicarbonate to **(7)** dissolved in a fixed human serum albumin (HSA) solution. A significant increase of the Eu emission and a shift in the $\Delta J = 2$ maximum from 614 to 616 nm were observed upon addition of sodium bicarbonate and these results were consistent with those observed when protein was not present. The terbium analogue **(8)** showed a change of less than 20% in spectral emission intensity following addition of the same concentration of bicarbonate. The different responses observed for **(7)** and **(8)** to the presence of bicarbonate in a fixed background of protein was exploited by Parker et al. to measure bicarbonate concentrations in a biological medium by monitoring the europium to terbium emission intensities ratio. This was achieved using a lanthanide-tandem system formed by a mixture of Eu(III) and Tb(III) complexes of a common ligand, where the terbium complex served as an internal reference for the strong emission intensity achievable with the europium analogue. Incremental additions of sodium bicarbonate to a mixture of **(7)** and **(8)** in 3:2 ratio, dissolved in a medium containing HSA, citrate, lactate, phosphate and ATP, were monitored by measuring the variation of the Eu/Tb emission intensities ratio. The higher proportion of the Eu(III) complex was essential to start at a point where the ratio of emission intensities was approximately unity, as terbium was the more emissive complex. An increase of the europium/terbium intensities ratio was observed upon bicarbonate addition, suggesting that this tandem system could be applied for bicarbonate concentration measurements in biological fluids. The tandem europium/terbium emission method was then tested in a human serum. Even in this case a significant increase of the europium/terbium emission intensities was observed upon addition of bicarbonate. The europium/terbium emission intensities ratio measured upon addition of bicarbonate allowed the estimation of unknown values of bicarbonate

concentration for real-life serum samples. The tandem europium/terbium emission method also proved to be effective for the calculation of mitochondrial levels of bicarbonate in several different cell types. In this assay the mitochondria were the target organelles since the Krebs cycle and glycolysis both produce mitochondrial CO_2 that is converted into bicarbonate for transport [34].

1.2.1.5 Examples of luminescent lanthanide complexes as cyanide and fluorine anions sensors

Other examples of luminescent lanthanide-based complexes able to detect the presence of anions in aqueous solutions were recently reported by Routledge *et al.* [35]. In this study the synthesis and anion binding behaviour of three Eu(III) complexes were reported. In particular, the ability of these complexes of signalling the presence of cyanide and fluorine anions in aqueous solutions was examined. The chemical structures of the lanthanide complexes **(9)**, **(10)** and **(11)** developed by Routledge *et al.* are shown in Figure 16.

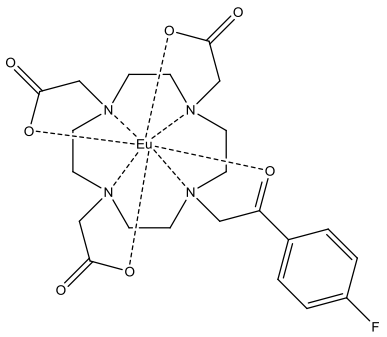

9

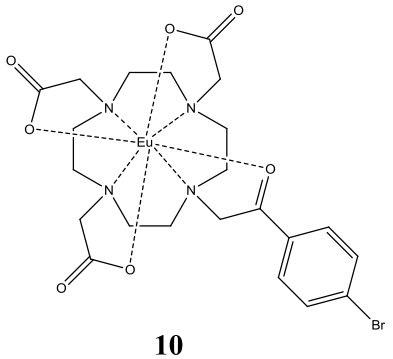

10

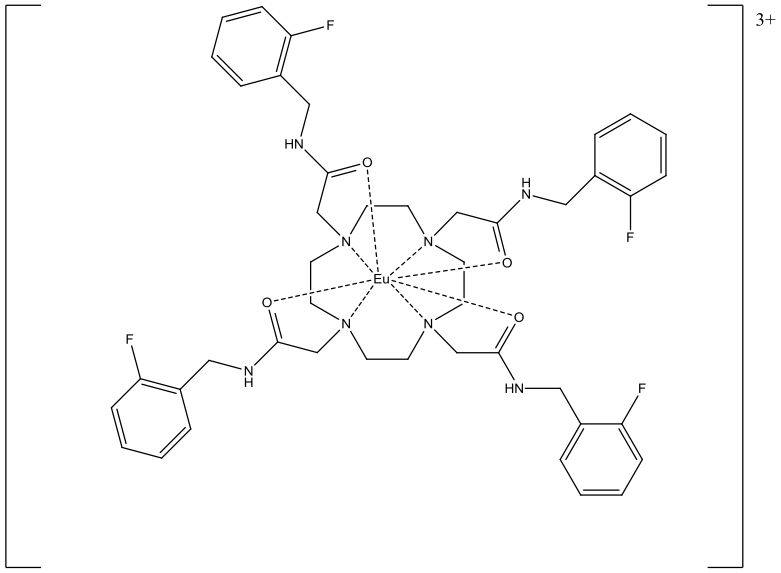

11

Figure 16. Chemical structures of complexes **(9)**, **(10)** and **(11)**.

Complexes **(9)** and **(10)** contain a phenacyl group that coordinates the Eu(III) through the carbonyl oxygen and in addition provides an antenna chromophore used for the sensitization of the lanthanide ion. The coordination of Eu(III) by the phenacyl group had two effects: it facilitated the energy transfer process from the chromophore to the lanthanide and in the meantime polarized the carbonyl group thus increasing its susceptibility to the attack by external nucleophiles. Such a binding event could cause a disruption of the chromophore antenna, thereby changing the effectiveness of energy transfer. The response of **(9)** and **(10)** to cyanide and fluoride ions was tested through emission and NMR spectroscopy and changes in emission and NMR spectra were

examined. A significant decrease in the relative intensity of the Eu(III) emission was observed for both complexes **(9)** and **(10)**. However, the Eu(III) emission spectra of **(9)** and **(10)** obtained upon the addition of cyanide ion did not show any difference in the peak shapes compared the Eu(III) emission spectra recorded before adding cyanide. This indicated that the coordination environment of the metal centre did not undergo any change, thus confirming that the water molecule was still involved in the lanthanide coordination and was not replaced by cyanide ion. Therefore, the decrease of the relative intensity of the Eu(III) emission could not be attributable to the perturbation of the coordination environment of Eu(III) caused by cyanide. It was rather the consequence of the nucleophilic attack by cyanide ion to the polarized carbonyl function of the phenacyl antenna, which was converted into its corresponding cyanohydrin form. This in turn caused a perturbation of the sensitizer antenna thus reducing the effectiveness of the energy transfer process from the antenna to the lanthanide ion, which resulted in a lowered intensity emission. This mechanism is illustrated in the Figure 17, which shows the reversible binding of the cyanide ion to **(9)** and **(10)** that led to the cyanohydrin formation.

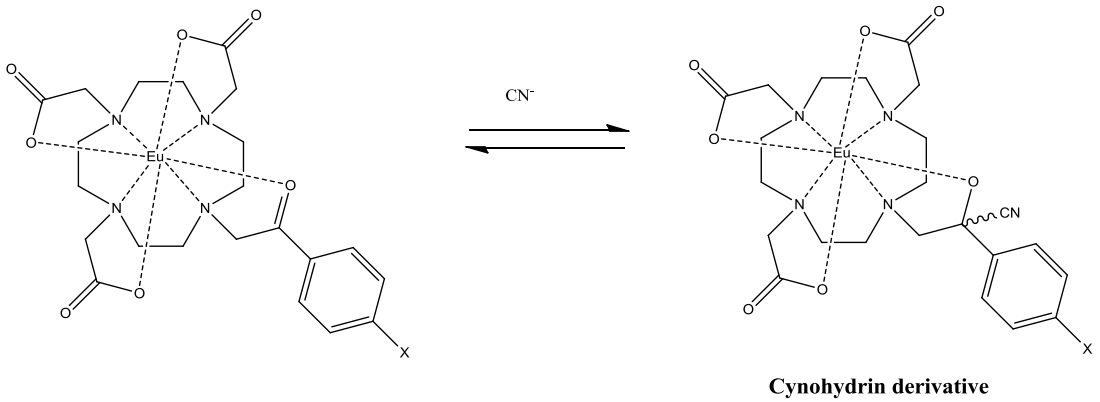

Figure 17. Cyanohydrin formation caused by the nucleophilic attack by cyanide ion to the carbonyl function of the antenna. X = F in complex **(9)** and X = Br in complex **(10)**.

The changes in the NMR spectra recorded for **(9)** and **(10)** following cyanide addition showed the presence of a cyanohydrin derivative thus confirming the mechanism responsible for the lowered Eu(III) emission observed upon cyanide addition. While both complexes **(9)** and **(10)** were responsive to the presence of cyanide ion, they did not show any response to changes in fluoride ion concentration. Indeed, a completely inverse situation was observed for complex **(11)** that proved to be responsive to changes in fluoride concentration and unresponsive to cyanide.

1.2.1.6 Examples of luminescent lanthanide complexes as phosphorylated amino acids and hexapeptides sensors

Other examples of luminescent lanthanide complexes were recently developed by Parker *et al.* to signal phosphorylated amino-acids and O-phosphorylated hexapeptides [36]. The two Eu(III) complexes, **(12)** and **(13)**, examined in this study were based on an achiral heptadentate triazacyclononane ligand bearing two strongly absorbing chromophores and their chemical structures are shown in Figures 18 and 19 respectively.

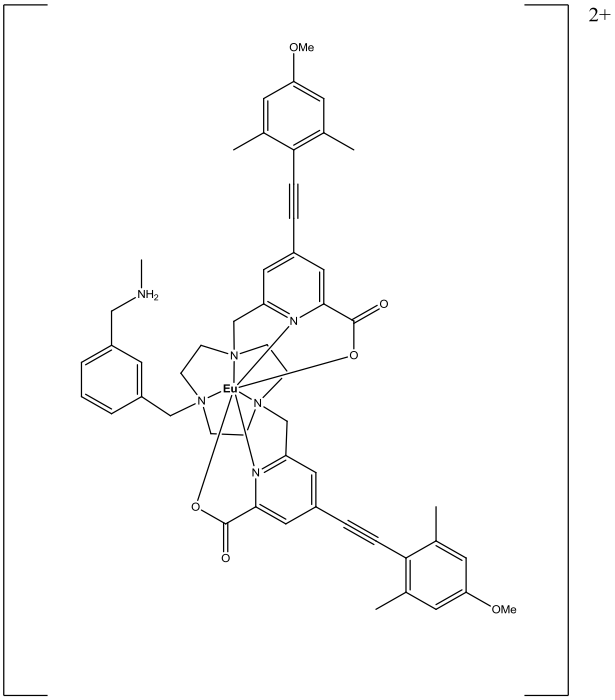

12

Figure 18. Chemical structure of **(12).**

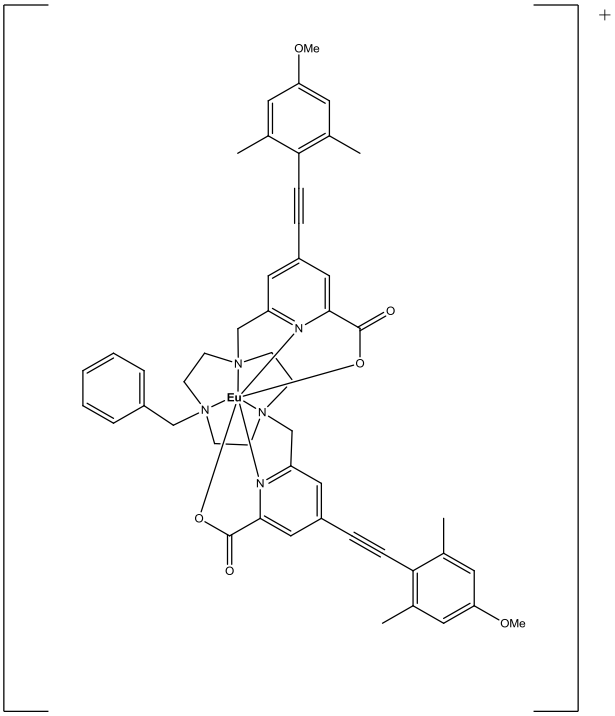

13

Figure 19. Chemical structure of **(13)**.

The two Eu(III) complexes were not coordinated by a solvent molecule since the steric hindrance caused by the benzylic substituent prevented solvent coordination. The anion binding properties of **(12)** and **(13)**, towards hydrogenphosphate were examined before studying the phosphorylated amino acid and hexapeptide anions. The emission of **(12)** and **(13)**, was monitored upon incremental addition of aqueous solutions containing hydrogen phosphate and the changes in the relative intensity and form of the Eu(III) emission spectrum were examined. Complex **(13)**, showed no change in europium spectral form with added hydrogenphosphate while complex **(12)** exhibited a significant modulation. The differences in hydorgenphosphate response shown by **(12)** and **(13)** were due to the fact that in **(12)**, the presence of the N-methyl ammonium group on the benzyl ring acting as hydrogen donor, favoured the hydrogen bonding with hydrogenphopshate, thus facilitating its incorporation into the coordination sphere of the metal centre, which in turn caused variation of the Eu(III) emission profile. The emission spectral changes of **(12)** were investigated following the addition of O-P-Ser, O-P-Thr and O-P-Tyr, which are O-phosphorylated amino acids. The Eu(III) emission spectra recorded upon the addition of the phopshorylated amino acids were all similar to that following the addition of hydrogenphosphate, and the changes that occurred were not significant, except in the $\Delta J = 4$ and $\Delta J = 1$ emissive bands. However, these changes were accompanied by a strong CPL signal upon addition of O-P-Ser or O-P-Thr to **(12)**. CPL stands for circularly polarized luminescence. No CPL signal was induced by addition of O-P-Tyr indeed, indicating that **(12)** was selective towards the O-phopshorylated serine and threonine. Moreover, the response of **(12)** to a series of phosphorylated amino acids was also investigated. Three phosphorylated peptides, containing the same amino acid sequence and only varying for the type of phosphorylated amino acid and the number of phosphorylated sites, were selected for this study. In particular, one peptide containing a phosphorylated residue of serine, one peptide containing a phosphorylated residue of tyrosine, and another peptide containing phosphorylated residues of serine and tyrosine were tested. The corresponding non-

phosphorylated peptide was also studied as a control. The addition of the non-phosphorylated control peptide resulted in no induced CPL indeed, providing further evidence that the peptide binds to the Eu(III) centre via the phosphate group. The induced CPL spectral response of the O-P-Ser peptide was opposite in sign and form to that of O-P-Tyr peptide, suggesting that the chiral structure of the entire peptide when bound to the lanthanide centre could be associated with the induced CPL response. The di-phosphorylated peptide, containing both a phosphorylated serine and tyrosine residue, induced a CPL signal much less intense than for the other two peptides, and seemed to be the result of an additive sum of the two separate spectra. This could be explained considering that **(12)** had no preferential binding site, as the calculated affinity constants for the O-P-amino acids were the same. Therefore, the emission spectrum observed was a combination of **(12)** bound to the O-P-Ser of the peptide and the O-P-Tyr residue.

The ligands used in the systems examined so far were almost symmetric since they were based on trisubstituted cyclen ligands containing two identical pendant arms or on tetrasubstituted cyclen ligands bearing three identical pendant arms. The luminescent lanthanide complexes that will be examined in the next section represent examples of more sophisticated systems whose ligands are based on asymmetrically substituted cyclen ligands, containing three different pendant arms [37], [38]. These examples will show how the use of asymmetrically substituted cyclen-based ligands allow a major control on the sensitization of the lanthanide ions and how this feature is particularly useful in sensing analytes difficult to be accurately detected in complex biological environments.

1.2.1.6 Examples of luminescent lanthanide complexes based on asymmetrically substituted cyclen ligands.

Most luminescent lanthanide complexes reported in the literature, some of which have been examined in the previous section, are able to signal the presence of substrates by

an increase or decrease in luminescence intensity or changes in the emission spectral form. This makes the analyte detection sometimes ambiguous. Bruce *et al.* reported a series of lanthanide-based luminescent sensors that were non-emissive in absence of the analytes of interest, and became emissive upon analyte binding [37]. This was be achieved by using unsymmetrical cyclen-based ligands incorporating an antenna and a quencher. The general chemical structures of these systems are shown in Figures 20 and 21.

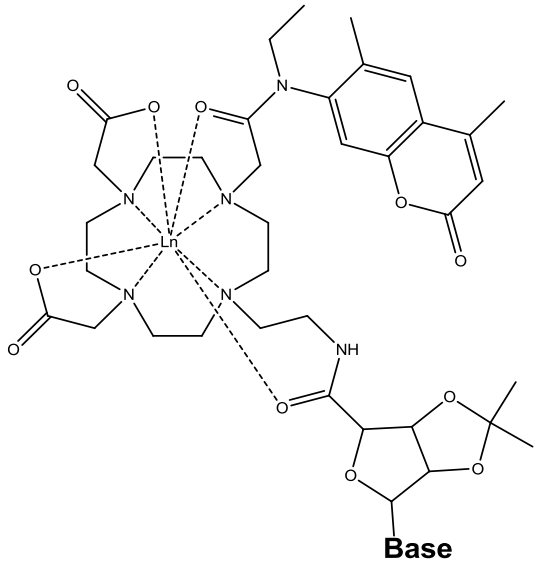

Base = U or A
Ln = Eu and Tb

Figure 20. General chemical structure of Eu(III) and Tb(III) complex developed in this study. Base is represented by uridine (U) or adenosine (A). The trivalent lanthanide ions (Ln) used in this system are Eu(III) and Tb(III). The sensitizer antenna is coumarin 2.

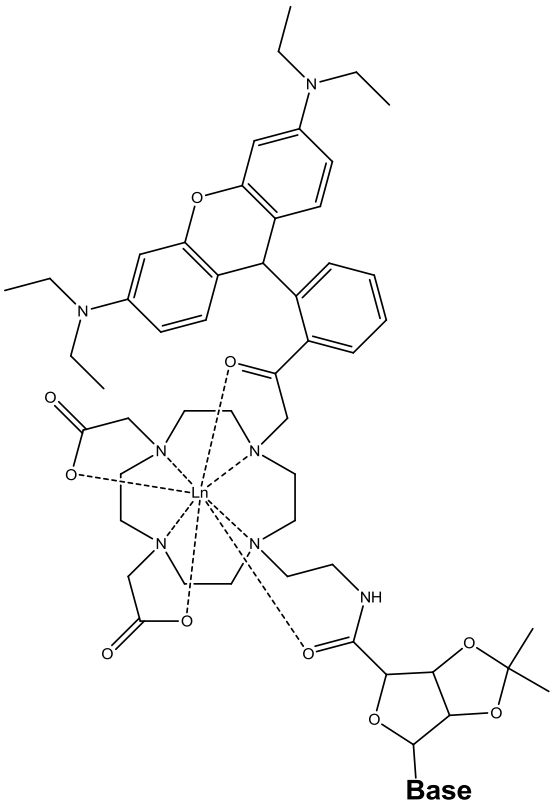

Base = U or A
Ln = Nd and Yb

Figure 21. General chemical structure of Nd(III) and Yb(III) complex developed in this study. Base is represented by uridine (U) or adenosine (A). The trivalent lanthanide ions (Ln) used in this system are Nd(III) and Yb(III). The sensitizer antenna is rhodamine.

In their systems, Eu(III) and Tb (III) were sensitised with coumarin 2, while Nd(III) and Yb(III) with rhodamine [37]. Both antennae were paired with nucleoside (uridine and adenosine) quenchers. The interaction between the quencher and the antenna could be regulated by the addition of the complementary base or DNA to the complexes, resulting in changes in the lanthanide luminescence intensity. In the absence of substrates, the quencher could disrupt the energy transfer from the antenna to lanthanide ion resulting in the inhibition of its luminescence. As the complementary base or DNA was added to the solution containing the complex, a strong luminescence from the lanthanide could be detected as consequence on quencher-complementary base or DNA interaction. Among

the systems developed in this study, the Nd (III)-based complex containing rhodamine as sensitizer and adenosine as base showed the desired switch off-on luminescence upon addition of DNA or the complementary base uridine. Quenching of the rhodamine antenna by the adenosine quencher was almost complete since only a very weak Nd(III)-based luminescence was observed in absence of substrate following excitation of the rhodamine antenna at 355 nm. Upon addition of substrate the non-luminescent probe was turned on and a strong Nd(III) based luminescent was observed upon excitation at 355 nm. The switching off-on property of the Nd(III)-based complex developed by Bruce et al. provides a valid example of how the use of asymmetrically substituted cyclen-based ligands can allow a tighter control the luminescence of lanthanide ion compared to the control achievable when more symmetric substituted cyclen-based ligands are employed. Other examples of how asymmetrically substituted cyclen-based ligands could be exploited to develop luminescent lanthanide-based sensors possessing a tight control of the lanthanide ion sensitization were reported by Bruce *et al*. [38]. In this study, the synthesis, characterization and photophysical properties of two asymmetrically substituted cyclen-based near IR-emitting lanthanide complexes were reported. Their chemical structures are shown in Figure 22. These systems possessed a common ligand based on an symmetrically substituted cyclen complexed with the near IR-emitting Nd(III) and Yb(III) in complex **(14)** and **(15)** respectively (Figure 22).

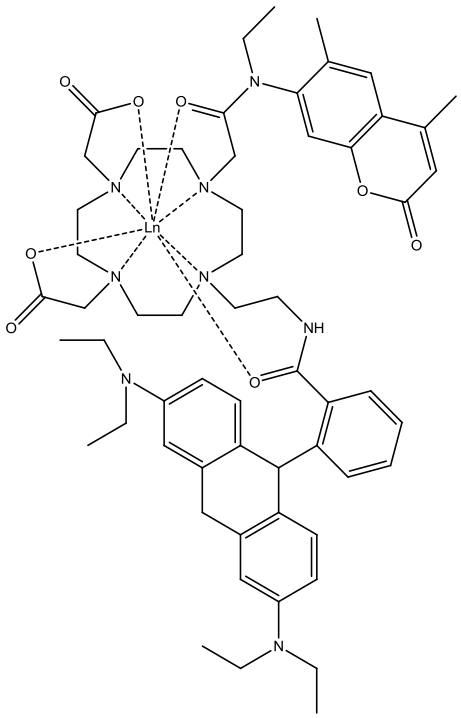

14 Ln = Yb
15 Ln = Nd

Figure 22. Chemical structures of compound **(14)** and **(15)** that were developed in this study.

The Nd(III) and Yb(III) were sensitised by rhodamine, which in turn is excited by energy transfer from a coumarin 2 moiety. An energy transfer cascade consisting of two processes occurred in these systems allowing the sensitization of Nd(III) and Yb(III): one energy transfer process from coumarin 2 to rhodamine and another from rhodamine to Nd(III) and Yb(III) in **(14)** and **(15)** respectively (Figure 23). The energy transfer cascade covered the UV-visible-near IR region of the spectrum, resulting in large Stokes shifts. Excitation of the coumarin 2 moiety at 355 nm resulted in the direct excitation of the rhodamine moiety and consequent emission from the lanthanide ion.

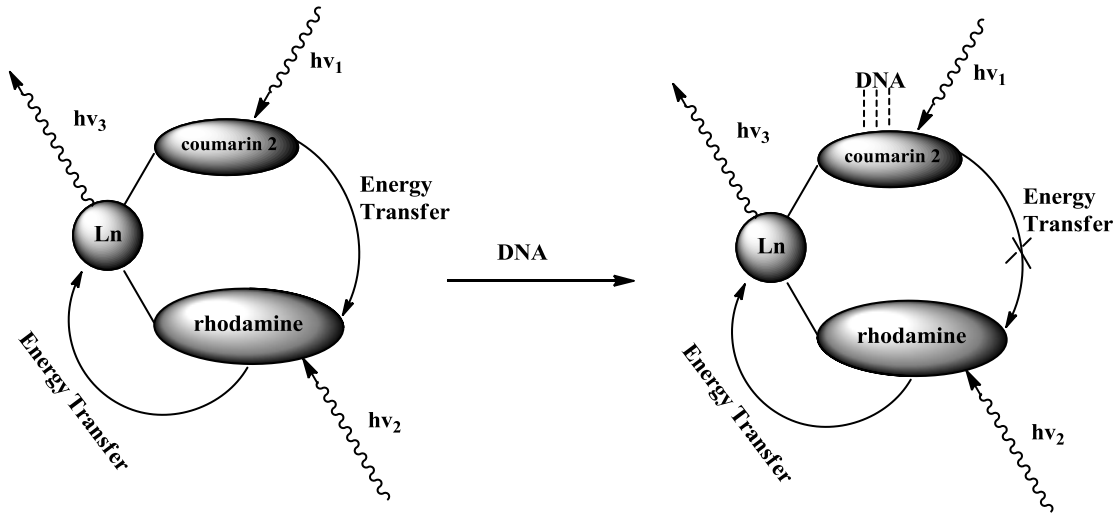

Figure 23. The energy transfer cascade initiated by excitation of the coumarin 2 moiety proceeds through the rhodamine antenna, resulting in lanthanide emission. The cascade can be disrupted by intercalative quenching of the coumarin 2 by DNA.

Both compounds **(14)** and **(15)** in methanol showed the characteristic near IR emission. **(14)** had an emission band at 890 nm and one at 1064 nm, while **(15)** emitted at 980 nm. The total emission intensity of **(14)** at 1065 nm showed a significant decrease upon treatment with 1 equiv. of *ds*DNA, due to quenching of the coumarin 2 moiety by the DNA-strands. This quenching effect resulted from an intercalation effect exerted by DNA on the coumarin 2. Changes similar to **(14)** emission were observed for **(15)** emission band at 980 nm, although the effect was less pronounced. The decrease of the lanthanide emission observed with both **(14)** and **(15)** upon DNA addition was due to the disruption of the energy transfer process from the coumarin 2 to rhodamine.

1.3 Reactive Oxygen Species (ROS)

In this section a description of ROS is provided since they represent the type of analytes for whose detection the lanthanide complexes developed in this project were designed. The ROS overview will be followed by a description of the biological processes involved in the ROS production and their biological roles. This would be help to understand the designing of the molecular systems studied in this project and the photophysical behaviour observed during both the cuvette- and cell- based tests performed to evaluate their ability to generate a ROS response, which are described in detail in the chapters 4 and 5 respectively. The detailed description of the mitochondrial electron transport chain (ETC) provided below will be also useful to understand the effects of the lanthanide complexes developed in this project on the mitochondrial and/or cellular functions during the cell- and isolated mitochondrial-based tests performed on these compounds to assess their potential mitochondrial or cellular toxicity. These tests and their related results are described in details in the chapter 5.

Reactive oxygen species (ROS) are chemically reactive molecules that are naturally produced within biological systems. There are diverse types of ROS including: superoxide anion, hydrogen peroxide, peroxide, hydroxyl radical and hydroxyl ion (Figure 24).

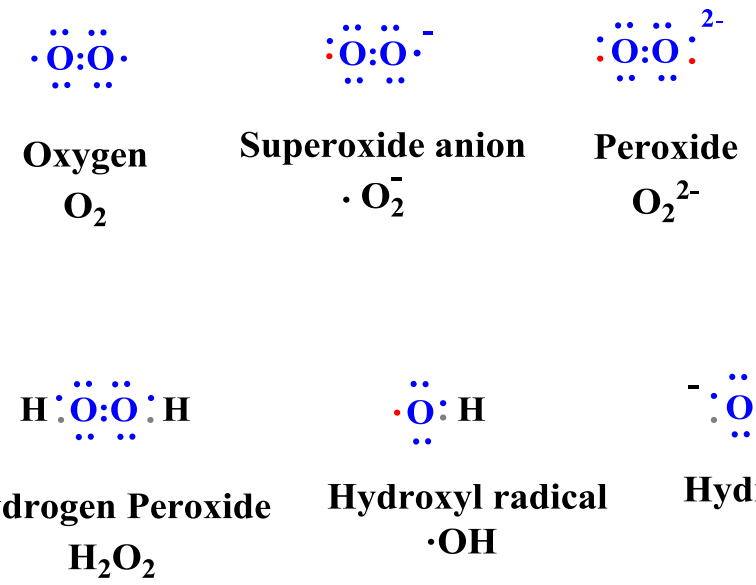

Figure 24. **Electron structures of common reactive oxygen species**. Each structure is provided with its name and chemical formula. The • designates an unpaired electron.

When the molecular oxygen O_2 is in its ground state (also called triplet state) it contains two unpaired electrons in the outer shell and so it is not highly reactive with the two electrons in a chemical bond. This is due to the fact that the two unpaired electrons in the molecular oxygen have the same spin and as consequence it can only react with one electron at a time. Molecular oxygen can be, however, converted to more reactive species containing oxygen. Energy transfer to O_2 leads to the formation of the more reactive molecular oxygen form, singlet oxygen ($^1O_2$). Singlet oxygen has paired electrons with opposite spins and as consequence it can quickly react with other pairs of electrons, especially those involved in a double bond [39], [41], [42]. Singlet oxygen can form during lipid peroxidation and contribute to damage because of its ability to readily oxidize lipids, proteins and DNA [40], [41], [42]. The reduction of oxygen by one electron produces relatively stable intermediates. Superoxide anion (O_2^{-}•), the product of a one-electron reduction of oxygen, is the precursor of most ROS and is involved in oxidative chain reactions. Dismutation of O_2^{-}• (either spontaneously or through a reaction catalyzed by superoxide dismutases) produces hydrogen peroxide (H_2O_2), which in turn may be fully reduced to water or partially reduced to hydroxyl radical (OH•), one of the

strongest oxidants in nature. The formation of OH• is catalyzed by reduced form of transition metals, which in turn may be re-reduced by O_2^{-}•, propagating this cyclic process [8], [43]. OH• can hydroxylate the position number 8 of the ring structure of guanine in DNA; the initial product is an 8-hydroxy-2'-deoxyguanosine radical, which can cause mutagenic lesion [44]. OH• can also attack other bases and the deoxyribose sugar in DNA, producing massive damage [45].

1.3.1 Electron transport chain (ETC) and Oxidative phosphorylation.

Oxidative phosphorylation is the process in which ATP is formed through electron transfer from NADH or $FADH_2$ to molecular oxygen via the electron transport chain (ETC) [46], [47]. Oxidative phosphorylation of eukaryotes takes place in the mitochondria. Mitochondria are ovoid shape cellular organelles, with a length of about 2 µm and a diameter of about 0.5 µm. The mitochondria have two systems of membranes: an outer membrane and a very extended and folded inner membrane. The inner membrane forms a series of folds called cristae. So there are two compartments in mitochondria: intermembrane space (the space between the inner membrane and the external membrane) and the matrix (the space delimited by the inner membrane) (Figure 25).

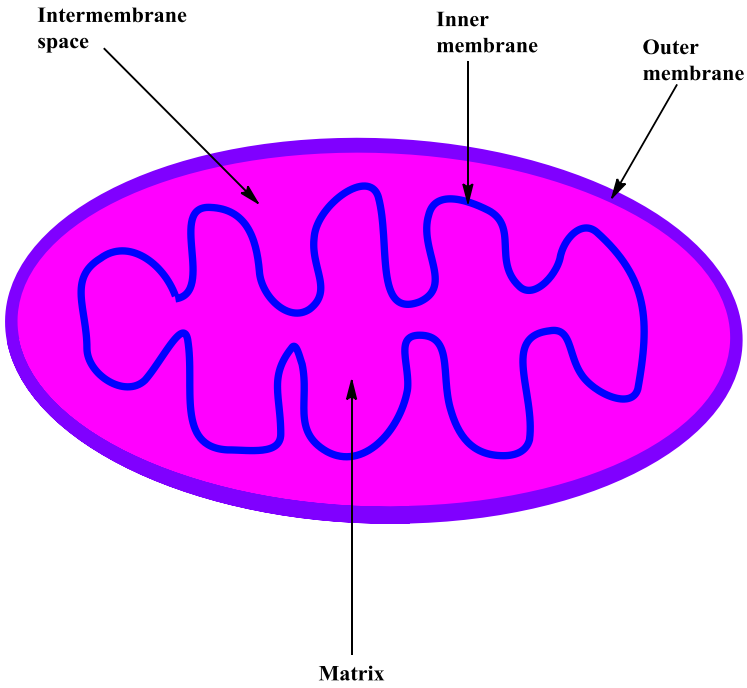

Figure 25. Mitochondrion

The driving force of oxidative phosphorylation is the electron transfer potential of NADH or $FADH_2$ relative to that of O_2. The related half-reactions are:

$$\frac{1}{2} O_2 + H^+ + 2e^- \rightarrow H_2O \qquad E'_0 = +0.82\ V \qquad (a)$$

$$NAD^+ + H^+ + 2e^- \rightarrow NADH \qquad E'_0 = -0.32\ V \qquad (b)$$

Subtracting reaction b from reaction a yields:

$$\frac{1}{2} O_2 + NADH + H^+ \rightarrow H_2O + NAD^+ \qquad \Delta E'_0 = +1.14V \qquad (c)$$

The redox potential for the NAD^+:NADH redox couple is E'_0 = -0.32 V, while the redox potential for the O_2:H_2O redox couple is E'_0 = +0.82 V, where E'_0 represents the reduction potential (also called the redox potential or oxidation-reduction potential). This means that the difference between the redox potentials of NADH and O_2 ($\Delta E'_0$) is +1.14V [44]. The electrons are transferred from NADH to oxygen through a chain of four protein complexes in the inner mitochondrial membrane. These complexes are numbered according to the order with which the electrons pass through them (Figure 26). The

electrons of NADH enter into the chain at the level of NADH-Q reductase (also called NADH dehydrogenase or Complex I). NADH binds to the complex I and the transfers its high-energy electrons to flavin mononucleotide (FMN) producing the reduced form $FMNH_2$ [46], [47]. The electrons are then transferred from $FMNH_2$ to a series of iron-sulphur (Fe-S) centres. The iron atoms of these centres cyclically pass from the ionization state +2 (reduced) to the state +3 (oxidized). The electrons are then transferred from the iron-sulphur centres of the NADH-Q reductase to the coenzyme Q, also known as ubiquinone. The ubiquinone is reduced to semiquinone free radical when it receives a single electron, while the reduction of this intermediate with a second electron leads to the formation of ubiquinol (QH_2) [46], [47]. The flow of two electrons from NADH to QH_2 through the NADH-Q reductase causes the transport of four H^+ ions from the matrix to the cytosolic side of the inner mitochondrial membrane. The electrons of $FADH_2$ are transferred to the coenzyme Q by the complex of the succinate-Q reductase (Complex II), producing the reduced form QH_2. The complex II is not a proton pump (it does not transfer H^+ ions) consequently, less ATP is formed by the oxidation of $FADH_2$ compared to the oxidation of NADH [46], [47]. The third complex of the respiratory chain is the cytochrome reductase (also called ubiquinol-cytochrome c reductase, cytochrome, cytochrome bc_1 complex or Complex III). In general, a cytochrome is a protein containing a heme prosthetic group that transports electrons [46], [47].

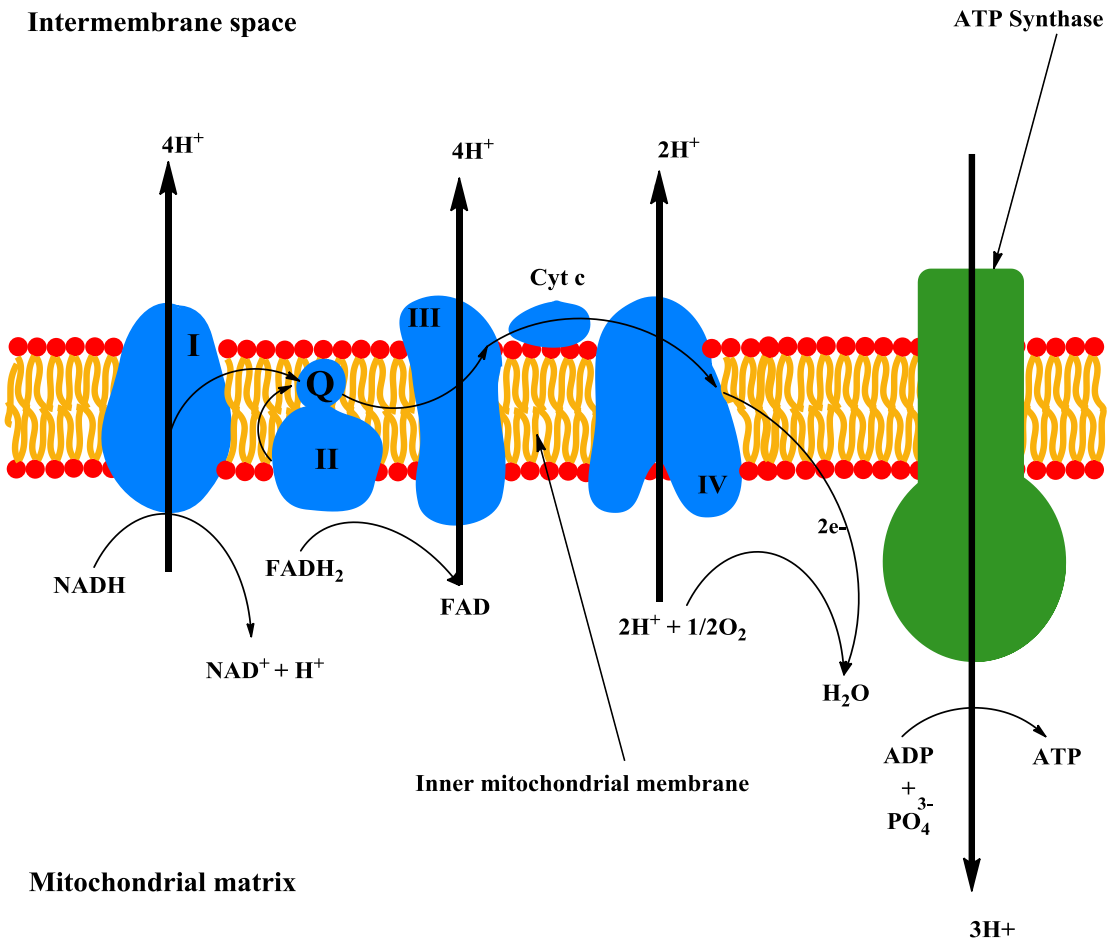

Figure 26. The picture shows a schematic representation of the mitochondrial electron transport chain.

Also in this case the iron of the heme group passes from the oxidation state +2 (reduced) to the oxidation state +3 (oxidized) and vice versa. The function of the cytochrome reductase is to catalyse the transfer of electrons from QH_2 to cytochrome 2, a water-soluble protein, and at the same time to transfer protons H^+ through the inner mitochondrial membrane. In particular the flow of two electrons through this complex causes the effective net transport of two H^+ to the cytosolic side, half of the yield obtained with the NADH-Q reductase due to a lower thermodynamic driving force. The final complex chain of electron transport is the cytochrome oxidase, (also called Complex IV), an enzyme that catalyses the transfer of electrons from ferrocytochrome c (the reduced form) to molecular oxygen, the final acceptor [46], [47], [41]:

4 cytochrome c (+2) + 4 H^+ + O_2 → 4 cytochrome c (+3) + 2 H_2O

For a complete reduction of O_2 to H_2O, four electrons are transferred from the cytochrome c to O_2 and concurrently protons (H^+) are transferred from the matrix to the cytosolic side of the inner mitochondrial membrane.

The electron transfer along the ETC causes the transport of protons (H^+) from the matrix side to the cytosolic side of the inner mitochondrial membrane [47], [48]. This generates a pH gradient across the inner mitochondrial membrane, with the pH higher in the matrix than in the intermembrane space of about 1 unit [47], [48], and a voltage gradient *(membrane potential,* ΔV*)* across the inner mitochondrial membrane, with the inside negative and the outside positive (as a result of the net outflow of H^+) [47], [48]. Together, the ΔpH and the ΔV thus generate an electrochemical proton gradient [47], [48]. The electrochemical proton gradient across the inner mitochondrial membrane is used to drive ATP synthesis in the process of oxidative phosphorylation. The synthesis of ATP is catalyzed by the enzyme ATP synthase or Complex V (Figure 26). This enzyme generates a hydrophilic pathway across the inner mitochondrial membrane that allows protons to flow from the inner membrane space to the matrix following their electrochemical gradient. As these ions flow down through the ATP synthase, they are used to promote the endergonic reaction of the ATP synthesis from ADP and P_i [46], [47].

1.3.2 ROS Production

In eukaryotes, the main biological system where ROS are produced is represented by the electron transport chain (ETC), located in internal mitochondrial membrane [49], [50], [51]. As discussed in the above paragraph (1.4.1), the transfer of four electrons from the cytochrome c to O_2 leads to the formation of a non-toxic product (two molecules of H_2O), while the partial reduction of O_2 generates potentially very dangerous compounds for the cells known as ROS [49], [50]. In mitochondria ROS are generated via escaping of electrons from ETC. The two principal sites of superoxide generation that have been identified in mitochondria are complex I and complex III. The amount of electrons

escaping ETC varies broadly and depends on physiological state of organisms [49], [51]. In living organisms under aerobic conditions more than 90% of oxygen consumed is reduced directly to water by cytochrome oxidase in ETC through four-electron mechanisms and without ROS production (Figure 27) [49], [50], [51]. Much less than 10% (1-5%) of oxygen consumed is reduced via one-electron pathways resulting in the partial reduction of molecular oxygen to superoxide anion radical ($O_2^{\bullet-}$) (Figure 27) [49], [50], [51]. The production of superoxide anion radical is followed by one-electron reduction with concomitant accepting of two protons to yield hydrogen peroxide (H_2O_2) (Figure 27) [49], [50], [51]. Then the hydrogen peroxide accepts one more electron and is converted into hydroxyl anion (HO^-) and hydroxyl radical ($OH\bullet$) (Figure 27). Finally, the hydroxyl radical reacts with one more electron and proton resulting in formation of water molecule. In biological systems, this reaction mainly occurs through the abstraction of a hydrogen atom from several compounds such as proteins and lipids and this results in the initiation of chain reaction processes [49], [50], [51].

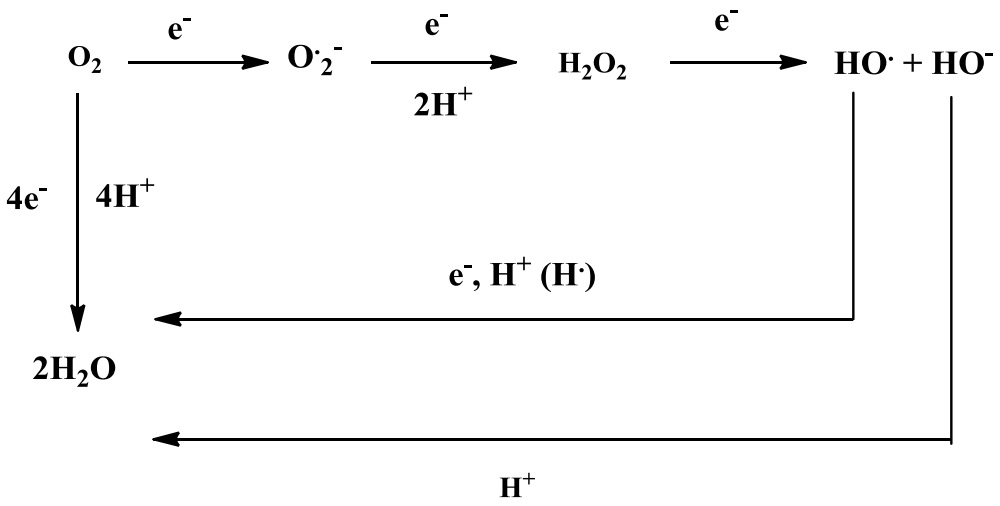

Figure 27. Reduction of molecular oxygen via four- and one-electron schemes.

The $O_2^{\bullet-}$ can be neutralized by the superoxide dismutase, an enzyme that catalyses the reaction between two $O_2^{\bullet-}$ to form H_2O_2 and H_2O [46].

$$O_2^{\bullet-} + O_2^{\bullet-} + 2H_3O^+ \rightarrow H_2O_2 + 2H_2O + O_2$$

The H_2O_2 formed by the reaction catalysed by the superoxide dismutase, is converted into H_2O and O_2 by the enzyme catalase [46].

$H_2O_2 + H_2O_2 \rightarrow 2\ H_2O + O_2$

The H_2O_2 can be also partially reduced to OH• by reduced transition metals. In the case of iron, this reaction is known as Fenton reaction [52]:

$Fe^{2+} + H_2O_2 \rightarrow Fe^{3+} + OH\bullet + OH^-$ *(Fenton reaction)*

$O_2\bullet^-$ participates in the Haber-Weiss reaction which combines a Fenton reaction and the reduction of Fe^{3+} by $O_2\bullet^-$, yielding Fe^{2+} and O_2 [11].

The Haber–Weiss reaction is:

$O_2\bullet^- + H_2O_2 \rightarrow O_2 + OH\bullet + OH^-$ *(Haber-Weiss reaction)*

Indeed, the reduction of Fe^{3+} by $O_2\bullet^-$ is:

$Fe^{3+} + O_2\bullet^- \rightarrow Fe^{2+} + O_2$

Apart from the mitochondria ETC, minor amounts of ROS are produced by ETC located in/at endoplasmic reticulum (ER), plasmatic, and nuclear membranes as well as some oxidases [53], [54]. ROS are also produced as consequence of the autoxidation of different small molecules of endo- and exogenous origin. Epinephrine (adrenalin) and norepinephrine provide a good example of endogenous molecules that undergo to autoxidation associated with ROS production [55]. ROS are also produced by ionizing and UV radiation and from the metabolism of a wide range of drugs and xenobiotics [40].

1.3.3 Dual role of ROS

The generation of ROS can be either beneficial or harmful. ROS at normal levels are involved in many cellular responses including cell growth and immune response [11], [56]. For example, during the oxidative burst occurring in an inflammatory process, activated neutrophils and macrophages produce large amount of $O_2\bullet^-$ and other ROS via the phagocytic isoform of NADPH oxidase. The concentration of H_2O_2 under such conditions may reach a level of 10-100 μM [11]. The rapid release of ROS during the oxidative burst represents a defence mechanism against pathogens [11]. ROS have also

a cell signalling role in many biological systems. ROS play important roles in cell proliferation, cell death, activation or suppression of many genes expression. ROS are also responsible for activating cell signalling cascades, such as those involving mitogen-activated protein kinases [57]. Although ROS play a key role in many physiological processes, overproduction of ROS results in oxidative stress that can be responsible for damage to important cell structures, such as lipids and membranes, proteins, and DNA. Cells possess enzymatic and non-enzymatic antioxidants that work in synergy to regulate the ROS levels and prevent oxidative damages [12]. The main cellular antioxidant enzymes are superoxide dismutase (SOD), glutathione peroxidase (GPX), and catalase (CAT). Other antioxidant enzymes, such as thioredoxin (TRX), glutaredoxin (GRX), and peroxiredoxin (PRX), also play important roles to protect cells against oxidation [56]. In addition to antioxidant enzymes, cells also contain several non-enzymatic antioxidants (e.g., glutathione (GSH), uric acid, and bilirubin). GSH is a tripeptide containing a thiol group that acts as reducing agent. GSH acts as electron and hydrogen atom ($H^+ + e^-$) donor to other molecules, including ROS, to neutralize them [58]. All these antioxidant systems developed by the cells contribute to the redox homeostasis, which is important to prevent the oxidative damage of important molecules, such as lipid, DNA and proteins. For example, unrepaired damage to mitochondrial DNA leads to defective complex I or III which in turn may cause an increased single-electron reduction of O_2 to $O_2^{\bullet}$. The consequent increased production of $O_2^{\bullet}$- may lead to oxidative stress. One of the main consequence of damaged mitochondrial DNA is the decreasing of the expression of the genes codifying for proteins playing important roles during the electron transport chain. This may lead to mitochondrial dysfunction [10].

Now that the beneficial and harmful roles of ROS have been elucidated, it is evident how important is to have means for detecting variation of ROS concentrations within the cells. This could be achieved by developing novel luminescent probes that could be used as ROS sensors allowing the measurement of the cellular oxidative stress.

1.4 ROS-responsive luminescent lanthanide complexes based on asymmetrically substituted cyclen-based ligands.

The molecular systems developed by Bruce *et al.* [37], [38], examined in the previous section, provided clear evidence of how advantageous it is to design lanthanide complexes based on asymmetrically substituted cyclen ligands to signal the presence of an analyte of interest, even in the complex cellular environment. Using unsymmetrically substituted cyclen-based ligands allows the introduction of several different arms on the cyclen ring, each exerting a specific function. This is particularly useful when designing a molecular sensor based on luminescent lanthanide complexes that should be able to signal the presence of an analyte localised in a particular cellular compartment. In this case, the use of an asymmetrically substituted-cyclen based ligand allows incorporation on the same cyclen ring a suitable sensitizer antenna, essential for achieving the sensitization of the lanthanide ion, a receptor unit, able to bind the analyte of interest, and a targeting moiety that selectively deliver the complex into a specific cellular compartment. This allows the development of sophisticated molecular systems that combine the unique photophysical properties of the luminescent lanthanide ions with the properties of the ligand. Taking advantage of asymmetrically substituted cyclen ligands, a series of luminescent lanthanide complexes were developed in this project with the aim of producing effective probes able to signal variation of ROS concentration thus allowing the measurement of cellular oxidative stress. Their general chemical structure is shown in Figure 28. Therefore, the lanthanide complexes developed in this project may be applied for studying the effects of oxidative stress on mitochondrial function/dysfunction, but also for the screening of drug candidates during the drug development phase to assess their potentially toxic effects on mitochondria.

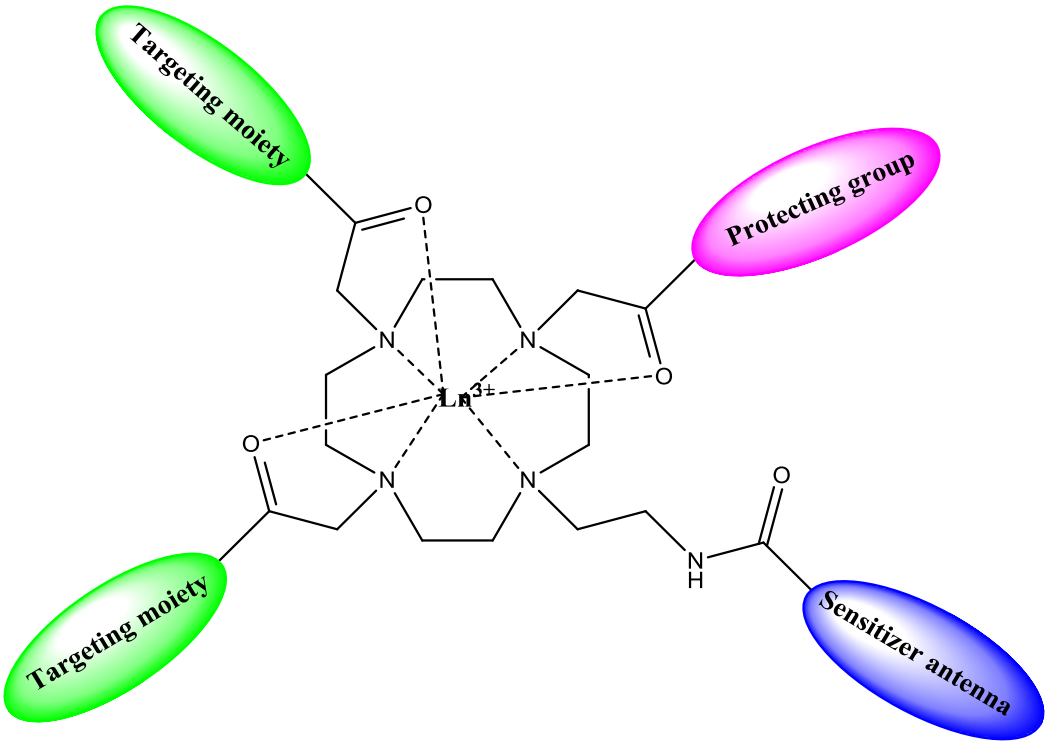

Figure 28. Representation of the general structure of the novel luminescent lanthanide complexes, based on asymmetrically substituted cyclen-based ligands, which contain two mitochondria targeting moieties.

2. Experimental Section

2.1 Materials and Methods

Cyclen, anhydrous europium(III) chloride, terbium(III) chloride, neodymium(III) chloride and ytterbium(III) chloride were obtained from Strem Chemicals. All other chemicals were purchased from Acros and Sigma Aldrich and used without further purification. All HPLC grade solvents were purchased from Sigma Aldrich and Fisher and were used as purchased. All anhydrous solvents were purchased from Sigma Aldrich and used as purchased. Thin Layer Chromatography was performed in Merck fluorescent silica or on Fluka fluorescent alumina plates with iodine, $KMnO_4$ or UV visualisation. ^{1}H NMR and ^{13}C NMR data were obtained using a 300 MHz and 400 MHz JEOL instruments manufactured by Oxford Instruments Limited. ESI Mass spectrometry (via direct injection) was performed on a TSQ Quantum instrument manufactured by Thermo Scientific. ESI-MS and MALDI-MS for the lanthanide complexes were obtained through the EPSRC Swansea Mass Spectrometry Service (University of Swansea). UV spectra were measured on a Genesys 10S UV-Vis spectrophotometer manufactured by Thermo Scientific. All UV spectra were recorded in aqueous solutions (unless differently stated) at a compound concentration of 0.3 mM (unless differently stated). Excitation and emission spectra of the Eu(III) and Tb(III) complexes were measured on a Fluoromax-P (Jobin-Yvon Horiba) fluorimeter. Excitation and emission spectra were recorded in aqueous solution at a compound concentration of 3 mM. The fluorescence intensity during the cellular ROS assay were read using a microplate reader Fluorostar OPTIMA instrument manufactured by BMG LABTECH. DMEM+Glutamax was purchased from GIBCO-Thermo Fisher. FBS (10% in medium) and HBSS were purchased from Sigma Aldrich. H_2O_2 30% and TBHP 70% were purchased from Sigma Aldrich. The MST was performed on a Seahorse Xfe96 analyser. All chemicals used in the MST and calcium loading capacity assay were supplied by Sigma Aldrich.

2.1.1 Synthesis of N-Boc-2-bromoethylamine (18)

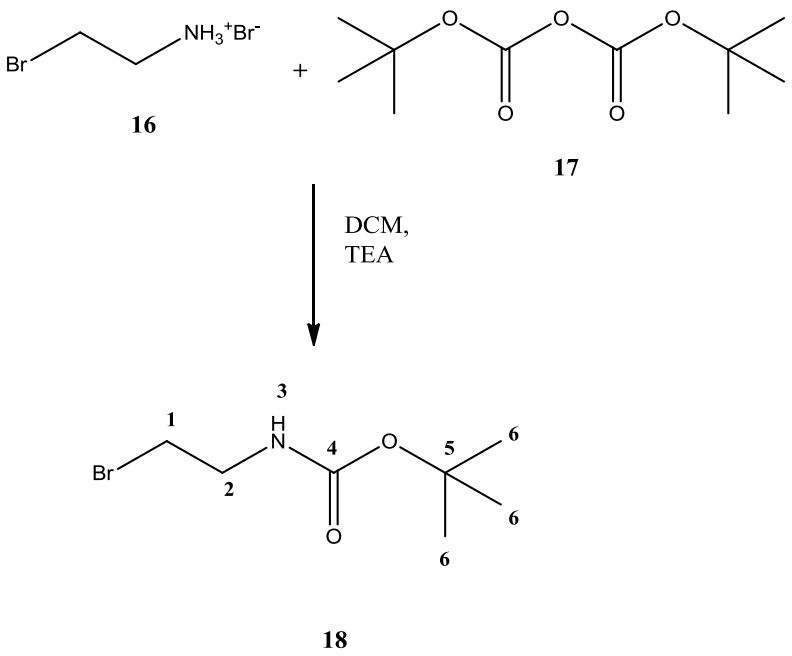

Synthetic procedure:

A suspension of 2-bromoethylamine hydrobromide (**16**) (10 g, 50 mmol) and di-*tert*butyl dicarbonate (**17**) (10.8 g, 50 mmol) in DCM (24 mL) was cooled to 0ºC, and TEA (8 mL) was added dropwise. After stirring for 24 h at room temperature (leaving the ice-water bath throughout the process), DCM (300 mL) was added to the mixture. The solution was then extracted with: water (200 mL), 0.1M HCl solution (200 mL), saturated solution of sodium bicarbonate (200 mL) and a saturated solution of NaCl. The mixture was dried over $MgSO_4$, filtered and concentrated in vacuum. Purification of the sample by column chromatography (silica column, elution with diethyl ether / hexane (2:8)) gave the product (**18**) as a colourless oil in 49% yield (8 g). ^{1}H NMR ($CDCl_3$, δ): 1.38 (s, 9 H, CH_3, H^6), 3.36-3.46 (m, 4 H, CH_2, $H^{1,2}$), 5.06 (br s, ~1 H, NH); ^{13}C NMR: 28.2 (CH_3, C^6), 32.5 (CH_2, C^1), 42.23 (CH_2, C^2), 79.6 (C_q, C^5), 155.51 (C=O, C^4).

2.1.2 Synthesis of 1-N-Boc ethylamine-1,4,7,10-tetraazacyclododecane (20)

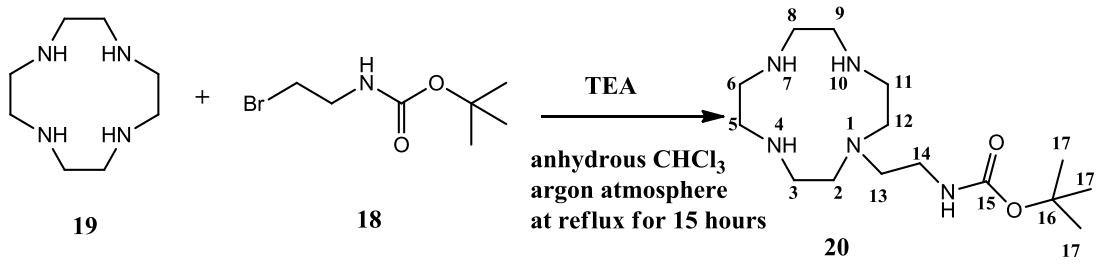

19 18 20

Synthetic procedure:

The N-Boc-2-bromoethylamine (**18)** (6.51 g; 0.029 mol; 1 eq) was added to a solution of cyclen (**19**) (25.00 g; 0.145 mol; 5 eq) and TEA (3.52 g; 0.035 mol; 1.2 eq) in one portion, in anhydrous $CHCl_3$ (500 mL). The resulting solution was heated under reflux for 18 h, under an argon atmosphere. After cooling to room temperature, the $CHCl_3$ was removed under vacuum and replaced with the same quantity of DCM (500 mL). The organic solution was washed with 1M sodium hydroxide solution (3 x 250 mL) to remove the excess of unreacted cyclen, and water (3 x 250 mL). The organic phase was dried over $MgSO_4$ and evaporated to give a withe powder in 76% yield (4.76 g): mp 119-120°C; MS: 316 $[M+H]^+$; ^1H NMR ($CDCl_3$, δ): 1.4 (s, 9 H, CH_3, H^{17}), 2.5 - 2.8 (m, 18 H, CH_2, $H^{2,3,5,6,8,9,11,12}$), 3.2 (m, 4 H, CH_2, $H^{13,14}$); ^{13}C NMR ($CDCl_3$, δ): 28.4 (CH_3, C^{17}), 38.5 (CH_2, $C^{6,8}$), 46.0 (CH_2, $C^{5,9}$), 47.1 (CH_2, $C^{11,3}$), 47.7 (CH_2, $C^{2,12}$), 52.0 (CH_2, C^{14}), 54.1 (CH_2, C^{13}), 78.8 (C_q, C^{16}), 156.0 (C=O, C^{15}).

2.1.3 Synthesis of coumarin 2 bromoacetate (23)

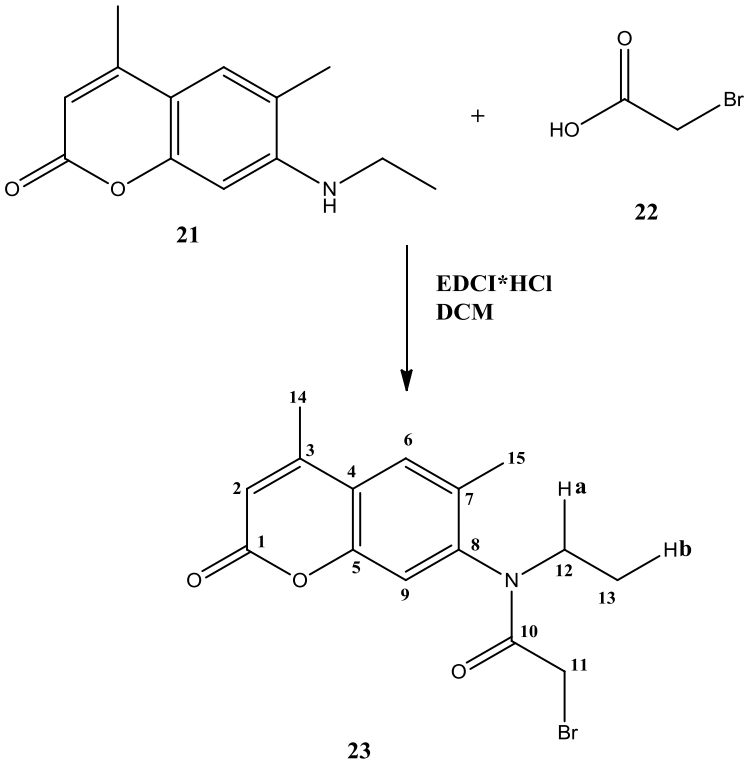

Synthetic procedure:

Coumarin 2 (**21**) (0.50 g, 2.30 mmol, 1 eq) and bromoacetic acid (**22**) (1.90 g, 13.8 mmol, 6 eq) were dissolved in DCM (30 mL), and EDCI*HCl (2.64 g, 13.8 mmol, 6 eq) was added in small portions to the vigorously stirred solution. The reaction was stirred at room temperature for 24 h. Water (50 mL) and DCM (30 mL) were added to the solution, the phases were separated and the product was extracted into DCM (2 x 30 mL). The combined organic phases were washed with water (40 mL) and 2 M NaOH (50 mL), dried over $MgSO_4$, filtered, and the DCM was evaporated in vacuum. The product (**23**) was isolated as a white solid in 84% yield (5.28 g). Analytically pure samples were obtained by chromatography on silica with EtAc / DCM (1:9): mp 170-173°C; ^{1}H NMR ($CDCl_3$, δ): 1.12-1.16 (t, 3 H, CH_3, H^{13}, $^3J_{Hb,a}$ 7.14 Hz), 2.31 (s, 3 H, CH_3, H^{15}), 2.43 (s, 3 H, CH_3, H^{14}), 3.16-3.29 (m, 1 H, CH_2, H^{12}, $^3J_{Ha,b}$ 7.14 Hz), 3.71 (s, 2 H, CH_2, H^{11}), 4.10-4.22 (m, 1 H, CH_2, H^{12}, $^3J_{Ha,b}$ 7.14 Hz), 6.32 (s, 1 H, CH, H^2), 7.12 (s, 1 H, CH, H^9), 7.52 (s, 1 H,

CH, H^{6}); ^{13}C NMR: 12.53 (CH_3, C^{13}), 17.54 (CH_3, C^{15}), 18.67 (CH_3, C^{14}), 41.55 (CH_3, C^{12}), 44.02 (CH_2, C^{11}), 116.10 (CH, C^{9}), 117.64 (CH, C^{6}), 120.41 (CH, C^{3}), 127.25 (C_q, C^{4}), 132.00 (C_q, C^{7}), 142.21 (C_q, C^{8}), 151.27 (C, C^{5}), 152.06 (CH, C^{2}), 159.98 (C=O, C^{10}), 165.49 (C=O, C^{1}).

2.1.4 Synthesis of 1-N-Boc-ethylamine-4-coumarin 2 acetamide-1,4,7,10-tetraazacyclododecane (24)

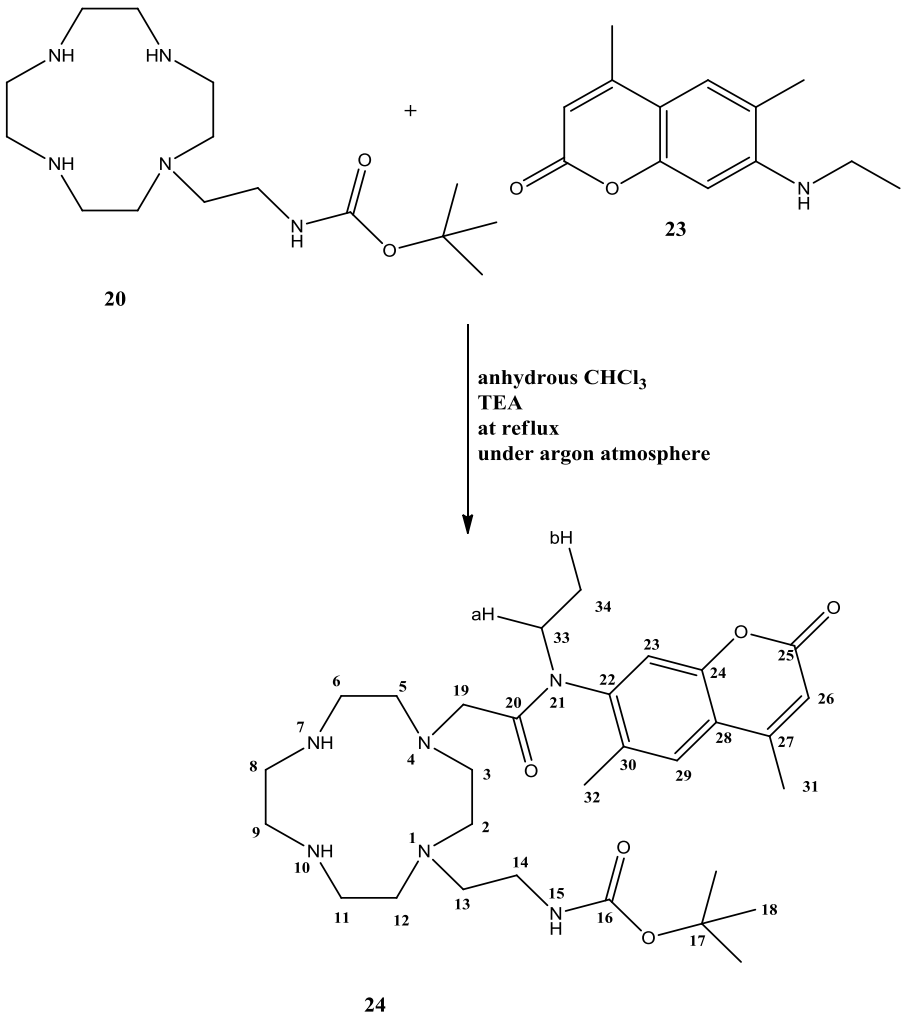

20 23

24

Synthetic procedure:

The 1-N-Boc ethylamine-1,4,7,10-tetraazacyclododecane (**20**) (1.54 g; 4.90 mmol; 1 eq) was dissolved in dry chloroform (100 mL), TEA (3.44 mL; 2.47 g; 24.5 mmol; 5 eq) was added to the solution, and the mixture was flushed with argon for 10 minutes. Coumarin 2 bromoacetate (**23**) (1.66 g; 4.90 mmol; 1eq) in chloroform (23 mL) was added dropwise (in 1 h) to the reaction mixture and the stirring was continued for 36 h at room temperature. Water (40 mL) was added, the phases were separated, and the organic phase was washed with water again (40 mL). The organic phase was dried over $MgSO_4$, filtered, and concentrated to ~5 mL. The desired product (**24**) was isolated by silica column chromatography by elution with DCM / $^{i}PrNH_2$ (2.5-10%) as a pale yellow solid in 13% yield (0.37 g): mp 54-56°C; ^{1}H NMR ($CDCl_3$, δ): 1.05 (t, 3 H, CH_3, H^{34}, $J_{Hb,a}$ = 7.14 Hz), 1.28 (s, 9 H, CH_3, H^{18}), 2.26 (s, 3 H, CH_3, H^{32}), 2.43 (s, 3 H, CH_3, H^{31}), 2.50-3.35 (m, 23 H, CH_2, $H^{2,3,5,6,8,9,11,12,13,14,19}$), 4.04 (m, 1 H, CH_2, H^{33}, $^{3}J_{Ha,b}$ = 7.14 Hz), 6.30 (s, 1 H, CH, H^{26}), 7.06 (s, 1 H, CH, H^{23}), 7.54 (s, 1 H, CH, H^{29}); ^{13}C NMR: 12.72 (CH_3, C^{34}), 17.22 (CH_3, C^{32}), 18.55 (CH_3, C^{31}), 28.19 (CH_3, C^{18}), 38.79 (CH_2, C^{33}), 43.09 (CH_2, C^{14}), 45.96 (CH_2, $C^{8,9}$), 47.41 (CH_2, C^{11}), 47.63 (CH_2, C^{6}), 51.49 (CH_2, $C^{12,5}$), 51.75 (CH_2, C^{3}), 51.98 (CH_2, C^{2}), 53.16 (CH_2, C^{13}), 53.35 (CH_2, C^{19}), 77.98 (C_q, C^{17}), 115.67 (CH, C^{26}), 117.07 (CH, C^{23}), 120.02 (CH, C^{29}), 127.25 (C_q, C^{22}), 131.65 (C_q, C^{30}), 142.70 (C_q, C^{28}), 151.44 (C_q, C^{24}), 152.05 (C_q C^{27}), 156.07 (C=O, C^{16}), 169.56 (C=O, C^{25}), 172.73 (C=O, C^{20}).

2.1.5 Synthesis of N-methyl-L-glucamine pentaacetate-bromoacetate (25)

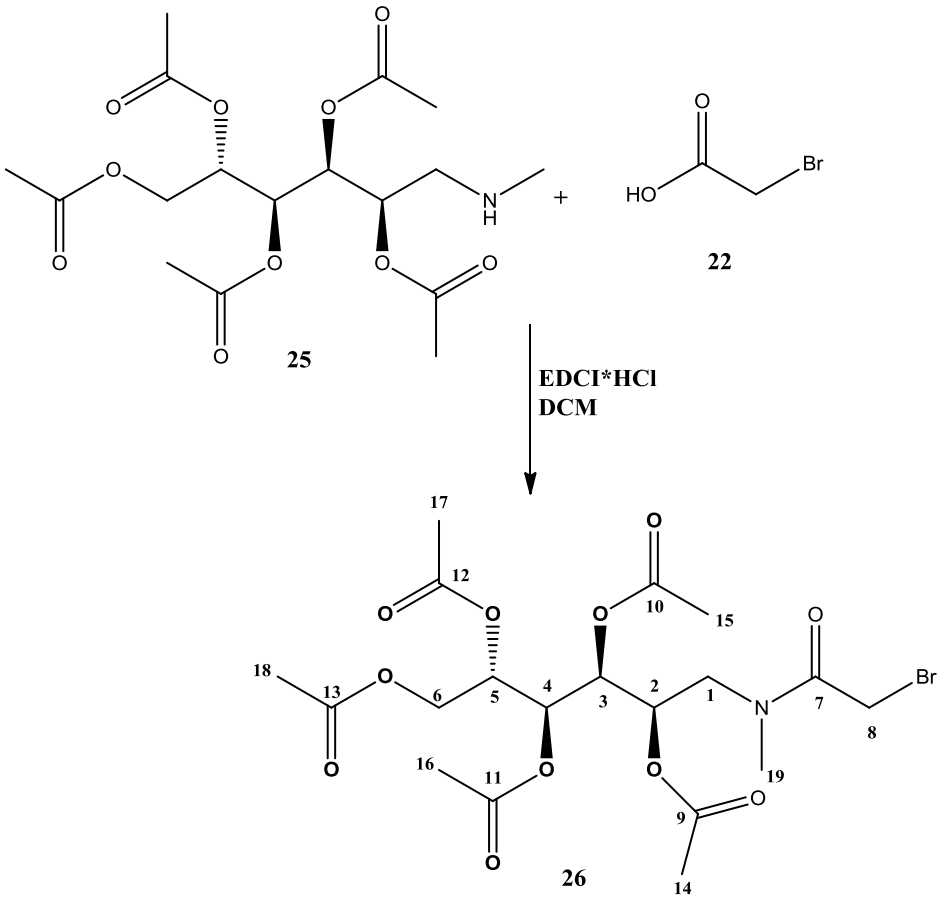

Synthetic procedure:

Bromoacetic acid (**22**) (1.38 g; 1 mmol; 1 eq) and N-methyl-L-glucamine (**25**) (1.95 g; 1 mmol; 1 eq) were dissolved in 15 mL water, EDCI (3.84 g; 2 mmol; 2 eq) was added to the solution, and the reaction was allowed to proceed for 12 h at room temperature. The water was removed at reduced pressure, the residue (colourless oil) was dissolved in dry pyridine (12 mL), and the solution was cooled in an ice-water bath for ten minutes. The solution was stirred vigorously while acetic anhydride (15 mL) was added to the solution in small portions. The reaction mixture was allowed to reach room temperature and the stirring was continued for another 12 h. The excess acetic anhydride was consumed by the addition of water (10 mL). DCM (30 mL) and water (40 mL) were afterwards added to the mixture, the phases were separated and the aqueous phase was extracted with DCM (3 x 30 mL). The combined organic phases were washed with

water (2 x 30 mL) and dilute acid (1 M HCl, 1 x 40 mL), dried over $MgSO_4$, filtered and the DCM was removed in vacuum. The product (**26**) was isolated as a colourless solid in 34% yield (1.80 g). ^{1}H NMR ($CDCl_3$, δ): 1.99-2.04 (m, 15 H, CH_3, $H^{14,15,16,17,18}$), 2.11 (s, 3 H, NCH_3, H^{19}), 2.96 (s, 2 H, $BrCH_2$, H^8), 3.50-3.60 (m, 2 H, CH_2, H^1), 4.04-4.09 (m, 1 H, CH, H^2), 4.22-4.23 (m, 1 H, CH, H^3), 4.99-5.02 (m, 1 H, CH, H^4), 5.25-5.29 (m, 1 H, CH, H^5), 5.38-5.41 (m, 2 H, CH_2, H^6); ^{13}C NMR: 20.37 (CH_3,C^{14}), 20.50 (CH_3, C^{15}), 20.66 (CH_3, C^{16}), 20.71 (CH_3, C^{17}), 20.76 (CH_3, C^{18}), 37.23 (CH_3, C^{19}), 47.74 (CH_2, C^8), 61.49 (CH_2, C^1), 68.60 (CH, C^2), 68.68 (CH, C^3), 68.78 (CH, C^4), 69.26 (CH, C^5), 69.60 (CH, C^6), 169.80 (C=O, C^9), 169.91 (C=O, C^{10}), 170.16 (C=O, C^{11}), 170.57 (C=O, C^{12}), 170.61 (C=O, C^{13}), 171.19 (C=O, C^7).

2.1.6 Synthesis of allyl bromoacetate (18)

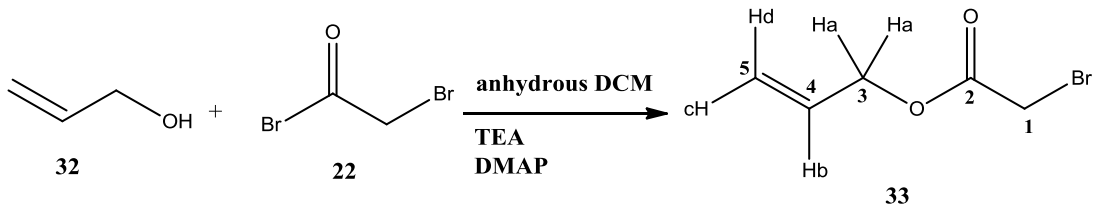

32 22 33

Synthetic procedure:

The allyl alcohol (**32**) (6.00 g; 0.103 mol; 1 eq) was dissolved in 200 mL of anhydrous dichloromethane. The solution was cooled down to 0°C and then TEA (11.48 g; 0.114 mol; 1.1 eq) and DMAP (63.53 mg; 0.520 mmol; 0.005 eq) were added. The mixture was stirred at 0°C and the bromoacetyl bromide (**22**) (20.85 g; 0.103 mol; 1 eq) was then added dropwise. The reaction was stirred overnight at room temperature and under argon atmosphere. The reaction mixture was washed three times with water, dried over $MgSO_4$ and filtered. The solvent (DCM) was removed under vacuum to give compound (**33**) as a very lachrymatory brown oil in 60% yield (11 g).

^{1}H NMR ($CDCl_3$, δ): 3.82 (s, 2 H, CH_2, H^1), 4.61-4.63 (d, 2 H, CH_2, H^3, $^3J_{Ha,b}$ = 6.8 Hz), 5.22-5.26 (dd, 1 H, CH_2, H^{5c}, $^3J_{Hc,b}$ = 10.3 Hz, $^2J_{Hc,d}$ = 1.3 Hz), 5.29-5.36 (dd, 1 H, CH_2,H^{5d} $^3J_{Hd,b}$ = 17.2 Hz, $^2J_{Hd,c}$ = 1.3 Hz) 5.82-5.95 (m, 1 H, CH, H^4, $^3J_{Hb,d}$ = 17.2, $^3J_{Hb,c}$ = 10.3, $^3J_{Hb,a}$ = 6.8 Hz); ^{13}C NMR ($CDCl_3$, δ): 25.7 (CH_2, C^3), 66.64 (CH_2, C^1), 119.01 (CH_2, C^5), 130.58 (CH, C^4), 166.80 (C=O, C^2).

2.1.7 Synthesis of 1-N-Boc ethylamine-4,7-diallyl acetate-1,4,7,10-tetraazacyclododecane (DABC) (34)

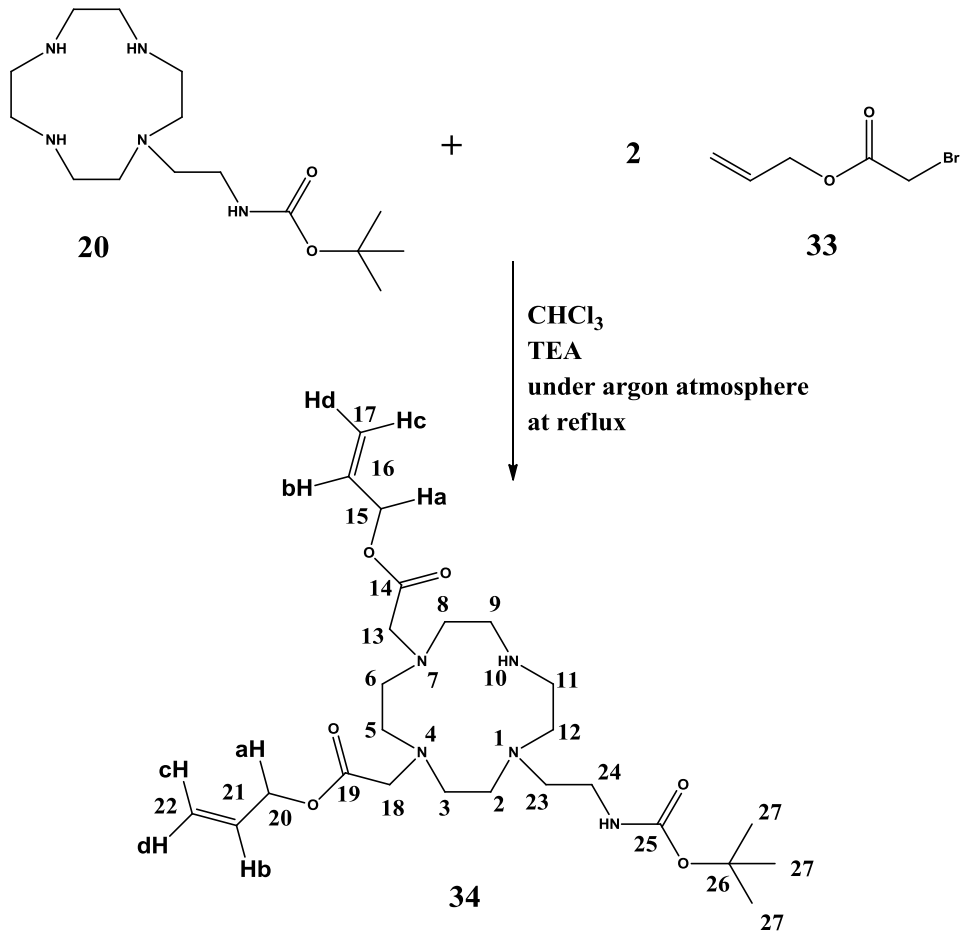

Synthetic Procedure:

The N-Boc ethylamine cyclen (**20**) (10.00 g; 0.032 mol; 1 eq) was dissolved in anhydrous chloroform (300 mL) with triethylamine (TEA) (1.60 g; 0.010 mol; 0.5 eq). The solution was heated under reflux and argon atmosphere. The allyl bromoacetate (**33**) (11.39 g; 0.064 mol; 2 eq) was dissolved in 100 mL of anhydrous chloroform and slowly added dropwise to the stirring solution. The reaction mixture was kept under argon atmosphere and at reflux for 16 h. The reaction mixture was cooled down and extracted with water (2 x 400 mL). The organic phase was anhydrified over $MgSO_4$ and filtered off. The solvent was evaporated under vacuum to give 16 g of crude mixture which was then purified through column chromatography using DCM/0.5-4% of TEA as eluent. The DABC **(34)** was isolated as an orange oil in 10% yield (1.478 g). MS: 512 $[M+H]^+$; ^{1}H NMR ($CDCl_3$, δ):1.43 (s, 9 H, CH_3, H^{27}), 2.14-3.50 (m, 24 H, CH_2, $H^{2,3,5,6,8,9,11,12,13,18,23,24}$), 4.61-4.63 (d, 4 H, CH_2, $H^{15,20}$, $^3J_{Ha,b}$ 6.8 Hz), 5.22-5.36 (m, 4 H, CH_2, $H^{17,22}$, $^3J_{Hc,b}$ 16.0 Hz, $^3J_{Hd,b}$ 10.3 Hz, $^2J_{Hc,d} = {}^2J_{Hdc}$ 1.3 Hz), 5.82-5.95 (m, 2 H, CH, $H^{16,21}$, $^3J_{Hb,c}$ 16.0 Hz, $^3J_{Hb,d}$ 10.3 Hz, $^3J_{Hb,a}$ 6.8 Hz). ^{13}C NMR ($CDCl_3$, δ): 28.52 (CH_3, C^{27}), 39.45 (CH_2, C^{24}), 47.14 (CH_2, C^9), 47.49 (CH_2, C^{11}), 50.62 (CH_2, C^{12}), 50.79 (CH_2, C^5), 51.12 (CH_2, C^6), 51.17 (CH_2, C^8), 52.19 (CH_2, C^3), 52.42 (CH_2, C^2), 53.40 (CH_2, C^{23}), 55.68 (CH_2, C^{13}), 56.04 (CH_2, C^{18}), 64.79 (CH_2, C^{15}), 64.83 (CH_2, C^{20}), 78.61(Cq, C^{26}),118.36 (CH_2, $C^{17,22}$), 132.02 (CH, $C^{16,21}$), 156.07 (C=O, C^{25}), 171.36 (C=O, C^{14}), 171.57 (C=O, C^{19}).

2.1.8 Synthesis of the 1-N-Boc ethylamine-4,7-diallyl acetate-10-benzyl acetate-1,4,7,10-tetraazacyclododecane (DABBC) (36)

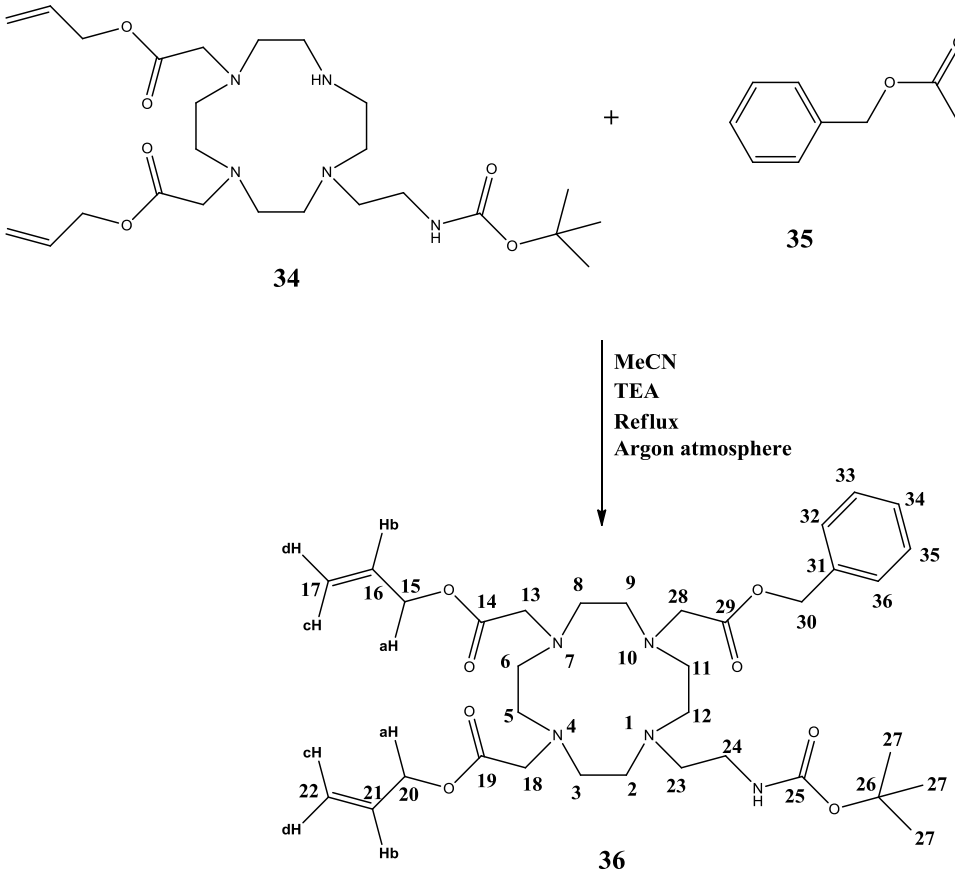

Synthetic procedure:

DABC (**34**) (1.46 g; 2.865 mmol; 1 eq) and TEA (0.43 g; 4.300 mmol; 1.5 eq) were dissolved in 200 mL of anhydrous acetonitrile. The reaction mixture was heated under reflux under argon atmosphere. The benzyl bromoacetate (**35**) (0.85 g; 3.720 mmol; 1.3 eq) was added to the solution dropwise and the reaction mixture was stirred at reflux under argon atmosphere overnight. After cooling to room temperature, the MeCN was removed under vacuum and replaced with the same quantity of DCM (200 mL). The organic solution was washed three times with water (3 x 120 mL). Afterwards the organic phase was dried over $MgSO_4$, filtered and evaporated to yield the desired compound

(**36**) as a dark brown oil in 95% yield (1.79 g). MS: 660 $[M+H]^+$; 682 $[M+Na]^+$; ^1H NMR ($CDCl_3$, δ): 1.38 (s, 9 H, CH_3, H^{27}), 2.74-3.75 (m, 26 H, CH_2, $H^{2,3,5,6,8,9,11,12,13,18,23,24,28}$), 4.55-4.57 (d, 4 H, CH_2, $^3J_{Ha,b}$ 6 Hz, $H^{15,20}$), 5.11-5.32 (m, 4 H, CH_2, $^3J_{Hc,b}$ 16 Hz, $^3J_{Hd,b}$ 10 Hz, $^2J_{Hc,d} = {}^2J_{Hd,c}$ 1.3 Hz, $H^{17,22}$), 5.79-5.94 (m, 2 H, CH, $^3J_{Hb,c}$ 16 Hz, $^3J_{Hb,d}$ 10 Hz, $^3J_{Hb,a}$ 6 Hz, $H^{16,21}$), 7.33 (s, 5 H, CH, $H^{32,33,34,35,36}$). ^{13}C NMR ($CDCl_3$, δ): 28.36 (CH_3, C^{27}), 39.05 (CH_2, C^{24}), 48.16 (CH_2, C^5), 50.19 (CH_2, C^6), 51.46 (CH_2, $C^{3,8}$), 52.42 (CH_2, $C^{2,9}$), 53.56 (CH_2, $C^{11,12}$), 54.69 (CH_2, C^{23}), 56.11 (CH_2, C^{28}), 65.58 (CH_2, $C^{13,18}$), 66.78 (CH_2, C^{30}), 79.65 (C_q, C^{26}), 119.12 (CH_2, $C^{17,22}$), 128.38 (CH, $C^{32,36}$), 128.45 (CH, C^{34}), 128.58 (CH, $C^{33,35}$), 131.48 (CH, $C^{16,21}$), 135.16 (C_q, C^{31}), 156.57 (C=O, C^{25}), 170.40 (C=O, C^{14}), 170.57 (C=O, C^{19}), 170.80 (C=O, C^{29}).

2.1.9 Synthesis of 1-N-Boc ethylamine-4,7-diacetic acid-10-benzyl acetate-1,4,7,10-tetraazacyclododecane (DAABBC) (37) / allyl ester group removal

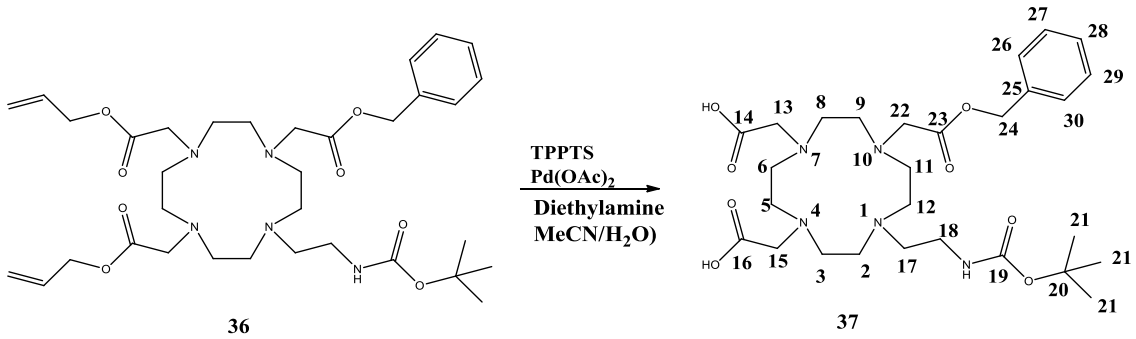

36 37

Synthetic procedure:

The doubly protected substrate (DABBC) (**36**) (0.90 g; 1.40 mmol; 1eq) was dissolved in MeCN:H_2O (3.5:0.5 v/v) under argon atmosphere. Diethylamine (0.50 g; 6.86 mmol; 5 eq) was added followed by rapid introduction of $Pd(OAc)_2$ (0.006 g; 0.03 mmol; 0.02 eq) and TPPTS (0.03 g; 0.055 mmol 0.04 eq). The reaction mixture went to completion after 2 h at room temperature. All solvents were removed under vacuum and the crude mixture was dissolved in chloroform (50 mL). The organic phase was then washed with 60 mL of water and the desired compound (**37**) was recovered from the aqueous phase. After removing all water under high vacuum, DAABBC (**37**) was obtained as a pale yellow oil in 97% yield (0.77 g).

MS: 580 $[M+H]^+$; 602 $[M+Na]^+$; ^{1}H NMR ($CDCl_3$, δ): 1.32 (s, 9 H, H^{21}), 2.58-3.56 (m, 26 H, CH_2, $H^{2,3,5.6,8,9,11,12,13,15,17,18,22}$), 5.04 (s, 2 H, CH_2, H^{24}), 7.27-7.32 (m, 5 H, 5CH, $H^{26,27,28,29,30}$), 9.40 (broad signal, 2 H, COOH); ^{13}C NMR ($CDCl_3$, δ): 28.12 (CH_3, C^{21}), 41.63 (CH_2 C^{18}), 51.17 (CH_2, $C^{2,9,11,12}$), 52.97 (CH_2, $C^{3,5,6,8}$), 56.95 (CH_2, $C^{17,22}$), 66.24 (CH_2,$C^{13,15}$), 66.70 (CH_2, C^{24}), 78.91 (C_q, C^{20}), 128.18 (CH, $C^{26,27,28,29,30}$), 134.89 (C_q, C^{25}); 155.93 (C=O, C^{19}), 170.33 (C=O, C^{23}), 174.14 (C=O, $C^{14,16}$).

2.1.10 Synthesis of (2-aminoethyl) triphenylphosphonium bromide (39)

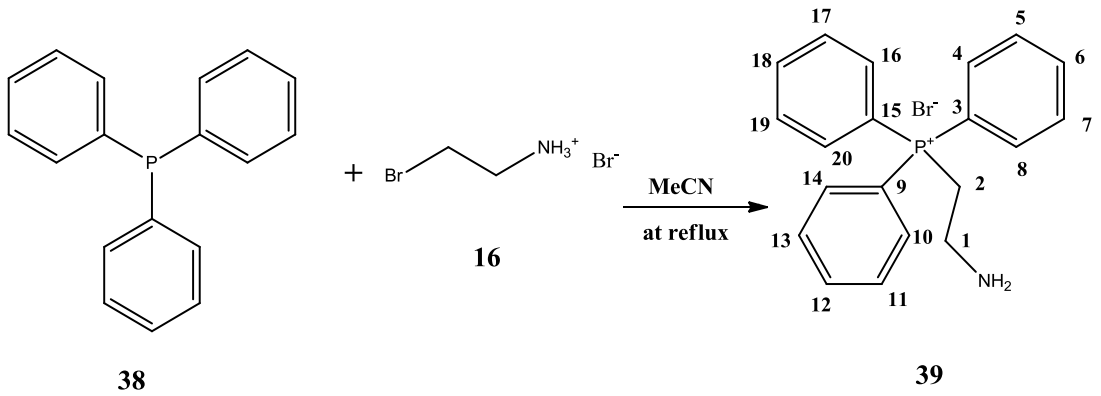

38 39

Synthetic procedure:

The (2-aminoethyl) triphenylphosphonium bromide (**39**) was prepared by dissolving the triphenyl phosphine (**38**) (10 g; 38.1 mmol; 1eq) and the bromoethylamine hydrobromide (**16**) (7.81 g; 38.1 mmol; 1eq) in anhydrous MeCN (50 mL) and heating the reaction mixture at reflux for 24 h. After 24 h, a white precipitate was formed. The reaction mixture was filtered when the acetonitrile was still hot and the white precipitate was washed for three times with 40 mL of hot acetonitrile in order to remove the impurities due to the unreacted starting materials (compound **38** and **16**) and triphenylphosphine oxide formed as byproduct. After removing the solvent, the hydrobromide salt of the (2-aminoethyl) triphenylphosphonium bromide was obtained without any further purification. To obtain the (2-aminoethyl) triphenylphosphonium bromide (**39**), the hydrobromide salt of **39** was dissolved in a sodium hydroxide aqueous solution (pH 9). The water was removed under high vacuum to give the desired product (**39**) in 80% yield (8.60 g): mp 227-233°C; MS: 306 $[M]^+$; ^{1}H NMR ($CDCl_3$, δ): 3.10-3.19 (m, 2 H, CH_2, H^1), 3.72-3.81 (m, 1 H, CH_2, H^2), 4.02-4.11 (m, 1 H, CH_2, H^2), 7.60-7.84 (m, 15 H, CH, $H^{4,5,6,7,8,10,11,12,13,14,16,17,18,19,20}$); ^{13}C NMR ($CDCl_3$, δ): 24.31 (CH_2, C^1), 41.90 (CH_2, C^2), 118.17 (CH, $C^{16,20}$),119.26 (CH, $C^{4,8}$), 119.32 (CH, $C^{14,10}$), 130.48 (CH, C^{17}), 130.51 (CH, C^{19}), 130.64 (CH, $C^{5,7}$), 130.68 (CH, $C^{11,13}$), 133.89 (CH, C^{18}), 134.01 (CH, C^6), 134.15 (CH, C^{12}), 134.80 (C_q, C^{15}), 135.08 (C_q, C^3), 135.12 (C_q, C^9).

2.1.11 Synthesis of 1-N-Boc-ethylamine-4,7-di-(triphenylphosphonium bromide ethyl)acetamide-10-benzyl acetate-1,4,7,10-tetraazacyclododecane (DTPPBBC) (40)

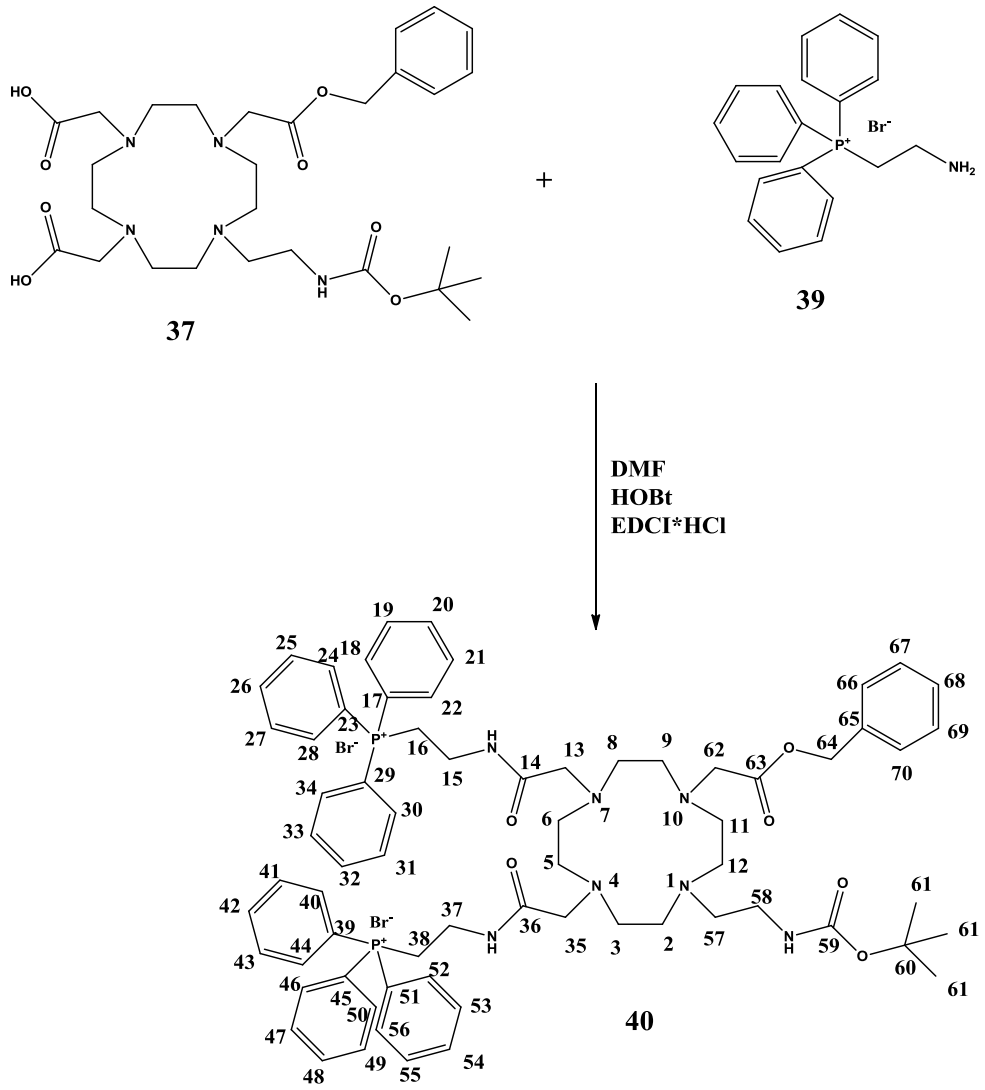

Synthetic procedure:

To the DAABBC (**37**) (0.85 g; 1.471 mmol; 1 eq) dissolved in anhydrous DMF (50 mL), HOBt (0.40 g; 2.942 mmol; 2 eq) and EDCI*HCl (0.56 g; 2.942 mmol; 2 eq) were added and the reaction mixture was stirred at room temperature and under argon atmosphere for 1 h. Then the (2-aminoethyl) triphenylphosphonium bromide (**39**) (1.43 g; 2.942 mmol; 2 eq) and DIPEA (0.76 g; 5.89 mmol; 4 eq) were added and the reaction mixture was stirred for 24 h at room temperature and under argon atmosphere. After stopping the

reaction the DMF was removed under vacuum and the crude mixture was dissolved in 40 mL of DCM and extracted one time with 40 mL of water. After the extraction the organic phase was dried over $MgSO_4$, filtered and dried to give the product (**40**) as a sticky light brown oil in 88% yield (1.5 g).

MS: 577 $[M]^{2+}$, 385 $[M+H]^{3+}$; ^{1}H NMR ($CDCl_3$, δ): 1.32 (s, 9 H, CH_3, H^{61}), 2.24-3.46 (m, 34 H, CH_2, $H^{2,3,5,6,8,9,11,12,13,15,16,35,37,38,57,58,62}$), 5.27 (s, 2 H, CH_2, H^{64}), 7.12-7.15 (m, 2 H, CH, $H^{66,70}$), 7.25-7.28 (m, 2 H, CH, $H^{67,69}$), 7.38-7.41 (m, 1 H, CH, H^{68}), 7.54-7.75 (m, 30 H, CH, $H^{18,19,20,21,22,24,25,26,27,28,30,31,32,33,34,40,41,42,43,44,46,47,48,49,50,52,53,54,55,56}$); ^{13}C NMR ($CDCl_3$, δ): 28.33 (CH_3, C^{61}), 34.19 (CH_2, C^{15}), 35.85 (CH_2, C^{37}), 41.82 (CH_2, $C^{16,38,58}$), 49.41 (CH_2, $C^{3,5,6,8}$), 52.39 (CH_2, $C^{2,9,11,12}$), 57.22 (CH_2, C^{57}), 65.95 (CH_2, $C^{13,35}$), 66.34 (CH_2, C^{62}), 66.73 (CH_2, C^{64}), 78.82 (C_q, C^{60}), 117.01 (CH, $C^{24,28}$), 117.47 (CH, $C^{46,50}$), 118.15 (CH, $C^{18,22,30,34}$), 118.31 (CH, $C^{40,44,52,56}$), 123.89 (CH), 125.10 (CH, C^{66}), 125.49 (CH, C^{70}), 128.16 (CH, C^{67}), 128.36 (CH, C^{69}), 128.56 (CH, C^{68}), 130.21 (CH, $C^{25,27}$), 130.39 (CH, $C^{47,49}$), 130.43 (CH,$C^{19,21,31,33}$), 130.60 (CH, $C^{41,43,53,55}$), 133.48 (CH, $C^{26,48}$), 133.62 (CH, $C^{20,32}$), 133.75 (CH, $C^{42,54}$), 134.69 (C_q, $C^{23,45}$), 135.18 (C_q, $C^{17,29,39,51}$), 142.96 (C_q, C^{65}), 157.5 (C=O, C^{59}), 170.9 (C=O, $C^{14,36}$), 171 (C=O, C^{63}).

2.1.12 Synthesis of 1-ethylamine-4,7-di-(triphenylphosphonium bromide ethyl)acetamide-10-benzyl acetate-1,4,7,10-tetraazacyclododecane (DTPPBC) (41)-BOC group removal

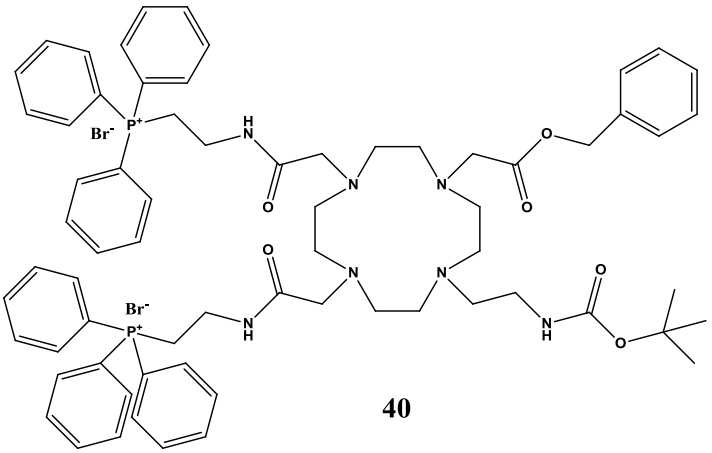

40

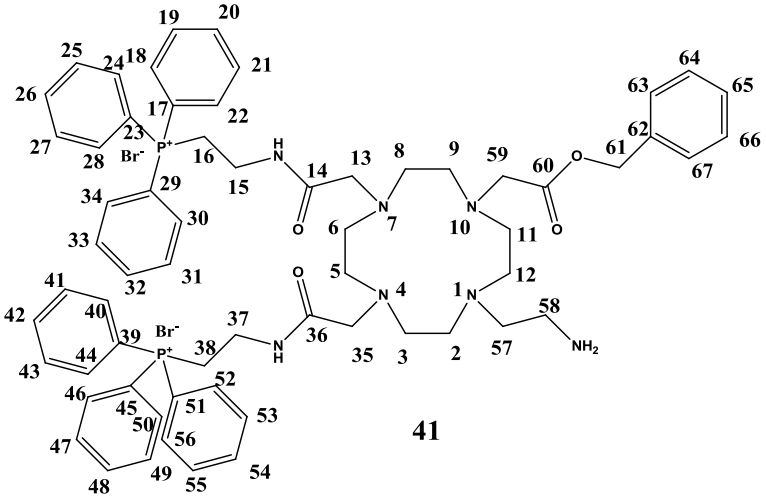

41

Synthetic procedure:

The DTPPBBC (**40**) (0.13 g; 0.115 mmol; 1eq) was dissolved in 6 mL of anhydrous DCM. Then 1.20 mL of TFA was added and the reaction mixture was stirred at room temperature for 2 h. After stopping the reaction 35 mL of DCM were added to the reaction mixture and extracted with 40 mL of 1M $NaHCO_3$ aqueous solution. After the extraction the organic phase was dried over $MgSO_4$, filtered and dried to give the product (**41**) as a sticky light brown oil in 84% yield (0.10 g).

MS: 527 $[M]^{2+}$, 352 $[M+H]^{3+}$; ^{1}H NMR ($CDCl_3$, δ): 2.10-3.63 (m, 34 H, CH_2, $H^{2,3,5,6,8,9,11,12,13,15,16,35,37,38,57,58,59}$), 5.02 (s, 2 H, CH_2, H^{61}), 7.19-7.24 (m, 5H, CH, $H^{63,64,65,66,67}$), 7.55-7.71 (m, 30 H, CH, $H^{18,19,20,21,22,24,25,26,27,28,30,31,32,33,34,40,41,42,43,44,46,47,48,49,50,52,53,54,55,56}$); ^{13}C NMR ($CDCl_3$, δ): 30.24 ($CH_2$, C^{58}), 33.23 (CH_2, C^{15}), 34.13 (CH_2, C^{37}), 37.36 (CH_2, $C^{16,38}$), 41.88 (CH_2, C^{57}), 49.96 (CH_2, $C^{5,6}$), 50.27 (CH_2, $C^{3,8}$), 50.98 (CH_2, $C^{9,11}$), 53.39 (CH_2, $C^{2,12}$), 57.42 (CH_2, C^{59}), 65.85 (CH_2, $C^{13,35}$), 66.48 (CH_2, C^{61}), 115.22, 117.06 (CH, $C^{24,48}$), 117.12 (CH, $C^{46,50}$) 117.81 (CH, $C^{18,22}$), 118.20 (CH, $C^{34,30}$), 118.26 (CH, $C^{40,44}$), 118.95 (CH, C^{52}), 119.14 (CH, C^{56}), 125.43 (CH, $C^{63,67}$), 128.12 (CH, C^{64}), 128.26 (CH, C^{66}), 128.31, 128.43, 128.50 (CH, C^{68}), 130.17 (CH, $C^{25,27}$), 130.34 (CH, $C^{47,49}$), 130.41 (CH, $C^{19,21}$), 130.49 (CH, $C^{31,33}$), 130.54 (CH, $C^{41,43}$), 130.58 (CH, $C^{53,55}$), 133.43 (CH, $C^{26,48}$), 133.56 (CH, $C^{20,32,42,54}$), 134.71 (C_q, C^{23}), 134.74 (C_q, C^{45}), 135.03 (C_q, C^{17}), 135.12 (C_q, C^{29}), 135.41 (C_q, $C^{39,51}$), 135.68, 135.74, 142.06 (C_q, C^{65}), 171.07 (C=O, C^{14}), 171.31 (C=O, C^{36}), 171.63 (C=O, C^{60}).

2.1.13 Synthesis of 1-N-(dihydrofluorescein diacetate)ethylamide-4,7-di-(triphenylphosphonium bromide ethyl)acetamide-10-benzyl acetate-1,4,7,10-tetraazacyclododecane (L1)

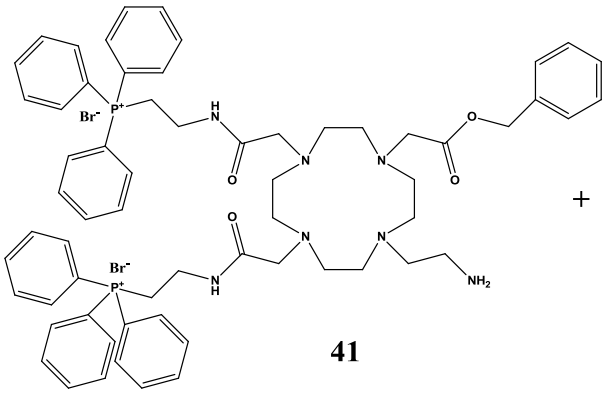

41

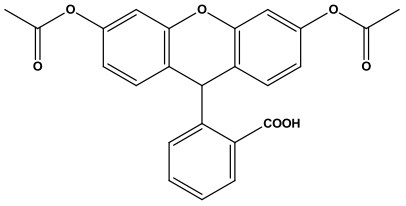

42

EDCI*HCl
HOBt
DIPEA

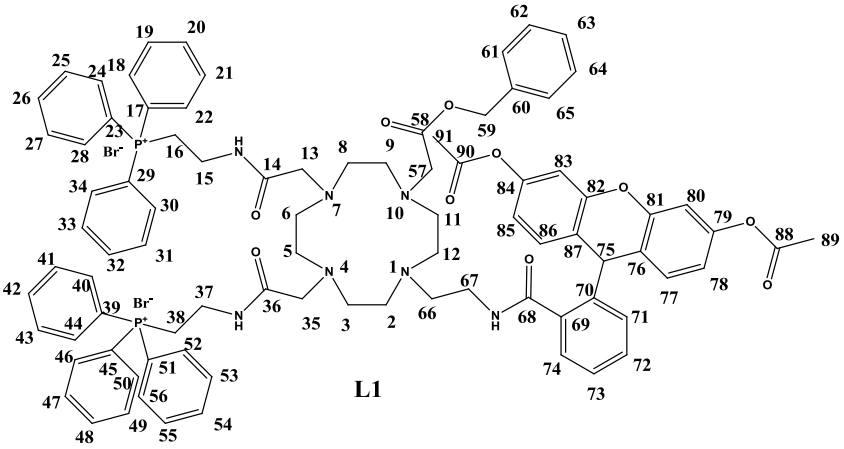

L1

Synthetic procedure:

To a solution of dihydrofluorescein diacetate (**42**) (0.05 g; 0.129 mmol; 1eq) dissolved in 20 mL of anhydrous DMF, EDCI*HCl (0.05g; 0.257 mmol; 2 eq) and HOBt (0.04 g; 0.257 mmol; 2 eq) were added and the reaction mixture was stirred for 1 h at room temperature and under argon atmosphere. After 1 h, the DTPPBC (**41**) (0.16 g; 0.129 mmol; 1 eq) and DIPEA (0.07 g; 0.566 mmol; 4.4 eq) were added to the reaction mixture that was kept under stirring for 24 h, at room temperature and under argon atmosphere. After 24 h the reaction was stopped and the DMF was removed under high vacuum and replaced with 40 mL of chloroform. The organic phase was then extracted with water (35 mL), dried over $MgSO_4$ and filtered. After removing the solvent, **L1** was obtained as a brown sticky oil in 60% yield (0.13 g). MS: 728 $[M]^{2+}$, 485 $[M+H]^{3+}$; ^{1}H NMR ($CDCl_3$, δ): 2.23 (s, 6 H, CH_3, $H^{89,91}$), 2.66-3.92 (m, 34 H, CH_2, $H^{2,3,5,6,8,9,11,12,13,15,16,35,37,38,57,66,67}$), 4.46 (s, 2 H, CH_2, H^{59}), 6.40-6.87 (m, 11 H, CH, $H^{61,62,63,64,65,77,78,80,83,85,86}$), 7.02-7.46 (m, 34 H, CH, $H^{18,19,20,21,22,24,25,26,27,28,30,31,32,33,34,40,41,42,43,44,46,47,48,49,50,52,53,54,55,56,71,72,73,74}$), 7.99 (s, 1H, CH, H^{75}); ^{13}C NMR ($CDCl_3$, δ): 21.21 (CH_3, $C^{89,91}$), 31.52 (CH_2, $C^{15,37}$), 36.58 (CH_2, $C^{16,38,67}$), 50.37 (CH_2, $C^{5,6}$), 51.65 (CH_2, $C^{8,9}$), 52.44 (CH_2, $C^{3,2}$), 53.84 (CH_2, $C^{11,12,57}$), 55.83 (CH_2, C^{66}), 65.56 (CH_2, $C^{13,35}$), 66.71 (CH_2, C^{59}), 109.66 (CH, C^{75}), 111.33 (CH), 118.12 (CH), 118.24 (CH), 119.70 (CH), 123.91 (CH), 124.56 (CH), 128.40 (CH), 128.45 (CH), 128.51 (CH), 128.66 (CH), 130.54 (CH), 130.98 (CH), 131.68 (CH), 136.20 (C_q), 143.26 (C_q), 149.89 (C_q), 150.85 (C_q), 162.65 (C=O, C^{68}), 169.26 (C=O, $C^{88,90}$), 170.53 (C=O, $C^{14,36}$), 170.57 (C=O, C^{58}).

2.1.14 Synthesis of 1-N-(coumarin 343)ethylamide-4,7-di-(triphenylphosphonium bromide ethyl)acetamide-10-benzyl acetate-1,4,7,10-tetraazacyclododecane (L2)

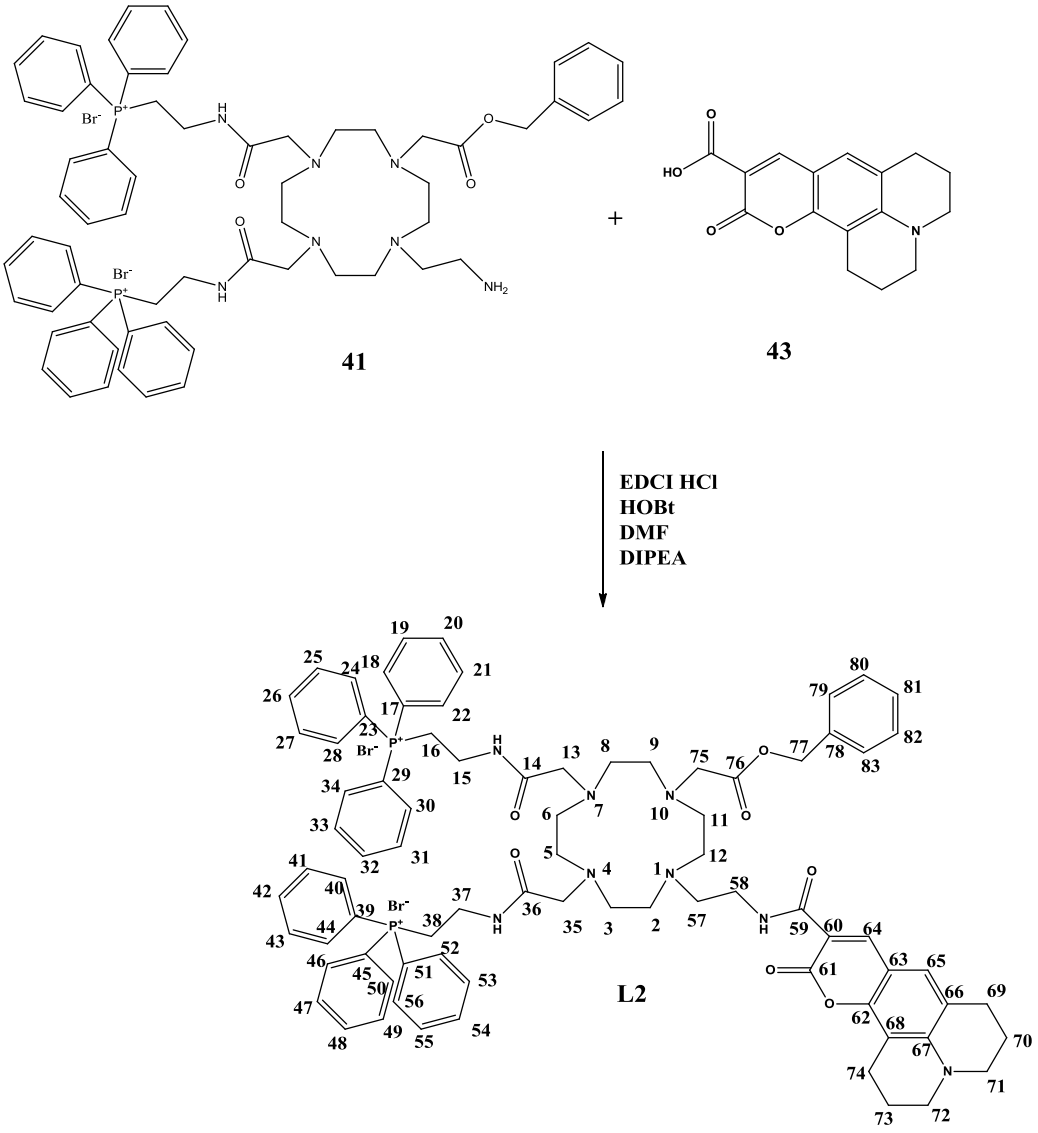

Synthetic procedure:

To the coumarin 343 (**43**) (0.04 g; 0.129 mmol; 1 eq), dissolved in 15 mL of dry DMF, HOBt (0.04 g; 0.257 mmol; 2.2 eq) and EDCI*HCl (0.05 g; 0.257 mmol; 2.2 eq) were added and the reaction mixture was stirred at room temperature under argon atmosphere for 1 h. Then DTPPBC (**41**) (0.16 g; 0.129 mmol; 1 eq) was added followed by DIPEA (0.07 g; 0.566 mmol; 4.4 eq). The reaction mixture was stirred under argon atmosphere and at room temperature for 24 h. After 24 h the reaction was stopped and the DMF was removed under high vacuum and replaced with 25 mL of chloroform. The organic phase was then extracted with water (20 mL), dried over $MgSO_4$ and filtered. After removing the solvent, **L2** was obtained as an orange oil in 30% yield (0.06 g).

MS: 661 $[M]^{2+}$, 441 $[M+H]^{3+}$. ^{1}H NMR ($CDCl_3$, δ): 1.93 (m, 8 H, CH_2, $H^{69,70,73,74}$), 2.47-4.05 (m, 38 H, CH_2, $H^{2,3,5,6,8,9,11,12,13,15,16,35,37,38,57,58,71,72,75}$), 6.96 (s, 2 H, CH_2, H^{77}), 7.10-7.17 (m, 5 H, CH, $H^{79,80,81,82,83}$), 7.43-7.97 (m, 28 H, CH, $H^{18,19,20,21,22,24,25,26,27,28,30,31,32,33,34,40,41,42,43,44,46,47,48,49,50,52,53,54,55,56}$), 8.44 (s, 1 H, CH, H^{65}), 8.51 (s, 1 H, CH, H^{64}); ^{13}C NMR ($CDCl_3$, δ): 20.05 (CH_2, $C^{70,73}$), 21.05 (CH_2, $C^{69,74}$), 29.91 (CH_2, $C^{71,72}$), 30.24 (CH_2, $C^{15,37}$), 33.23 , 34.13 (CH_2, C^{16}), 34.31 (CH_2, C^{38}), 41.88 (CH_2, C^{58}), 49.96 (CH_2, $C^{5,6}$), 50.27 (CH_2, $C^{2,3}$), 50.98 (CH_2, $C^{8,9}$), 53.39 (CH_2, $C^{11,12}$), 57.42 (CH_2, C^{57}), 58.51 (CH_2, C^{75}), 65.85 (CH_2, $C^{13,35}$), 66.48 (CH2, C^{77}), 115.22 (CH), 117.06 (CH), 117.81 (CH), 118.20 (CH), 118.26 (CH), 118.95 (CH), 119.14 (CH), 125.43 (CH), 128.06 (CH), 128.31 (CH), 128.43 (CH), 128.50 (CH), 130.17 (CH), 130.34 (CH), 130.41 (CH), 130.49 (CH), 130.54 (CH), 130.58 (CH), 133.43 (CH), 133.56 (CH), 134.71 (C_q), 134.74 (C_q), 135.03 (C_q), 135.12 (C_q), 135.41 (C_q), 135.68 (C_q), 135.74 (C_q), 137.41 (C_q), 140.90 (C_q), 142.06 (C_q), 143.73 (CH, C^{65}), 148.81 (CH, C^{64}), 162.01 (C=O, C^{61}), 167.56 (C=O, C^{59}), 171.07 (C=O, C^{36}), 171.31 (C=O, C^{14}), 171.63 (C=O, C^{76}).

2.1.15 Synthesis of 1-N-(rhodamine B)ethylamide-4,7-di-(triphenyl phosphonium bromide ethyl)acetamide-10-benzyl acetate-1,4,7,10-tetraazacyclododecane (L3)

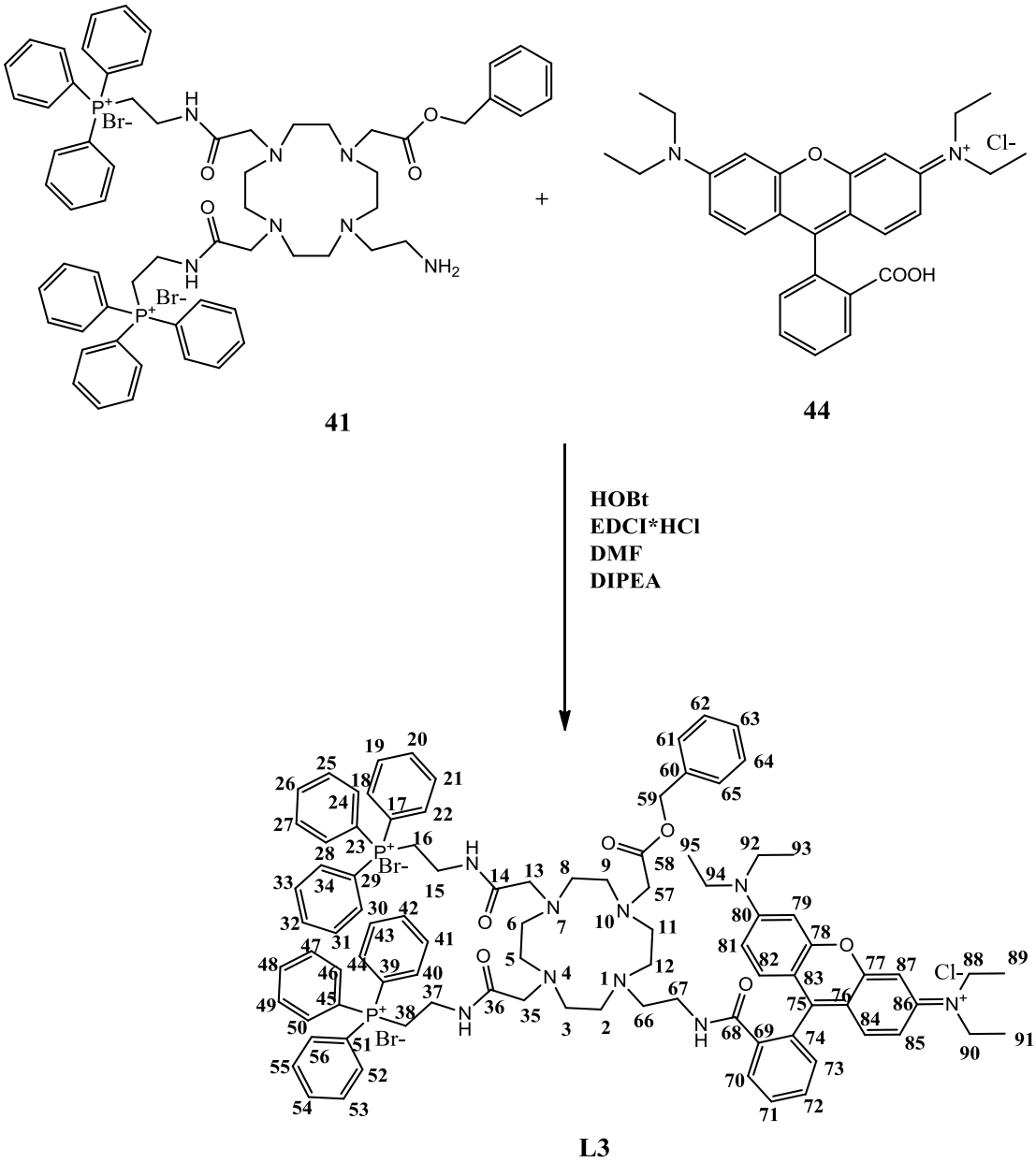

Synthetic procedure:

To the rhodamine B (**44**) (0.04 g; 0.076 mmol; 1 eq), dissolved in 20 mL of dry DMF, HOBt (0.02 g; 0.167 mmol; 2.2 eq) and EDCI*HCl (0.03 g; 0.167 mmol; 2.2 eq) were added and the reaction mixture was stirred at room temperature under argon atmosphere

for 1 h. Then DTPPBC (**41**) (0.09 g; 0.076 mmol; 1 eq) was added followed by DIPEA (0.04 g; 0.334 mmol; 4.4 eq). The reaction mixture was stirred under argon atmosphere and at room temperature for 24 h. After 24 h the reaction was stopped and the DMF was removed under high vacuum and replaced with 30 mL of chloroform. The organic phase was then extracted with water (25 mL), dried over $MgSO_4$ and filtered. After removing the solvent, (**L3**) was obtained as a dark pink oil in 93% yield (0.12 g). MS: 740 $[M]^{2+}$, 493 $[M]^{3+}$. ^1H NMR ($CDCl_3$, δ): 09-1.12 (m, 20H, CH_3 ($H^{89,91,93,95}$)), CH_2 ($H^{88,90,92,94}$), 2.12-3.51 (m, 34 H, CH_2, $H^{2,3,5,6,8,9,11,12,13,15,16,35,37,38,57,66,67}$), 4.99 (s, 2H, CH_2, H^{59}), 6.30-6.51 (m, 9 H, CH, $H^{61,62,63,64,65,79,81,82,85}$), 7.03-7.57 (m, 35 H, CH, $H^{18,19,20,21,22,24,25,26,27,2830,31,32,33,34,40,41,42,43,44,46,47,48,49,50,52,53,54,55,56}$), 7.95 (s, 2H, CH, $H^{84,87}$); ^{13}C NMR ($CDCl_3$, δ): 27.45 (CH_3, $C^{89,91,93,95}$), 30.28 (CH_2, $C^{15,37}$), 34.19 (CH_2, $C^{16,38}$), 35.85 (CH_2), 41.82 (CH_2), 42.94 (CH_2, C^{67}), 48.83 (CH_2, $C^{88,89,92,94}$), 49.41 (CH_2, $C^{5,6}$), 52.39 (CH_2, $C^{2,3,8,9,11,12}$), 57.22 (CH_2, $C^{66,57}$), 65.95 (CH_2, $C^{13,35,59}$), 78.82 (C), 110.77 (CH), 117.01 (CH), 117.47 (CH), 118.15 (CH), 118.31 (CH), 123.89 (CH), 125.10 (CH), 125.49 (CH), 128.16 (CH), 128.36 (CH), 128.56 (CH), 130.21 (CH), 130.39 (CH), 130.43 (CH), 130.60 (CH), 133.48 (CH), 133.62 (CH), 133.75 (C_q), 134.69 (C_q), 135.18 (C_q), 144.52 (C_q) 147.76 (C_q), 155.32 (C_q), 163.21 ($C=N^+$, C^{86}), 167.91 (C=O, C^{68}), 170.34 (C=O, $C^{14,36}$), 171.36 (C=O, C^{58}).

2.1.16 Synthesis of 1-N-(coumarin 3 carboxylic acid)ethylamide-4,7-di-(triphenyl phosphonium bromide ethyl)acetamide-10-benzyl acetate-1,4,7,10-tetraazacyclododecane (L4)

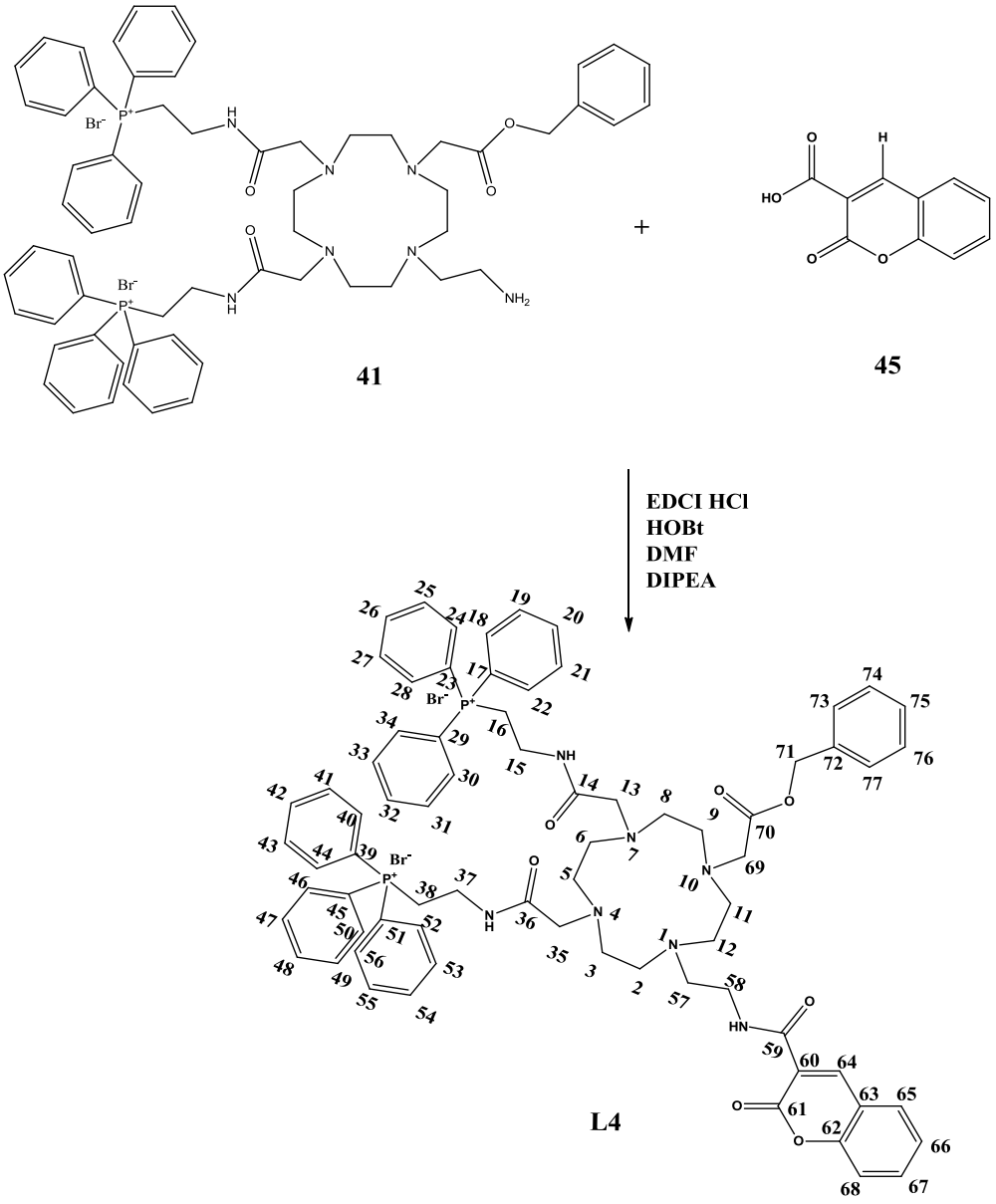

Synthetic procedure:

To the coumarin-3-carboxylic acid (**45**) (0.01 g; 0.046 mmol; 1 eq), dissolved in 20 mL of dry DMF, HOBt (0.01 g; 0.101 mmol; 2.2 eq) and EDCI*HCl (0.02 g; 0.102 mmol; 2.2 eq)

were added and the reaction mixture was stirred at room temperature under argon atmosphere for 1 h. Then DTPPBC (**41**) (06 g; 0.046 mmol; 1 eq) was added followed by DIPEA (0.03 g; 0.203 mmol; 4.4 eq). The reaction mixture was stirred under argon atmosphere and at room temperature for 24 h. After 24 h the reaction was stopped and the DMF was removed under high vacuum and replaced with 30 mL of chloroform. The organic phase was then extracted with water (25 mL), dried over $MgSO_4$ and filtered. After removing the solvent, (**L4**) was obtained as a pale yellow oil in 94% yield (60 mg). MS: 614 $[M]^{2+}$, 409 $[M+H]^{3+}$; ^1H NMR ($CDCl_3$, δ): 2.28-4.31 (m, 34 H, CH_2, $H^{2,3,5,6,8,9,11,12,13,15,16,35,37,38,57,58,69}$), 4.52 (s, 2 H, 1 CH_2, H^{71}), 7.11-7.30 (m, 5 H, CH, $H^{65,66,67,68}$), 7.61-7.66 (m, 35 H, CH, $H^{18,19,20,21,22,24,25,26,27,28,30,31,32,33,34,40,41,42,43,44,46,47,48,49,50,52,53,54,55,56,73,74,75,76,77}$), 8.72 (s, 1 H, CH, H^{64}); ^{13}C NMR ($CDCl_3$, δ): 30.13 (CH_2, $C^{15,37}$), 32.26 (CH_2, $C^{16,38}$), 34.20 (CH_2), 37.43 (CH_2), 40.80 (CH_2, C^{58}), 48.96 (CH_2, $C^{5,6}$), 50.67 (CH_2, $C^{2,3}$), 51.98 (CH_2, $C^{8,9}$), 53.79 (CH_2, $C^{11,12}$), 56.72 (CH_2, $C^{57,69}$), 65.75 (CH_2, $C^{13,35}$), 66.48 (CH_2, C^{71}), 115.22 (CH), 117.06 (CH), 117.12, 117.81 (CH), 118.20 (CH), 118.26 (CH), 118.75 (CH), 119.34 (CH), 125.33 (CH), 128.06 (CH), 128.31 (CH), 128.43 (CH), 128.50 (CH), 130.17 (CH), 130.34 (CH), 130.41 (CH), 130.49(CH), 130.54(CH), 130.58 (CH), 133.43 (CH), 133.56 (CH), 134.71 (C_q), 134.74 (C_q), 135.03 (C_q), 135.12 (C_q), 135.41 (C_q), 135.68 (C_q), 135.74 (C_q), 142.06 (C_q), 153.7 (C_q), 162.01 (C=O, C^{61}), 166.53 (C=O, C^{59}), 171.07 (C=O, C^{14}), 171.31 (C=O, C^{36}), 171.63 (C=O, C^{70}).

2.1.17 Synthesis of 1-N-Boc-ethylamine-4,7-di-(coumarin 151)-N-acetamide-10-benzyl acetate-1,4,7,10-tetraazacyclododecane (L5)

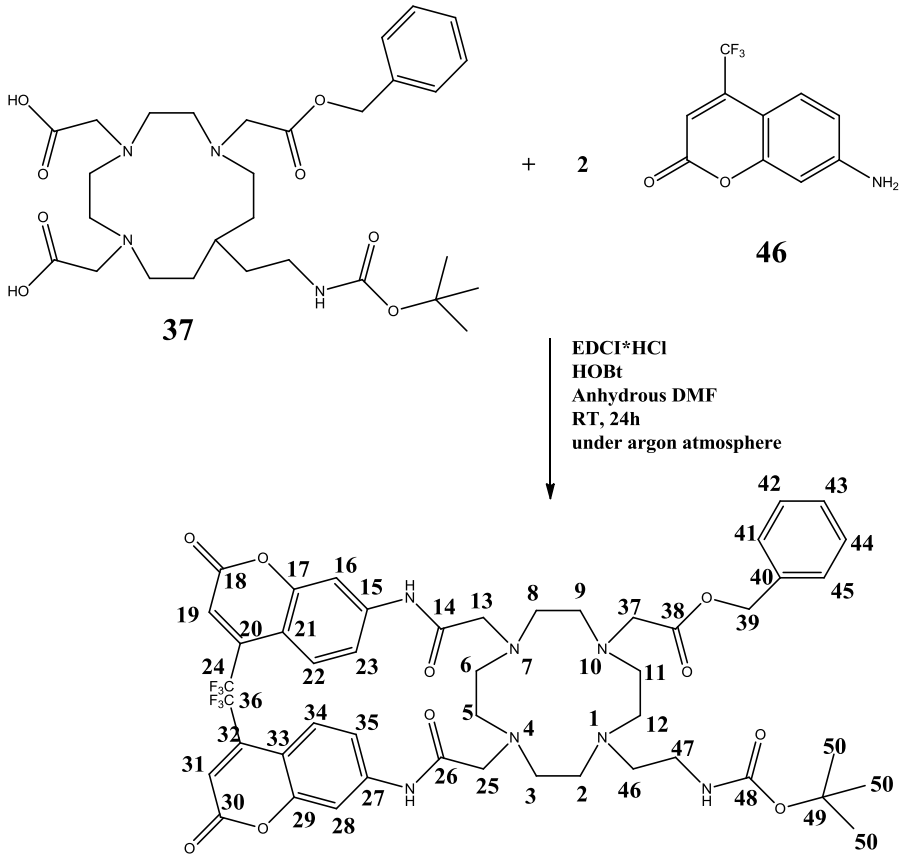

Synthetic procedure:

The acid (DAABBC) (**37**) (0.15 g; 0.259 mmol; 1eq) was dissolved in 30 mL of anhydrous DMF. Then HOBt (0.11 g; 0.777 mmol; 3eq) and EDCI*HCl (0.15 g; 0.777 mmol; 3eq) were added and the reaction was kept under stirring, under argon atmosphere and at room temperature for about 1h. The amine, the coumarin 151 (**46**) (0.12 g; 0.518 mmol; 2 eq) was added to the reaction mixture, followed by DIPEA (0.15 g; 1.140 mmol; 4.4 eq) and the reaction mixture was kept under stirring, under argon atmosphere and at room temperature for 24 h. After 24 h the reaction mixture was stopped and the DMF was

removed under high vacuum. The crude mixture was then dissolved into 40 mL of $CHCl_3$ and extracted with H_2O (3 x 40 mL). After removing the solvent, the product (**L5**) was obtained as a pale yellow oil in 46% yield (0.12 g). MS: 690 $[M_1+H]^+$; 712 $[M_1+Na]^+$; 677 $[M_2+H]^+$; ^1H NMR ($CDCl_3$, δ): 1.39 (s, 9 H, CH_3, H^{50}), 2.79-3.64 (m, 26 H, CH_2, $H^{2,3,5,6,8,9,11,12,13,25,37,46,47}$), 4.47 (s, 2 H, CH_2, C^{39}), 5.08 (s, 2 H, CH, $H^{23,35}$), 6.43 (s, 2 H, CH, $H^{16,28}$), 6.57 (s, 2 H, CH, $H^{22,34}$), 7.16-7.31 (m, 7 H, CH, $H^{41,42,43,44,45,19,31}$); ^{13}C NMR ($CDCl_3$, δ): 13.15 (CH_2), 14.38 (CH_2), 28.61 (CH_3, C^{50}), 40.32 (CF_3, $C^{24,36}$), 41.45 (CH_2, C^{47}), 51.31 (CH_2, $C^{5,6,3,8}$), 52.24 (CH_2, $C^{2,9,11,12}$), 66.55 (CH_2, $C^{13,25,39}$), 78.80 (C_q, C^{49}), 101.148 (CH), 104.69 (CH), 109.73 (CH), 112.56 (CH), 118.25 (CH), 120.09 (CH), 123.53 (CH), 126.63 (CH), 128.45 (CH), 128.71 (CH), 142.34 (C_q), 143.73 (C_q), 151.55 (C=O, C^{48}), 156.85 (C=O, $C^{14,26}$), 160.29 (C=O, C^{38}).

2.1.18 Deprotection of the Boc group from the 1-N-Boc-ethylamine-4,7,10- triallyl acetate-1,4,7,10-tetraazacyclododecane (TABC) (47)

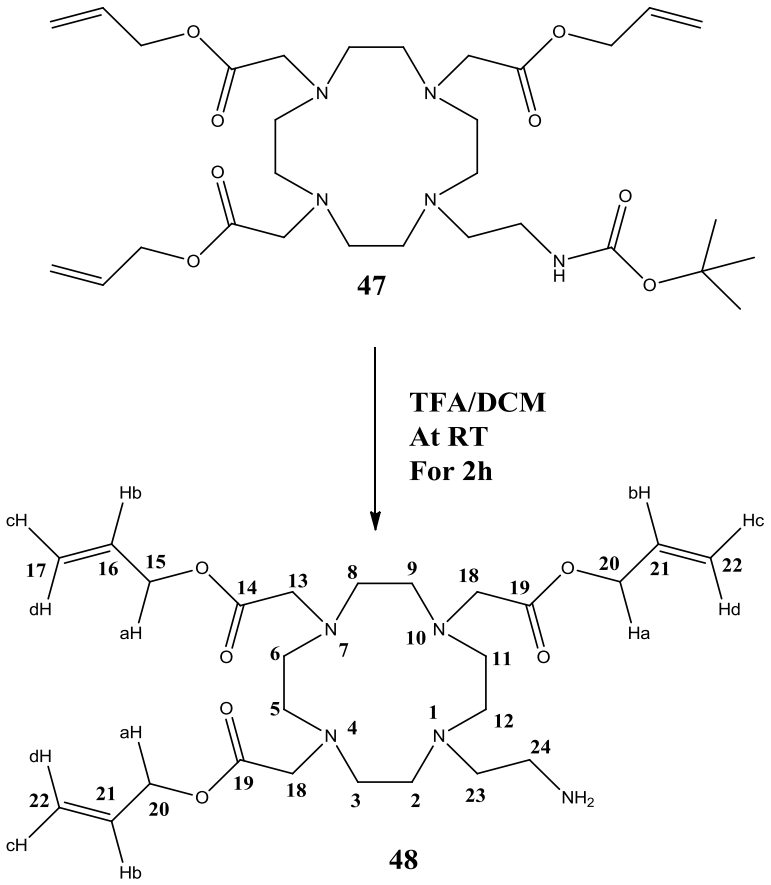

Synthetic procedure:

The TABC (**47**) was recovered as by product during the column chromatography performed for the purification of the reaction mixture obtained during the synthesis of DABC (**36**). The TABC (**47**) (0.16 g; 0.263 mmol) was dissolved in 10 mL of anhydrous DCM. Then 1 mL of TFA was added and the reaction mixture was stirred at room temperature for 2 hours. After stopping the reaction, 20 mL of DCM were added to the reaction mixture and extracted with 30 mL of 1M $NaHCO_3$ aqueous solution. After the extraction the organic phase was dried over $MgSO_4$ and filtered. After removing the solvent, the product (**48**) was obtained as a light brown oil in 45% yield (0.06 g). MS: 510 $[M+H]^+$. ^1H NMR ($CDCl_3$, δ): 2.52-3.43 (m, 36 H, CH_2, $H^{2,3,5,6,8,9,11,12,13,18,23,24}$), 4.53-4.55 (d, 6 H, CH_2, $^3J_{Ha,b}$ 6 Hz, $H^{15,20}$), 5.16-5.29 (m, 6 H, CH_2, $^3J_{Hd,b}$ 16 Hz, $^3J_{Hc,b}$ 10 Hz, $^2J_{Hc,d}$

= $^{2}J_{Hd,c}$ 1.4 Hz, $H^{17,22}$), 5.79-5.92 (m, 3H, CH, $^{3}J_{Hb,d}$ 16 Hz, $^{3}J_{Hb,c}$ 10 Hz, $^{3}J_{Hb,a}$ 6 Hz, $H^{16,21}$). ^{13}C NMR ($CDCl_3$, δ): 39.45 (CH_2 C^{24}), 47.14 (CH_2, C^{6}), 47.49 (CH_2, C^{8}), 50.62 (CH_2, C^{5}), 50.79 (CH_2, C^{9}), 51.12 (CH_2, C^{3}), 51.17 (CH_2, C^{11}), 52.19 (CH_2, C^{2}), 52.42 (CH_2, C^{12}), 53.40 (CH_2), 55.68 (CH_2, C^{23}), 56.04 (CH_2, $C^{13,18}$), 64.79 (CH_2, C^{15}), 64.83 (CH_2, C^{20}), 118.36 (CH_2, $C^{17,22}$), 132.02 (CH, $C^{16,21}$), 171.36 (C=O, C^{14}), 171.57 (C=O, C^{19}).

2.1.19 Synthesis of 1-N-(coumarin 343)ethylamide-4,7,10-triallyl acetate-1,4,7,10-tetraazacyclododecane (L6)

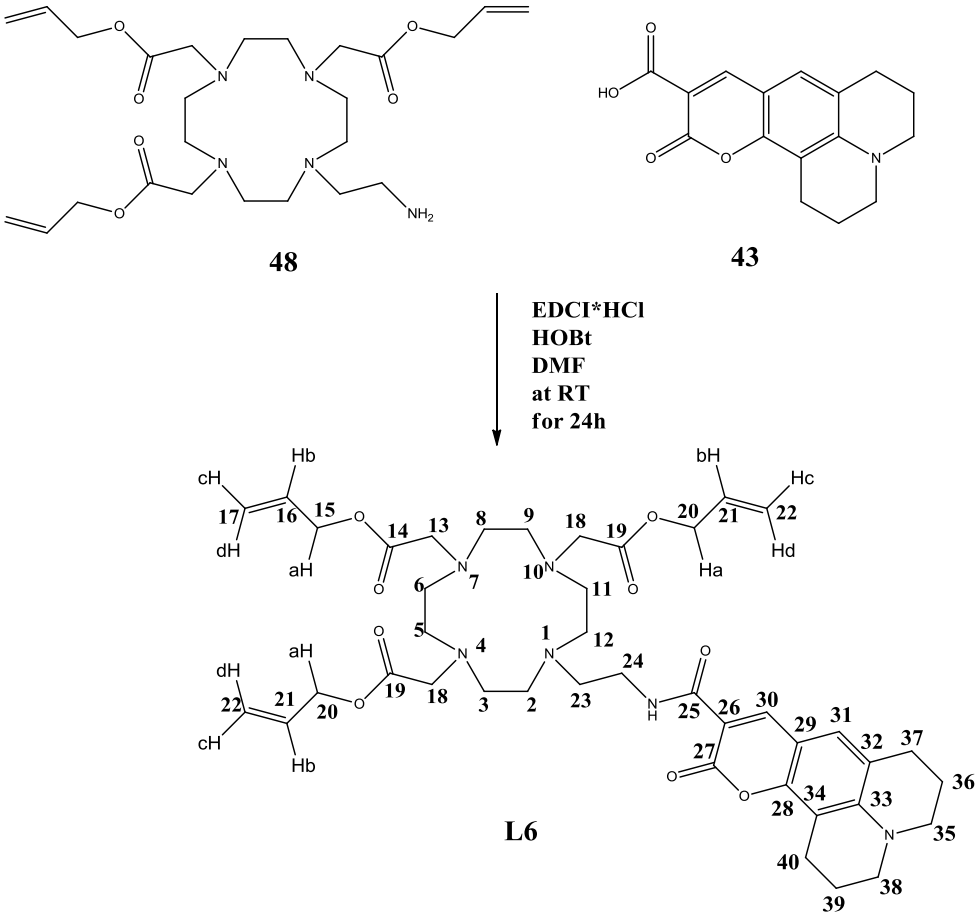

Synthetic procedure:

The acid (coumarin 343) (**43**) (0.03 g; 0.118 mmol; 1 eq) was dissolved in 30 mL of anhydrous DMF. Then HOBt (0.02 g; 0.177 mmol; 1.5 eq) and EDCI*HCl (0.03 g; 0.177 mmol; 1.5 eq) were added and the reaction mixture was kept under stirring for 1h at room temperature. After 1h, the amine, TAC (**48**), (0.06 g; 0.118 mmol; 1 eq) was added, followed by DIPEA (0.03 mg, 0.259 mmol; 2.2 eq). The reaction mixture was stirred under argon atmosphere and at room temperature for 24 h. After 24 h the reaction was stopped and the DMF was removed under high vacuum and replaced with 30 mL of chloroform. The organic phase was then extracted with water (2 x 25 mL), dried over $MgSO_4$ and filtered. After removing the solvent **L6** was obtained as a yellow oil in 77% yield (0.07 g). MS: 777 $[M+H]^+$, 799 $[M+Na]^+$. ^1H NMR ($CDCl_3$, δ): 1.93 (m, 4 H, CH_2, $H^{36,39}$), 2.71-3.61 (m, 34 H, CH_2, $H^{2,3,5,6,8,9,11,12,13,18,23,24,35,3738,40}$), 4.53-4.55 (d, 6 H, CH_2, $^3J_{Ha,b}$ 6 Hz, $H^{15,20}$), 5.16-5.29 (m, 6 H, CH_2, $^3J_{Hd,b}$ 16 Hz, $^3J_{Hc,b}$ 10 Hz, $^2J_{Hc,d} = {}^2J_{Hd,c}$ 1.4 Hz, $H^{17,22}$), 5.79-5.92 (m, 3 H, CH, $^3J_{Hb,d}$ 16 Hz, $^3J_{Hb,c}$ 10 Hz, $^3J_{Hb,a}$ 6 Hz H, $H^{16,21}$), 6.84 (s, 1 H, CH, H^{31}), 8.49 (s, 1 H, CH, H^{30}). ^{13}C NMR ($CDCl_3$, δ): 20.05 (CH_2, $C^{36,39}$), 21.05 (CH_2, $C^{37,40}$), 27.40 (CH_2, C^{35}), 29.63 (CH_2 C^{38}), 36.43 (CH_2, $C^{15,20}$), 49.63 (CH_2, C^6), 49.77 (CH_2, C^8), 50.01 (CH_2, C^5), 50.19 (CH_2, C^9), 52.23 (CH_2, $C^{11,3}$), 52.60 (CH_2, $C^{2,12}$), 54.36 (CH_2, C^{23}), 55.83 (CH_2, $C^{13,18}$), 64.99 (CH_2, C^{15}), 105.61(CH_2), 106.05 (CH_2), 110.97 (CH_2), 118.45 (CH_2, C^{17}), 119.58 (CH_2, C^{22}), 128.150 (CH, C^{16}), 131.86 (CH, C^{21}), 143.54 (C_q), 144.84 (C_q), 147.91(CH, C^{31}), 148.21 (CH, C^{30}), 152.69 (C_q), 162.67 (C=O, C^{25}), 164.04 (C=O, C^{27}), 170.86 (C=O, $C^{14,19}$).

2.1.20 Deprotection of the Boc group from DABBC (36)

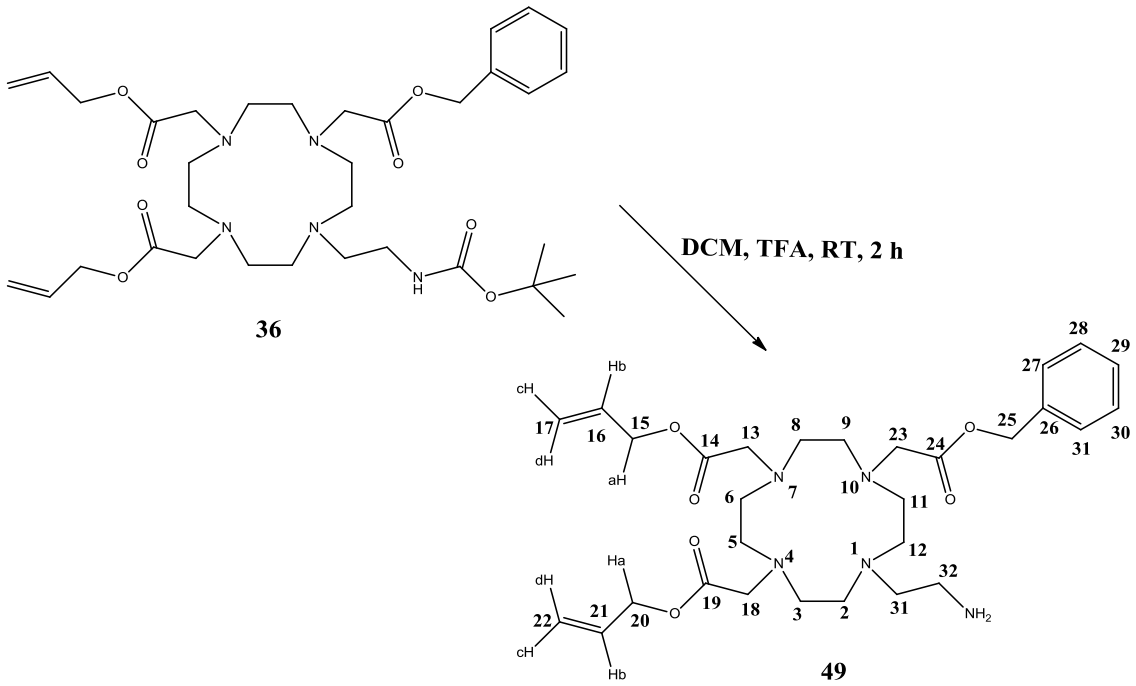

36

49

Synthetic procedure:

The DABBC (**36**) (0.31 g; 0.470 mmol; 1 eq) was dissolved in 20 mL of DCM and 1 mL of TFA was added. The reaction was kept under stirring for 2 h. After 2 h the reaction was stopped and 20 mL of DCM were added to the reaction mixture and extracted with 30 mL of 1M $NaHCO_3$ aqueous solution. After the extraction, the organic phase was dried over $MgSO_4$, filtered and the solvent was removed to give the DABnC (**49**) in 53% yield (0.14 g). MS: 560 $[M+H]^{2}$; 582 $[M+Na]^{+}$. ^{1}H NMR ($CDCl_3$, δ): 2.70-3.70 (m, 26 H, CH_2, $H^{2,3,5,6,8,9,11,12,13,18,23}$), 4.51-4.52 (d, 4 H, CH_2, $^{3}J_{Ha,b}$ 6Hz, $H^{15,20}$), 5.08 (s, 2 H, CH_2. H^{25}), 5.15-5.27 (m, 4 H, CH_2, $^{3}J_{Hd,b}$ 16.2 Hz, $^{3}J_{Hc,b}$ 10.3 Hz, $^{2}J_{Hd,c} = {}^{2}J_{Hc,d}$ 1.3 Hz, $H^{17,22}$), 5.75-5.87 (m, 2 H, CH, $^{3}J_{Hb,d}$ 16.2 Hz, $^{3}J_{Hb,c}$ 10.3 Hz, $^{3}J_{Hb,a}$ 6 Hz, $H^{16,21}$), 7.21-7.30 (m, 5 H, CH, $C^{27,28,29,30,31}$).

2.1.21 1-N-(dihydrofluorescein diacetate)ethylamide-4,7-diallyl acetate-10-benzyl acetate-1,4,7,10-tetraazacyclododecane (L7)

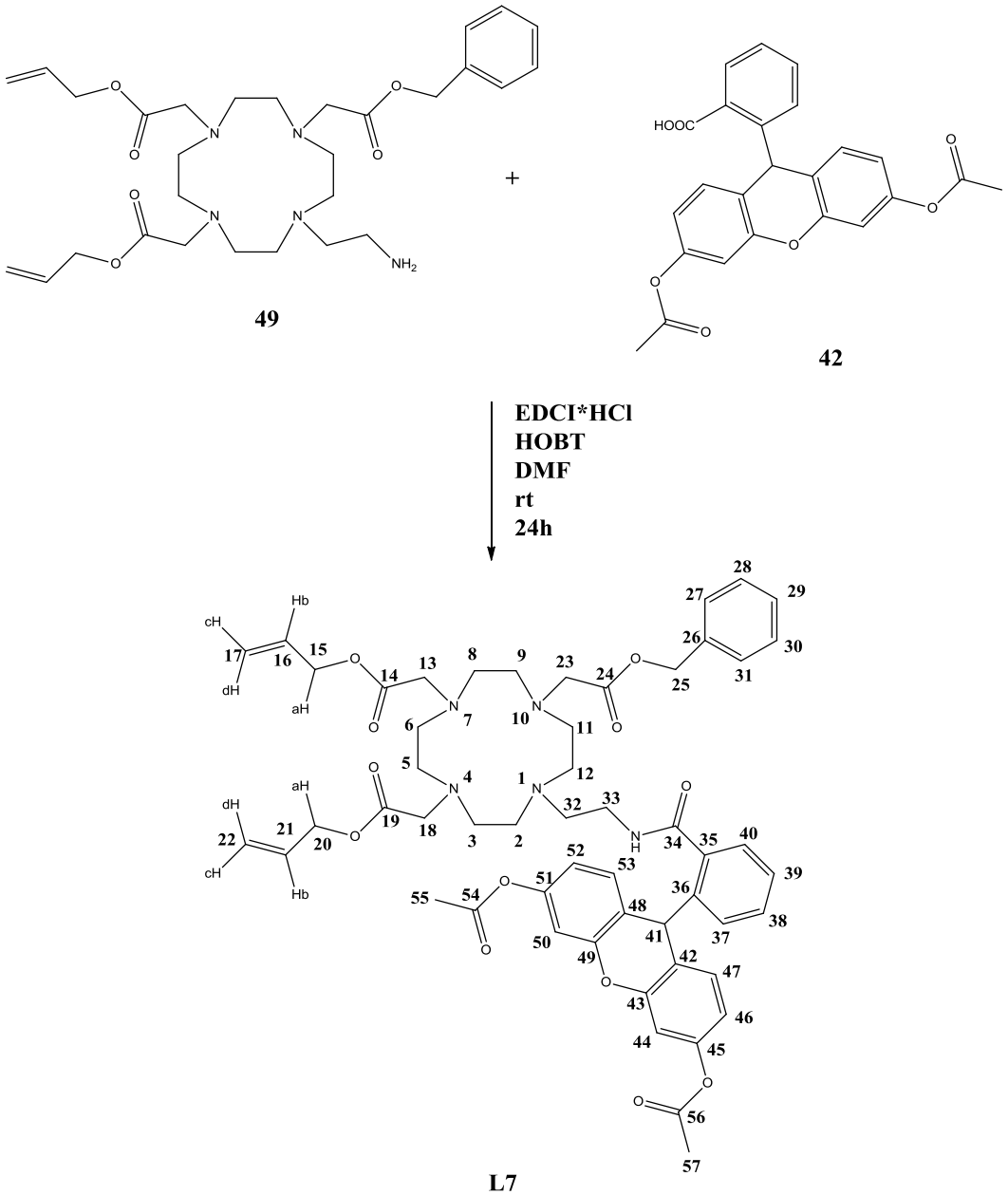

Synthetic procedure:

The acid (dihydrofluorescein diacetate) (**42**) (0.11 g; 0.251 mmol; 1 eq) was dissolved in 40 mL of anhydrous DMF. Then HOBt (0.07 g; 0.5014 mmol; 2 eq) and EDCI*HCl (0.09 g; 0.501 mmol; 2 eq) were added and the reaction mixture was kept under stirring for 1 h at room temperature. After 1 h, the amine, the DABnC (**49**), (0.14 g; 0.251 mmol; 1eq) was added, followed by DIPEA (0.10 g; 0.752 mmol; 3 eq). The reaction mixture was stirred under argon atmosphere and at room temperature for 24 h. After 24 h the reaction was stopped and the DMF was removed under high vacuum and replaced with 40 mL of chloroform. The organic phase was then extracted with water (2 x 30 mL), dried over $MgSO_4$ and filtered. After removing the solvent, **L7** was obtained as yellow oil in 68% yield (0.14 g). MS: 960 $[M+H]^+$; 982 $[M+Na]^+$. ^1H NMR ($CDCl_3$, δ): 1.95 (s, 6 H, CH_3, $H^{55,57}$), 2.70-3.70 (m, 26 H, CH_2, $H^{2,3,5,6,8,9,11,12,13,18,23,32,33}$), 4.51-4.52 (d, 4 H, CH_2, $^3J_{Ha,b}$ 6 Hz, $H^{15,20}$), 5.08 (s, 2 H, CH_2, H^{25}), 5.15-5.27 (m, 4 H, CH_2, $^3J_{Hd,b}$ 16 Hz, $^3J_{Hc,b}$ 10 Hz, $^2J_{Hd,c}$ = $^2J_{Hc,d}$ 1.3 Hz, $H^{17,22}$), 5.75-5.87 (m, 2 H, CH, $^3J_{Hb,d}$ 16 Hz, $^3J_{Hb,c}$ 10 Hz, $^3J_{Hb,a}$ 6 Hz, $H^{16,21}$), 6.43-6.84 (m, 10 H, CH, $H^{37,38,39,40,44,46,47,50,52,53}$), 7.21-7.30 (m, 5 H, CH, $H^{27,28,29,30,31}$), 8.49 (s, 1 H, CH, H^{41}).

2.1.22 Complexation of L1 with Eu(III): synthesis of EuL1

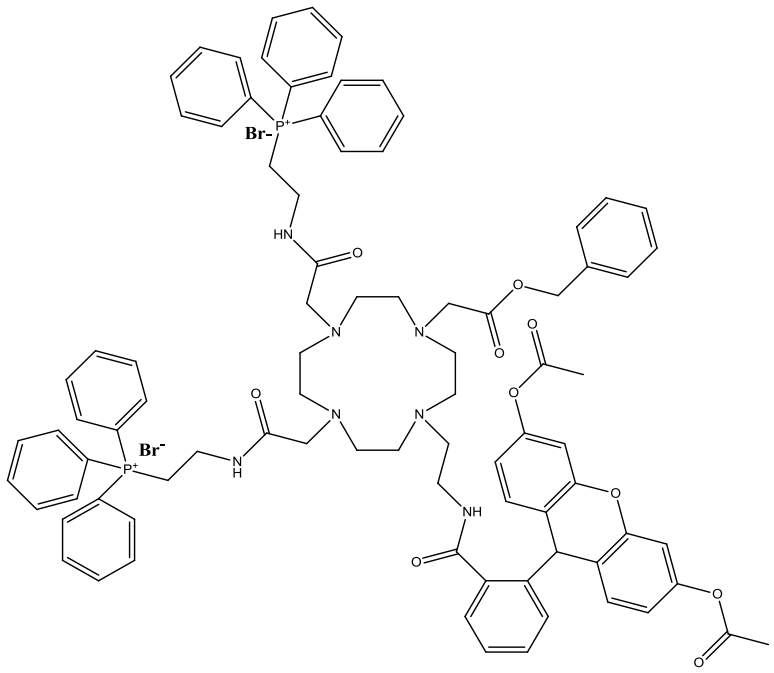

L1

$EuCl_3$ MeOH

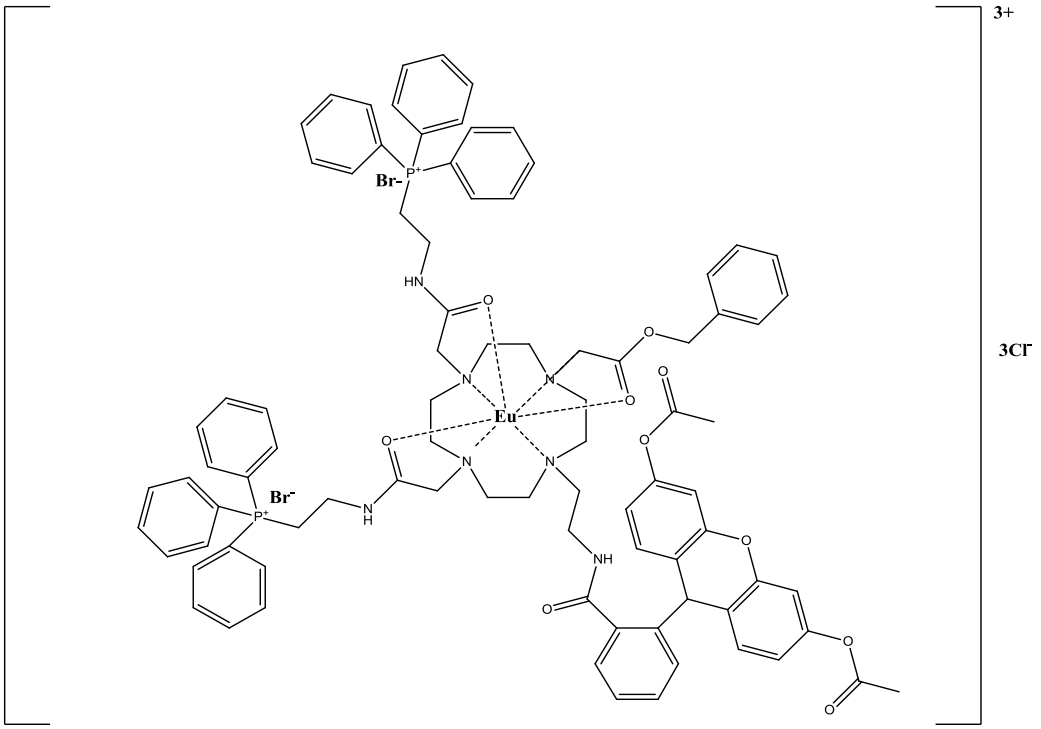

Desired product EuL1

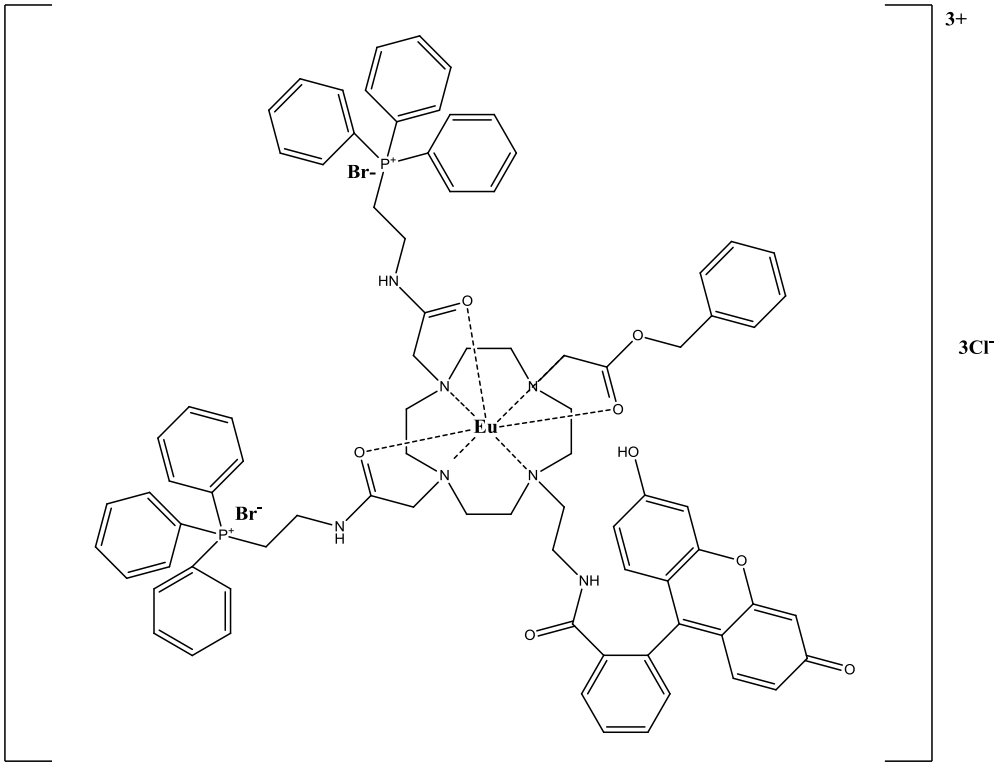

Observed product EuL1

Synthetic procedure:

L1 (0.03 g; 0.017 mmol; 1 eq) and anhydrous europium chloride ($EuCl_3$) (0.004 g; 0.017 mmol; 1eq) were dissolved in 20 mL of anhydrous methanol. The reaction mixture was heated under reflux and argon atmosphere for 15 h. The reaction was monitored through ESI mass spectrometry via direct injection and TLC (DCM/isopropylamine 95:0.5). The reaction was stopped when no peak related to the free ligand (**L1**) was observed in the mass spectrum and no spot related to the free ligand (**L1**) was observed on TLC plate. The reaction mixture was allowed to cool back to room temperature and was poured into cold diethyl ether (15 mL). The mixture was centrifuged and the ether was poured off the pale yellow precipitate. The precipitated was dissolved in distilled water (5 mL) and the sample was freeze-dried. The observed product (**EuL1**) was obtained as pale yellow solid in 96% yield (based on **L1** containing the acetate groups) (0.03 g). **EuL1** was characterized via mass spectrometry and absorption and emission spectroscopy. λ_{max} =

489 nm; MS (ESI) *m/z*: $[L1+Eu+Br+2H_2O-2COCH_3]^{4+}$ Calcd for $[C_{83}H_{89}Br^{153}EuN_7O_{10}P_2]^{4+}$ 409.3630; Found 409.1623; MS (MALDI) *m/z*: $[L1+Eu+Br+2H_2O-2COCH_3]^{4+}$ Calcd for $[C_{83}H_{89}Br^{153}EuN_7O_{10}P_2]^{4+}$ 409.3630; Found 409.2.

2.1.23 Complexation of L1 with Tb(III): synthesis of TbL1

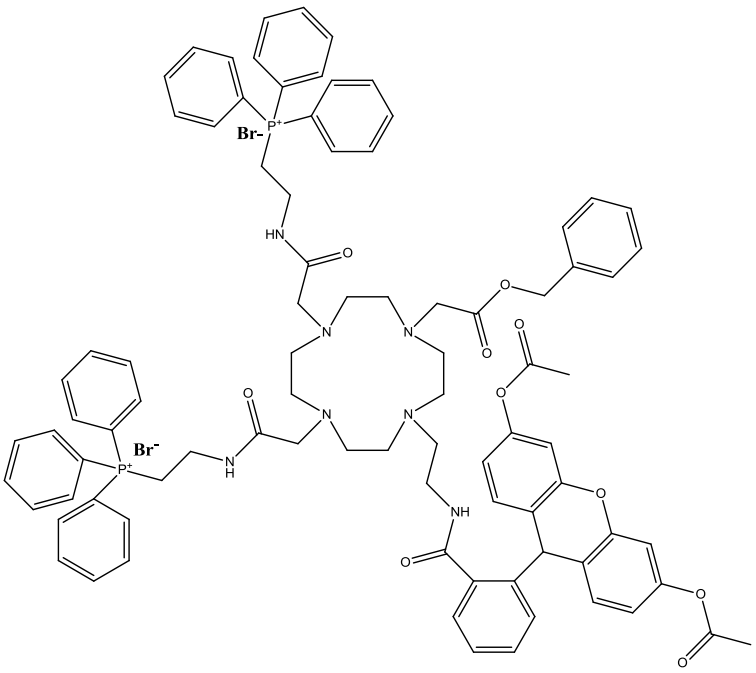

L1

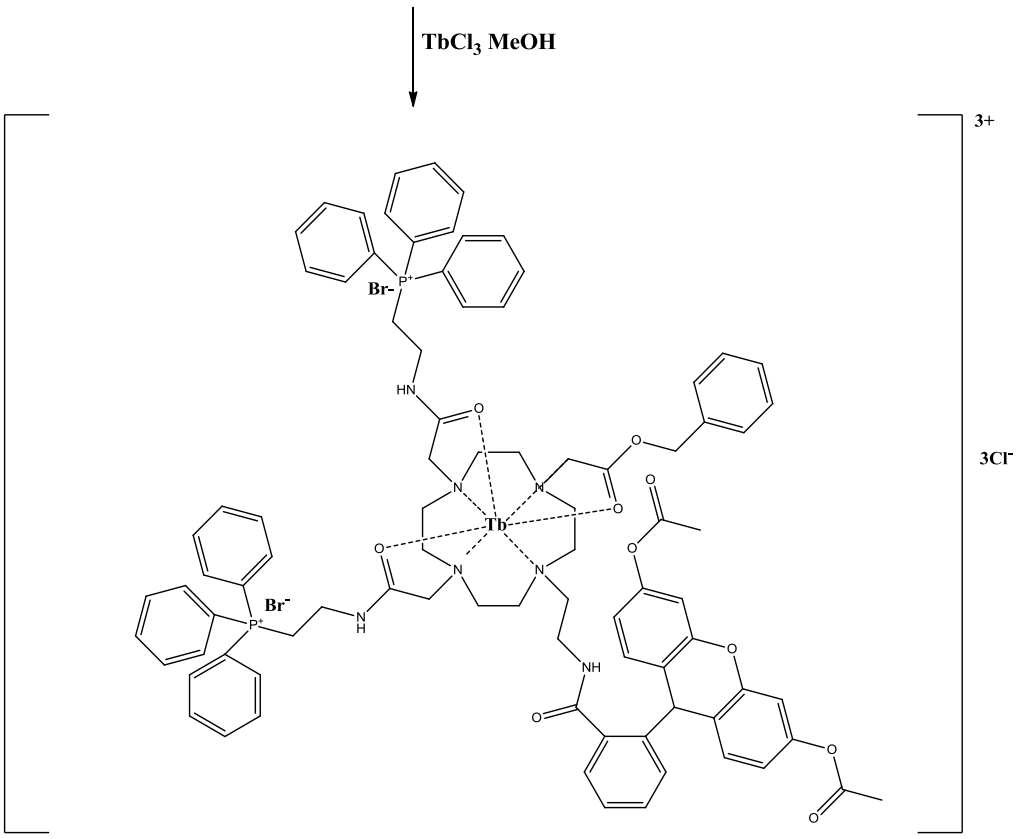

Desired product TbL1

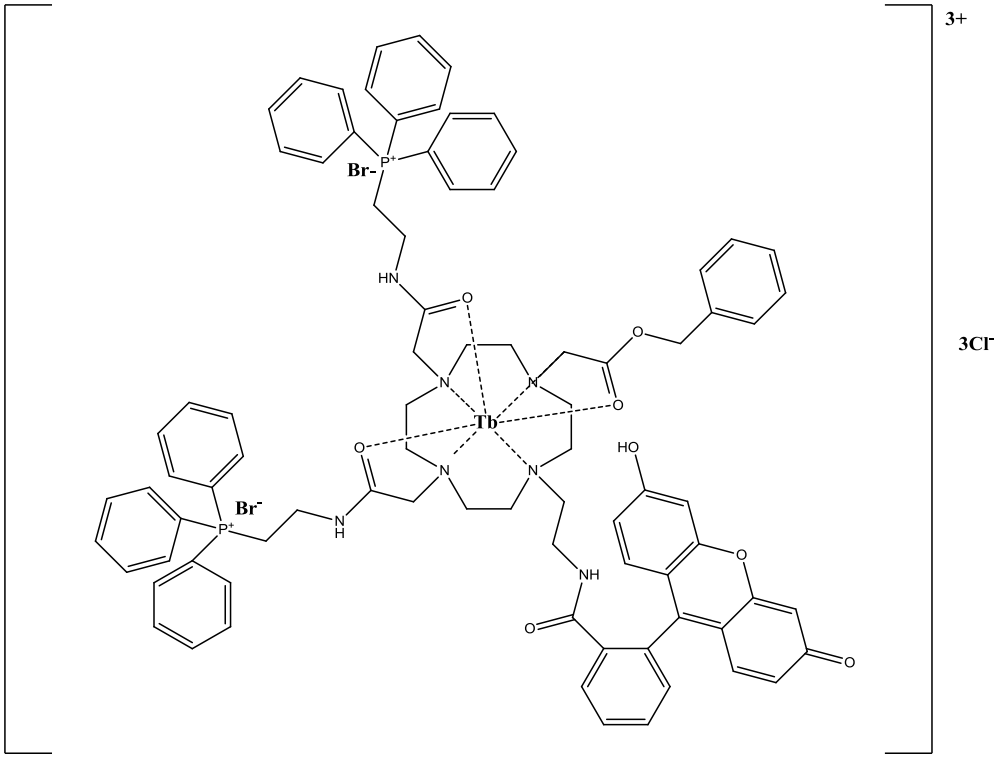

Observed product TbL1

Synthetic procedure:

L1 (0.03 g; 0.021 mmol; 1 eq) and anhydrous terbium chloride ($TbCl_3$) (0.005 g; 0.021 mmol; 1 eq) were dissolved in 20 mL of anhydrous methanol. The reaction mixture was heated under reflux and argon atmosphere for 15 h. The reaction was monitored through ESI mass spectrometry via direct injection and TLC (DCM/isopropylamine 95:0.5). The reaction was stopped when no peak related to the free ligand (**L1**) was observed in the mass spectrum and no spot related to the free ligand (**L1**) was observed on TLC plate. The reaction mixture was allowed to cool back to room temperature and was poured into cold diethyl ether (15 mL). The mixture was centrifuged and the ether was poured off the pale yellow precipitate. The precipitated was dissolved in distilled water (5 mL) and the sample was freeze-dried. The observed product (**TbL1**) was obtained as pale yellow solid in 98.9 % yield (based on **L1** containing the acetate groups) (0.04 g). **TbL1** was

characterized via mass spectrometry and absorption and emission spectroscopy. λ_{max} = 489 nm; MS (ESI) *m/z*: [L1+Tb+Br-2COCH$_3$]$^{4+}$ Calcd for [$C_{83}H_{85}BrN_7O_8P_2Tb$]$^{4+}$ 401.8588; Found 402.1225.

2.1.24 Complexation of L2 with Eu(III): synthesis of EuL2

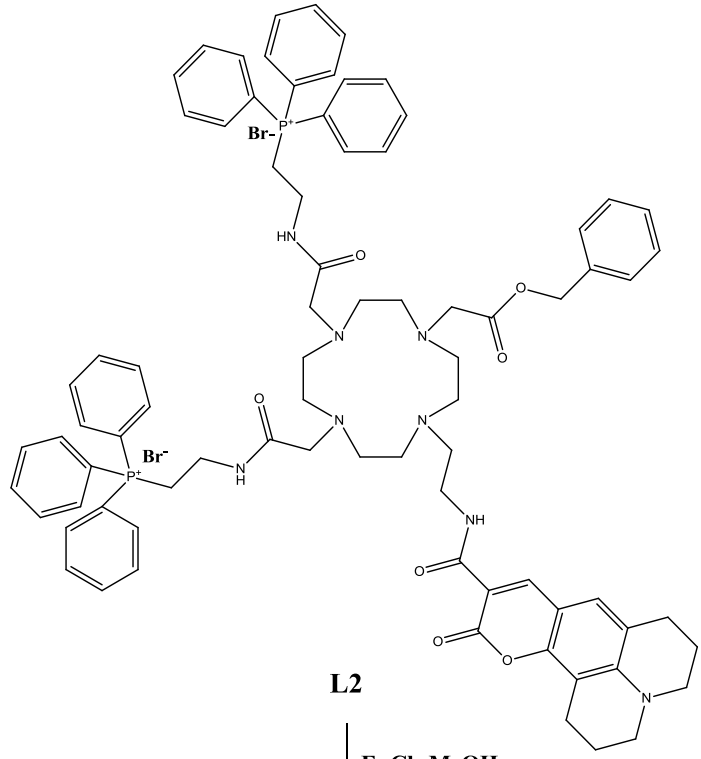

L2

$EuCl_3$ MeOH

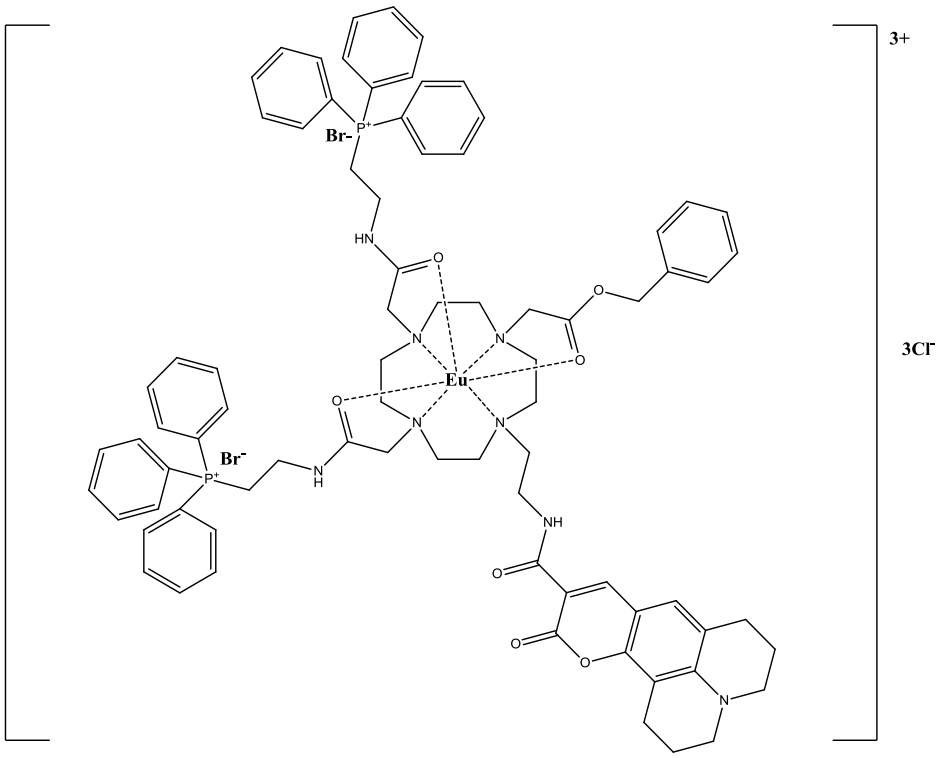

EuL2

Synthetic procedure:

L2 (0.04 g; 0.029 mmol; 1 eq) and anhydrous europium chloride ($EuCl_3$) (0.008 g; 0.029 mmol; 1 eq) were dissolved in 20 mL of anhydrous methanol. The reaction mixture was heated under reflux and argon atmosphere for 15 h. The reaction was monitored through ESI mass spectrometry via direct injection and TLC (DCM/isopropylamine 95:0.5). The reaction was stopped when no peak related to the free ligand (**L2**) was observed in the mass spectrum and no spot related to the free ligand (**L2**) was observed on TLC plate. The reaction mixture was allowed to cool back to room temperature and was poured into cold diethyl ether (15 mL). The mixture was centrifuged and the ether was poured off the orange precipitate. The precipitated was dissolved in distilled water (5 mL) and the sample was freeze-dried. The complex (**EuL2**) was obtained as orange solid in 99 % yield (0.05 g). **EuL2** was characterized via mass spectrometry and absorption and emission spectroscopy. λ_{max} = 447 nm; MS (MALDI) *m/z*: $[L2+Eu+Br+4H_2O]^{4+}$ Calcd for $[C_{79}H_{96}Br^{153}EuN_8O_{11}P_2]^{4+}$ 406.6262; Found 407.2.

2.1.25 Complexation of L2 with Tb(III): synthesis of TbL2

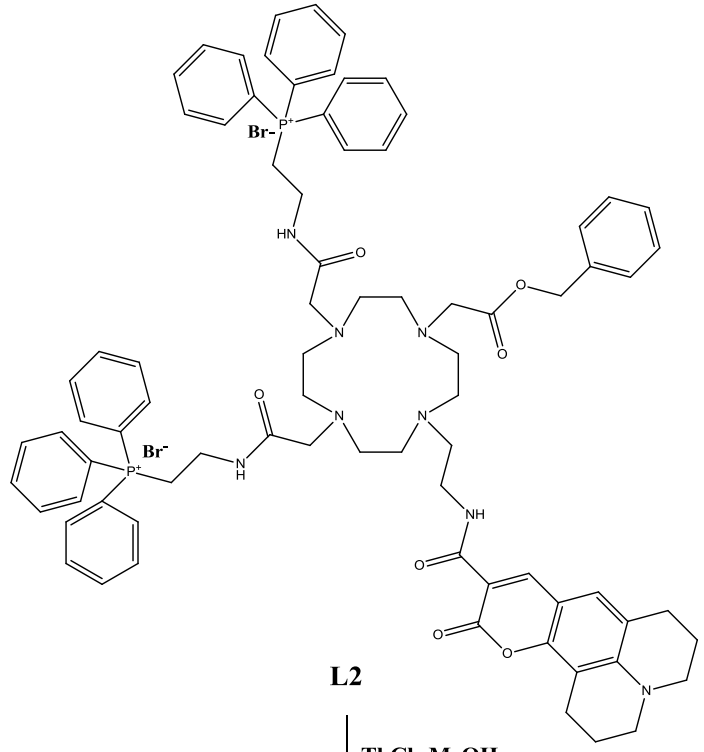

L2

$TbCl_3$ MeOH

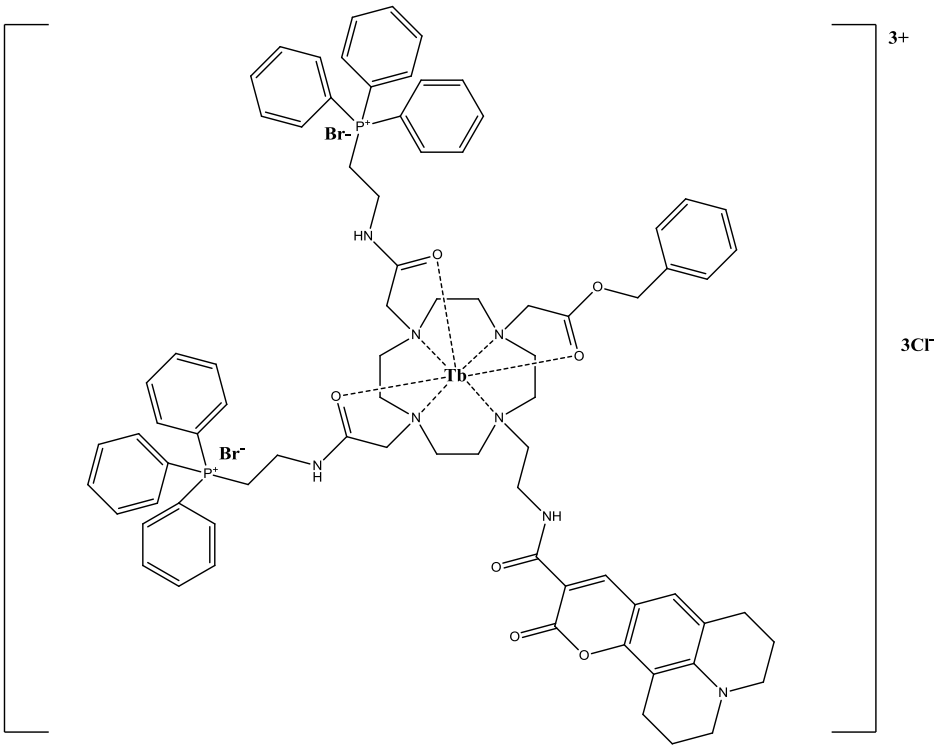

TbL2

Synthetic procedure:

L2 (0.04 g; 0.027 mmol; 1 eq) and anhydrous terbium chloride ($TbCl_3$) (0.01 g; 0.027 mmol; 1 eq) were dissolved in 20 mL of anhydrous methanol. The reaction mixture was heated under reflux and under argon atmosphere for 15 h. The reaction was monitored through ESI mass spectrometry via direct injection and TLC (DCM/isopropylamine 95:0.5). The reaction was stopped when no peak related to the free ligand (**L2**) was observed in the mass spectrum and no spot related to the free ligand (**L2**) was observed on TLC plate. The reaction mixture was allowed to cool back to room temperature and was poured into cold diethyl ether (15 mL). The mixture was centrifuged and the ether was poured off the orange precipitate. The precipitated was dissolved in distilled water (5 mL) and the sample was freeze-dried. The complex (**TbL2**) was obtained as orange solid in 81 % yield (0.04 g). **TbL2** was characterized via mass spectrometry and absorption and emission spectroscopy. λ_{max} = 447 nm; MS (MALDI) *m/z*: $[L2+Tb+4H_2O+Br]^{4+}$ Calcd for $[C_{79}H_{96}BrN_8O_{11}P_2Tb]^{4+}$ 408.1272; Found 408.2; MS (ESI) *m/z*: $[L2+Tb+4H_2O+Br]^{4+}$ Calcd for $[C_{79}H_{96}BrN_8O_{11}P_2Tb]^{4+}$ 408.1272; Found 408.1692.

2.1.26 Complexation of L4 with Eu(III): synthesis of EuL4

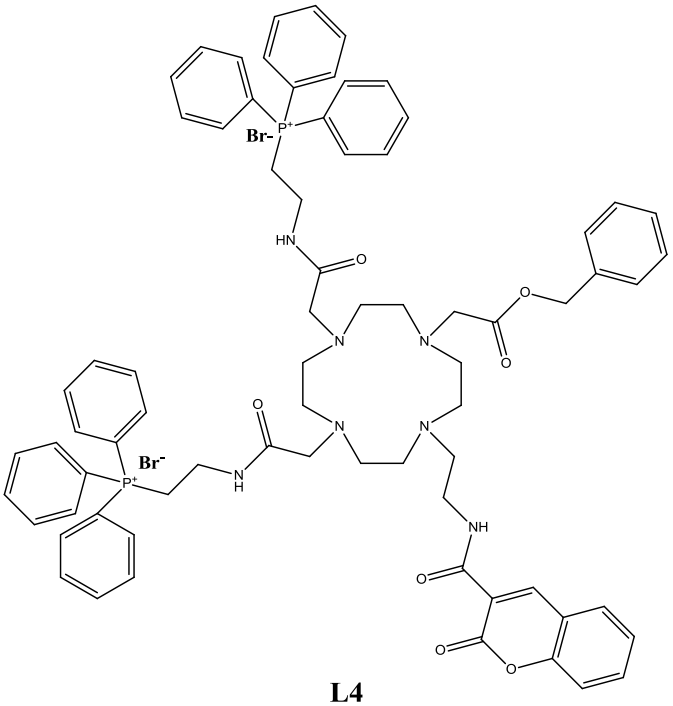

L4

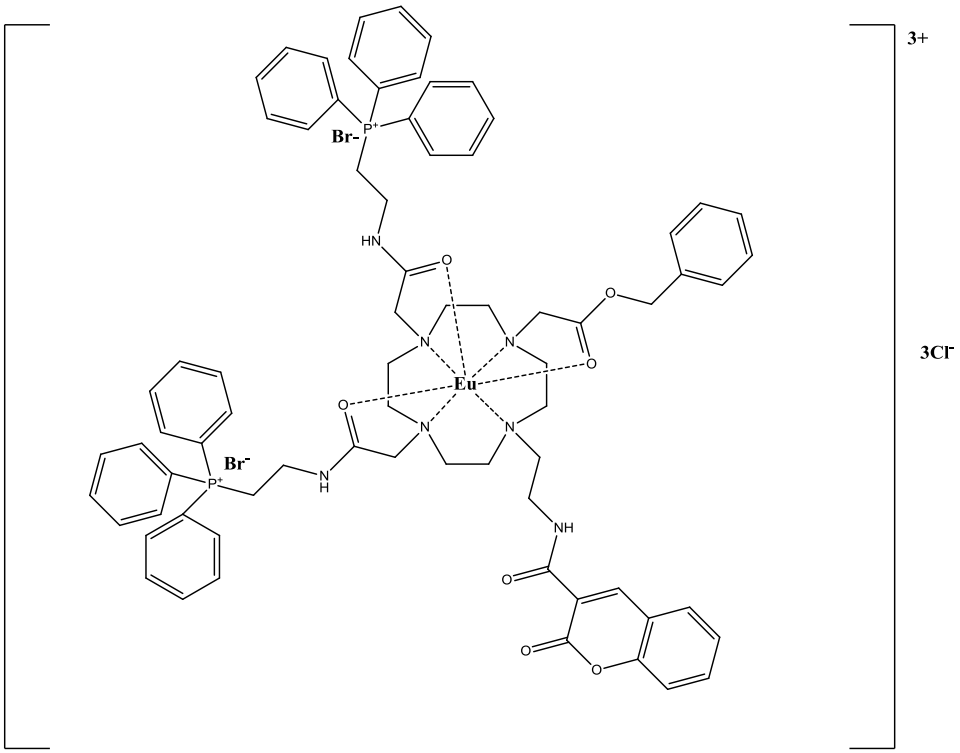

EuL4

Synthetic procedure:

The ligand (**L4**) (0.03 g; 0.022 mmol; 1 eq) and anhydrous europium chloride ($EuCl_3$) (0.01 g; 0.022 mmol; 1 eq) were dissolved in 20 mL of anhydrous methanol. The reaction mixture was heated under reflux and argon atmosphere for 15 h. The reaction was monitored through ESI mass spectrometry via direct injection and TLC (DCM/isopropylamine 95:0.5). The reaction was stopped when no peak related to the free ligand (**L4**) was observed in the mass spectrum and no spot related to the free ligand (**L4**) was observed on TLC plate. The reaction mixture was allowed to cool back to room temperature and was poured into cold diethyl ether (20 mL). The mixture was centrifuged and the ether was poured off the pale yellow precipitate. The precipitated was dissolved in distilled water (5 mL) and the sample was freeze-dried. The complex (**EuL4**) was obtained as pale yellow solid in 97% yield (0.03 g). **EuL4** was characterized via mass and absorption and emission spectroscopy. λ_{max} = 298 nm; MS (ESI) *m/z*: $[L4+Eu+H_2O]^{5+}$ Calcd for $[C_{73}H_{81}{}^{153}EuN_7O_8P_2]^{5+}$ 279.6961; Found 279.0936.

2.1.27 Complexation of L5 with Eu(III): synthesis of EuL5

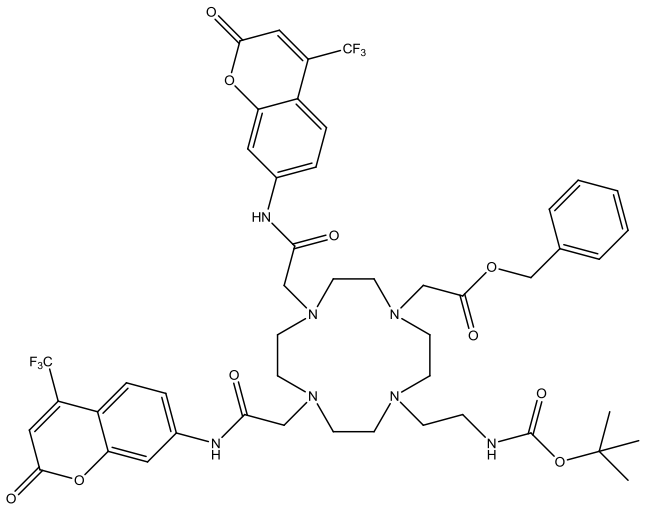

L5

$EuCl_3$
MeOH

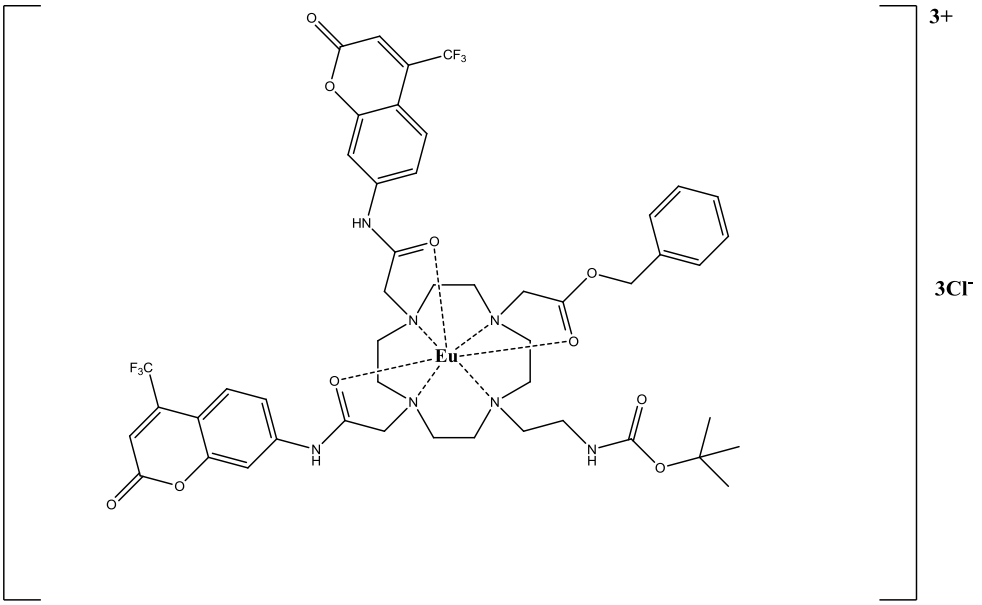

EuL5

Synthetic procedure:

The ligand (**L5**) (0.03 g; 0.033 mmol; 1 eq) and anhydrous europium chloride ($EuCl_3$) (0.01 g; 0.033 mmol; 1 eq) were dissolved in 20 mL of anhydrous methanol. The reaction mixture was heated under reflux and argon atmosphere for 15 h. The reaction was monitored through ESI mass spectrometry via direct injection and TLC (DCM/isopropylamine 95:0.5). The reaction was stopped when no peak related to the free ligand (**L5**) was observed in the mass spectrum and no spot related to the free ligand (**L5**) was observed on TLC plate. The reaction mixture was allowed to cool back to room temperature and was poured into cold diethyl ether (20 mL). The mixture was centrifuged and the ether was poured off the pale yellow precipitate. The precipitated was dissolved in distilled water (5 mL) and the sample was freeze-dried. The complex (**EuL5**) was obtained as pale yellow solid in 94% yield (0.04 g). **EuL5** was characterized via mass spectrometry and absorption and emission spectroscopy. λ_{max} = 339 nm; MS (ESI) *m/z*: $[L5+Eu+Cl]^{2+}$ Calcd for $[C_{48}H_{53}Cl^{153}EuF_6N_7O_{10}]^{2+}$ 594.6324; Found 595.2107.

2.1.28 Complexation of L6 with Eu(III): synthesis of EuL6

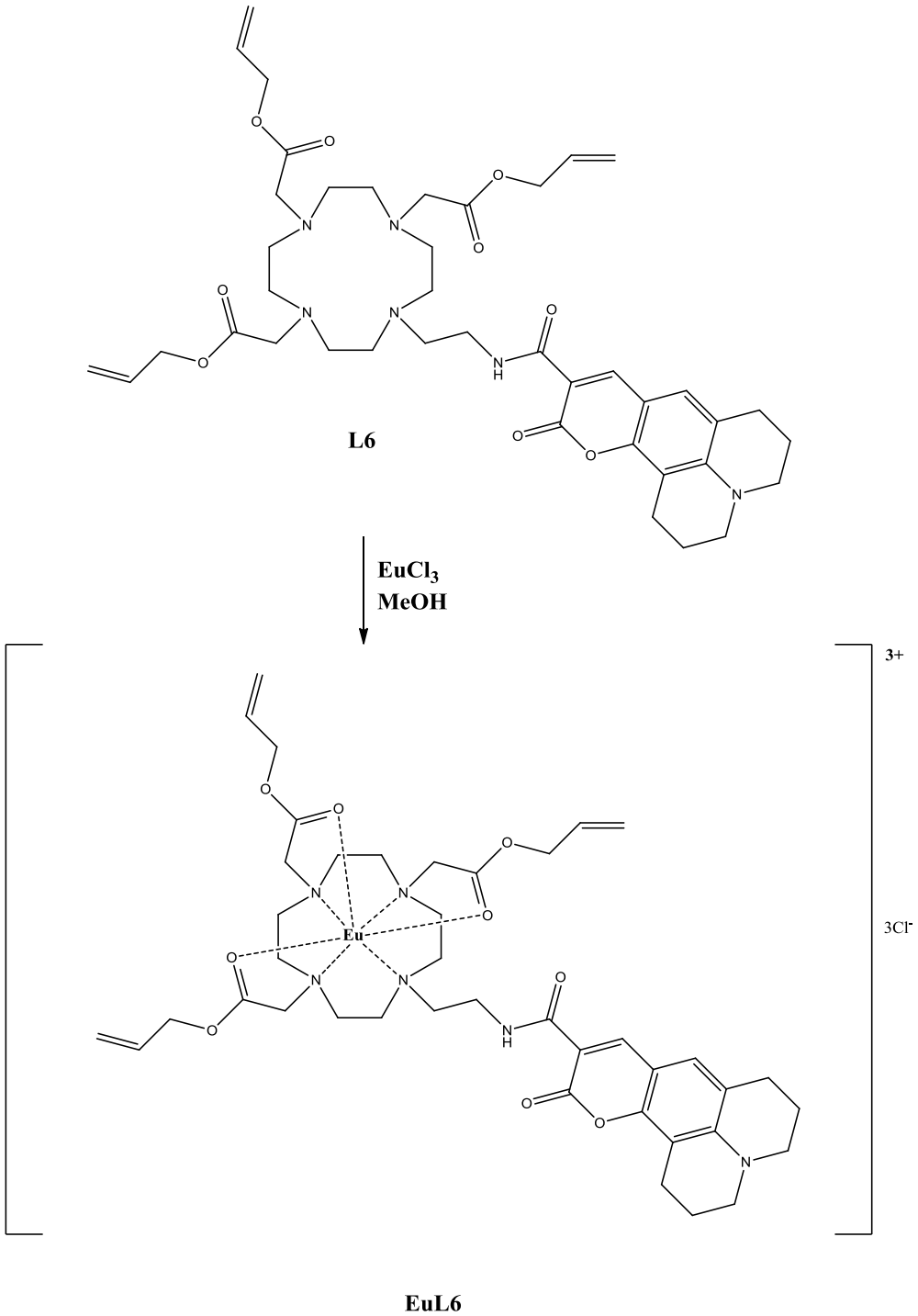

EuL6

Synthetic procedure:

The ligand (**L6**) (0.04 g; 0.045 mmol; 1 eq) and anhydrous europium chloride ($EuCl_3$) (0.01 g; 0.045 mmol; 1 eq) were dissolved in 20 mL of anhydrous methanol. The reaction

mixture was heated under reflux and argon atmosphere for 15 h. The reaction was stopped when no peak related to the free ligand (**L6**) was observed in the mass spectrum and no spot related to the free ligand (**L6**) was observed on TLC plate. The reaction mixture was allowed to cool back to room temperature and was poured into cold diethyl ether (20 mL). The precipitated was dissolved in distilled water (5 mL) and the sample was freeze-dried. The mixture was centrifuged and the ether was poured off the yellow precipitate. The complex (**EuL6**) was obtained as yellow solid in 87% yield (34 mg). **EuL6** was characterized via mass spectrometry and absorption and emission spectroscopy. λ_{max} = 275 nm, λ_{max} = 452 nm; MS (MALDI) *m/z*: $[L6+Eu+5H_2O+Cl]^{2+}$ Calcd for $[C_{41}H_{66}Cl^{153}EuN_6O_{14}]^{2+}$ 527.1764; Found 526.5.

2.1.29 Complexation of L7 with Eu(III): synthesis of EuL7

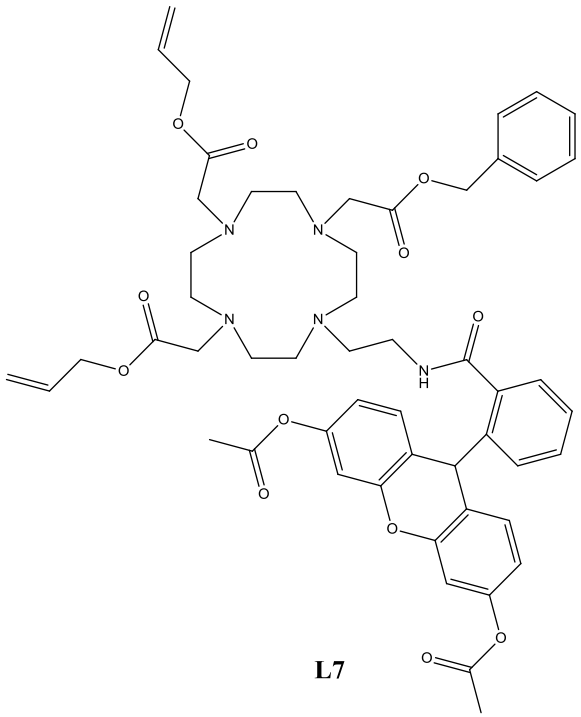

L7

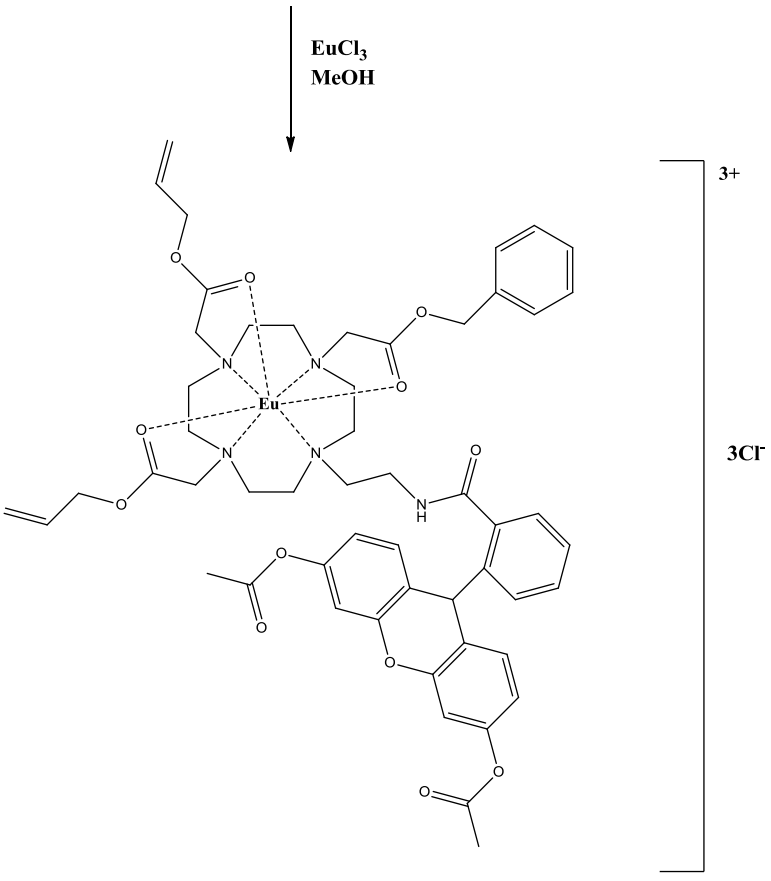

Desired product EuL7

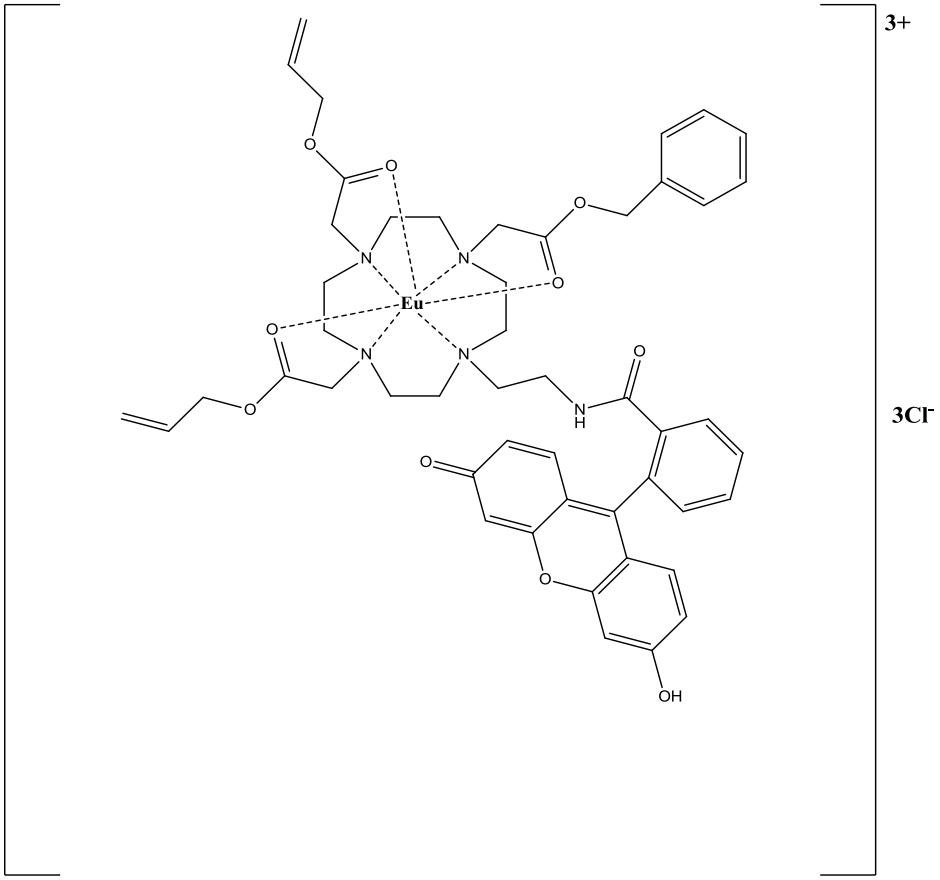

Observed product EuL7

Synthetic procedure:

The ligand (**L7**) (0.04 g; 0.036 mmol; 1 eq) and anhydrous europium chloride ($EuCl_3$) (0.01 g; 0.036 mmol; 1 eq) were dissolved in 20 mL of anhydrous methanol. The reaction mixture was heated under reflux and argon atmosphere for 15 h. The reaction was monitored through ESI mass spectrometry via direct injection and TLC (DCM/isopropylamine 95:0.5). The reaction was stopped when no peak related to the free ligand (**L7**) was observed in the mass spectrum and no spot related to the free ligand (**L7**) was observed on TLC plate. The reaction mixture was allowed to cool back to room temperature and was poured into cold diethyl ether (20 mL). The mixture was centrifuged and the ether was poured off the pale yellow precipitate. The precipitated was dissolved in distilled water (5 mL) and the sample was freeze-dried. The complex (**EuL7**) was obtained as pale yellow solid in 90% yield (0.04 g). **EuL7** was characterized via mass

spectrometry and absorption and emission spectroscopy. λ_{max} = 280 nm, λ_{max} = 309 nm, λ_{max} = 483 nm; MS (MALDI) *m/z*: $[L7+Eu+Cl-2COCH_3]^+$ Calcd for $[C_{49}H_{54}Cl^{153}EuN_5O_{10}]^+$ 1060.2766; Found 1060.5.

2.2 Assay Protocols

2.2.1 Mitochondrial Isolation

Mitochondria were prepared from the livers of control using the Qproteome™ Mitochondria Isolation kit (Qiagen, Limburg, Netherlands) according to the manufacturer's instructions with minor modifications. Briefly, 1.3 g of liver was minced using a scalpel prior to homogenisation in ice cold lysis buffer using a Qiagen Tissue Ruptor. The homogenate was incubated on an end-over-end shaker for 10 minutes at 4°C prior to centrifugation at 1300 g for 13 minutes. The resulting pellet was resuspended in disruption buffer firstly by gentle pipetting and secondly using a Dounce homogenizer (4 strokes at 200 rpm). The resulting lysate was centrifuged at 1000g for 13 minutes with the resulting supernatant washed and pelleted twice at 6000g for 13 minutes. The crude mitochondrial pellet was finally resuspended in Incubation Buffer B (130 mM sucrose, 50 mM KCl, 2.5 mM KH_2PO_4 and 5 mM N-2-hydroxyethylpiperazine-N'-2-ethanesulfonic acid [HEPES], pH7.4 with KOH) and protein content was measured using a bicinchoninic acid (BCA) protein assay kit (Pierce, Rockford, IL, USA).

2.2.2 Calcium Retention Capacity

Mitochondria were suspended at 0.2mg/ml in Incubation Buffer B, supplemented with 100 µM arsenazo III, 2.5 µM rotenone and 1 µg/mL oligomycin in each well of a 96 well microplate and absorbance measured every 2 seconds at 650 nm in a FlexStation3 microplate reader (Molecular Devices, Sunnyvale, CA, USA). After approximately 1

minute of reading, Ca^{2+} was added (1µmol/mg mitochondrial protein) shortly followed by the addition of 10 mM succinate as the mitochondrial substrate. The CRC was calculated as the difference in optical density (ΔOD) between the point at which mitochondria were energised and were undergoing mitochondrial permeability transition (i.e. the lowest OD reading following calcium release via MPT).

The direct effect of complexes (**EuL1**, **TbL1**, **EuL2**, **TbL2**, **NdL3**, **YbL3**, **EuL4** and **TbL4**) on CRC was examined as above by treating freshly isolated mitochondria with prior exposure to compounds **EuL1**-**TbL4**. All complexes were added in a six point concentration range (250 µM, 125 µM, 62.5 µM, 15.6 µM, 3.9 µM and 0.97 µM) alongside 0.5% DMSO (vehicle control) and 1 µM cyclosporine A (mPTP inhibitor positive control) to the mitochondrial suspension prior to reading. And the effect of the compounds on CLC assessed as above.

2.2.3 Measurement of Oxygen Consumption Rate in HepG2 Cells

Human hepatocellular liver carcinoma (HepG2) cells were obtained from the European collection of cell cultures (ECCAC, Sailsbury UK). Cells were grown in DMEM medium (Invitrogen #11966) supplemented with 10 mM galactose, 100 µM sodium pyruvate, 5 mM HEPES, 2 mM GlutaMAX, 10% fetal bovine serum and 5 µg/ml gentamycin. Cells were maintained in a 37°C, 5% CO_2 humidified atmosphere. HepG2 cells were seeded in an XF96-well plate at 20,000 cells / 80 µL cell culture medium / well and incubated in a 37°C, 5% CO_2 humidified atmosphere for 24 hours. Following incubation the culture medium was replaced with 175 µL pre-warmed, serum-free XF Base Assay Media (Seahorse Bioscience, Billerica, MA), supplemented with 2 mM L-glutamine, 1 mM sodium pyruvate and 10 mM glucose (pH 7.4) and incubated at 37°C for one hour. Compounds **EuL1**-**TbL4** were maintained in DMSO and a five point dose response (200 µM – 0.8 µM), plus 0.1% DMSO control, was diluted to 8X concentration in XF Assay media and 25 µL was loaded into Port A of the XF Assay Cartridge (2 technical replicates

per concentration of Compound / DMSO control). Oligomycin (2 µM final), FCCP (0.25 µM final) and antimycin A / rotenone (1 µM final) were loaded into ports B, C and D at 9X, 10X and 11X concentrations respectively (all 25 µL volume). Following calibration of the XF Assay Cartridge, the cell plate was inserted into the analyser and 2 basal measurements were made using a 3 minute mix, 3 minute measure protocol. The compounds were then injected pneumatically into each well from ports A-D (compounds **EuL1** to **TbL4** first followed by mito-stress test compounds) with ten, 1 minute mix, 2 minute measure cycles performed over a 1 hour incubation with compounds **EuL1**-**TbL4**. This was followed by three 2 minute mix 2, minute measure cycles following each injection with the exception of AA/Rot which had two 2 minute mix and 2 minute measure cycles. Data is expressed in pmol/min OCR and represent the mid-point of each measurement period.

2.2.4 Cellular ROS assay protocol

100000 cells per well were seeded and left to incubate at 37°C with 5% CO_2 overnight in DMEM+Glutamax medium supplemented with 10% FBS (serum) and 1% P/S (penicillin/streptomycin) in a 96 wells per plate. The following day the cells were exposed to H_2O_2 50 µM and TBHP 150 uM and incubated for 30 minutes at 37°C. After 30 minutes of incubation, the H_2O_2 and TBHP solutions were removed and replaced with the **EuL4** and **EuL5** at concentrations of 1 µM, 10 µM and 100 µM, and with the Mitosox at 2.5 µM and 5 µM concentrations. The medium was removed from other cells that were not previously exposed to H_2O_2 and TBHP and replaced with **EuL4** and **EuL5** at concentrations of 1 µM, 10 µM and 100 µM and Mitosox at 2.5 µM and 5 µM concentrations. Mitosox was used as positive control. After 30 minutes the plates were read with a microplate reader. Second time reading was made by washing all wells twice with HBSS, a transparent medium.

3. Results and Discussion: design and synthesis of lanthanide complexes based on asymmetrically substituted cyclen ligands

This chapter describes how lanthanide complexes based on asymmetrically substituted cyclen ligands were designed in order to produce molecular sensors able to signal the presence of ROS species. A detailed description of the synthetic routes that were applied to the synthesis of these molecular sensors is provided. Two different synthetic routes were used to synthesize the final asymmetrically substituted cyclen-based ligands before the complexation with the lanthanide ions. The first synthetic route was based on the direct and selective N-alkylation of four pendant arms on the cyclen ring. This synthetic approach required that the pendant arms had to be synthesised separately and then could be used for the direct N-alkylation. This route presented many issues such as very low yields, due to the low stability of the products during the purification by column chromatography. In order to overcome the issues encountered with the first synthetic route, a new synthetic scheme based on a different synthetic approach was developed. It involved the synthesis of an intermediate ligand that was called “the generic ligand” since it possesses a chemical structure that could be modified in many ways in order to produce different types of ligands. The generic ligand was designed and synthesised by exploiting an orthogonal protection strategy (Scheme 3.1). Starting from the generic ligand and selectively removing the protecting groups attached to it, it was possible to synthesise different types of asymmetrically substituted cyclen based ligands.

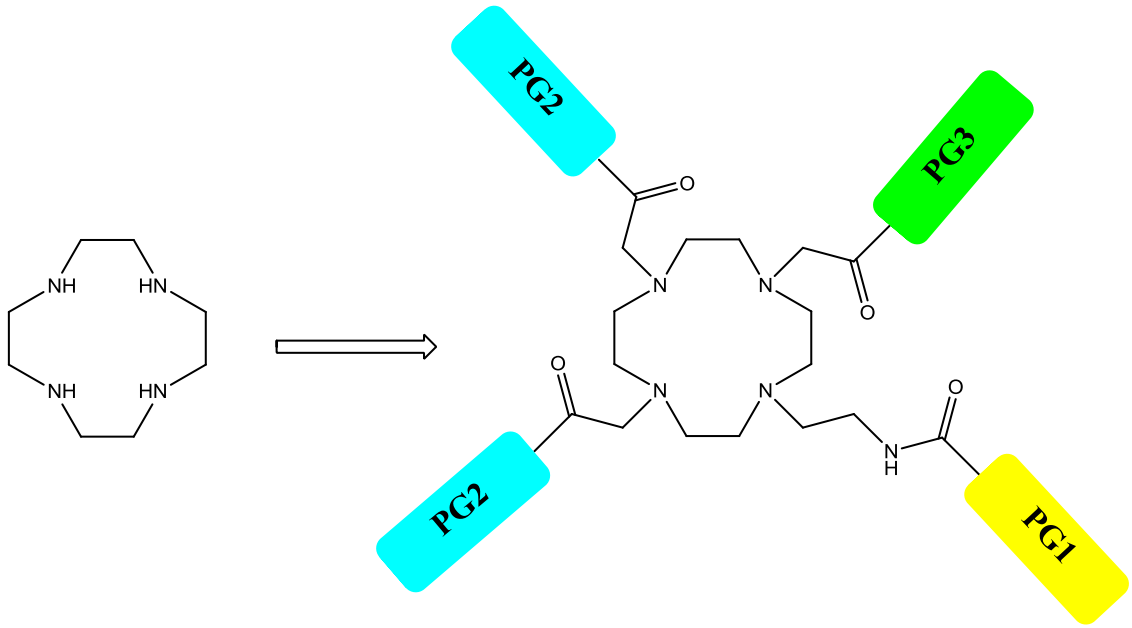

Scheme 3.1 A strategy for the synthesis of asymmetrically substituted cyclen based on orthogonal protecting groups (PG).

3.1 Designing ROS-responsive luminescent lanthanide complexes based on asymmetrically substituted cyclen-based ligands.

Taking advantage from the lanthanide complexes based on asymmetrically substituted cyclen ligands developed by Bruce and co-workers. [37], [38], which were examined in the chapter 1, a series of lanthanide complexes based on asymmetrically substituted cyclen ligands were designed in this project in order to develop ROS-responsive luminescent probes. The general structure of the lanthanide complexes designed in this project is shown in Figure 29.

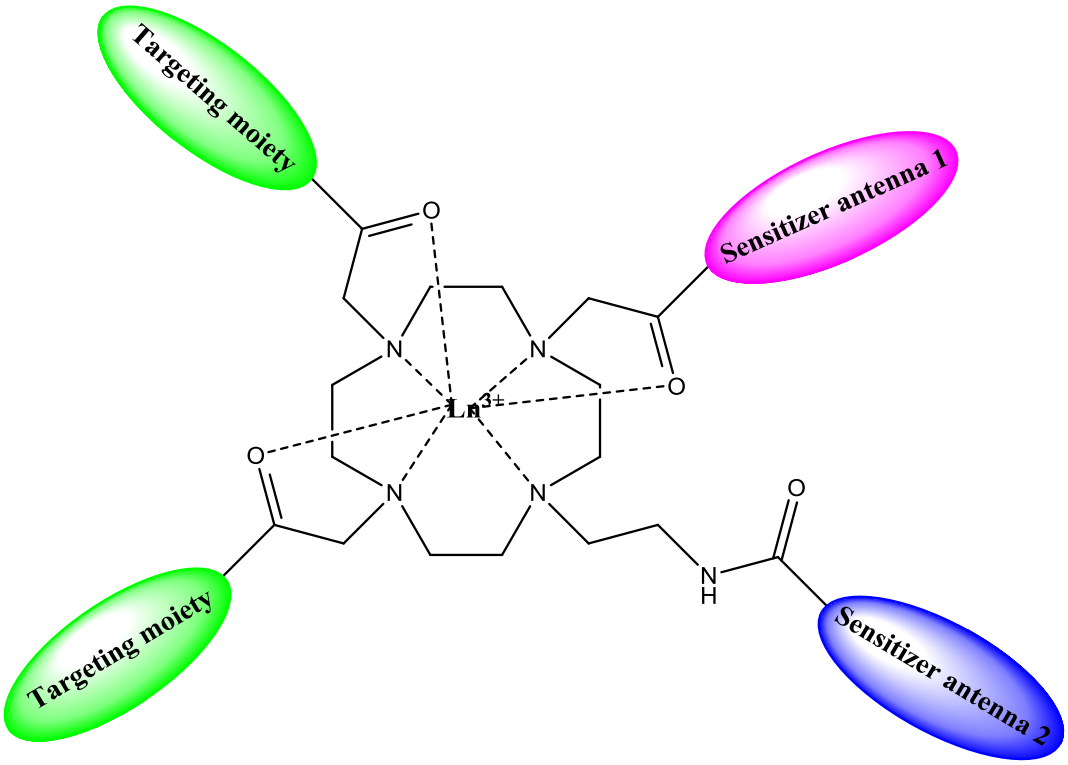

Figure 29. A cartoon representation of the general structure of a lanthanide complex based on asymmetrically substituted cyclen ligand that was designed to be responsive to ROS species.

The ligand structure of the molecular system shown in Figure 29 is formed by an asymmetrically substituted cyclen bearing four pendant arms. Two arms containing targeting molecules were introduced on the cyclen ring in order to increase the permeability of the complex through the cellular and mitochondrial membranes. This was to allow not only to achieve a high concentration of the complex within the cells, but also to target it to the mitochondria that represent the targeted organelles since, as discussed in the chapter 1, they are the main source of ROS. The other two moieties attached to the cyclen ring were two chromophore antennae that were chosen to act as sensitizers towards the trivalent lanthanide ion and in meantime to be able to sense the presence of ROS species. In this system one of the two antennae, for example antenna 2, could be an organic chromophore, such as a fluorescein or coumarin derivative, which acts as sensitizer of the trivalent lanthanide ion and in the meantime should be oxidized by a ROS species, such as H_2O_2 or OH•. The oxidation of antenna 2 by a ROS species should

cause changes in its photophysical properties that in turn should cause changes in the lanthanide emission. In fact, a quenching or an enhancement and/or spectral form changes of lanthanide emission could take place as results of changes of photophysical properties of the sensitizer antenna. This means that changes in the lanthanide emission are indicative of the presence of ROS species. The other antenna introduced on the cyclen ring, namely antenna 1, should be able to reduce back the antenna 2 thus restoring its reduced form that can react again with other ROS species. Moreover, the sensitisation of the lanthanide ion achievable by using two sensitizer antennae could be more effective than the sensitisation achievable by using one antenna, and using two antennae allows a wider wavelength range. Finally, the three carbonyl functions present on three pendant arms of the cyclen ring participate together with the four nitrogen atoms of the cyclen ring to the coordination of the trivalent lanthanide ion.

3.2 Design and synthesis of the first asymmetrically substituted cyclen-based ligand

An asymmetrically substituted cyclen-based ligand was designed at the beginning of this project in order to have all the properties mentioned in the section 3.1 that would have allowed the development of a ROS responsive molecular sensor. The chemical structure of this ligand is shown in Figure 30.

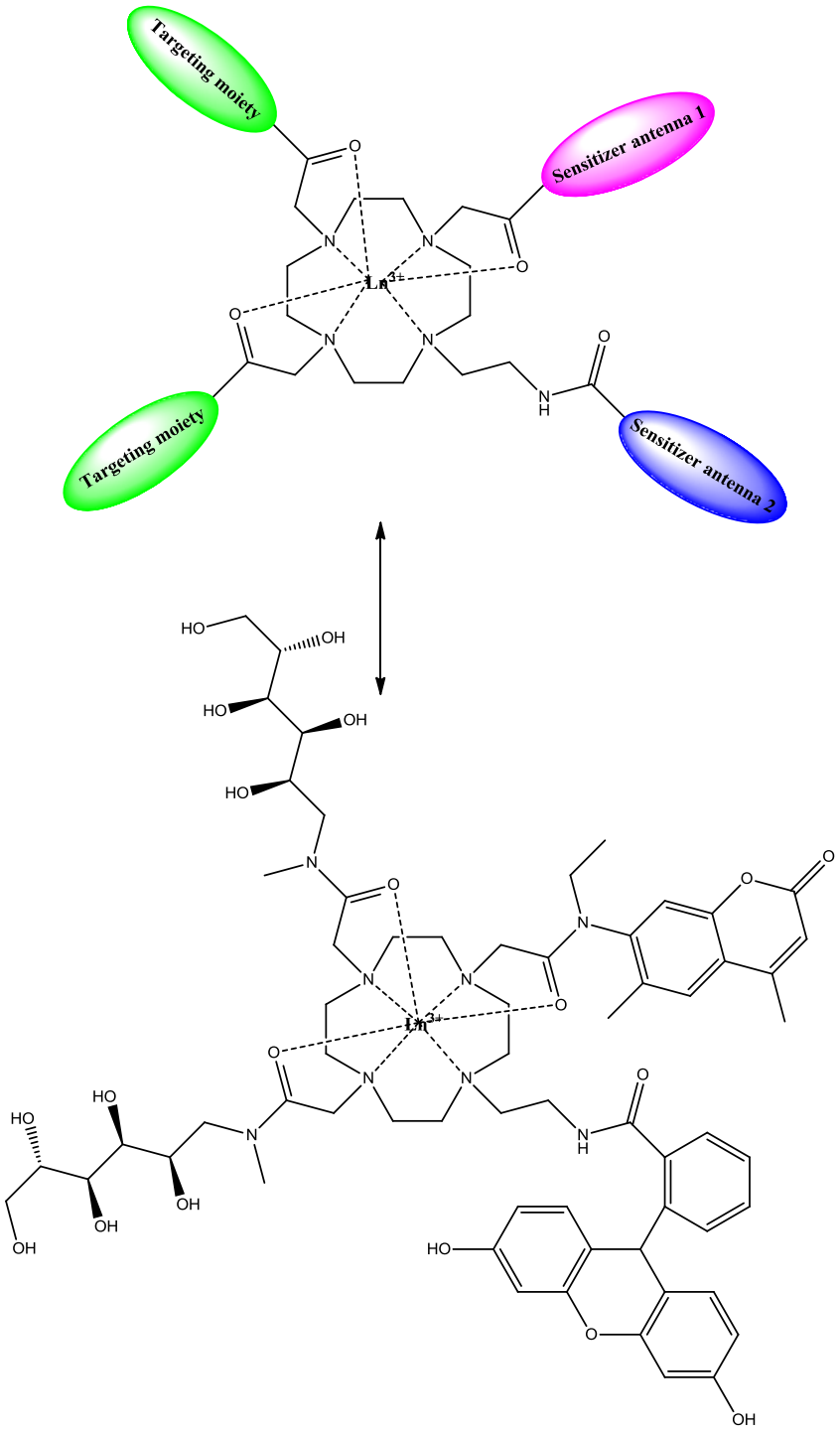

Figure 30. The first asymmetrically substituted cyclen-based ligand designed in this project.

The ligand shown in Figure 30 is formed by an asymmetrically substituted cyclen to which four pendant arms are attached. The two arms containing the N-methyl-L-glucamine derivative were chosen in order to increase the hydrophilicity of the ligand thanks to the presence of ten hydroxyl functions thus making the ligand an amphiphilic molecule. It

was thought that adding two high hydrophilic moieties like N-methyl-L-glucamine derivative would have provided the ligand with similar properties of plasma and mitochondria membranes, facilitating its diffusion through these systems of membranes. It is well known that the plasma membrane as well as the mitochondrial membranes are formed by a phospholipid bilayer, which are amphiphilic molecules since they possess a hydrophilic phosphate head and a hydrophobic tail consisting of two fatty acid chains (C1-8). The synthetic route that was applied to the synthesis of the asymmetrically substituted cyclen-based ligand shown in Figure 30, is illustrated Figure 31. The synthetic approach used in this synthetic route required that the pendant arms of the cyclen had to be synthesised separately and then could be used for the N-alkylation reaction thus allowing the functionalization of the cyclen ring.

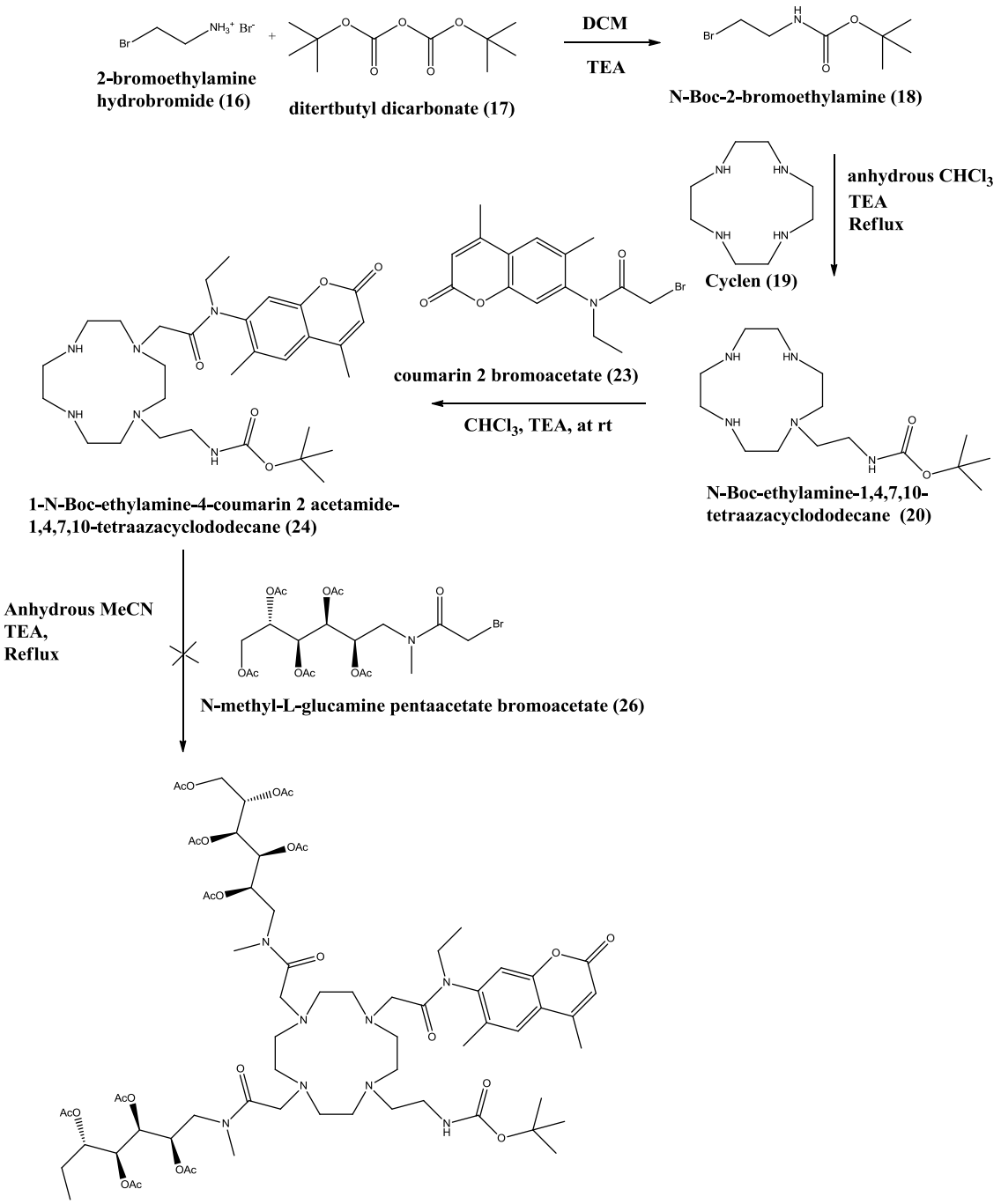

1-N-Boc-ethylamine-4-coumarin 2-acetamide-7,10-di-N-methyl-L-glucamine pentaacetate-N-acetamide-1,4,7,10-tetraazacyclododecane (27)

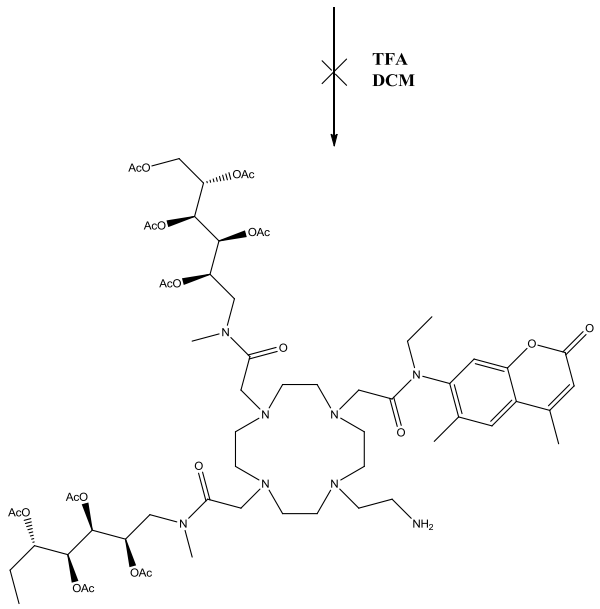

1-ethylamine-4-coumarin 2-acetamide-7,10-di-N-methyl-L-glucamine pentaacetate-N-acetamide-1,4,7,10-tetraazacyclododecane (28)

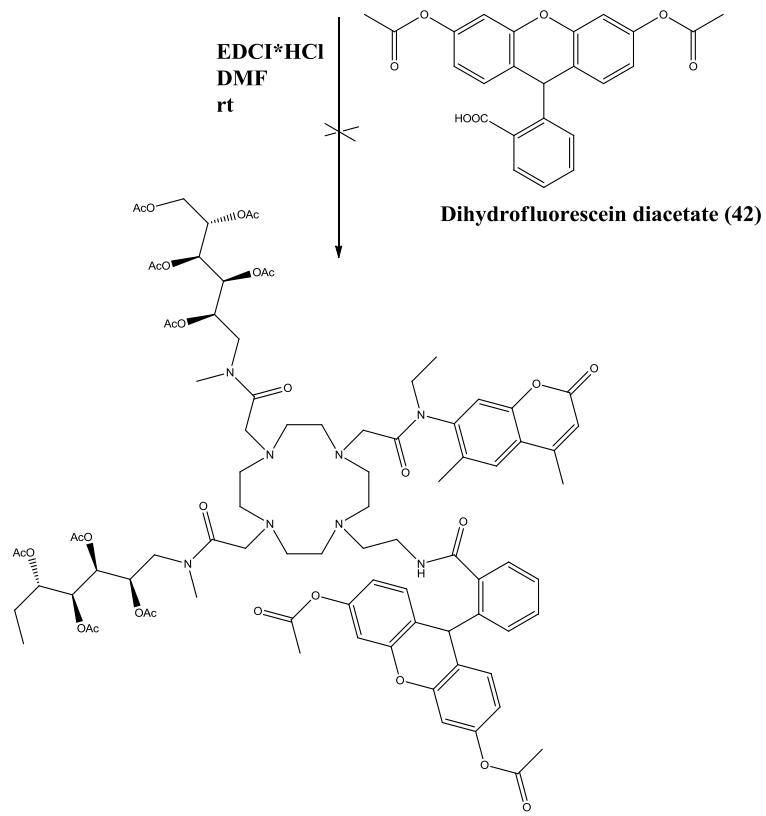

Dihydrofluorescein diacetate (42)

1-ethylamide-dihydrofluorescein diacetate-4-coumarin 2-acetamide-7,10-di-N-methyl-L-glucamine pentaacetate-N-acetamide-1,4,7,10-tetraazacyclododecane (30)

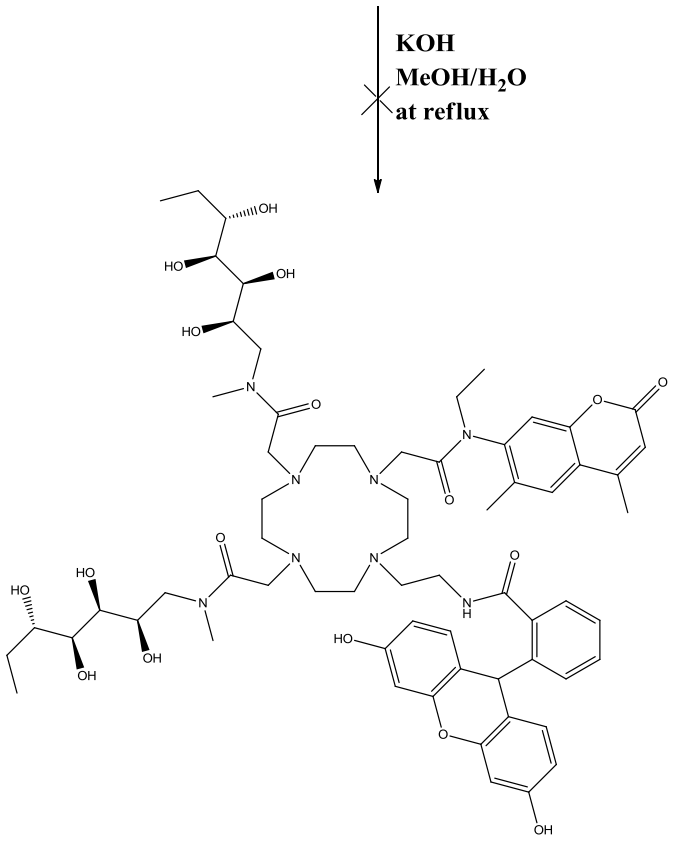

1-ethylamide-dihydrofluorescein-4-coumarin 2-acetamide-7,10-di-N-methyl-L-glucamine-N-acetamide-1,4,7,10-tetraazacyclododecane (31)

Figure 31. Schematic representation of the synthetic route applied to the synthesis of the 1-ethylamide-dihydrofluorescein-4-coumarin 2-acetamide-7,10-di-N-methyl-L-glucamine-N-acetamide-1,4,7,10-tetraazecyclododecane **(31)**.

The synthetic route started with the synthesis of the N-Boc-2-bromoethylamine **(18)**, which was synthesised starting from the bromoethylamine hydrobromide **(16)** and di-*tert*butyl dicarbonate **(17)**. This reaction allowed the introduction of the Boc group on the amino function to protect it and prevent it from reacting during the following steps. The protection of the primary amino function with the Boc group was essential in order to prevent its participation during the following N-alkylation reactions of the cyclen ring. In fact, if the reactivity of the amino function had not been properly masked by a protecting group (such as the Boc group), then the amino function would have competed with the secondary amino functions of the cyclen ring during the nucleophile substitution

reactions employed for the cyclen ring functionalization. The Boc group is widely used to protect amino functions and is stable towards most nucleophiles and bases. It is usually removed using moderate acidic conditions such as trifluoroacetic acid in DCM [58], [59].

3.2.1 Synthesis of the N-Boc-ethylamine-1,4,7,10-tetraazacyclododecane (20)

The N-Boc-2-bromoethylamine **(18)** was then introduced on the cyclen **(19)** ring to obtain the N-Boc-ethylamine-1,4,7,10-tetraazacyclododecane **(20)** through a mono alkylation reaction. The first attempt to obtain the monosubstituted cyclen **(20)** was made using both the cyclen and the N-Boc bromoethylamine in 1:1 ratio, anhydrous chloroform as solvent and triethylamine as base. This reaction turned out to be not selective since a complex mixture of mono-, di-, and tri- substituted cyclen was observed during the monitoring of the crude mixture with TLC (DCM/isopropylamine 9.5:0.5) and NMR spectroscopy. The formation of mono-, di-, and tri- substituted cyclen suggested that the reactivity of the cyclen and the mono- and di- substituted cyclen was approximately the same. Unfortunately many attempts to purify the monosubstituted cyclen and recover it through column chromatography were made, using different combinations of eluents and stationary phase, but all failed (Table 1).

Mobile phase	Stationary phase
hexane/ethyl acetate (80:20)	Silica gel
DCM/isopropylamine (from 0.5 to 10%)	Silica gel
DCM/methanol (90:10)	Silica gel
hexane/ethyl acetate (80:20)	Alumina gel
DCM/isopropylamine (from 0.5 to 10%)	Alumina gel
DCM/methanol (90:10)	Alumina gel

Table 1. Combination of solvents and stationary phases used to purify the reaction mixture obtained with the first procedure applied to the synthesis of the monosubstituted cyclen.

The combinations of solvents used as mobile phase were: hexane/ethyl acetate (80:20), DCM/isopropylamine (from 0.5 to 10%) and DCM/methanol (90:10). Silica and alumina gel were used as stationary phase with the combinations of solvents mentioned above but no product was recovered from the column. In order to overcome the issue related to the impossibility of recovering the monosubstituted cyclen from the column chromatography, a different synthetic procedure, which did not require the purification by column chromatography, was used [60]. According to the new procedure applied to the synthesis of the monosubstituted cyclen, 5 equivalents of cyclen per equivalent of N-Boc-2-bromoethylamine were used as starting material [60]. The reaction was carried out in anhydrous $CHCl_3$, under argon atmosphere and kept under reflux conditions for 16 hours. The reaction mixture was monitored by TLC (DCM/isopropylamine 95:0.5) and mass spectrometry via direct injection. In particular, the TLC performed on the reaction mixture after 15 hours at reflux showed the presence of two spots: one spot was related to the excess of unreacted cyclen and the other spot was obtained to the alkylated cyclen formed during the reaction. No spot related to the N-Boc bromoethylamine was observed on the TLC confirming that the reaction went to completion. The results obtained with the mass spectrometry performed on the reaction mixture after 15 hours at reflux

confirmed the presence of two main peaks: one peak related to the excess of unreacted cyclen at *m/z* 173 and another peak at *m/z* $[M+1]^+$ 316, which corresponded to the monosubstituted cyclen. No peaks related to the di-, tri-, and tetrasubstituted cyclen were observed in the mass spectrum. The results obtained with the mass spectrometry were aligned with the results obtained with the TLC and confirmed that one of the two spots seen on the TLC plate was related to the monosubstituted cyclen. The results obtained with the TLC and mass spectrometry proved that the excess of cyclen used in the new procedure applied to the synthesis of the monosubstituted cyclen had proved to be effective in preventing the polyalkylation of the cyclen ring. The excess of unreacted cyclen was easily recovered from the aqueous phase after extracting the reaction mixture three times with a 2M NaOH aqueous solution [60]. The monosubstituted cyclen was recovered from the organic phase with a high degree of purity and without the necessity to perform column chromatography.

3.2.2 Synthesis of the coumarin 2 bromoacetate (23)

The following pendant arm that was introduced on the cyclen was the coumarin 2 bromoacetate **(23)**, which was synthesized from coumarin 2 and bromoacetic acid and using EDCI * HCl as coupling agent and DCM as solvent at room temperature [61]. The reaction was performed six times using each time different equivalents of EDCI*HCl and bromoacetic acid per equivalent of coumarin 2 as shown in the Table 2.

Coumarin 2 (eq)	Bromoacetic acid (eq)	EDCI*HCl (eq)	Reaction time (hour)	Yield %
1	1	1	24	reaction not complete
1	2	2	24	reaction not complete
1	3	3	24	reaction not complete
1	4	4	24	reaction not complete
1	5	5	24	reaction not complete
1	6	6	24	84

Table 2. Reaction conditions used during the peptide coupling reaction that lead to the synthesis of the coumarin 2 bromoacetate **(23)**.

When 1-5 equivalents of bromoacetic acid and EDCI*HCl were used the reaction did not go to completion when observed using TLC. After 24 hours there was still decreasing amounts of unreacted coumarin 2 present. It was found that the reaction went to completion when 6 equivalents of bromoacetic acid and 6 equivalents of EDCI*HCl per equivalent of coumarin 2 were used. This was shown by the TLC results related to the reaction monitoring, where no spot related to the unreacted coumarin 2 was observed after 24 hours.

3.2.3 Synthesis of the 1-N-Boc-ethylmine-4-coumarin 2 acetamide-1,4,7,10-tetraazacyclododecane (24)

The coumarin 2 bromoacetate was introduced in the position 4 of the cyclen ring through a selective 1-4 N-alkylation [62] to obtain the 1-N-Boc-ethylmine-4-coumarin 2

acetamide-1,4,7,10-tetraazacyclododecane **(24)**. In order to obtain the 1-4 substituted cyclen, the coumarin 2 bromoacetate and **(20)** were reacted in a 1:1 ratio. The reaction was performed using 1.1 equivalents of TEA as base and anhydrous $CHCl_3$ as solvent and keeping the reaction mixture under argon atmosphere at room temperature. The 1-4 regioselectivity is observed in less polar and aprotic solvent such as chloroform at room temperature [62], [38]. This can be explained by the fact that after the first N-alkylation of the cyclen, the two N-H groups of the position number 4 of the cyclen ring will be intraannular and bonded through hydrogen bonds to the two lone pairs of the nitrogen atoms in position number 1 and 7. This means that the lone pair of the nitrogen atoms in position number 7 will be intraannular and so not available to act as nucleophile during the alkylation reaction. The only lone pairs that can act as nucleophile and be further alkylated are the ones in position number 4, since they are extraannular [62]. The 1-4 disubstituted cyclen **(24)** was purified through column chromatography using a combination of DCM and isopropylamine from 0.5 to 5% as eluent.

3.2.4 Synthesis of the 1-N-Boc-ethylamine-4-coumarin 2 acetamide-7,10-di-N-methyl-L-glucamine pentaacetate-N-acetamide-1,4,7,10-tetraazacyclododecane (27)

The two pendant arms of N-methyl-L-glucamine pentaactetate bromoacetate **(26)** that had to be introduced on the 1-4 disubstituted cyclen **(24)** were synthesized separately in a two-step reaction. The first step was the synthesis of the N-methyl-L-glucamine pentaactetate-bromoacetate **(26)**, which was a peptide coupling reaction, performed using bromoacetic acid and N-methyl-L-glucamine as starting materials and EDCI as coupling reagent [61]. The second step was the protection of the five hydroxyl functions with acetate protecting group. This reaction was performed by dissolving the crude mixture obtained with the first step in dry pyridine and adding an excess of acetic anhydride in small portions [63]. The excess of acetic anhydride was consumed by the addition of water and the compound was recovered into the organic layer after first

extracting the reaction mixture with DCM and water and then with DCM and diluted acidic aqueous solution. Three attempts (Table 3) to introduce the two arms of the N-methyl-L-glucamine pentaactetate-bromoacetate **(26)** in position 7 and 10 of **(24)** through a direct N-alkylation reaction were made but all were unsuccessful since no signal of the two N-methyl-L glucamine pentaacetate moieties were found in the proton NMR spectra performed on the crude mixtures obtained from each attempt. The reaction was generally performed using one equivalent of **(24)**, two equivalents of N-methyl-L-glucamine pentaactetate-bromoacetate **(26),** TEA as base and anhydrous acetonitrile as solvent and the reaction mixture was kept under argon atmosphere under reflux conditions [37].

1-4 disubstituted cyclen (1 eq)	**N-methyl-L-glucamine pentaactetate bromoacetate (2 eq)**	**TEA (eq)**	**Reaction Time (hour)**	**Product: (27)**
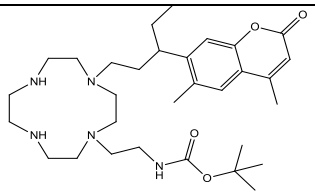	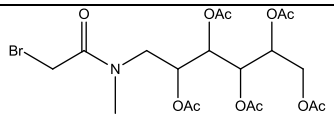	**2**	**12**	-
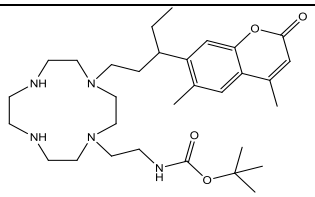	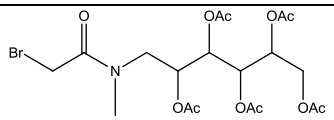	**5**	**24**	-
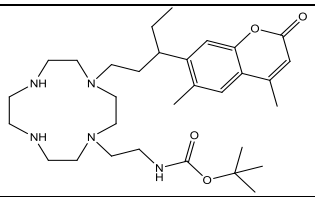	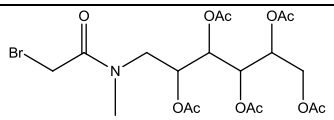	**10**	**36**	-

Table 3. The three attempts were made to synthesize the 1-N-Boc-ethylamine-4-coumarin 2 acetamide-7,10-di-N-methyl-L-glucamine pentaacetate-N-acetamide-1,4,7,10-tetraazacyclododecane **(27)**.

As it shown in Table 3, the first attempt of introducing two moieties of N-methyl-L glucamine pentaacetate-bromoacetate **(26)** on the 1-4 disubstituted cyclen **(24)** was made using 2 equivalents of TEA per equivalent of 1-4 disubstituted cyclen **(24)** and

keeping the reaction under argon atmosphere under reflux conditions for 12 hours. The proton NMR spectroscopy performed on the crude mixture obtained from this reaction did not show the peaks related to hydrogen atoms of the N-methyl-L-glucamine pentaacetate-bromoacetate **(26)** moieties, indicating that no product was formed. This could be due to the fact that the reaction conditions used to perform the reaction were not suitable to introduce the two moieties of N-methyl-L glucamine pentaacetate-bromoacetate **(26)** in position 7 and 10 of the 1-4 disubstituted cyclen **(24).** The reaction was repeated again increasing both the amount of TEA and the reaction time. In particular, 5 equivalents of TEA per equivalent of 1-4 disubstituted cyclen **(24)** were used and the reaction mixture was kept 24 h at reflux. Unfortunately the proton NMR spectrum of the reaction mixture after 24 hours at reflux, did not show the peaks related to the hydrogens of the N-methyl-L-glucamine pentaacetate-bromoacetate **(26)** moieties, indicating that also in this case no product was formed. The reaction was repeated again increasing the amount of TEA up to 10 equivalents per equivalent of 1-4 disubstituted cyclen **(24)** and the reaction time up to 36 hours (Table 1). Even in this case the proton NMR performed on the reaction mixture did not revealed the presence of hydrogen atoms related to the N-methyl-L-glucamine pentaacetate-bromoacetate **(26)** moieties, indicating that no product was formed. This suggested that probably the N-methyl-L glucamine pentaacetate-bromoacetate **(26)** was not stable to the reaction conditions used for running the reaction. It could be possible that the conditions caused a decomposition of the N-methyl-L glucamine pentaacetate-bromoacetate **(26)**, explaining why the proton NMR spectra related to the reaction mixtures obtained from the three attempts made to synthesize the 1-N-Boc-ethylamine-4-coumarin 2-acetamide-7,10-di-N-methyl-L-glucamine pentaacetate-N-acetamide-1,4,7,10-tetraazacyclododecane **(27)** did not show the peaks related to the hydrogen atoms of the N-methyl-L glucamine pentaacetate-bromoacetate **(26).** It was also thought the steric hindrance of the two N-methyl-L glucamine pentaacetate-bromoacetate **(26)** moieties could in some way prevent the N-alkylation reaction of the 1-4 disubstituted cyclen **(24)** from taking place.

3.3 The second synthetic route applied to the synthesis of asymmetrically substituted cyclen-based ligands

Based on the hypothesis that the N-methyl-L-glucamine pentaacetate-bromoacetate **(26)** was not stable under reflux conditions used for the direct N-alkylation, it was replaced by another moiety, which was thought to be stable under reflux conditions. In particular, two moieties of a lipophilic triphenylphosphonium cation were used. Moreover, based on the hypothesis that the steric hindrance of the two N-methyl-L-glucamine pentaacetate-bromoacetate **(26)** moieties could be responsible for the failure of the direct N-alkylation reaction, a different synthetic approach for the synthesis of the asymmetrically substituted cyclen-based ligands was used. It involved the synthesis of an intermediate ligand, the 1-N-Boc ethylamine-4,7-diallyl acetate-10-benzyl acetate-1,4,7,10-tetraazacyclododecane (DABBC) **(36)**, which was called “the generic ligand” since it possesses a generic chemical structure that could be modified in many ways in order to produce different types of ligands. The chemical structure of DABBC **(36)** (generic ligand) is shown in Figure 32.

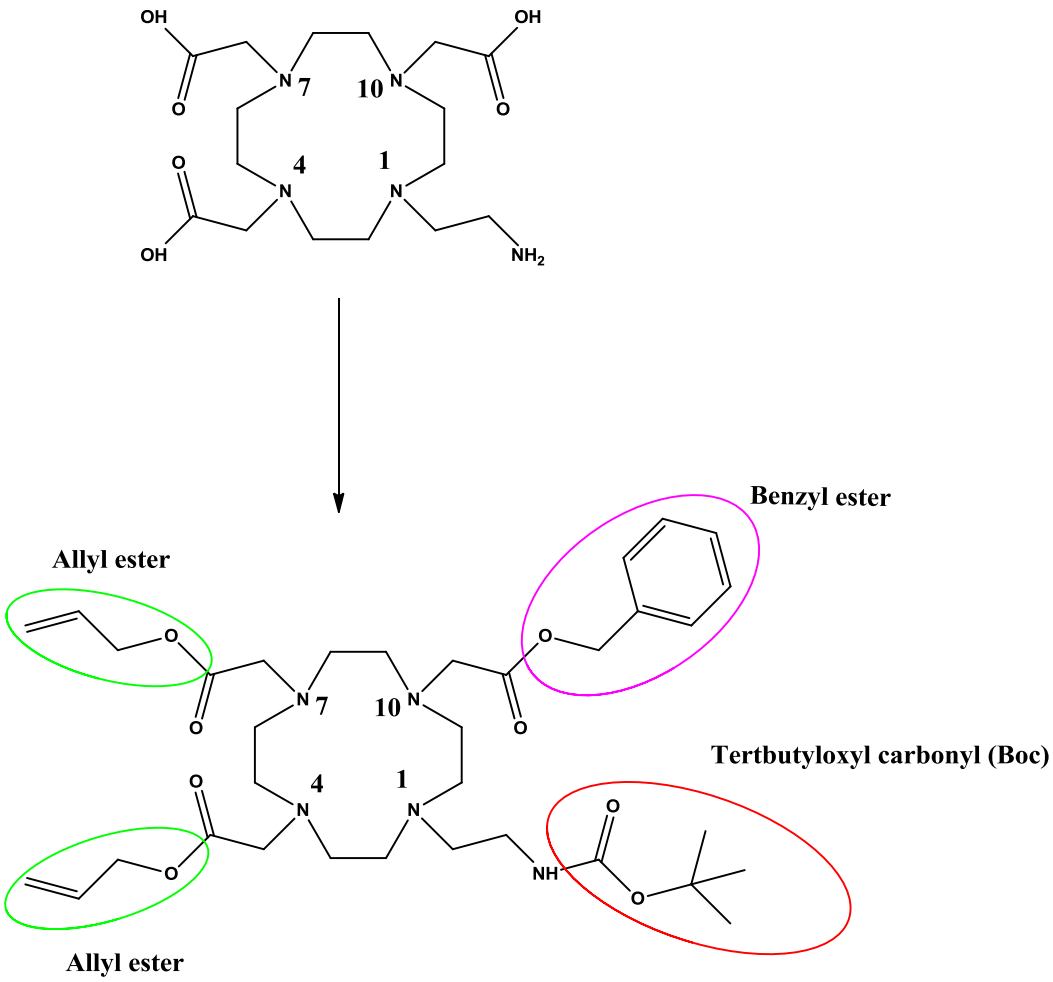

Figure 32. 1-N-Boc ethylamine-4,7-diallyl acetate-10-benzyl acetate-1,4,7,10-tetraazacyclododecane (DABBC) (Generic Ligand) **(36)**

The generic ligand **(36)** was designed and synthesized by exploiting an orthogonal protection strategy. Orthogonal protection is a synthetic strategy allowing the sequential deprotection of protective groups one at a time each with a dedicated set of reaction conditions without affecting the other [64]. The generic ligand was designed in a way that it contained three different protecting groups, used for masking the reactivity of carboxyl and amino functions. These protecting groups could be selectively and sequentially removed allowing to insert different pendant arms on the cyclen ring. The sequential attachment of different pendant arms to the cyclen ring, after that each protecting group has been removed, would allow to obtain an asymmetrically substituted cyclen-based ligand and could be achieved using a peptide coupling reaction. The peptide coupling

reaction could be performed using EDCI*HCl and HOBt as coupling agent and anhydrous DMF as the solvent. The three protecting groups that were chosen for the synthesis of the general ligand are: one Boc group, two allyl ester groups and one benzyl ester group. The two allyl ester groups were chosen to protect two of the three carboxylic functions shown in Figure 32. The two carboxylic functions protected via allyl ester were the ones on the pendant arms in position 4 and 7 of the cyclen ring. The esterification represents a useful and well established way to protect a carboxylic function and prevent its reactivity during the following steps of a multistep synthesis, such as the one involving the synthesis of peptides. There are many alcohols that can be used for esterifying carboxylic functions and the benzyl alcohol and the allyl alcohol are an example of alcohols widely employed for carboxylic functions esterification [65]. The Boc group was used to protect the primary amino function on the pendant arm in position 1 of the cyclen ring (Figure 32). The use of protecting groups able to mask the reactivity of the three carboxylic functions and the amino function was essential for the selective and sequential introduction of different pendant arms on the cyclen ring in order to achieve an asymmetrically substituted cyclen-based ligand. In fact, if the carboxylic and amino functions were not protected, they would have reacted during the subsequent peptide coupling reactions randomly, giving rise to many side products, which could be difficult to purify. The second synthetic route, which involved the synthesis of the intermediate generic ligand, presented two important advantages over the previous route:

1. Although the attachment of the pendant arms containing the protecting groups to the cyclen ring to obtain the generic ligand would involve reactions under reflux conditions, once the protecting groups are removed, the incorporation of the pendant arms can be achieved using a peptide coupling reaction. Since the coupling reaction is performed at room temperature, it can be applied when the starting materials are thought to be unstable to the high temperature required for the refluxing conditions, as hypothesized for the N-methyl-L-glucamine pentaacetate-bromoacetate **(26).**

2. The peptide coupling reactions are less susceptible to the steric hindrance compared to the nucleophilic substitution reactions and in some cases the peptide coupling is achievable using sterically hindered substrates [66]. The N-alkylation of the cyclen is a nucleophilic substitution reaction and as such it is widely affected by the steric hindrance of both substrates taking part in the reaction. In the case of the N-alkylation reactions applied to the functionalization of the cyclen, the latter acts as nucleophile and the pendant arm to be introduced, containing a bromine (or a chlorine) as leaving group, acts as electrophile. Although the peptide coupling reactions may be affected by steric hindrance of the substrates involved in the reaction, they are more influenced by the ability of the coupling agent to activate the carboxyl function. In the peptide coupling reactions, two substrates containing respectively a carboxyl function and an amino function are bound together via an amide (or peptide) bond. In order to make the reaction possible, it is necessary to increase the electrophilicity of the carboxyl function by converting it into a more reactive form [61]. This can be achieved by converting the carboxyl function into an acyl chloride (or bromide) or an activated ester. In the latter case a wide range of coupling agents are employed to convert the carboxyl function into an activated ester and among these the combination of HOBt, EDCI is one of the most effective [61]. The chance that the peptide coupling reactions could be applied sometimes to sterically hindered substrates represents an important advantage over the N-alkylation reaction since it would allow the functionalization of the cyclen ring using sterically hindered substrates, such as the ones containing bulky groups like triphenylphophonium cations.

3.3.1 Orthogonal protection strategy

This section describes the orthogonal protection strategy that was exploited to synthetize asymmetrically substituted cyclen based ligands and overcome the issues encountered with the first synthetic route discussed in the previous sections. An important advantage of the orthogonal protection strategy applied to the synthesis of the intermediate ligand, namely the DABBC or generic ligand **(36)** (Figure 32) is that it could be achieved in two different ways. One way is to start with the two allyl ester groups removal, using Pd(0)-catalyzed allyl transfer to diethylamine as the accepting nucleophile, also called a scavenger (Figure 33). The Pd(0)-catalyst can be generated in situ from $Pd(OAC)_2$ (palladium acetate) and TPPTS (triphenylphosphinotrisulfonate sodium salt) [71]. In chemistry, a scavenger is defined as a chemical substance that is added to a reaction mixture in order to remove or deactivate reactive intermediate formed during a reaction. In the specific case of the allyl ester deprotection, an excess of diethylamine is added in order to react with the allyl cations formed as result of the allyl ester bond breaking catalysed by the Pd(0). The deactivation of the allylic cations by using an excess diethylamine is important to prevent their reactivity during the reaction that may lead to the formation of unwanted side products. Under the reaction conditions used for the allyl ester removal, both the benzyl ester and the Boc groups should be unaffected. Once the allyl ester groups have been removed, it is possible to couple two moieties, bearing a primary or secondary amino function, to the free carboxylic acid functions using a peptide coupling reaction, such as the one involving EDCI*HCl and HOBt as coupling agents (Figure 33). Then the benzyl ester group can be cleaved in a selective manner using a catalytic hydrogenation reaction, which can be performed using 10% palladium on charcoal as catalyst and gaseous molecular hydrogen (H_2) as hydrogen donor (Figure 33). These reaction conditions should leave intact the Boc group. After the benzyl ester group deprotection, it is possible to couple another moiety containing a primary or secondary amino function that can take part in a peptide coupling with the free carboxylic function. Also in this case a peptide coupling reaction, involving the use of EDCI*HCl and

HOBt as coupling agents, could be applied. Finally, the Boc group can be removed in a mild acidic environment, using TFA and DCM. This reaction frees the amino function, whose reactivity had been masked by Boc group, and allows introducing another moiety, bearing a free carboxylic function, via peptide coupling reaction (Figure 33).

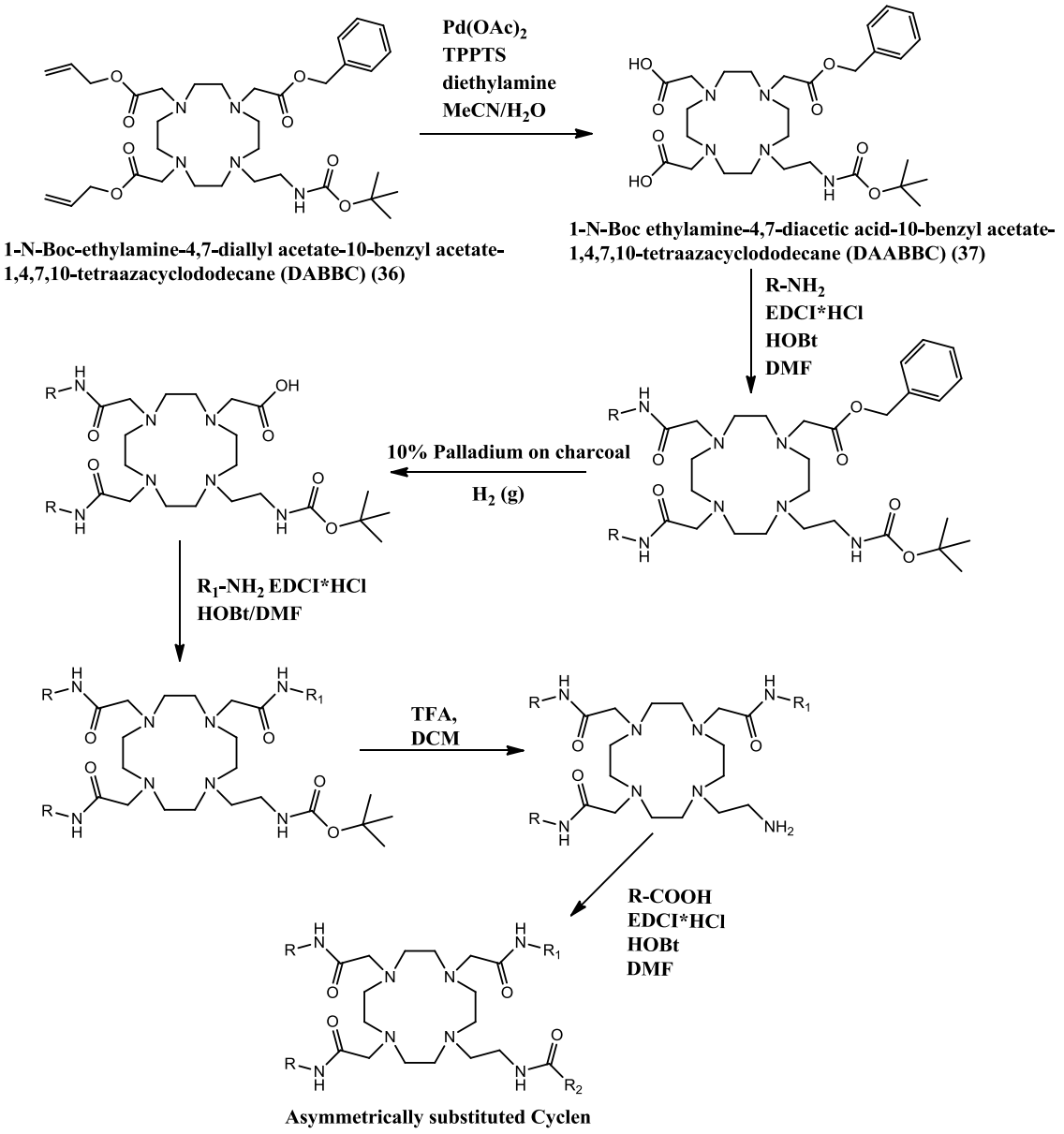

Figure 33. Schematic representation of an orthogonal deprotection strategy involving the generic ligand **(36)**.

The deprotection strategy descried so far can be applied only if the pendant arms that are sequentially added to the cyclen via peptide coupling reactions are stable to the mild acidic conditions used for the final Boc group removal. If one or more than one pendant arms used to functionalize the cyclen are unstable under the mild acidic condition used for the Boc deprotection, then an alternative orthogonal deprotection strategy is required. This can be achieved by changing the order by which the protecting groups are selectively removed from the generic ligand. An alternative orthogonal deprotection strategy, applied to the generic ligand to obtain asymmetrically substituted cyclen-based ligands, is shown in Figure 34. It starts with the selective removal of the Boc group using TFA and DCM, followed by the introduction of the acid labile moiety via a peptide coupling reaction. This should guarantee that one or more acid labile pendant arms can be introduced on the cyclen ring without being affected from the reaction conditions used in following steps. This is possible since the Boc group is the only protecting group among those that were used for the synthesis of the generic ligand that can be only removed in mild acidic conditions. Although the benzyl ester can be removed using a catalytic hydrogenation reaction, it can be also removed in acidic conditions. However in this case stronger acidic conditions are required for the deprotection compared to the mild acidic condition required for the Boc deprotection. The mild acidic conditions used for the Boc group cleavage should leave intact both benzyl ester and allyl ester groups. Once the Boc group has been cleaved and a pendant arm has been introduced via a peptide coupling reaction, the two allyl groups can be selectively removed (Figure 34). As discussed above, the two allyl ester groups can be removed using $Pd(OAc)_2$ and TPPTS as catalyst and an excess of diethylamine as scavenger. These reaction conditions should leave intact the benzyl ester group that can be removed, once two pendant arms have been introduced into the cyclen ring via a peptide coupling reaction to replace the two allyl ester groups. Finally, after the benzyl ester group removal via catalytic hydrogenation performed using 10% palladium on charcoal as catalyst and

gaseous molecular hydrogen (H_2) as hydrogen donor, it is possible to introduce a further pendant arm via a peptide coupling reaction.

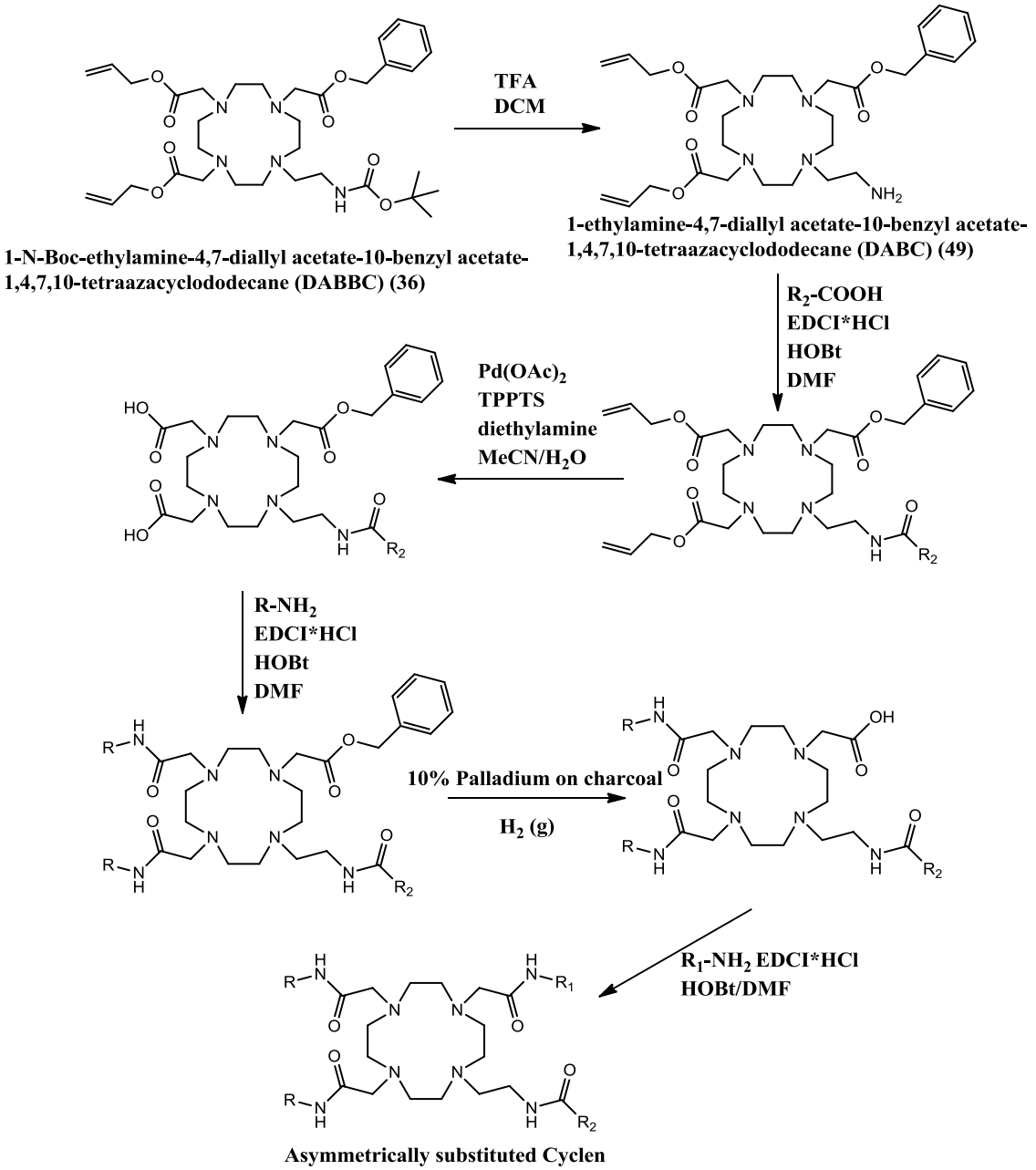

Figure 34. Schematic representation of an orthogonal deprotection strategy, applicable when using acid labile pendant arms.

The two orthogonal deprotection strategies discussed so far allow the synthesis of asymmetrically substituted cyclen ligands starting from the DABBC **(36)** (generic ligand).

The flexibility that can be achieved in terms of using two different types of orthogonal deprotection strategies allows a synthesis of several different asymmetrically substituted cyclen-based ligands starting from the same intermediate molecule of generic ligand. In the next section the synthetic route that was applied to the synthesis of the generic ligand will be discussed.

3.3.2 Synthesis of the 1-N-Boc-ethylamine-4,7-diallyl acetate-10-benzyl acetate-1,4,7,10-tetraazacyclododecane (DABBC) (36): the generic ligand

The synthetic route applied to the synthesis of the DABBC **(36)** or generic ligand is a multistep organic synthesis consisting of five steps (Figure 35). It requires that the four pendant arms attached to the general ligand have to be introduced via selective direct N-alkylation reactions. The arms in position 1, 4 and 7, containing respectively a Boc-protected amino function and two allyl ester groups (Figure 32), were synthetized separately, while the arm in position 10, containing the benzyl ester group (Figure 32), was commercially available.

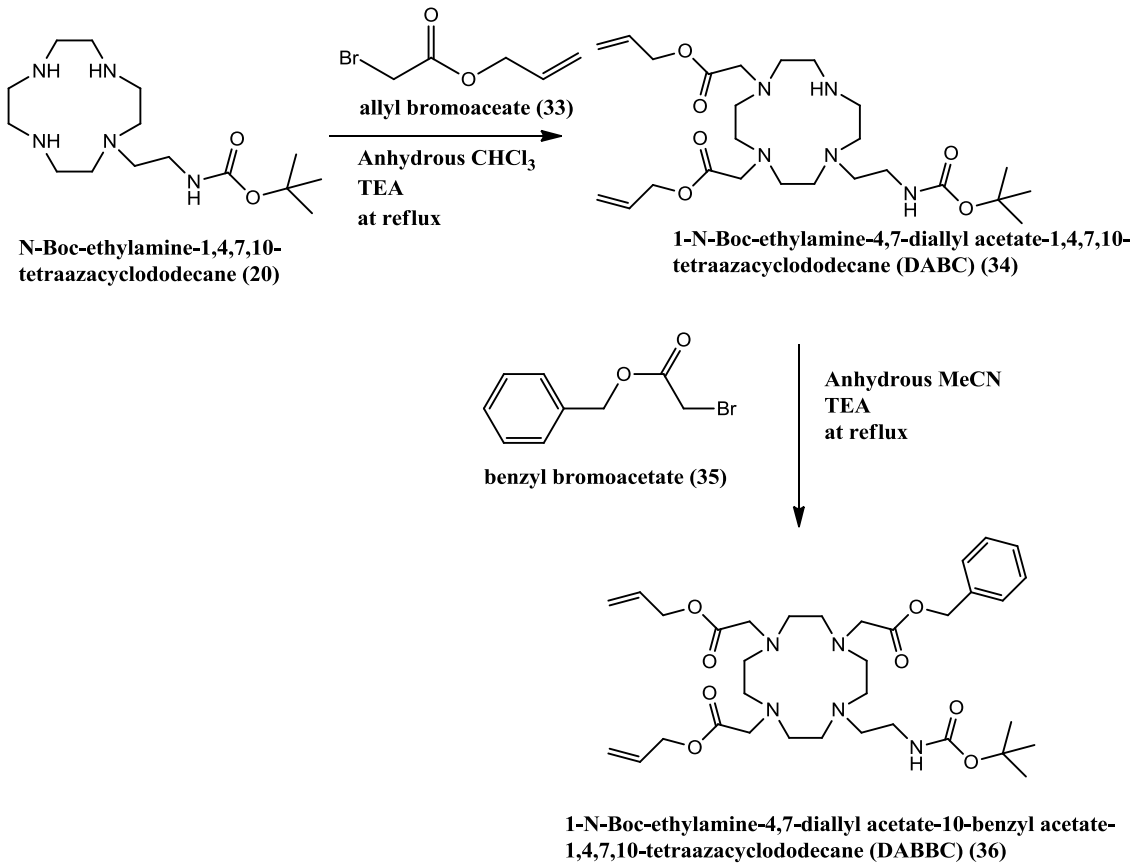

Figure 35. Synthesis of the 1-N-Boc-ethylamine-4,7 diallyl acetate-10-benzyl acetate-1,4,7,10-tetraazacyclododecane (DABBC) **(36)**.

The first two steps of the synthesis of the DABBC **(36)**, the generic ligand, were the same first two steps of the previous synthetic route, and are illustrated in the Figure 31 and described in detail in the section 3.1. The following three steps that led to the synthesis of the DABBC **(36)** (generic ligand) starting from N-Boc-ethylamine-1,4,7,10-tetraazacyclododecane **(20)** are illustrated in the Figure 35. The synthesis of the DABBC **(36)** started with the introduction of two allyl ester groups on the N-Boc-ethylamine-1,4,7,10-tetraazacyclododecane **(20)**. The allyl ester groups were introduced as allyl bromoacetate **(33)**, which was synthetized from allyl alcohol and bromoacetyl bromide [64]. The allyl esters introduction was performed using 1 equivalent of monosubstituted cyclen **(20)**, 2 equivalents of allyl bromoacetate **(33)** and two equivalents of triethylamine as base [37]. The reaction was conducted in anhydrous acetonitrile under reflux

conditions and under argon atmosphere [34]. The product of this reaction, namely the 1-N-Boc-ethylamine-4,7-diallyl acetate-1,4,7,10-tetraazacyclododecane (DABC) **(34),** was successfully synthesised and purified through the column chromatography. However, the yield obtained after the column was about 20% due to the loss of some product in the overlapping fractions containing both the DABC **(34)** and the 1-N-Boc-ethylamine-4,7,10-triallyl acetate-1,4,7,10-tetraazacyclododecane (TABC) **(47)**, a side product formed during the reaction. In order to increase the yield of the DABC **(34)** it was essential to prevent or at least reduce the formation of TABC **(47)**. In this way the reaction mixture would have been less complex and easier to purify by column chromatography. In order to reduce the formation of TABC the reaction was repeated three more times changing some reaction parameters such as amount of TEA and reaction time, as shown in the Table 4. It was found that reducing the reaction time from 15 hours to 7 hours increased the yield from 20% to 50% since it reduced the formation of TABC, making the reaction mixture less complex and easier to purify via column chromatography.

N-Boc-ethylamine-1,4,7,10-tetraazacyclododecane (20) (1 eq)	Allyl bromoacetate (2 eq)	TEA (eq)	Time hour	Product: DABC (34)	Yield (%)
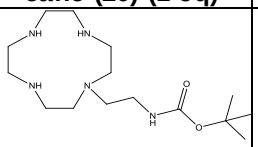	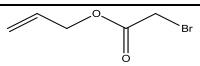	2	15	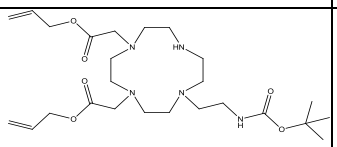	20%
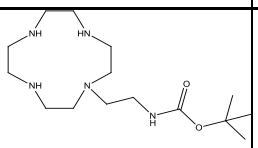	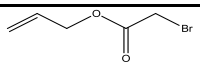	1	15	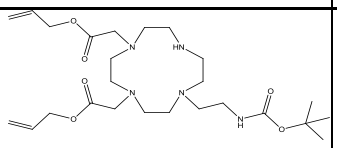	20%
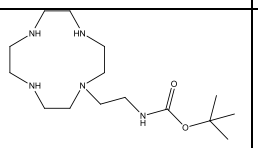	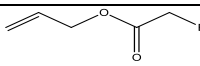	0.5	15	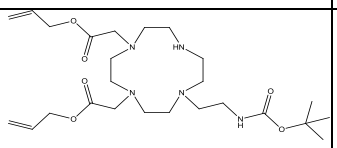	20%
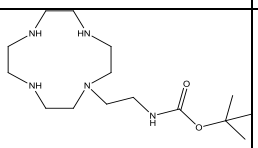	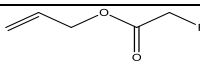	2	7	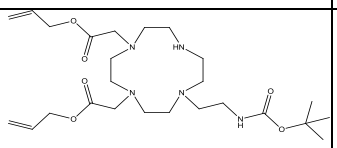	50%

Table 4. Results obtained with the synthesis of the DABC **(34)** changing some reaction parameters.

The final step of the DABBC **(36)** synthesis was the introduction of the benzyl ester group on the DABC **(34)** (Figure 35). The benzyl ester group was introduced as benzyl bromoacetate **(35)**, which was commercially available, and the reaction was performed using one equivalent of DABC **(34)**, 1.2 equivalents of benzyl bromoacetate **(35)**, 2 equivalents of triethylamine as base and anhydrous acetonitrile as solvent. The reaction was kept under reflux conditions and argon atmosphere for about 24 hours. The DABBC

(36) (generic ligand), was successfully synthesized with a high degree of purity that did not require the column chromatography.

3.3.3 Orthogonal deprotection strategy applied to the synthesis of asymmetrically substituted cyclen-based ligands

In the previous section, the synthetic route applied to the synthesis of the DABBC **(36)** was described. In this section a description of the orthogonal deprotection strategy that starting from the DABBC **(36)** led to the synthesis of ligands, based on asymmetrically substituted cyclen containing two triphenylphosphonium cation moieties and a chromophore antenna, is provided. In this project, four ligands of this type were synthesised and their chemical structures are shown in Figure 36. They were named **L1**, **L2**, **L3** and **L4** (which **L** stands for ligand). As it is possible observe in the Figure 36, all ligands possess a common core structure formed by a cyclen ring functionalised with two arms containing a triphenylphosphonium derivative, one containing a benzyl ester group and one containing a variable chromophore antenna. They only differ from one other for the chromophore antenna. In **L1** the dihydrofluorescein diacetate was used as sensitizer towards the visible emitting Eu(III) and Tb(III) and in meantime as ROS receptor unit. The coumarin 343 and the coumarin 3 carboxylic acid were used in **L2** and **L4** respectively as sensitizers of Eu(III) and Tb(III) and as ROS receptor unit. In **L3** the rhodamine B was used for the sensitization of the near infrared emitting Nd(III) and Yb(III) and as ROS receptor unit. The triphenylphosphonium derivative was used to target the complexes to the mitochondria since, as discussed in the chapter 1, they represent the main source of ROS within the cells.

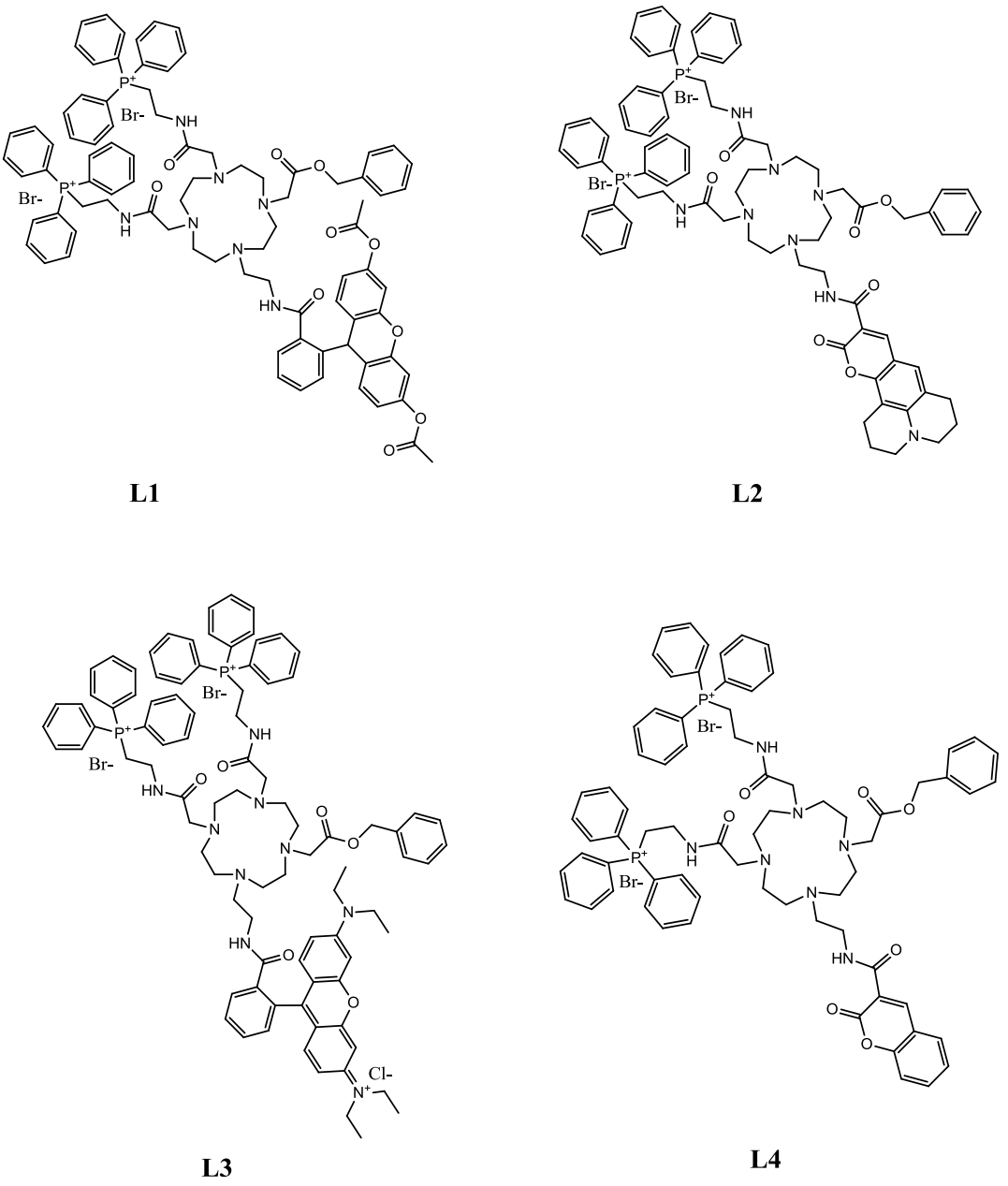

Figure 36. Chemical structures of the four ligands synthesised in this project, bearing two arms of a triphenylphosphonium derivative, a benzyl ester group and a chromophore antenna.

The orthogonal deprotection strategy described in this section was applied to the synthesis of **L1**, **L2**, **L3** and **L4**. Since all the steps involved in this orthogonal deprotection route were the same for all ligands (**L1**, **L2**, **L3** and **L4**) with the exception of the last step, namely the coupling of the sensitizer antenna, in this section only the one that led to the synthesis of 1-N-(coumarin 343)ethylamide-4,7-di-

(triphenylphosphonium bromide ethyl)acetamide-10-benzyl acetate-1,4,7,10-tetraazacyclododecane **(L2)** is discussed in detail as representative of this ligand series. One of the orthogonal deprotection strategies discussed in the section 3.3.1 and shown in Figure 37, was applied to the synthesis of **L2**, as well as for **L1**, **L3** and **L4** synthesis. The strategy starting with the allyl ester groups' removal was chosen as would have prevented the chromophore antenna, such as coumarin 343, being affected by reaction conditions required for the allyl ester groups' removal. In fact, if the allyl ester and/or benzyl ester groups had been deprotected after cleaving the Boc group and incorporating the chromophore antenna, the unsaturated bond present on the antenna would have been reduced by the reducing agents employed for cleaving the allyl ester and/or benzyl ester groups.

.

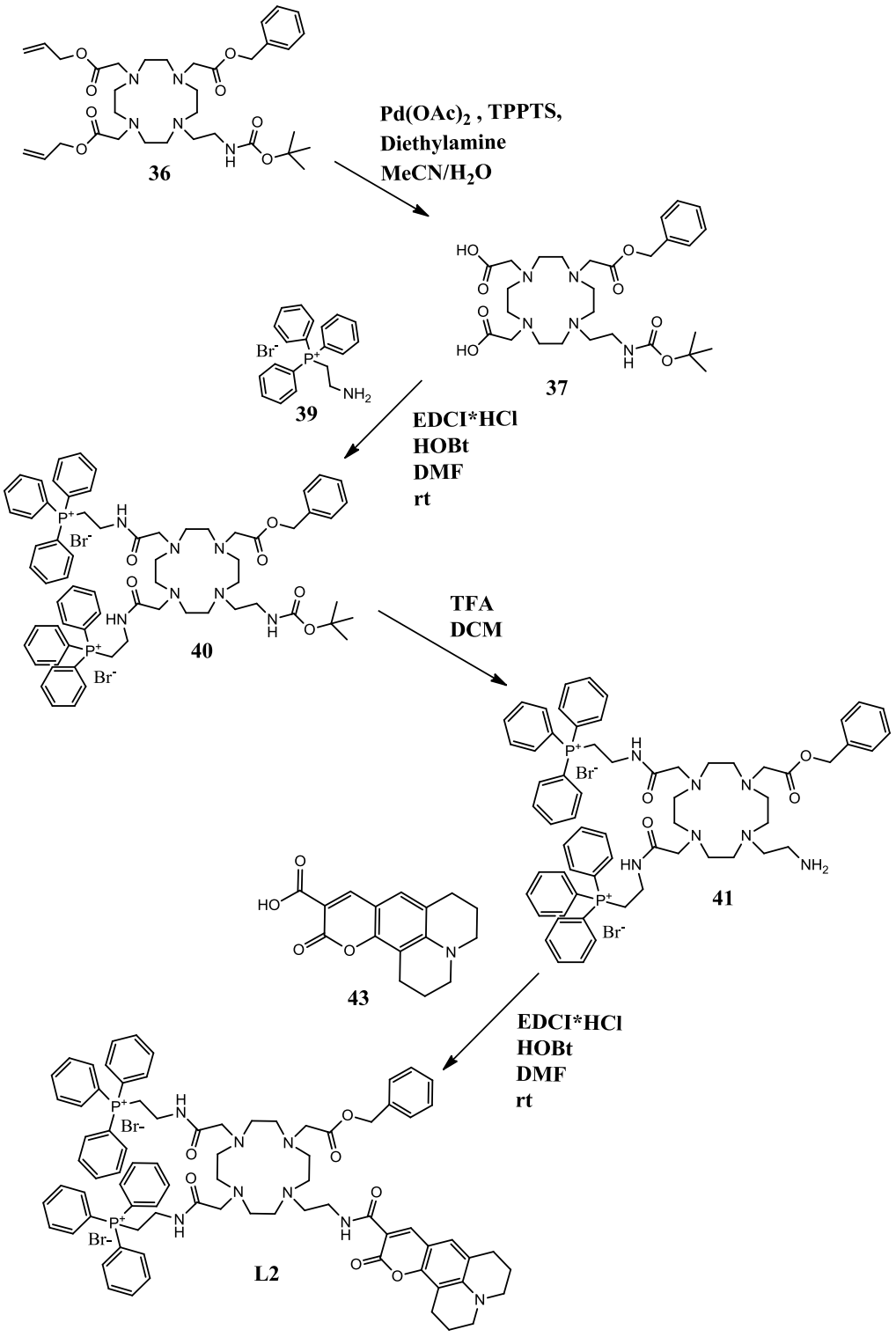

Figure 37. Schematic representation of the synthesis of **(L2)** starting from the generic ligand **(36)**.

The removal of the two allyl esters groups was successfully performed using a combination of palladium acetate $Pd(OAc)_2$ and triphenylphosphinotrisulfonate sodium salt (TPPTS) as catalyst and the dimethylamine as scavenger [71]. However, an initial

procedure performed using tetrakis-(triphenylphosphine)-palladium and morpholine in dichloromethane at room temperature was unsuccessfully applied to the removal of the two allyl ester groups [68], [69], [70]. According to the initial procedure [68], [70] the reaction would have been kept under stirring for about three hours to achieve the allyl ester groups' deprotection. Although the mass spectrum of the reaction mixture obtained after 24 hours confirmed that both the benzyl ester and the Boc groups were stable under the chemical conditions used for the deprotection, two main peaks were found in the mass spectrum. One peak at *m/z* 570 related to the mono allyl-removal product and one peak at *m/z* 530 related to the product derived from the deprotection of both allyl groups (Figure 38).

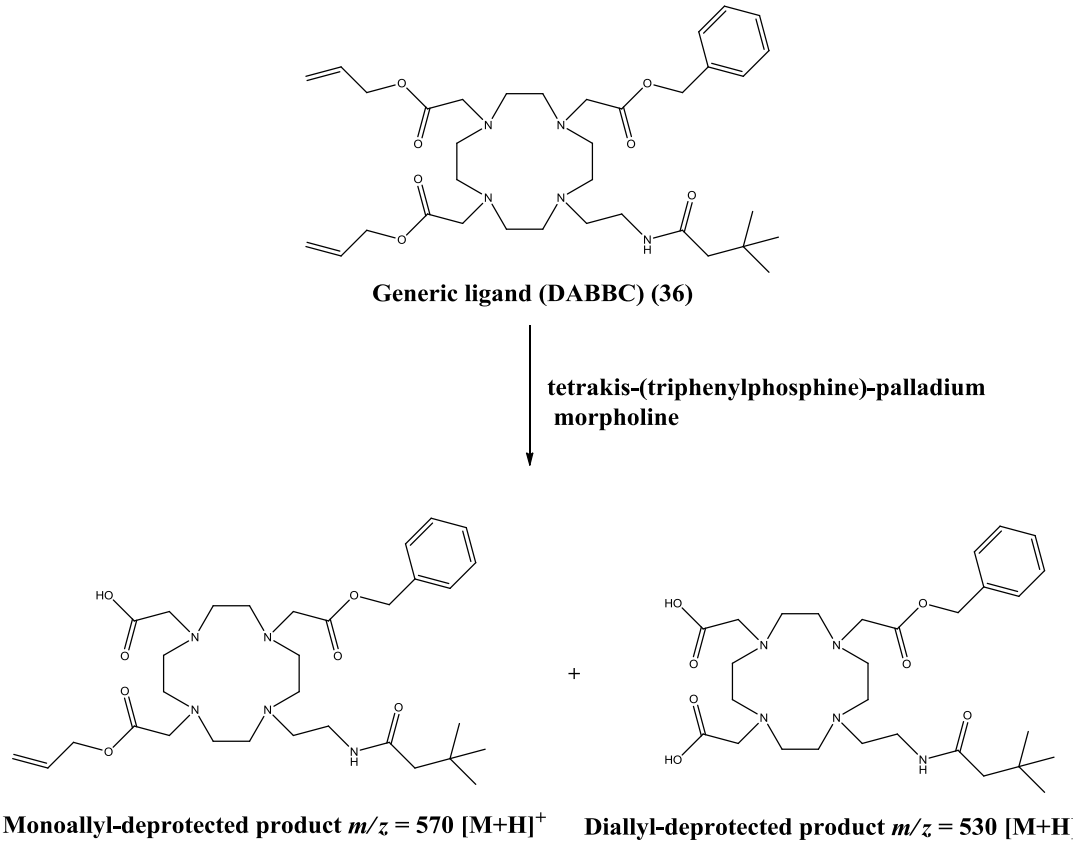

Figure 38. The two main products formed during the allyl deprotection procedure performed using tetrakis-(triphenylphosphine)-palladium as catalyst and morpholine as scavenger.

This indicated that, although the procedure involving the use of tetrakis-(triphenylphosphine)-palladium and morpholine could be successfully applied to remove one allyl ester group, was not suitable for the simultaneous cleavage of two allyl ester groups. In fact, the reaction did not go to completion even though it was kept under stirring for 24 hours and repeated three times using increasing concentrations of tetrakis-(triphenylphosphine)-palladium and morpholine, as it is shown in Table 5.

Substrate (1eq)	**Catalyst (eq)**	**Scavenger (eq)**	**Solvent/s**	**Time (hour)**	**Product/s**
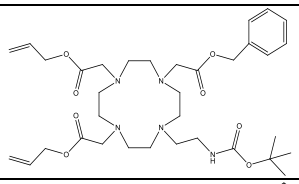	tetrakis-(triphenylphosphine)-palladium (0.2eq)	Morpholine (10eq)	CH_2Cl_2	24	Mono allyl deprotected (m/z 570) + Diallyl deprotected (m/z 530)
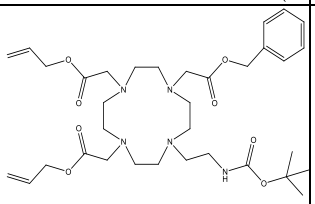	tetrakis-(triphenylphosphine)-palladium (0.5eq)	Morpholine (20eq)	CH_2Cl_2	24	Mono allyl deprotected (m/z 570) + Diallyl deprotected (m/z 530)
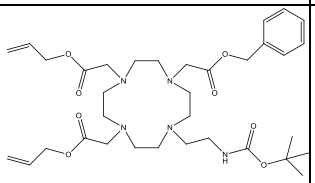	tetrakis-(triphenylphosphine)-palladium (1eq)	Morpholine (20eq)	CH_2Cl_2	24	Mono allyl deprotected (m/z 570) + Diallyl deprotected (m/z 530)
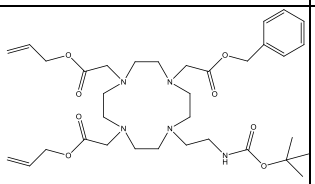	$Pd(OAc)_2$ (0.02eq) TPPTS (0.04eq)	Diethylamine (5eq)	MeCN/ H_2O	2	Diallyl deprotected (m/z 530)

Table 5. Results obtained with the deprotection of the allyl ester groups from the generic ligand **(36)** using different reaction conditions.

After the allyl ester groups deprotection, it was possible to introduce the two moieties of triphenylphosphine on the two free carboxylic functions of the 1-N-Boc ethylamine-4,7-diacetic acid-10-benzyl acetate-1,4,7,10-tetraazacyclododecane (DAABBC) **(37)** (Figure 37). This was achieved by synthesising the (2-aminoethyl) triphenylphosphonium

bromide **(39)**, a molecule containing both the triphenylphosphonium cation and the amino functions [69]. The latter was essential to obtain the formation of the amide bond with the free carboxylic function. The (2-aminoethyl) triphenylphosphonium bromide **(39)** was synthesised by stirring at reflux for 24 hours the 2-bromoethylamine hydrobromide **(16)** and triphenylphosphine in 1:1 ratio [72]. The two arms containing the triphenylphosphonium cations were successfully introduced through a peptide coupling reaction performed using HOBT and EDCI*HCl as coupling agent, DIPEA as base and anhydrous DMF as solvent [61], [73], [59]. The reaction mixture was kept under argon atmosphere and at room temperature for 24 hours. The desired product, 1-N-Boc-ethylamine-4,7-di-(triphenylphosphonium bromide ethyl)acetamide-10-benzyl acetate-1,4,7,10-tetraazacyclododecane (DTPPBBC) **(40)** (Figure 37), was obtained with 90% of yield and with a high degree of purity, as it was shown by the related mass spectrometry and carbon and proton NMR spectroscopy results. The synthesis of the final ligand proceeded with the cleavage of the Boc group from the amino function of DTPPBBC **(40)** to obtain the 1-ethylamine-4,7-di-(triphenylphosphonium bromide ethyl)acetamide-10-benzyl acetate-1,4,7,10-tetraazacyclododecane (DTPPBC) **(41)** (Figure 37). The Boc cleavage was performed using trifluoroacetic acid and dichloromethane as solvent [56]. The mild acidic conditions used for the Boc group cleavage allowed a selective deprotection that did not affect the benzyl group and the two triphenylphosphonium cation containing moieties. DTPPBC **(41)** was used as starting material to couple several types of organic fluorophores such as fluorescein, rhodamine and coumarin derivatives. Figure 39 provides a schematic representation of the coupling reaction between the coumarin 343 **(43)** acid and DTPPBC **(41)**. The reaction was performed using the same conditions described above [61], [73], [59], for the amide bond formation between the (2-aminoethyl) triphenylphosphonium bromide **(39)** and the DAABBC **(37)**. The coupling reaction shown in Figure 39 allowed obtaining the final ligand, namely the 1-N-(coumarin 343)ethylamide-4,7-di-(triphenylphosphonium bromide ethyl)acetamide-10-benzyl

acetate-1,4,7,10-tetraazacyclododecane **(L2)**, in high yield and with a high degree of purity, which did not require the use of column chromatography.

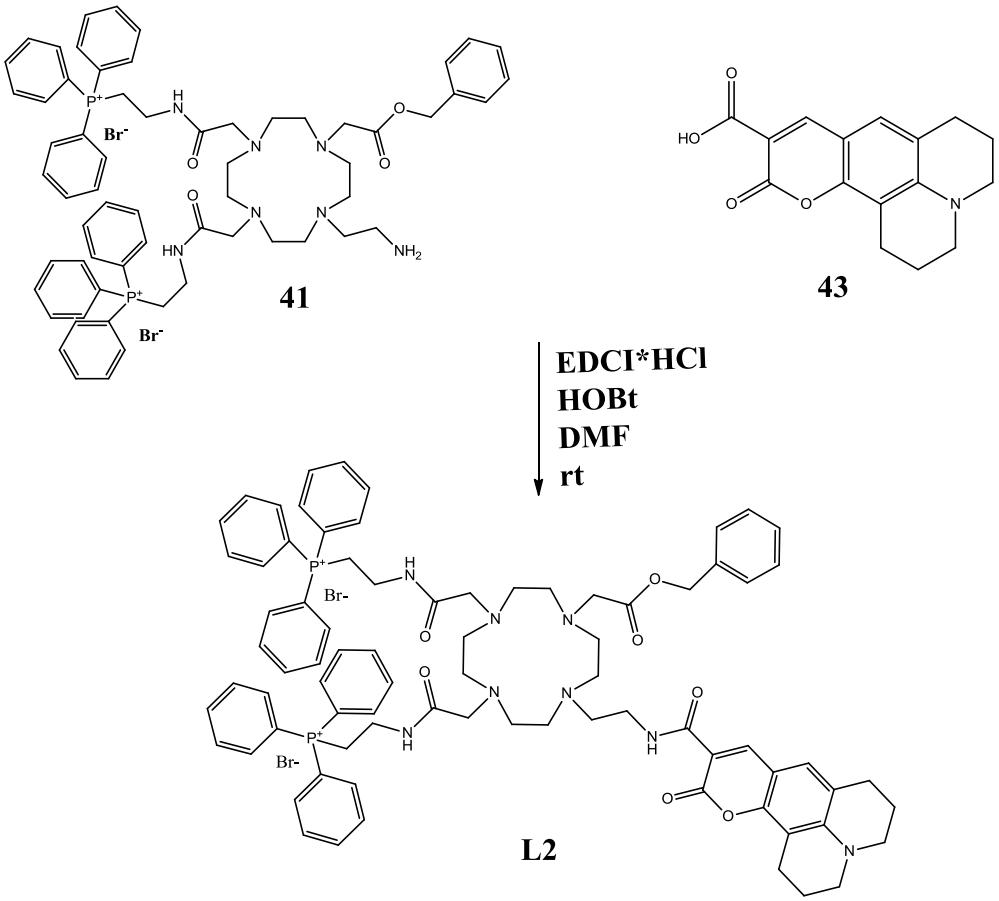

Figure 39. Peptide coupling reaction between the coumarin 343 **(43)** and the DTPPBC **(41).**

The orthogonal deprotection strategy applied to the synthesis of the DTPPBC **(L2)** starting from the DABBC **(36)** was successfully applied to the synthesis of all other ligands of the series, namely **L1**, **L2**, **L3** and **L4**. This indicated that the synthetic route involving the synthesis of the intermediate ligand DABBC **(36)**, can be applied to the asymmetrical functionalization of the cyclen ring and represents an alternative way to the synthesis of the asymmetrically substituted cyclen via direct N-alkylation when the stability and/or the steric hindrance of the pendant arms is an issue. The synthesis of four ligands, bearing two triphenylphosphonium derivatives, one benzyl ester group and one chromophore antenna has been described so far. Apart from these ligand series,

another series of ligands, which did not incorporate triphenylphosphonium derivatives, was synthesized in this project as “model ligands” used to investigate and understand the effect of the triphenylphosphonium derivatives on the lanthanide emission (see chapter 4). The following section describes the synthetic routes applied to the synthesis of three model ligands, not incorporating triphenylphosphonium derivatives.

3.3.4 Synthesis of the ligands that did not incorporate triphenyl phosphonium derivatives

In this section a description of the synthetic routes applied to the synthesis of the three model ligands is provided. These ligands were synthetized in order to investigate the effects of the triphenylphosphonium cations on the lanthanide emission. In particular, it was necessary to verify if the lack of lanthanide-based emission observed with both europium and terbium complexes of **L1** and **L2** could be attributable in some way to the presence of the triphenylphosphonium cations (see chapter 4 for a detailed description). Figure 40 shows the chemical structures of three model ligands that did not incorporate triphenylphosphonium derivative moieties. The 1-N-Boc-ethylamine-4,7-di-(coumarin 151)-N-acetamide-10-benzyl acetate-1,4,7,10-tetraazacyclododecane **(L5)** is the first model ligand shown in Figure 40. **L5** contains two coumarin 151 derivative moieties, which were chosen to sensitize the visible emitting lanthanide Eu(III). The remaining pendant arms contain a benzyl ester group and a Boc group to protect respectively the carboxylic and primary amino function. Either the benzyl ester and Boc groups were not cleaved off to prevent that the free carboxylic function and/ or the free amino function could have a quenching effect on the Eu(III) emission [20] thus interfering with the sensitization process.

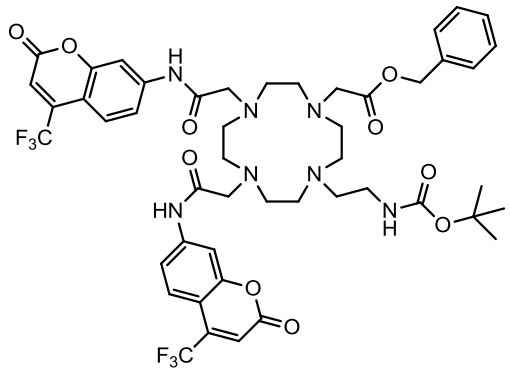

L5

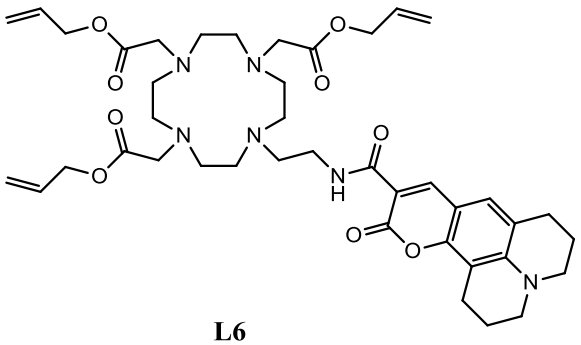

L6

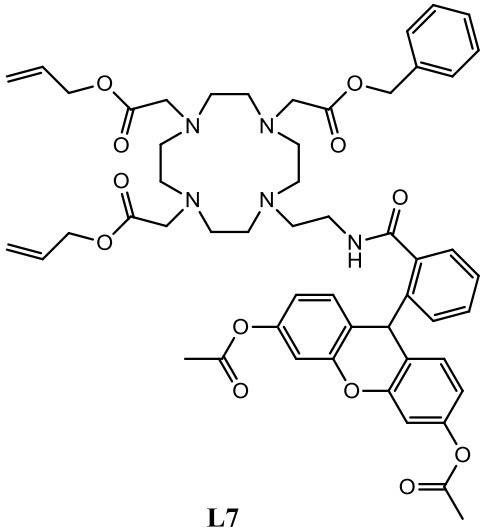

L7

Figure 40. Chemical structures of the ligands that did not contain the triphenylphosphonium derivative moieties.

L5 was synthesized starting from the generic ligand, DABBC **(36)**, by selectively removing both allyl ester groups and replacing them with two molecules of coumarin 151

(Figure 41). The allyl ester groups were removed using the same procedure described in the section, using $Pd(OAc)_2$ and TPPTS as catalyst and dimethylamine as scavenger. The reaction was conducted in a mixture of MeCN and H_2O at room temperature for two hours and was monitored by mass spectrometry via direct injection. The mass spectrum related to the reaction mixture after 2 hours of running indicated that the reaction went to completion within this time since only one two intense peaks at *m/z* = 580 $[M+H]^+$ and *m/z* = 602 $[M+Na]^+$, both related to the DAABBC **(37)**, were found. After cleaving the allyl ester groups, two molecules of coumarin 151 **(46)**, which was commercially available, were coupled to both allyl-deprotected carboxylic functions of DAABBC **(37)** (Figure 41). The peptide coupling reaction between the two free carboxylic functions on DAABBC **(37)** and the primary amino function of each coumarin 151 molecule was performed using EDCI*HCl and HOBt as coupling agents and was conducted in DMF at room temperature for 24 hours.

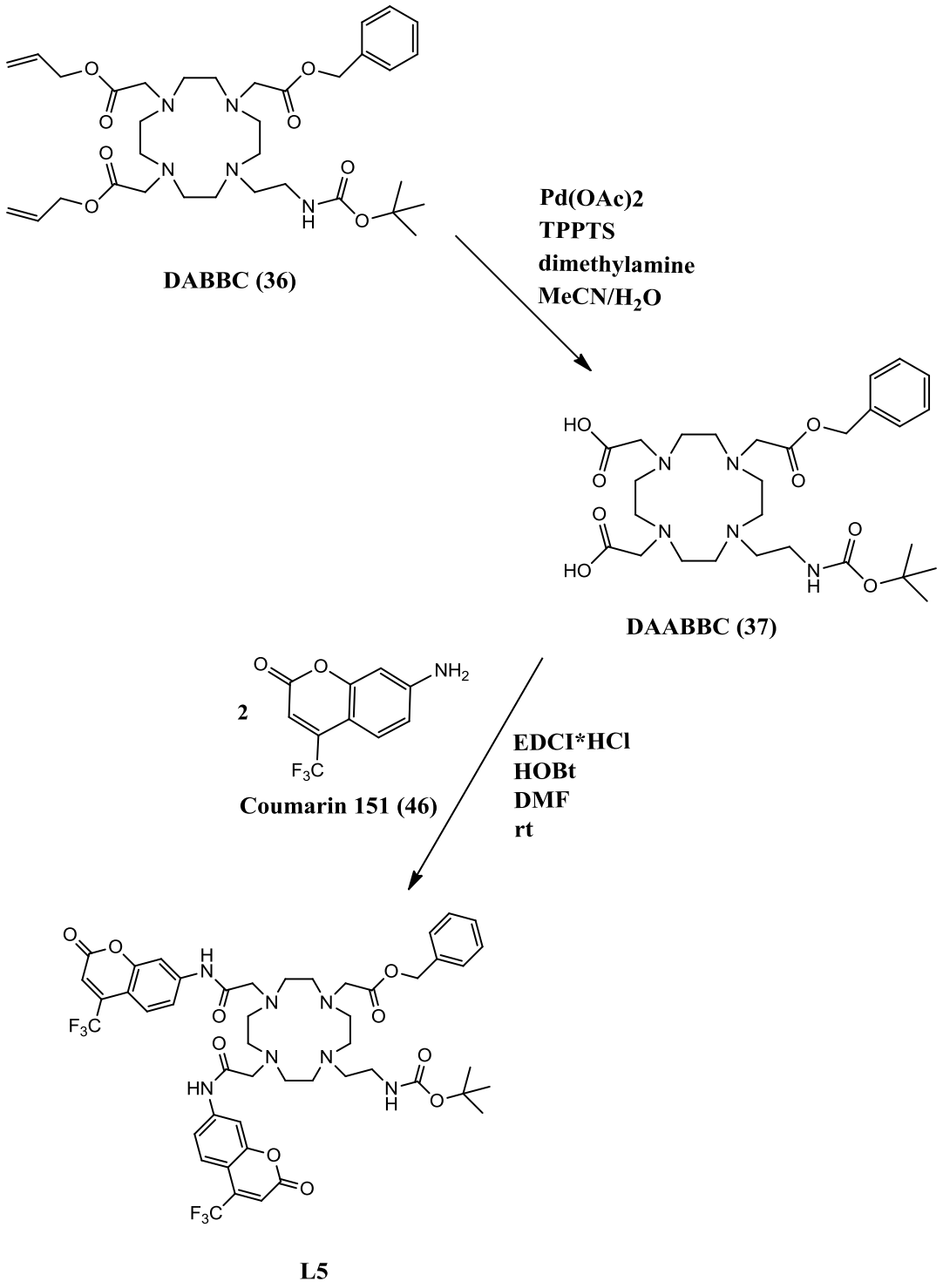

Figure 41. Synthetic route that starting from DABBC **(36)** led to the synthesis of **L5.**

The peptide coupling reaction between DAABBC **(37)** and coumarin 151 **(46)** was successfully performed, as it was shown by the proton and carbon NMR spectra obtained

after purifying the related reaction mixture with extraction. The second ligand shown in Figure 40 is the 1-N-(coumarin 343)ethylamide-4,7,10-triallyl acetate-1,4,7,10-tetraazacyclododecane **(L6)**. This model ligand was obtained starting from the TABC **(47)**, a side product recovered after the chromatography column performed to purify the reaction mixture related to the synthesis of the DABC **(34)** (see section 3.3.2). The coumarin 343 used in **L6** was chosen to sensitize the lanthanide Eu(III). Figure 42 shows a schematic representation of the steps that led to the synthesis of **L6** starting from the TABC **(47)**. The first step of this synthesis was the removal of the Boc group from **(47)**, which was performed in mild acidic condition using TFA. The reaction was conducted at room temperature in DCM and monitored by mass spectrometry via direct injection. The presence on the mass spectrum, obtained after 1 hour, of an intense peak at *m/z* = 960 $[M+H]^+$ and a small peak at *m/z* = 982 $[M+Na]^+$, both related to the Boc-cleaved product, and the absence of the peak at *m/z* = 610 $[M+H]^+$ and its sodium adduct at *m/z* = 632, which were related to the starting material **(47)** and both observed at the beginning of reaction monitoring, confirmed that the reaction went to completion in 1 hour. Indeed, the absence of any peak related to the either mono-, di- and tri-allyl ester-cleaved products confirmed that the Boc group could be selectively removed using mild acidic condition (TFA/DCM) without affecting the stability of the allyl ester group.

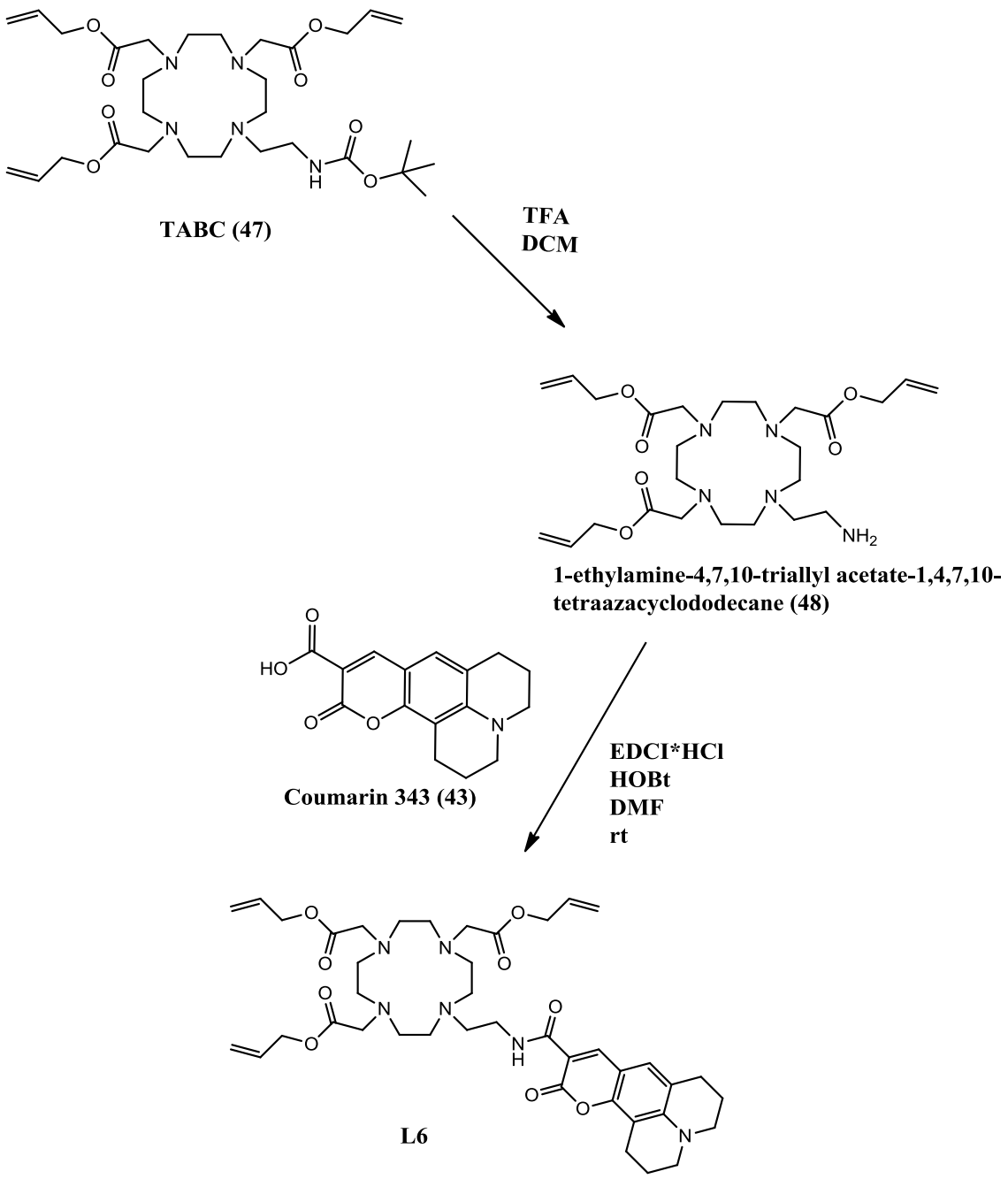

Figure 42. Synthetic route that starting from the TABC **(47)** led to the synthesis of **L6.**

After the Boc removal from TABC **(47)**, the coumarin 343 **(43)** was coupled to the free amino function of 1-ethylamine-4,7,10-triallyl acetate-1,4,7,10-tetraazacyclododecane TAC **(48)**, using the same peptide coupling procedure previously described for the last step of **L5**. The peptide coupling reaction between was successfully performed and the desired product **(L6)**, was obtained with a high degree of purity and without preforming

the column chromatography. The synthetic steps involved in the synthesis of the 1-N-(dihydrofluorescein diacetate)ethylamide-4,7-diallyl acetate-10-benzyl acetate-1,4,7,10-tetraazacyclododecane **(L7)** are shown in Figure 43. The first step of the synthesis was the Boc group removal using TFA and DCM. The reaction was monitored by mass spectrometry via direct injection. The mass spectrum related to the reaction mixture after 1 hour showed only the presence of an intense peak at *m/z* = 560 $[M+H]^+$, which was related to the 1-ethylamine-4,7-diallyl acetate-10-benzyl acetate-1,4,7,10-tetraazacyclododecane (DABnC) **(49)**, and a small peak at *m/z* = 582, which was related to its sodium adduct. This indicated that under the mild acidic conditions used to cleave the Boc group off either the allyl ester and the benzyl ester groups remained unaffected. This was an important result since it proved that the orthogonal deprotection strategy applied to the generic ligand **(36)**, which was discussed in the section 3.2.1 and shown in the Figure 33, could effectively start from the Boc group removal and the incorporation on the cyclen ring of acidic labile moiety. The Boc deprotection was followed by the peptide coupling reaction between the DABnC **(49)** and the dihydrofluorescein diacetate **(42)**. Also in this case the coupling reaction was performed in DMF and performed using EDCI*HCl and HOBt as coupling agents.

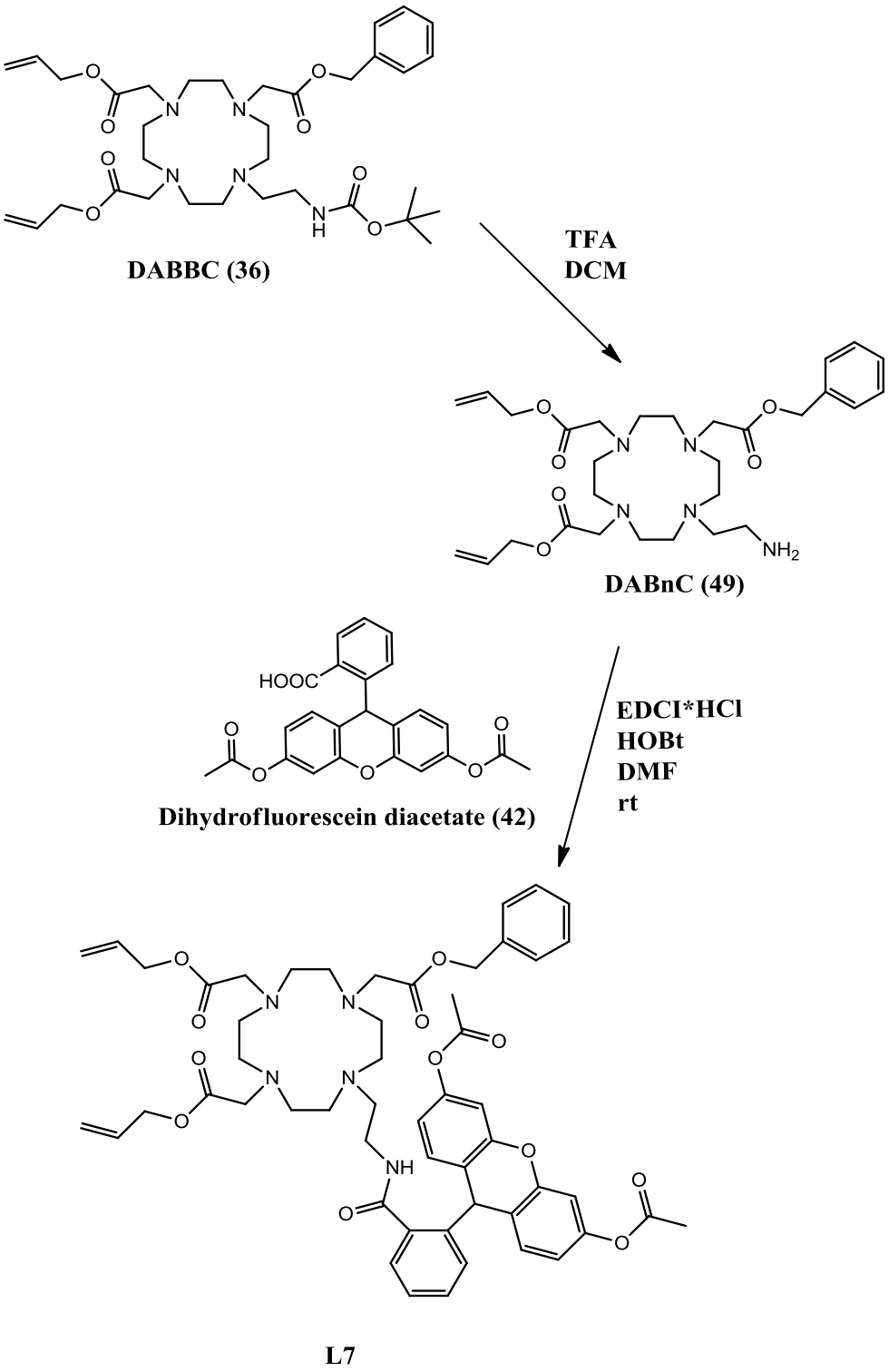

Figure 43. Synthetic route that starting from the DABBC **(36)** led to the synthesis of **(L7).**

The new synthetic route, based on the orthogonal deprotection strategy, overcame the issues encountered with the direct N-alkylation strategy and synthesising different types

of ligands, based on asymmetrically substituted cyclen, whose synthesis have been described so far. However the goal of producing reversible redox systems able to distinguish between transient increase of ROS production and chronically elevated ROS levels was not achieved and a detailed explanation to this follows in the next section.

3.4 Benzyl ester group removal

As discussed in the section 3.2.3, four ligands (**L1**, **L2**, **L3** and **L4**), based on symmetrically substituted cyclen and bearing two pendant arms containing a triphenylphosphonium cation as mitochondria targeting moiety and one pendant arm containing a sensitizer antenna that in the meantime could react with ROS species, were successfully synthesised in this project. However it was not possible to introduce a further antenna that could have generated a reversible system of antennae described in the section 3.1. This was due to the fact that one step of the multistep orthogonal deprotection strategy, which started from the DABBC **(36)** led to the synthesis of **L1**, **L2**, **L3** and **L4**, did not work even if many attempts were made. Figure 44 is a schematic representation of the orthogonal deprotection strategy step involving the benzyl ester group removal from the 1-N-Boc-ethylamine-4,7-di-(triphenylphosphonium bromide ethyl)acetamide-10-benzyl acetate-1,4,7,10-tetraazacyclododecane (DTPPBBC) **(40)**.

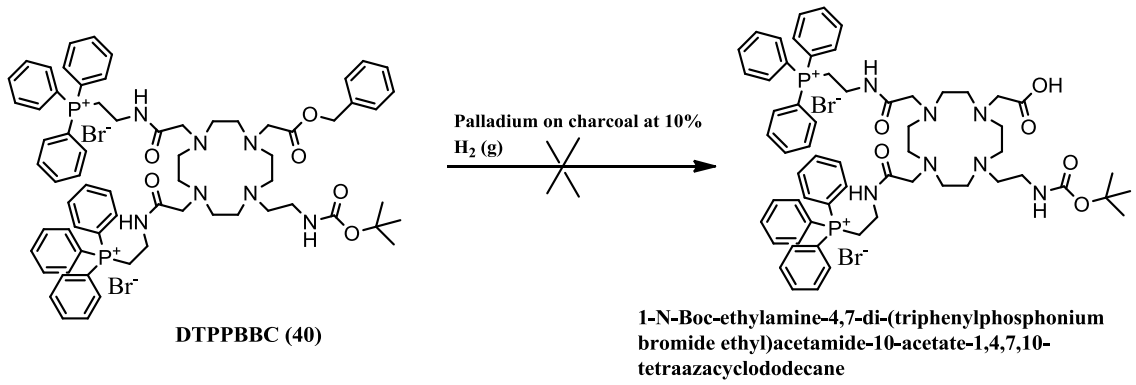

Figure 44. Schematic representation of the benzyl ester group removal.

Two synthetic procedures were applied to the cleavage of the benzyl ester group but they were both unsuccessful. The first synthetic procedure that was applied to the benzyl ester group removal was a catalytic hydrogenation reaction. The reaction was performed by treating the compound containing the benzyl ester group to be cleaved, the DTPPBBC **(40)**, with 10% Palladium on charcoal and bubbling gaseous molecular hydrogen (H_2) into the reaction mixture [59]. The palladium on charcoal would have acted as catalyst and the molecular hydrogen as reducing agent. The reaction was conducted using anhydrous methanol as solvent at room temperature (Table 6) and was monitored through TLC and mass spectrometry via direct injection. The TLC (DCM/isopropylamine 9.5:0.5) and mass spectrometry results of the reaction monitoring obtained after 1, 6, 12 and 24 hours from the starting time confirmed that no product was formed and the starting material was quantitatively recovered unaffected by filtering the reaction mixture through a celite pad. The reaction was repeated a second time by gently heating the reaction mixture (Table 6) but no product formation was observed and the starting material was recovered via celite pad filtration. Since the conventional procedure used to cleave the benzyl ester group [59] was unsuccessful, a different synthetic procedure was applied [74] where molecular hydrogen was replaced by a hydrogen donor, the triethylsilane, the palladium on charcoal at 10% was used as catalyst and the anhydrous

methanol was used as solvent [74] (Table 6). When the reaction was performed at room temperature no product formation was observed. The same results were obtained after repeating the reaction by gently heating the reaction mixture (Table 6) since no product formation was observed.

Substrate (40)	Reducing agent	Catalyst	Solvent	Temperature
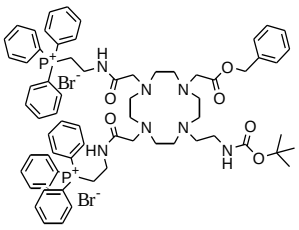	H_2	10% Palladium on charcoal	MeOH	room temperature
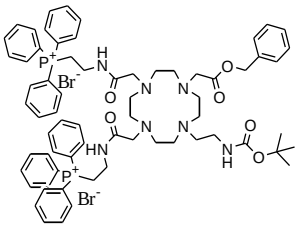	H_2	10% Palladium on charcoal	MeOH	room temperature
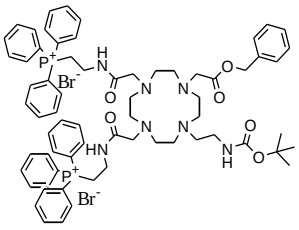	triethylsilane	10% Palladium on charcoal	MeOH	reflux
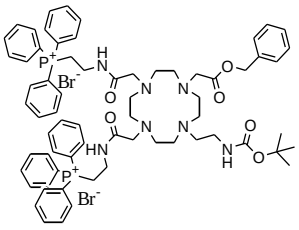	triethylsilane	10% Palladium on charcoal	MeOH	reflux

Table 6. Summary of the reaction conditions used for the benzyl ester group removal.

Since after each attempt the starting ligand **(40)** was quantitatively recovered unaffected by celite pad filtration, the unsuccessful benzyl ester removal could be due to an adsorption of the ligand on the palladium catalyst surface, in such a way as to prevent allyl arms from reaching the surface. Alternatively the tetrafunctionalized cyclen ring may assume a conformation hinders the approach of hydrogen to the double bond

3.5 Complexation of ligands with lanthanide ions

L2, **L3**, **L4**, **L5** and **L6** were successfully complexed with trivalent lanthanide ions, giving rise to eleven lanthanide complexes:

1. **L2** was complexed with Eu(III) and Tb(III) to give **EuL2** and **TbL2** respectively (Figure 45)
2. **L4** was complexed with Eu(III) and Tb(III) to give **EuL4** and **TbL4** respectively (Figure 47)
3. **L5** and **L6** were complexed with Eu(III) to give **EuL5** and **EuL6** respectively (Figure 48).
4. **L3** was complexed with near infrared Nd(III) and Yb(III) to give **NdL3** and **YbL3** respectively (Figure 46).

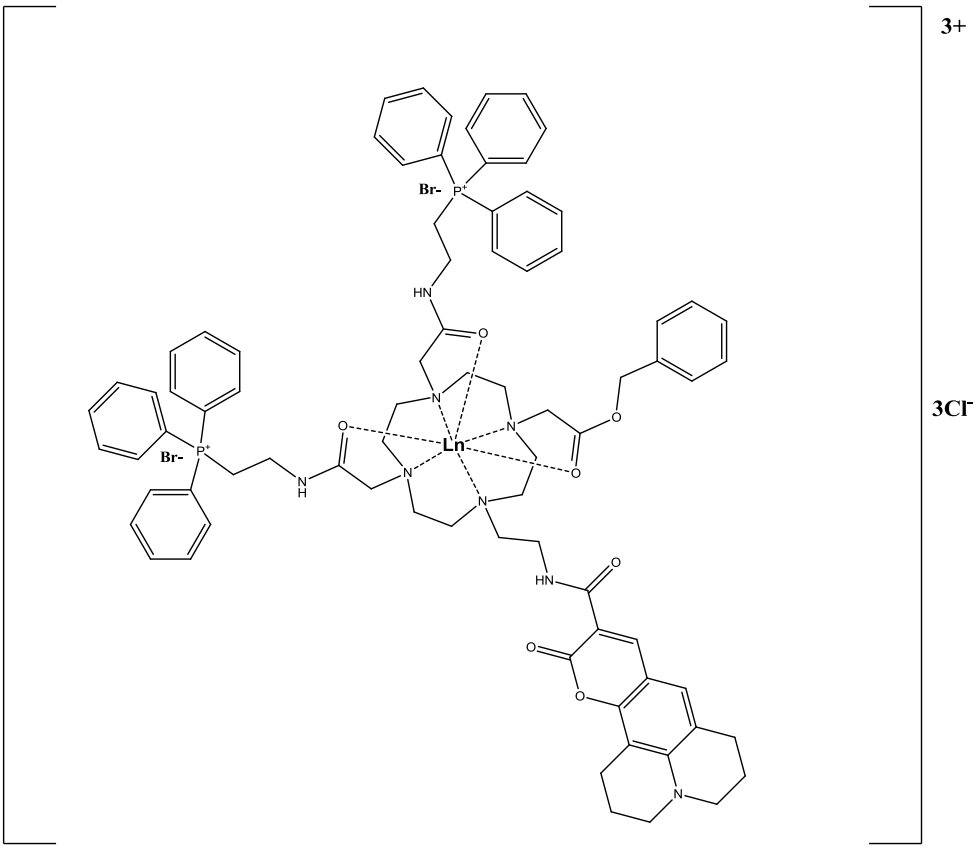

EuL2: Ln = Eu
TbL2: Ln = Tb

Figure 45. Chemical structures of the lanthanide complexes **EuL2** and **TbL2**.

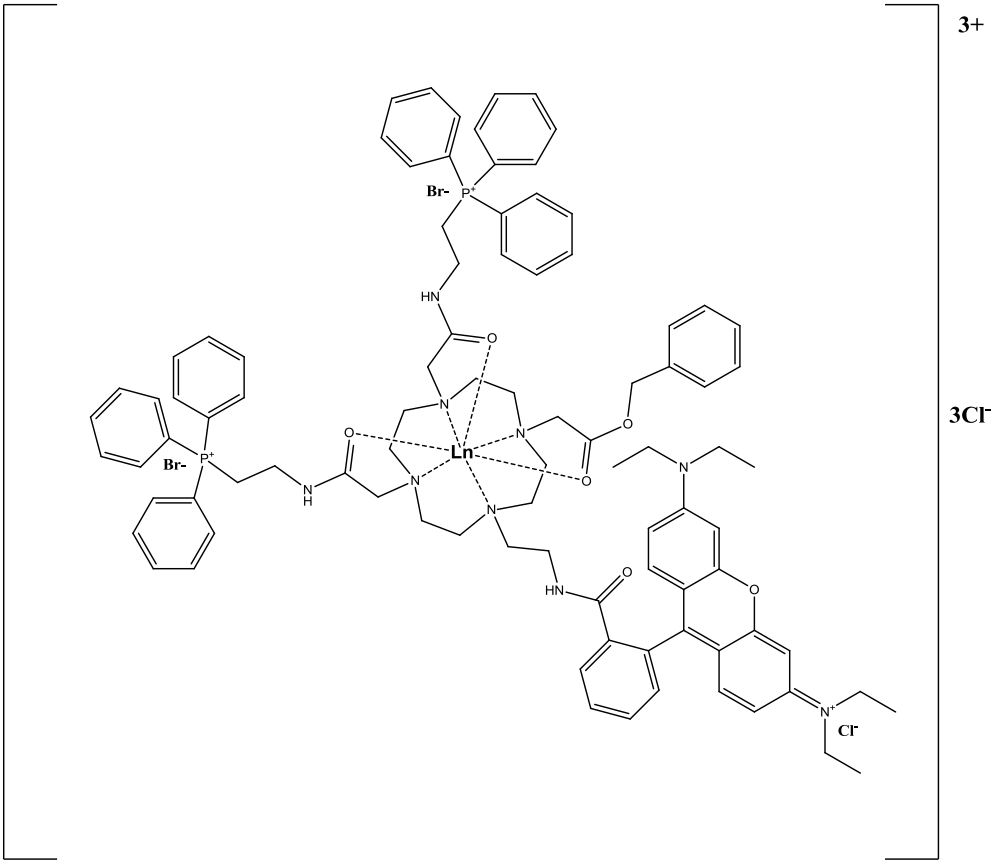

NdL3: Ln = Nd
YbL3: Ln = Yb

Figure 46. Chemical structures of the lanthanide complexes **NdL3** and **YbL3**.

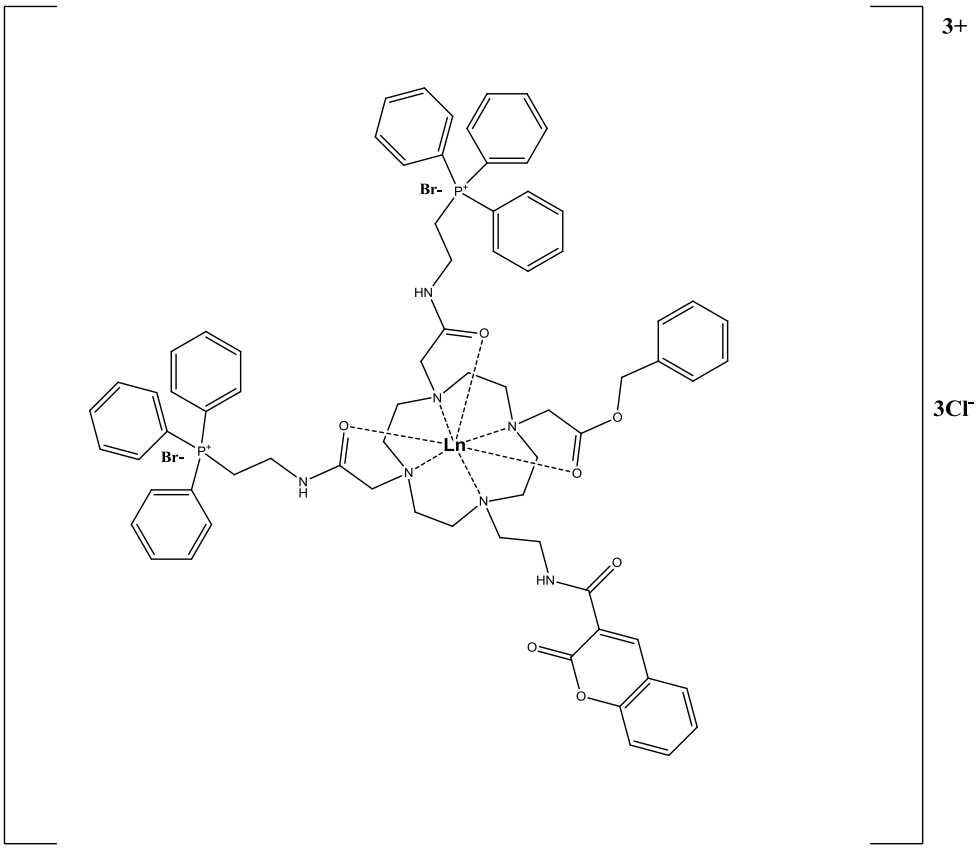

EuL4: Ln = Eu
TbL4: Ln = Tb

Figure 47. Chemical structures of the lanthanide complexes **EuL4** and **TbL4**.

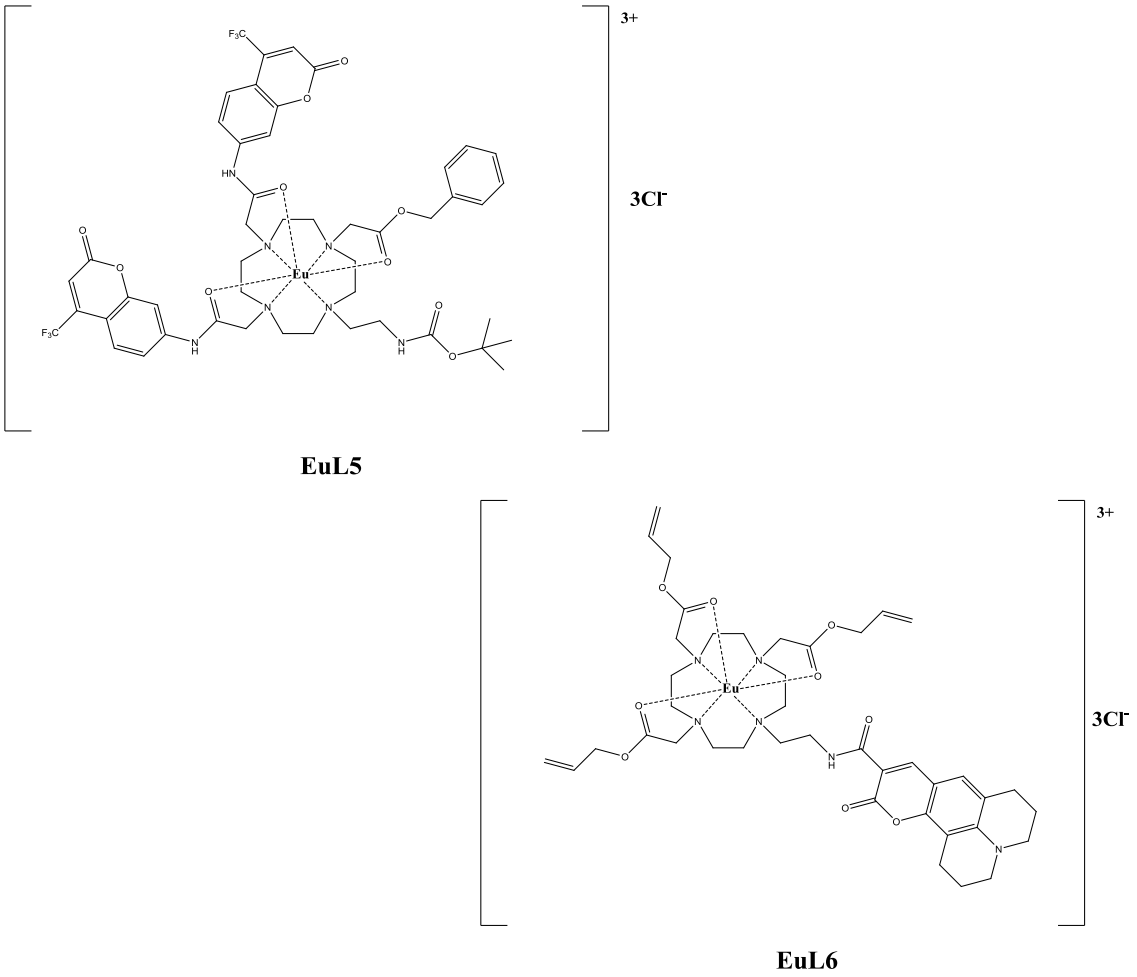

Figure 48. Chemical structures of the lanthanide complexes **EuL5** and **EuL6**.

The general synthetic procedure applied to the complexation of each ligand synthetized in this project with the related lanthanide ion was performed by reacting the free ligand and anhydrous lanthanide chloride ($LnCl_3$) in 1:1 ratio, in anhydrous methanol, under reflux conditions and under argon atmosphere for 15 hours [75]. The complexation reaction was monitored through TLC (DCM/isopropyl amine 95:0.5) and mass spectrometry via direct injection. The reaction was stopped when no free ligand peak was observed in the mass spectrum related to the reaction mixture and no spot related to the free ligand was observed on TLC plate. After the reaction went to completion, most of the methanol was removed under vacuum leaving only a minimal amount necessary to dissolve the mixture. Then cold diethyl ether was added and the formation

of a precipitate was observed [75]. The precipitate was allowed to settle down and the reaction mixture was centrifuged. The supernatant was removed, the precipitate was dissolved in a minimum amount of water and the aqueous solution was freeze-dried overnight. The lanthanide complexes were characterized by mass spectrometry (see chapter 2) and absorption and emission spectroscopy (see chapter 4).

3.5.1 Complexation of L1 and L7 with Eu(III)

The general procedure described in the previous section and applied to the complexation of the L(III) ions with the ligands synthesised in this project was also applied to the complexation of **L1** with Eu(III) and Tb(III), and **L7** with Eu(III). However in this case the loss of the acetate groups was observed after the complexation reaction. This could be due to a transesterification reaction that occurred during the complexation of **L1** and **L7** with the Ln(III), which was performed using methanol as the solvent. The hydroxyl function of methanol could probably replace the hydroxyl functions of the dihydrofluorescein molecules resulting in the loss of the acetate groups from **L1** and **L7**. This hypothesis was confirmed by the mass spectrometry data reported in chapter 2 and photophysical data discussed in chapter 4. The chemical structures of **EuL1** and **TbL1**, obtained after the complexation of **L1** with $EuCl_3$ and $TbCl_3$ respectively are reported in Figure 49, whilst the chemical structure of **EuL7**, which was obtained after the complexation of **L7** with $EuCl_3$, is reported in Figure 50.

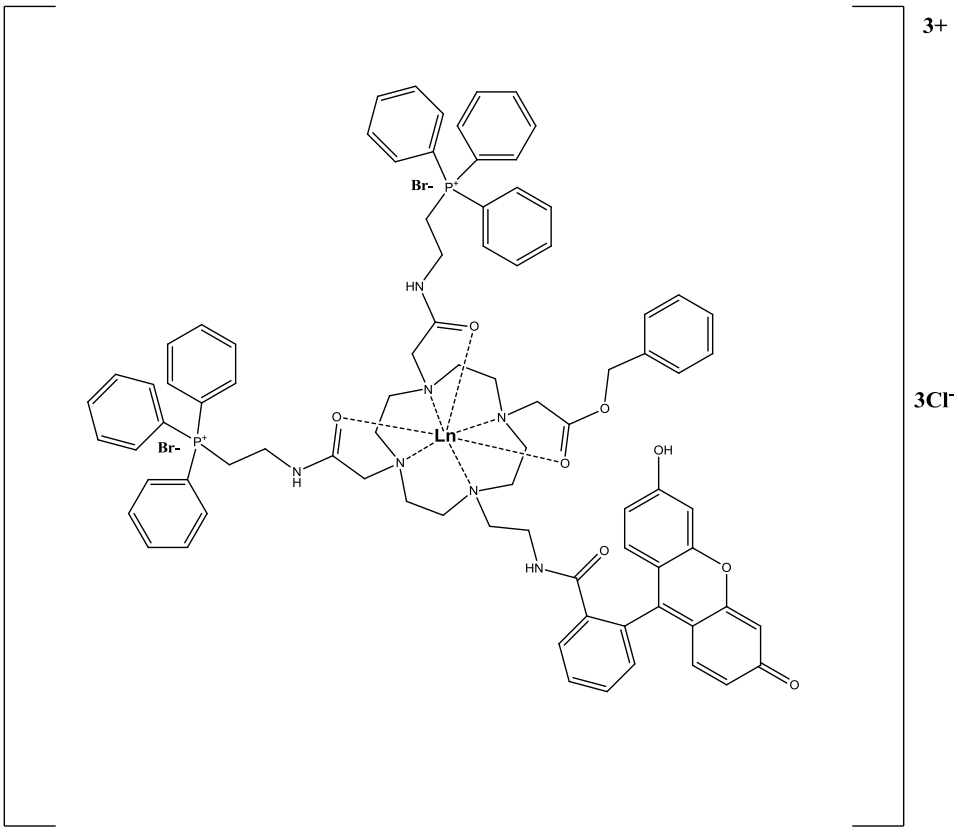

EuL1: Ln = Eu
TbL1: Ln = Tb

Figure 49. Chemical structures of the lanthanide complexes **EuL1** and **TbL1**.

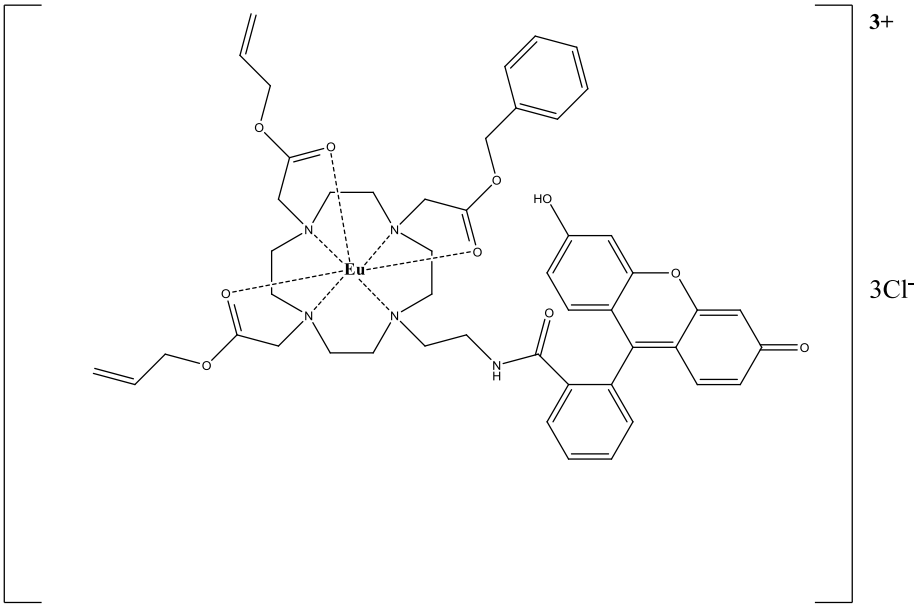

EuL7

Figure 50. Chemical structures of the lanthanide complex **EuL7**.

4. Photophysical properties of Lanthanide Complexes

This chapter describes the photophysical studies performed on the lanthanide complexes that were synthesised in this project starting from the asymmetrically substituted cyclen-based ligands described in the chapter 3. The trivalent lanthanide ions europium and terbium were used in the complexes described in this chapter, while different types of organic chromophores, such as fluorescein and coumarin derivatives, were used as antennae-sensitizers of the Ln^{3+}. The use of a sensitizer antenna is required for an effective excitation of Ln^{3+} since, because of their low molar absorption coefficient, direct excitation of lanthanide ions only produces weak Ln^{3+}-based emission [76]. In some cases no lanthanide emission is achieved upon Ln^{3+} direct excitation. The function of the sensitizing group or "antenna" is to absorb strongly at a suitable wavelength and to transfer this excitation energy to the Ln^{3+} which may then emit its characteristic luminescence [76]. The photophysical properties of all Eu(III) and Tb(III) complexes synthesized in this project were measured with absorption and emission spectroscopy. The absorption spectroscopy was also applied to measure the absorbance of the fluorescein and coumarin derivatives used as sensitizer of Eu(III) and Tb(III) emission. Moreover the emission properties of two Eu(III) complexes were also investigated in presence of different concentrations of H_2O_2, in order to verify whether or not these complexes were able to detect the presence of H_2O_2 through changes in the Eu(III) -based luminescence.

4.1 EuL1 and TbL1 photophysical studies

EuL1 and **TbL1** were synthetized starting from the **L1** ligand, containing two arms of triphenyl phosphonium, one benzyl ester group and one moiety of dihydrofluorescein diacetate. The ligand was complexed with Eu(III) in **EuL1** and Tb(III) in **TbL1** (Figure 51).

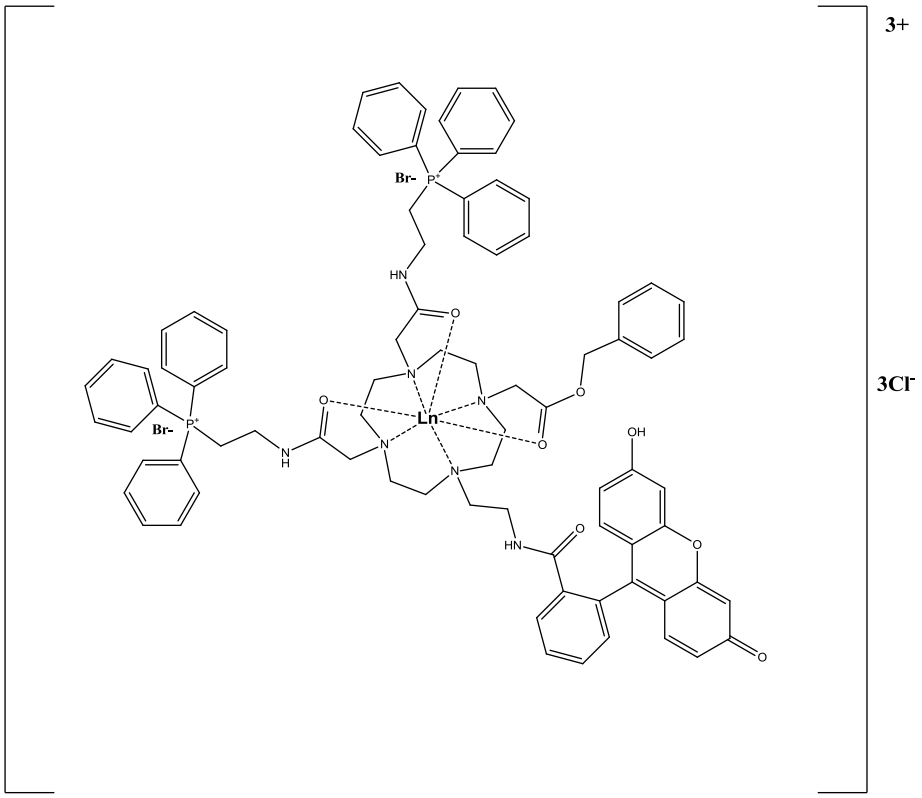

Figure 51. Chemical structure of **EuL1** and **TbL1**.

The dihydrofluorescein diacetate was used as sensitizer antenna towards both trivalent lanthanide ions. Since the excitation wavelengths used during the emission acquisition of all complexes corresponded to the maximum peaks found in the absorption spectrum of each complex and the absorption spectrum of the related chromophore antenna, the absorption spectra of each complex will be described together with the absorption spectrum related to the antenna used. The absorption spectra of **EuL1** and **TbL1** showed a similar trend with a maximum peak at 489 nm, which was related to the

chromophore antenna, and an intense absorbance region between 250 and 350 nm (Figure 52).

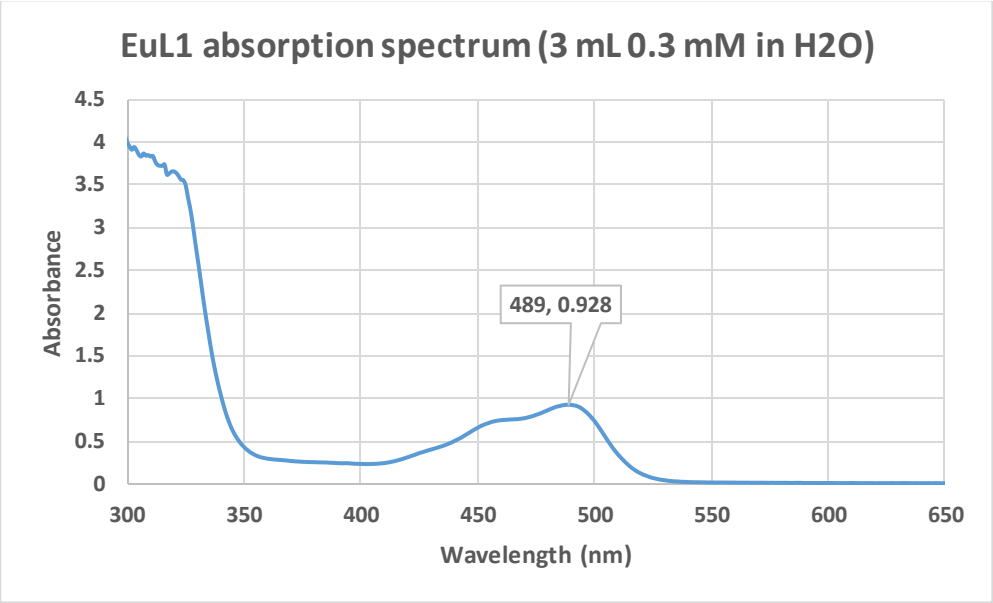

Figure 52. Absorption spectrum of **EuL1** (3 mL 0.3 mM in H_2O).

The dihydrofluorescein acetate absorbance was measured in ethanol, due to its poor solubility in H_2O. The dihydrofluorescein diacetate absorption spectrum showed a maximum peak at 275 nm and a broad region between 220 and 260 nm (Figure 53). However no peaks were found above 310 nm.

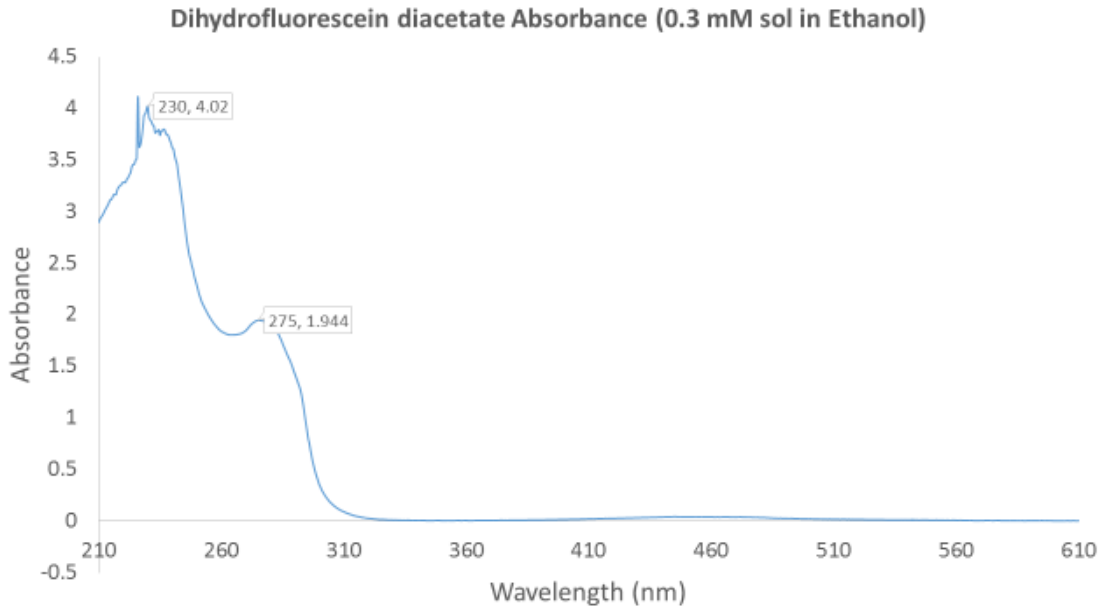

Figure 53. Absorption spectrum of dihydrofluorescein diacetate (3 mL 0.3 mM in ethanol).

The absence of a peak at 489 nm in the dihydrofluorescein diacetate absorption spectrum did not confirm the hypothesis that the peak at 489 nm, found in the **EuL1** and **TbL1** absorption spectra, was related to the chromophore antenna. This suggested indeed that the peak at 489 nm could be related to the formation of a conjugated system on the dihydrofluorescein diacetate that could be due to its oxidation. The formation of a conjugated system would have explained the long absorption wavelength at 489 nm present in the **EuL1** and **TbL1** absorption spectra. Another possibility could be that the dihydrofluorescein diacetate derivative lost the acetate groups and the resulting dihydrofluorescein derivative showed a maximum absorption peak around 489 nm. Therefore it was necessary to investigate the photophysical properties of the dihydrofluorescein diacetate in order to understand what gave rise to the presence of an absorption peak at 489 nm on the **EuL1** and **TbL1** absorption spectra.

4.1.1 Photophysical properties of dihydrofluorescein diacetate

In order to further investigate the photophysical properties of the dihydrofluorescein diacetate, its absorbance was recorded in absence and presence of NaOH and H_2O_2. The NaOH was used to favour the cleavage of the acetate groups that would have converted the dihydrofluorescein diacetate to dihydrofluorescein. This choice was made since one of the procedures used for the acetate group removal involves the treatment of the compound whose hydroxyl functions are protected with acetate groups with a KOH or NaOH methanol solution [77]. The H_2O_2 was used as oxidant species that should have been able to oxidise the dihydrofluorescein to fluorescein and generate a conjugated system. According to the data reported in the literature [78], the dihydrofluorescein diacetate is a not fluorescent molecule that is used as probe for detecting a broad range of intracellular oxidants, such as H_2O_2 [79]. The dihydrofluorescein diacetate represents the reduced form of the fluorescein, whose two hydroxyl functions are protected as acetate groups. The reduced form of the fluorescein, namely the dihydrofluorescein diacetate, is a non-fluorescent molecule, which upon the cleavage of the acetate groups and oxidation by an intracellular oxidant, such as H_2O_2, becomes fluorescent [78]. The dihydrofluorescein does not absorb light at 500 nm but its oxidation to fluorescein by H_2O_2, which is possible only after the cleavage of the acetate groups by cellular esterases or OH^-, generates a conjugated system responsible for the longer absorption wavelength at 500 nm (Figure 54) [79]. It is known from the literature [80] that the conjugation causes a red shift (a so-called bathochromic shift) of the absorption and emission maximum peaks of a molecule. This means that when a conjugated system is generated, the molecule will absorb and emit light to longer wavelengths depending on the nature of the conjugated system that has been generated [80]. The strong emission from the fluorescein at 512 nm upon the oxidation of the dihydrofluorescein diacetate indicates the presence of oxidant species [78].

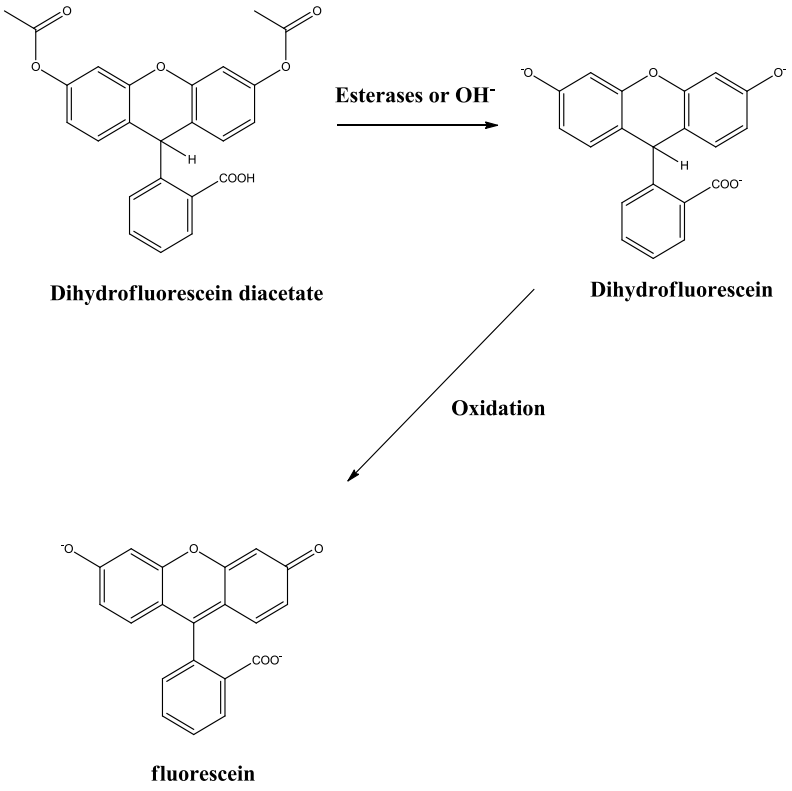

Figure 54. Oxidation of the dihydrofluorescein diacetate to fluorescein upon removal of the acetate groups by OH^- or cellular esterases.

It is evident from the literature that the oxidation of the dihydrofluorescein diacetate is responsible for the red shift observed in the absorption spectrum of its oxidised form. However it does not give any information regarding the possibility that the cleavage of the acetate groups on the fluorescein diacetate could be also responsible for the red shift. In order verify whether the presence of a peak at 489 nm observed in the **EuL1** and **TbL1** absorption spectra was due to the dihydrofluorescein diacetate oxidation or the loss of its acetate groups, the absorption of the dihydrofluorescein diacetate was measured at different conditions. In particular the absorption of the dihydrofluorescein diacetate (3 mL 0.3 mM in ethanol) was recorded upon the addition of 20 uL of 5 M NaOH aqueous (Figure 55) to verify if the cleavage of the acetate groups, favoured by the basic NaOH solution, could cause any changes in the absorption spectrum.

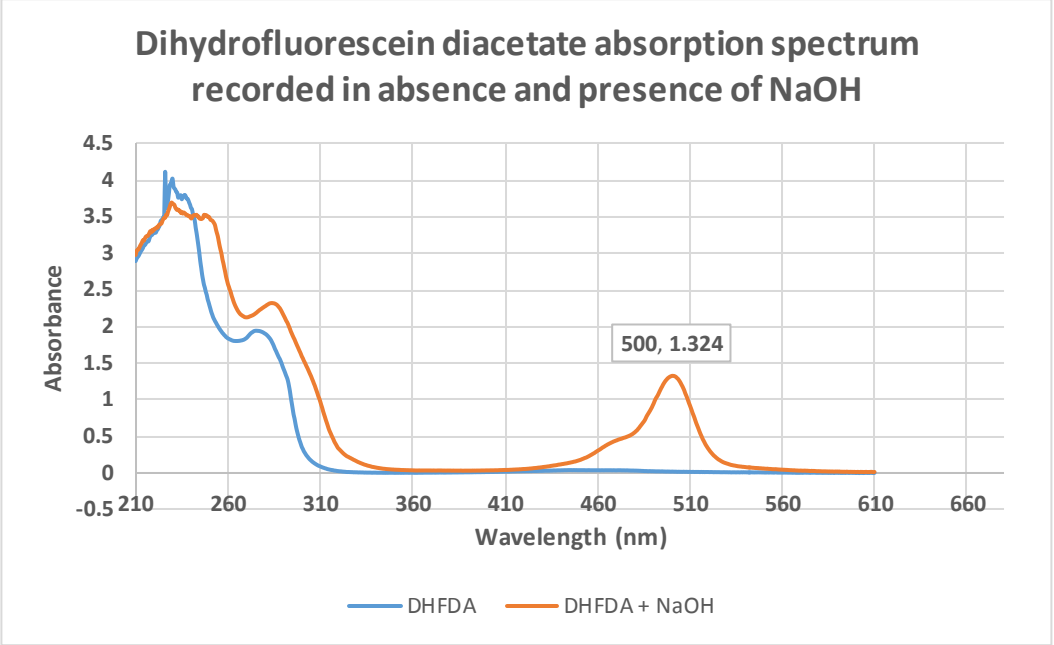

Figure 55. Absorption spectra of dihydrofluorescein diacetate (3 mL 0.3 mM in ethanol) recorded in absence and presence of 20 uL of 5 M NaOH.

The fluorescein diacetate absorption spectrum was also recorded upon the addition of 20 uL of 30% H_2O_2 to the main solution, already containing the NaOH, and it was monitored after 1 hour and 6 hours (Figure 56).

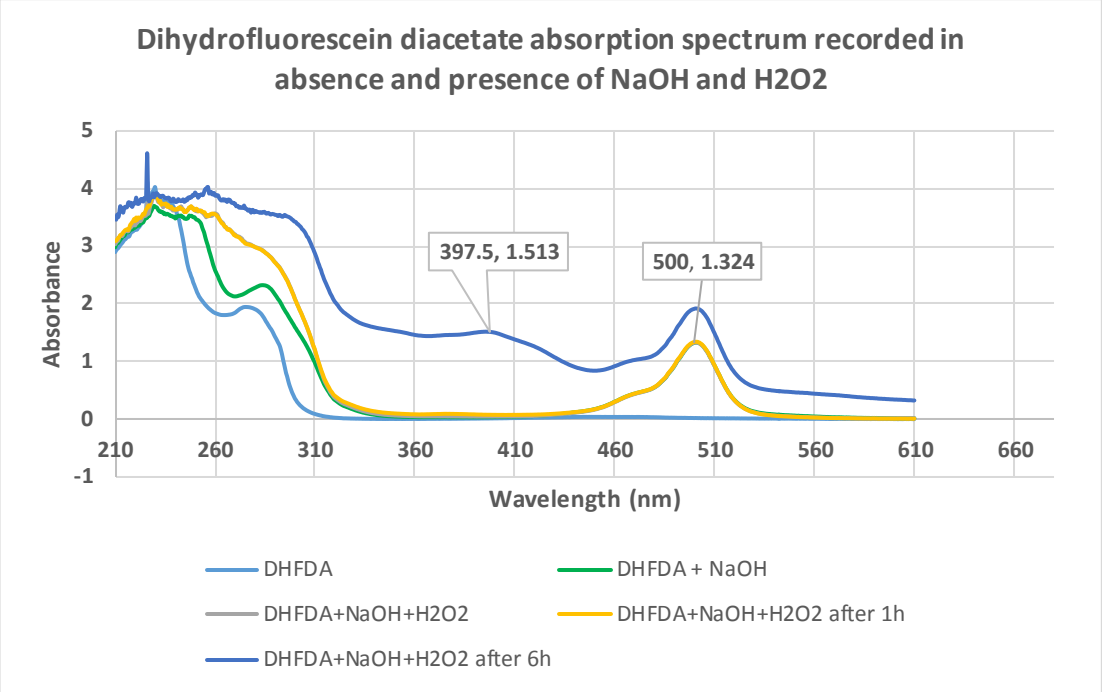

Figure 56. Absorption spectra of dihydrofluorescein diacetate (3 mL 0.3 mM in ethanol) recorded in absence and presence of 20 uL of 5 M NaOH and 20 uL of 30% H_2O_2.

The absorption spectrum of the dihydrofluorescein diacetate recorded immediately after the addition of 20ul of 5M NaOH aqueous solution showed a strong absorption peak at 500 nm (Figure 55), suggesting that the cleavage of the acetate groups by NaOH was responsible for the red shift at 500 nm. The dihydrofluorescein absorption spectrum was also recorded immediately upon the addition of the H_2O_2 and after 1 hour and 6 hours form added H_2O_2. No changes in the dihydrofluorescein diacetate absorption spectrum in the region between 450 and 610 nm were observed after 1 hour from the H_2O_2 addition compared to the absorption spectrum recorded upon NaOH addition. However an increase of the absorbance intensity at 500 nm was observed after 6 hours and this was accompanied by a broad absorption band between 320 and 450 nm, with a maximum absorption peak at 397 nm (Figure 56). The presence of a peak at 489 nm and the absence of a broad absorption region between 320 and 450 nm in **EuL1** and **TbL1** absorption spectra suggested that the peak at 489 nm was related to the cleavage of the

acetate groups and not to the formation of a conjugated system on the dihydrofluorescein diacetate derivative caused by its oxidation. The cleavage of the acetate groups on **EuL1** and **TbL1** could take place during the complexation reaction of **L1** with the $LnCl_3$. Since the complexation reaction was performed by refluxing **L1** with the related $LnCl_3$ in methanol for about 15 hours, it was likely that a transesterification reaction was responsible for the acetate groups' removal, as discussed in section 3.5.1.

4.1.2 EuL1 and TbL1 emission profiles

The emission of **EuL1** was recorded upon excitation at 489 nm, 275 nm and 397 nm. The excitation wavelength of 489 nm was used since it was the one of the maximum peak found in the **EuL1** absorption spectrum that, as discussed above, could be probably due to the dihydrofluorescein, whilst 397 nm was used as it is the typical wavelength employed for the direct excitation of Eu(III) [81]. The excitation at 275 nm was used to excite the dihydrofluorescein antenna. The emission spectrum of **EuL1** recorded upon exciting the antenna at 275 nm did not show the characteristic Eu(III)-based luminescence, indicating that no sensitization of europium was achieved using the dihydrofluorescein as antenna. No Eu(III) emission was observed upon Eu(III) direct excitation at 397 nm. Similar results were obtained upon exciting the antenna at 489, indicating that the dihydrofluorecein derivative, formed as consequence of the acetate groups' cleavage, was not able to sensitize the lanthanide emission.

The emission of **TbL1** was recorded using different excitation wavelengths according to the data obtained with the absorption spectra of **TbL1** and the dihydrofluorescein. The emission of **TbL1**, recorded upon excitation of the dihydrofluorescein antenna at 275 nm, did not show the characteristic Tb(III)-based emission profile, indicating that no sensitization of Tb(III) was achieved using the dihydrofluorescein as antenna. Similar results were obtained upon Tb(III) direct excitation at 378 nm [81] and dihydrofluorescein at 489 nm.

4.2 EuL2 and TbL2 photophysycal studies

EuL2 and **TbL2** were synthetized starting from **L2** containing two arms of triphenyl phosphonium derivatives, one benzyl ester group and one moiety of coumarin 343. The ligand was complexed with Eu(III) in **EuL2** and Tb(III) in **TbL2** (Figure 57).

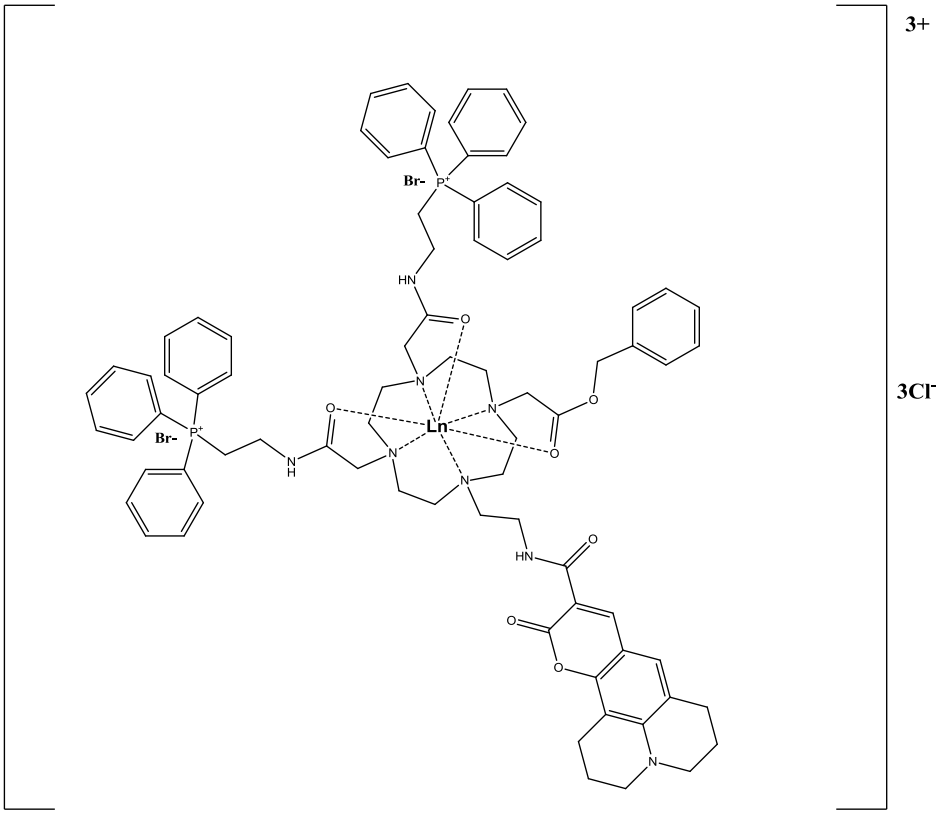

EuL2: Ln = Eu
TbL2: Ln = Tb

Figure 57. Chemical structure of EuL2 and TbL2.

The coumarin 343 was used to act as sensitizer toward the lanthanide ions via antenna effect. The absorption spectrum of the coumarin 343, the chromophore antenna used in **EuL2** and **TbL2**, was recorded in water in order to have information about which wavelengths should be used to excite the chromophore antenna in **EuL2** and **TbL2**

during their emission profiles acquisition. The absorption spectrum of the coumarin 343 showed two intense peaks at 418 nm and 275 nm and a less intense peak at 264 nm (Figure 58).

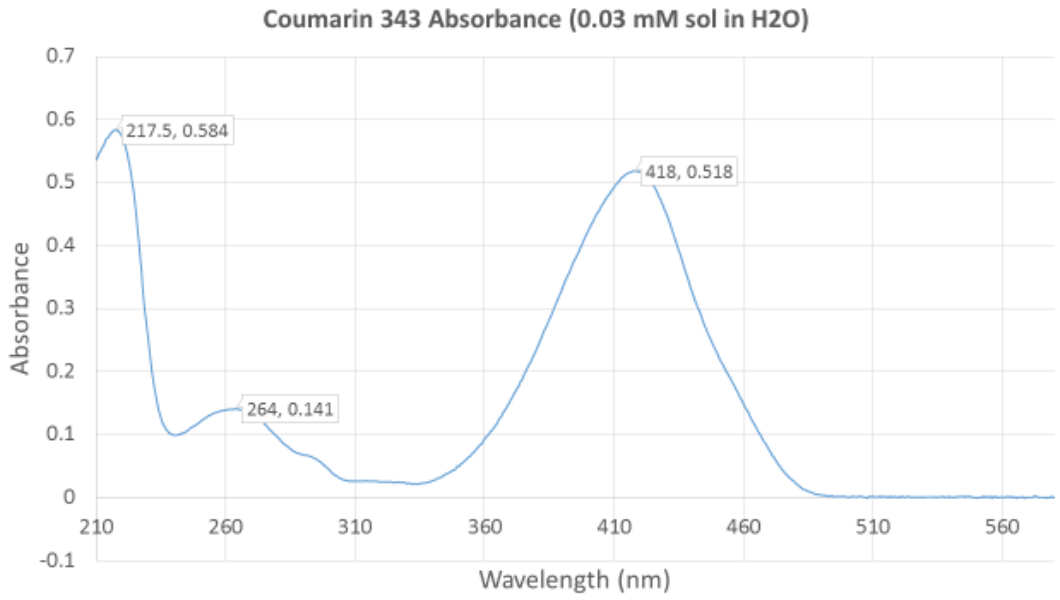

Figure 58. Coumarin 343 absorption spectrum (3 mL 0.03 mM in H_2O).

The absorption spectra of **EuL2** and **TbL2** showed an intense peak at 447 nm, which was related to the coumarin 343 chromophore antenna. The emission of **EuL2** was recorded at different excitation wavelengths. The excitation wavelengths used during the emission acquisition of **EuL2** were the ones corresponding to the maximum peaks found in the **EuL2** (447 nm) and coumarin 343 (217 nm, 264 nm and 418 nm) absorption spectra. It was also used as the excitation wavelength normally used to directly excite Eu(III) (397 nm) [81]. The characteristic Eu(III)-based emission was not observed upon excitation of **EuL2** at 447 nm, indicating that no sensitization of Eu(III) was achieved at 447 nm. No emission from the Eu(III) was observed upon Eu(III) direct excitation at 397 nm. Similar results were obtained upon excitation of **EuL2** at 217 nm, 264 nm and 418

nm, namely the wavelengths corresponding to the maximum peaks found in the absorption spectrum of coumarin 343, indicating that no sensitization of Eu(III) was achieved using the coumarin 343 derivative as antenna. The emission of **TbL2** was recorded using the same excitation wavelengths employed for **EuL2**, except the direct excitation wavelength of the lanthanide ion. While an excitation wavelength of 397 nm was used to direct excite Eu(III) in **EuL2** [81], in **TbL2** the Tb(III) direct excitation was achieved using 378 nm [81]. Also with **TbL2**, no emission from Tb(III) was observed upon excitation at 447 nm, indicating that no sensitization of Tb(III) was achieved at 447 nm. Similar results were obtained upon Tb(III) direct excitation at 378 nm and coumarin 343 excitation at 217 nm, 264 nm and 418 nm, indicating that the coumarin 343 could not be able to act as Tb(III) sensitizer antenna. The absence of lanthanide emission in **EuL1**, **TbL1**, **EuL2** and **TbL2** could be due to a number of factors. It was hypothesized that the two triphenyl phosphonium containing moieties could be responsible for the lanthanide luminescence quenching. It was also hypothesized that the linker spacer that separated the antenna from the lanthanide could affect the efficiency of the energy transfer process from the antenna to the lanthanide ion. In this case the energy content of the photon absorbed by the antenna would have been emitted rather than transferred to the lanthanide. Another explanation to the absence of lanthanide emission could be that the energy gap between the lowest energy level of the ligand triplet state and the receiving energy level of the Ln^{3+} was too small. This means that upon excitation of the ligand, although an energy transfer process could occur from the ligand triplet state to the Ln^{3+} emissive state, it could be followed by a thermally activated back energy transfer from the Ln^{3+} excited state to the ligand [82].

4.3 Photophysical properties of a new series of lanthanide complexes

In order to fully understand the photophysical behaviour of the lanthanide complexes examined so far and find a solution to overcome the problem of the lack in lanthanide

emission, a new series of lanthanide complexes was synthetized and their photophysical properties were measured. The new series comprised four different complexes that were named **EuL4**, **EuL5**, **EuL6** and **EuL7**. The Ln^{3+} used in the new series of complex was Eu(III). In the following sections, the photophysical properties of the new series of lanthanide complexes will be analysed.

4.3.1 EuL6 and EuL7 photophysical properties

The first lanthanide complexes of the new series synthesized in this project were **EuL6** and **EuL7** (Figure 59). **EuL6** and **EuL7** were Eu(III) based complexes obtained starting from **L6** and **L7** respectively.

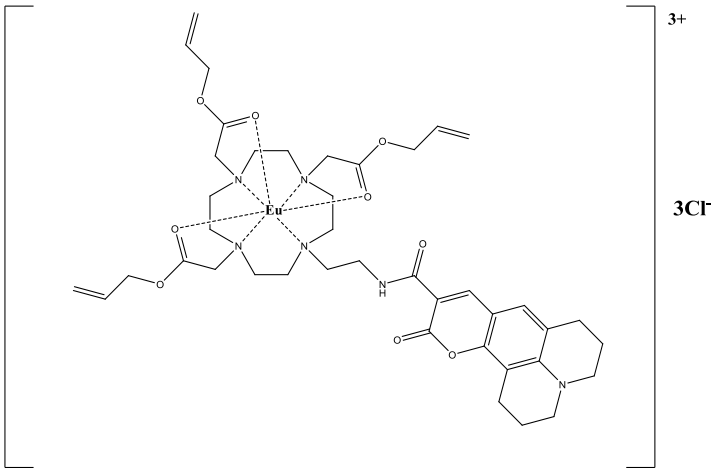

EuL6

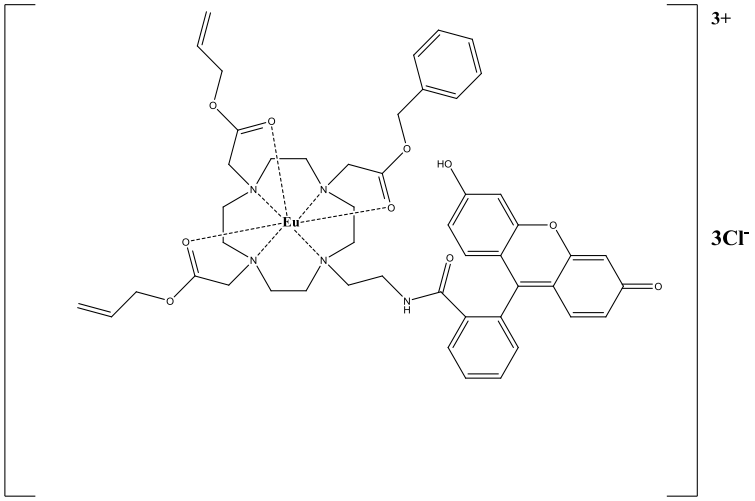

EuL7

Figure 59. Chemical structures of **EuL6** and **EuL7**.

As it is shown in Figure 59, **EuL6** and **EuL7** did not contain any pendant arms bearing triphenyl phosphonium derivatives, which were indeed present on **EuL1**, **TbL1**, **EuL2** and **TbL2**. This choice was made in order to assess whether or not the two triphenyl phosphonium derivatives could be responsible for the absence of the Ln^{3+} luminescence in **EuL1**, **TbL1**, **EuL2** and **TbL2**. It was also important at this stage using the same chromophore antennae used in **EuL1**, **TbL1**, **EuL2** and **TbL2** placed at the same position. This would have allowed to understand if the absence of Ln^{3+} emission in **EuL1**, **TbL1**, **EuL2** and **TbL2** could be due to the type of antenna used and/or to the linker

spacer length separating it from the Ln^{3+}. For this reason the sensitizer antenna used in **EuL6** was the same used in **EuL2** and **TbL2**, namely the coumarin 343, while the sensitizer antenna used in **EuL7** was the same used in **EuL1** and **TbL1**, namely the dihydrofluorescein diacetate.

4.3.1.1 EuL6 absorption and emission properties

The **EuL6** absorption spectrum showed a maximum peak at 452 nm and a broad absorption band between 260 and 310 nm, with a maximum at 275 nm, which were likely due to the absorbance of the coumarin 343 moiety (Figure 60).

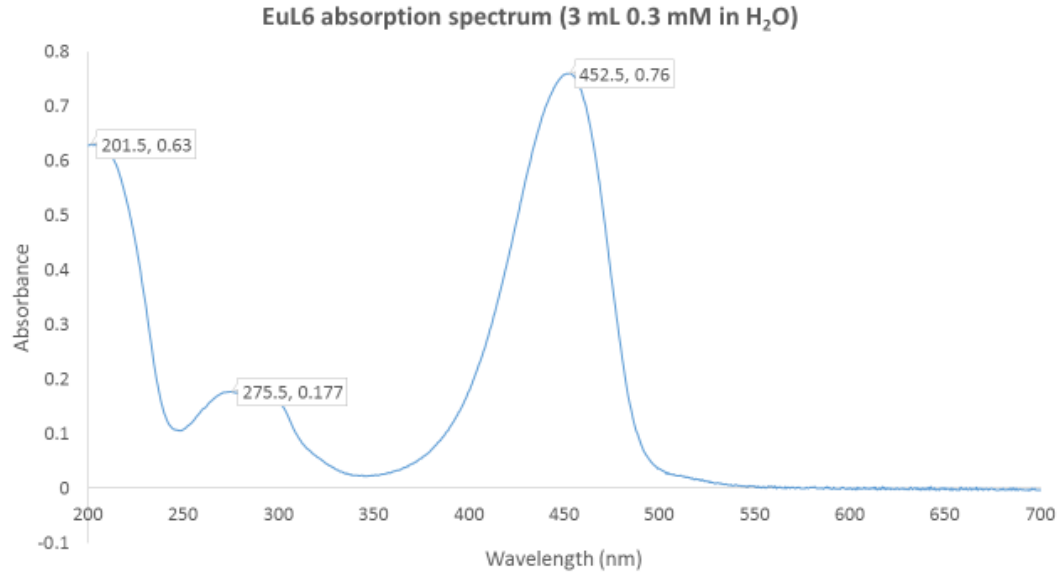

Figure 60. **EuL6** absorption spectrum (3 mL 0.3 mM in H_2O).

The **EuL6** emission recorded upon excitation of the chromophore antenna at 452 nm did not show the characteristic Eu(III) emission, indicating that no energy transfer process occurred from the coumarin 343 to the Eu(III). Therefore it was tried to achieve the sensitization of Eu(III) emission by changing the excitation wavelengths of the coumarin 343 moiety at 275 nm and 310 nm. However also in these cases no Eu(III) emission was observed, indicating that the coumarin 343 was not able to act as sensitizer antenna of

Eu(III). This could be due to the too small energy gap between the between the lowest energy level of the ligand triplet state and the receiving energy level of the Eu(III) or to the linker spacer length separating the chromophore antenna from the Eu(III) core. These results also suggested that the triphenyl phosphinium derivatives were not responsible for the absence of Ln^{3+} emission in **EuL1**, **TbL1**, **EuL2** and **TbL2** since no Eu(III) emission was observed in **EuL6** despite it did not contain any triphenyl phosphonium derivatives.

4.3.1.2 EuL7 absorption and emission properties

The photohysical properties of **EuL7** were measured in order to understand the photophysical behaviour of **EuL1** and **TbL1** that, as mentioned before, contained the same chromophore antenna of **EuL7**. As it was hypothesized in the sections 3.5.1 and 4.1.1, the cleavage of the acetate groups of dihydrofluorescein diacetate could be responsible for the absence of Ln^{3+}-based emission in **EuL1** and **TbL1** since the new antenna generated upon the acetate groups cleavage, namely the dihydrofluorescein, was not able to act as sensitizer toward Eu(III) and Tb(III). For this reason, the complexation of **L7** with $EuCl_3$ that led to the formation of **EuL7** was performed by heating the starting materials for 6 hours rather than for 15 hours, as it was made for **EuL1** and **TbL1**. It was thought that lowering the reaction time would have prevented the cleavage of the acetate groups from the dihydroluorescein diacetate in **EuL7**. The **EuL7** absorption spectrum showed an intense peak at 280 nm and, similarly to **EuL1** and **TbL1**, a less intense peak at 489 nm (Figure 61). The peak at 489 nm suggested that the acetate groups present on the dihydrofluorescein diacetate in **EuL7** were cleaved.

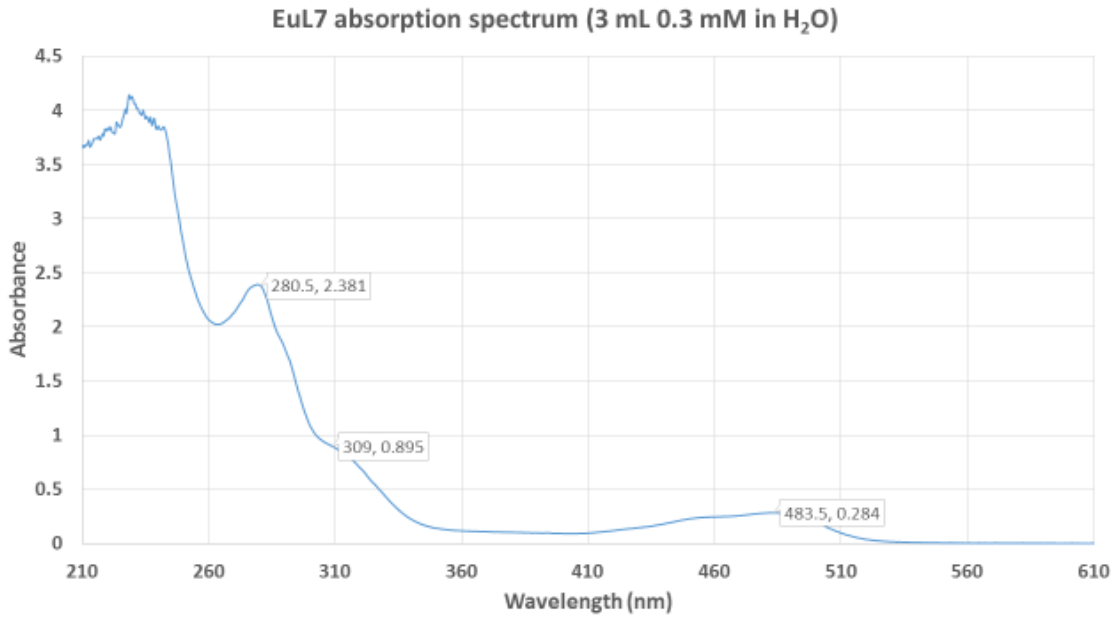

Figure 61. **EuL7** absorption spectrum (3 mL 0.3 mM in H_2O).

However, the peak at 489 nm in **EuL7** was much lower in intensity compared to the peak intensity at 489 nm observed in the **EuL1** and **TbL1** absorption spectra, despite the absorbance of **EuL7**, **EuL1** and **TbL1** was recorded starting from the same concentration of complexes, namely 0.3 mM. This suggested that **EuL7** was probably a mixture of two complexes, one containing the dihydrofluorescein diacetate and the other one containing the dihydrofluorescein, namely the product of the acetate groups' cleavage. The **EuL7** emission, recorded upon exciting the dihydrofluorescein diacetate at 275 nm, did not show the characteristic Eu(III) based luminescence (Figure 62).

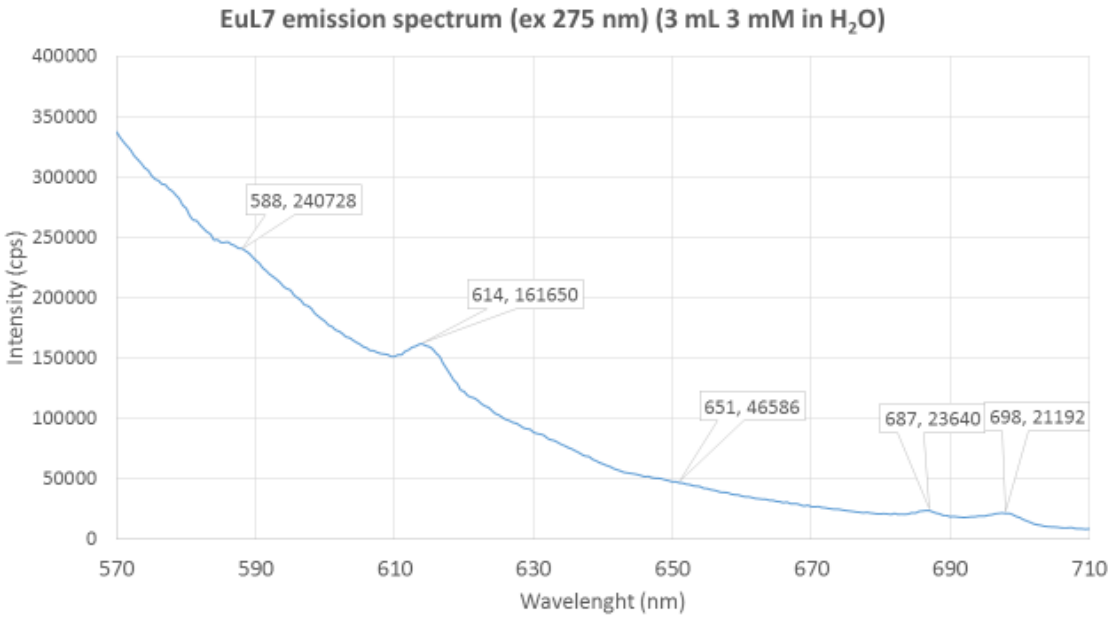

***Figure 62*. EuL7** emission spectrum recorded upon excitation at 275 nm (3 mL 3 mM in H_2O).

However some features characteristic of Eu(III) emission were observed. This is particularly evident in Figure 63, where the **EuL7** emission profile is compared with the $EuCl_3$ emission profile recorded upon Eu(III) direct excitation at 397 nm.

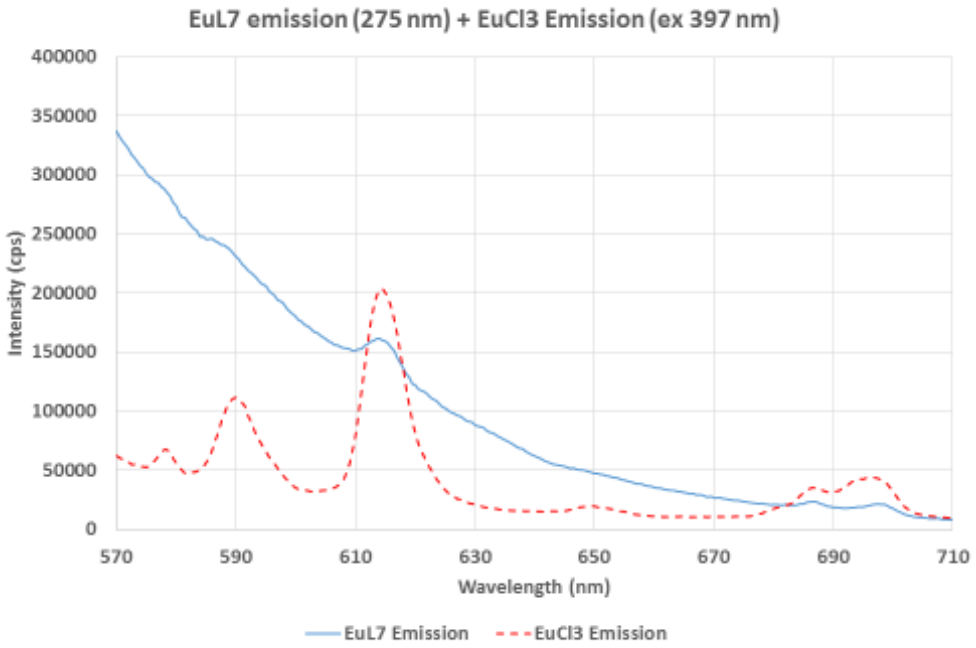

Figure 63. **EuL7** Emission spectrum recorded upon excitation at 275 nm (solid blue line) and the $EuCl_3$ emission spectrum recorded upon Eu(III) direct excitation at 397 nm (dashed red line).
(**EuL7** and $EuCl_3$ 3 mL 3 mM in H_2O)

The presence of some features characteristic of Eu(III) emission profile observed in **EuL7** emission spectrum indicated that a very low antenna effect was achieved upon excitation of dihydrofluorescein diacetate at 275 nm. This low antenna effect could be due to a low amount of dihydrofluorescein diacetate that survived to the acetate group's cleavage, which was hypothesized to occur during the complexation reaction. Similarly to **EuL1** and **TbL1**, the emission of **EuL7** recorded upon excitation at 489 nm did not show the characteristic Eu(III) emission, indicating that no antenna effect was achieved upon excitation of the dihydrofluorescein antenna at 489 nm. The results obtained with the photophysical properties studies of the Ln^{3+} complexes described so far, namely **EuL1**, **TbL1**, **EuL2**, **TbL2**, **EuL6** and **EuL7** suggested that:

- The absence of the Ln^{3+}-based luminescence in **EuL2** and **TbL2** was due to the type of chromophore antenna used to achieve the Eu(III) and Tb(III) sensitization,

namely the coumarin 343, rather than a Ln^{3+} luminescence quenching by the triphenyl phosphonium moieties. This was confirmed by the fact that no Eu(III) emission was achieved using the coumarin 343 as sensitizer antenna in **EuL6**, despite the latter did not contain any triphenyl phosphonium moieties.

- The absence of the Ln^{3+}-based luminescence in **EuL1** and **TbL1** was due to the fact that the dihydrofluorescein diacetate could undergo removal of acetate groups and the resulting diacetate-deprotected product, namely the dihydrofluorescein, was not able to sensitize the Eu(III) and Tb(III) emission. The acetate group removal probably occurred during the complexation reaction performed by treating **L1** with the $LnCl_3$ in methanol at reflux for about 15 hours. In this case the long exposure at refluxing conditions of **L1** to the $LnCl_3$ methanol solution could favour the acetate groups' cleavage. The results obtained with **EuL1** and **TbL1** photophysical properties studies were in line with the results obtained with the photophysical properties studies performed on **EuL7**, which contained the same chromophore antenna used in **EuL1** and **TbL1**. Although no Eu(III) emission was observed upon exciting the dihydrofluorescein diacetate antenna at 275 nm, some features characteristic of the Eu(III) emission profile were observed in **EuL7** emission spectrum. This was probably due to a low fraction of the dihydrofluorescein diacetate that did not undergo to the acetate groups' removal during the complexation reaction. This could be also an indication that that dihydrofluorescein diacetate would have been a suitable Eu(III) sensitizer if it would have not been converted into its diacetate-deprotected product. However it could not be excluded that the low Eu(III) sensitization achieved upon exciting **EuL7** at 275 nm (Figure 62) could be due to a low Eu(III) sensitization by the carbonyl functions rather than a possible low fraction of dihydrofluorescein diacetate survived to the acetate cleavage since the typical wavelength used to excite the carbonyl functions is 280 nm.

The inability of the coumarin 343 and the diacetate-deprotected product of the dihydrofluorescein diacetate to act as sensitizer antennae towards Eu(III) and Tb(III) was due to their relatively long absorption wavelengths, which were respectively 418 and 489 nm. This was in line what was found in the literature [83]. According to the data reported by Steemers et al. [83], the long wavelength absorption edge of the antenna cannot be much above 346 nm for Tb^{3+} or above 385 nm for Eu^{3+} complexes in order to obtain a fast and irreversible energy transfer process from the antenna to the lanthanide ion [83]. Since no Ln^{3+} emission was observed with the complexes examined so far due to the absorption properties of chromophore antennae used in these complexes, it was necessary to synthesize another complex bearing a different sensitizer antenna. The following section describes the photophysical properties of **EuL5**, which was synthesized with the aim to investigate the sensitization of Eu(III) with a chromophore antenna absorbing the light at shorter wavelengths compared to the chromophore antennae used in the complexes examine so far.

4.3.2 EuL5 Photophysical Studies

EuL5 was synthesized starting from the ligand **L5** and complexing it with Eu(III). As it is shown in Figure 64, **EuL5** contained two chromophore antennae of coumarin 151 used to sensitize the Eu(III) emission. The coumarin 151 was used to have an antenna that absorbed the light at shorter wavelength compared to the coumarin 343 used in **EuL2**, **TbL2** and **EuL6** that showed a maximum absorption peak at 418 nm. This would have allowed to overcome the issue of the long-wavelength absorption chromophore antenna responsible for the absence of Ln^{3+} emission in the previous complexes.

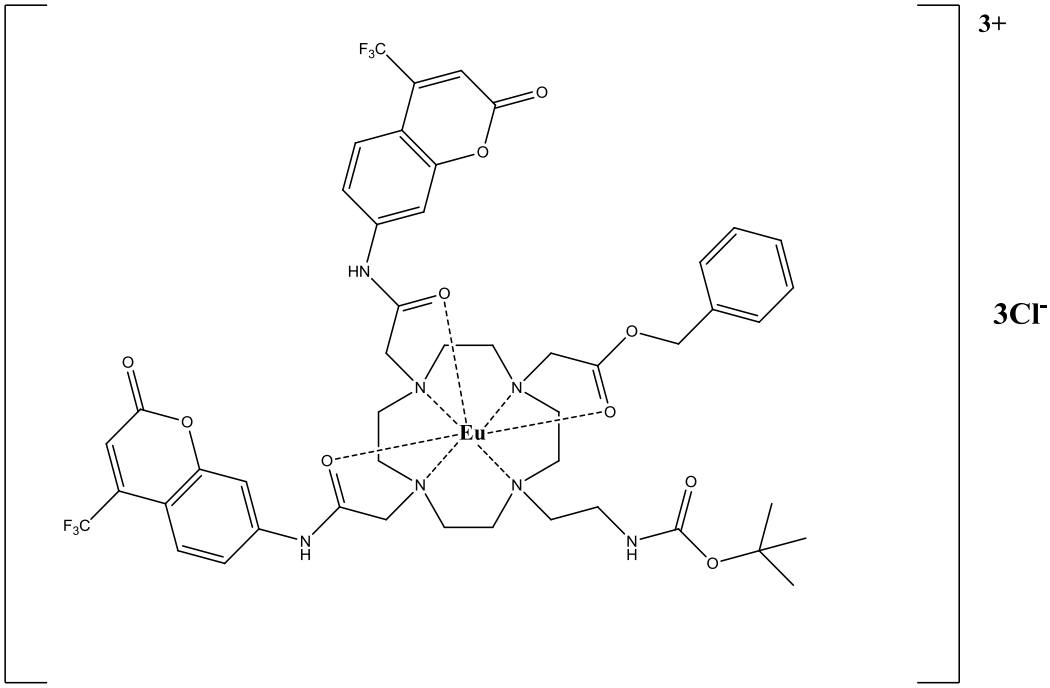

EuL5

Figure 64. Chemical structure of **EuL5**.

The absorption spectrum of **EuL5** (Figure 65) showed one peak at 339 nm and a very intense peak in the region comprises between 200 and 230 nm. The peak at 339 nm was related to the absorbance of the coumarin 151 antenna, which is known to absorb the light at around 350 nm.

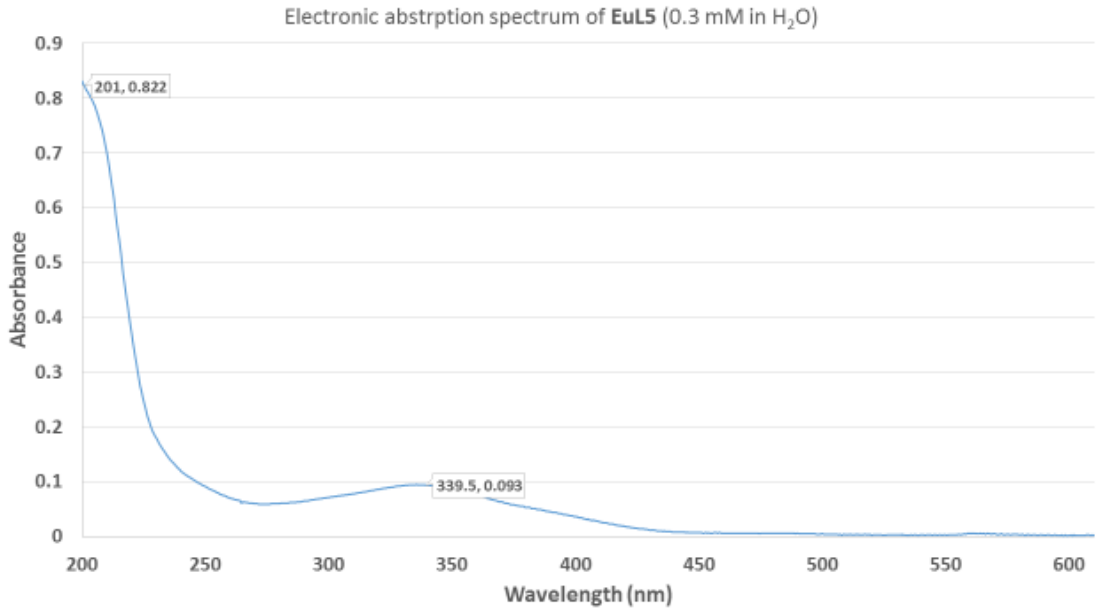

Figure 65. Electronic absorption spectrum of **EuL5** (3 mL 0.3 mM in H_2O).

No emission from the lanthanide europium was observed following Eu(III) direct excitation at 397 nm, whilst the characteristic Eu(III)-based luminescence was observed following excitation of the chromophore antennae at 339 nm (Figure 66). This indicated that the coumarin 151 antenna was able to sensitize the Eu(III) emission. The **EuL5** emission spectrum presented the five bands $\Delta J = 0$, $\Delta J = 1$, $\Delta J = 2$, $\Delta J = 3$ and $\Delta J = 4$ characteristic of the Eu(III) emission and that arise from $^5D_0 \rightarrow {}^7F_J$ transitions [84], [20], [24] (Figure 66).

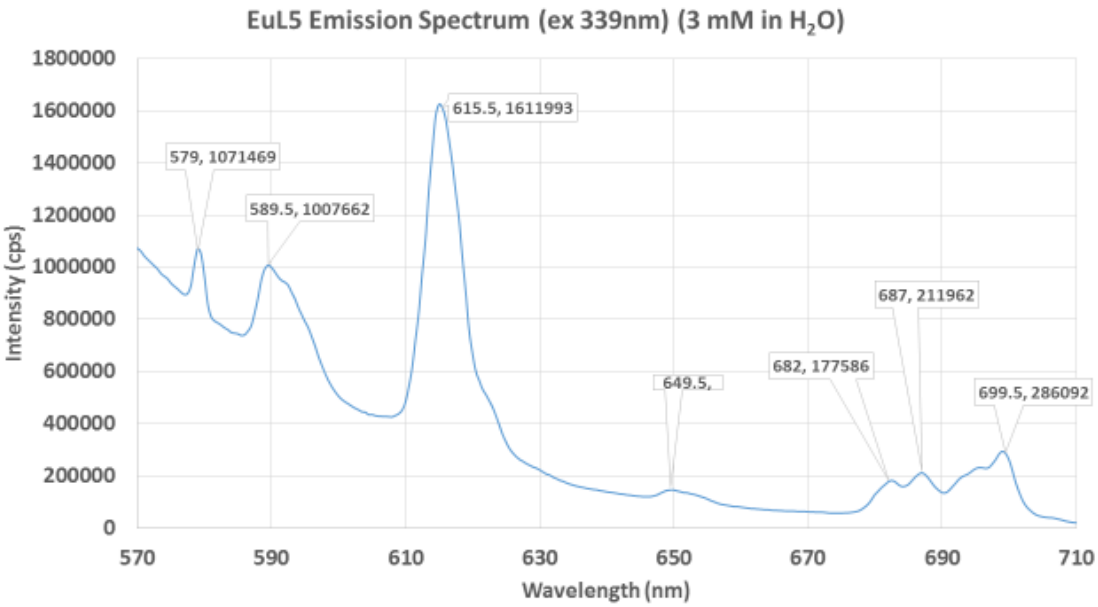

Figure 66. Emission spectrum of **EuL5** (3 mL 3 mM in H_2O) recorded upon excitation of the coumarin 151 antennae at 339 nm. The ΔJ values are shown on the spectrum.

The fact that the sensitization of the Eu(III) emission in **EuL5** was achieved using the coumarin 151 as sensitizer antennae having a maximum absorption peak below 385 nm was consistent with the data reported in the literature by Steemers *et al.* [83], which were discussed above. This was also a further proof that in the previous complexes, namely **EuL1**, **TbL1**, **EuL2**, **TbL2**, **EuL6** and **EuL7** the Eu(III) and Tb(III) sensitization were not achieved using the coumarin 343 and the dihydrofluorescein diacetate as sensitizer antennae because of their absorption properties. The coumarin 343 was not able to sensitize the Eu(III) and Tb(III) emission because of its relative long absorption wavelength at 418 nm, while the absence of Ln^{3+} emission in **EuL1**, **TbL1** and **EuL7** was due to the cleavage of the acetate groups of the dihydfrofluorescein diacetate, probably occurring during the complexation reaction, which converted it into its diacetate deprotected product, the dihydrofluorescein, which could not act as Eu(III) and Tb(III) sensitizer since it presented a maximum absorption peak at 489 nm.

The **EuL5** excitation spectrum (Figure 67) was recorded by monitoring the Eu(III) emission at 616 nm, which is the emission wavelength corresponding to the electric-dipole allowed transition $^5D_0 \rightarrow {}^7F_2$ [81], [84]. It showed an intense band between 340 and 360 nm. The similarity between the **EuL5** absorption and excitation spectra confirmed that the energy transfer process from coumarin 151 to Eu(III) was not efficient.

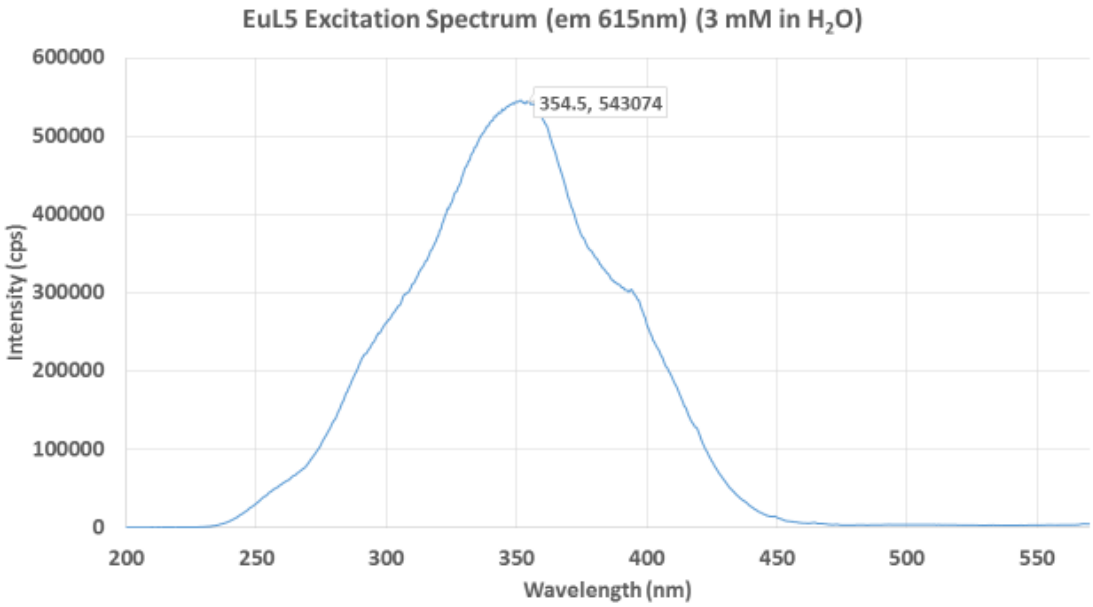

Figure 67. **E**xcitation spectrum of **EuL5** (3 mL 3 mM in H_2O) recorded by monitoring the Eu(III) emission at 616 nm.

From the results examined so far, it was evident that the triphenyl phosphonium derivatives in **EuL1**, **TbL1**, **EuL2** and **TbL2**, as well as the spacer length separating the antenna from the Ln^{3+} core in **EuL1**, **TbL1**, **EuL2**, **TbL2, EuL6** and **EuL7**, were not responsible for the absence of the characteristic Ln^{3+} based emission observed with these complexes. It was demonstrated that for an efficient Eu(III) sensitization the use of a chromophore antenna absorbing below 389 nm was essential to obtain a fast and irreversible energy transfer process from the antenna to the lanthanide ion [83]. With this in mind, two complexes, **EuL4** and **TbL4**, were synthesized starting from the same ligand

L4, which was functionalised with two pendant arms containing the triphenyl phosphonium derivatives and a pendant arm containing a low-wavelength absorbing sensitizer antenna, separated from the Ln^{3+} with the same spacer used in **EuL1**, **TbL1**, **EuL2**, **TbL2, EuL6** and **EuL7**. **L4** was complexed with Eu(III) in **EuL4** and with Tb(III) in **TbL4**. The photophysical properties of **EuL4** and **TbL4** will be discussed in the following section.

4.3.3 EuL4 and TbL4 Photophysical Studies

The chemical structures of **EuL4** and **TbL4** are shown in the figure 68.

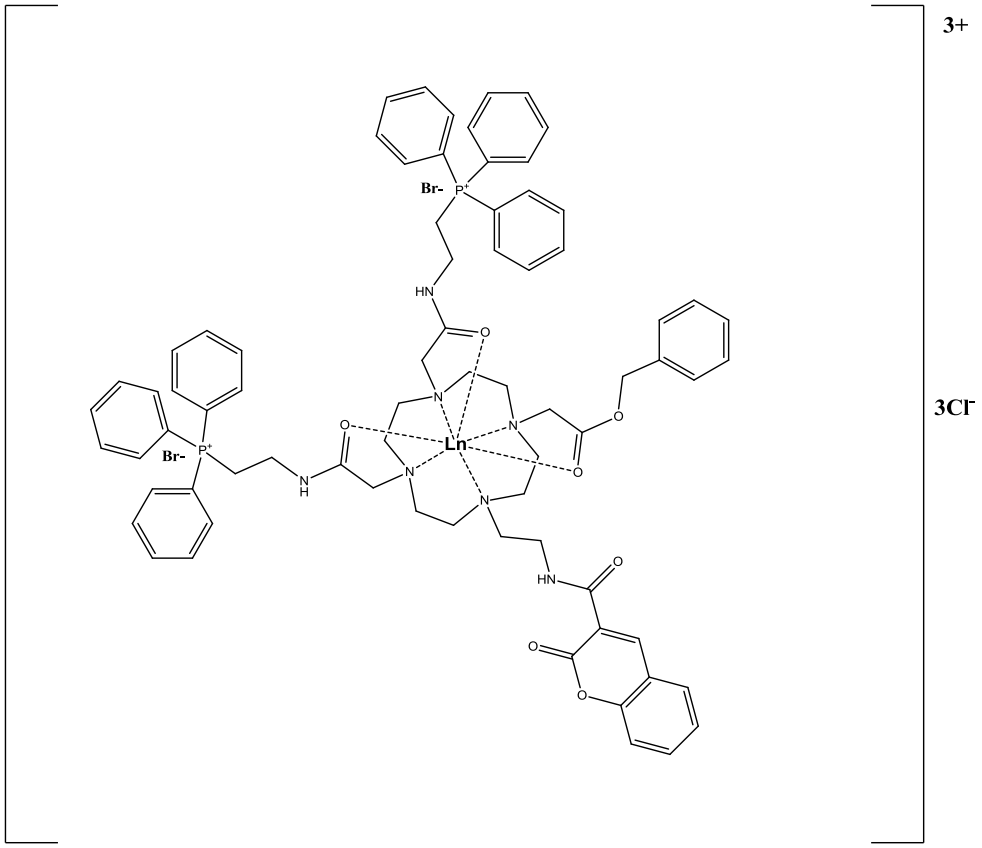

EuL4: Ln = Eu
TbL4: Ln = Tb

Figure 68. Chemical structure of **EuL4** and **TbL4.**

The coumarin 3 carboxylic acid was used as Eu(III) sensitizer antenna in **EuL4** and as Tb(III) sensitizer antenna in **TbL4**. To sensitize the Ln^{+3} emission in **EuL4** and **TbL4** it was necessary to use an antenna absorbing the light below 385 nm. This was achieved using the coumarin 3 carboxylic acid since it contained a free carboxylic function that could be coupled to the free primary amino function of the (DTPPBC) **(41)** during the final step of **L4** synthesis and presents two intense absorption peaks at 214 and 290 nm and lower intense peak at 329 nm, as shown in Figure 69.

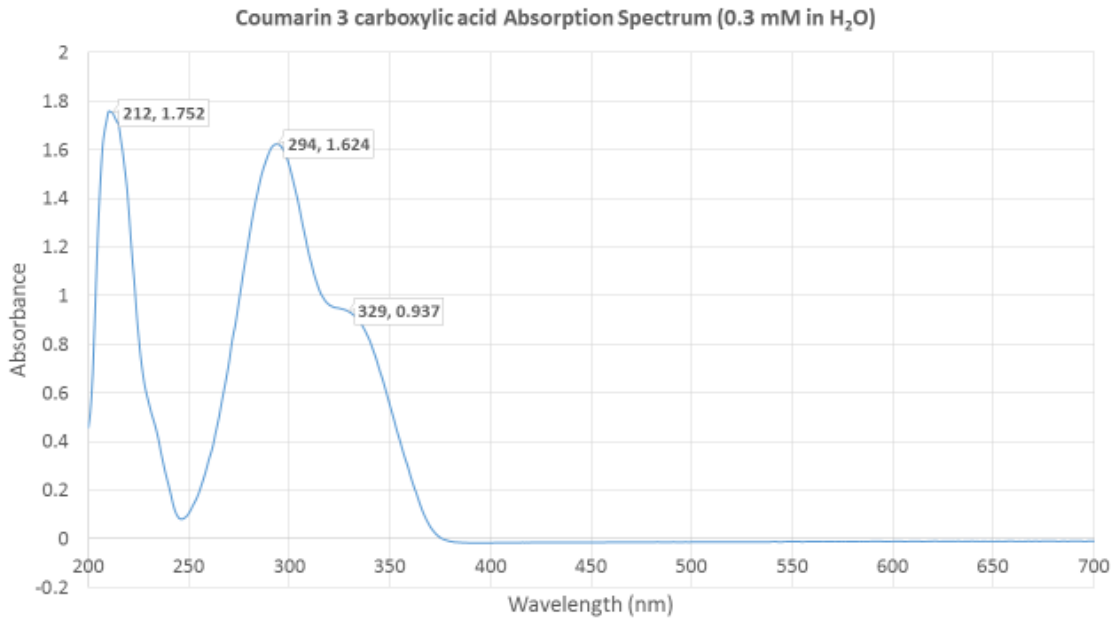

Figure 69. Absorption spectrum of coumarin 3 carboxylic acid (3 mL 0.3 mM in H_2O).

The absorption spectrum of **EuL4** (Figure 70) presented a relative intense absorption peak at 298 nm, which was related to the coumarin 3 carboxylic acid antenna, and another intense absorption peak at 206 nm.

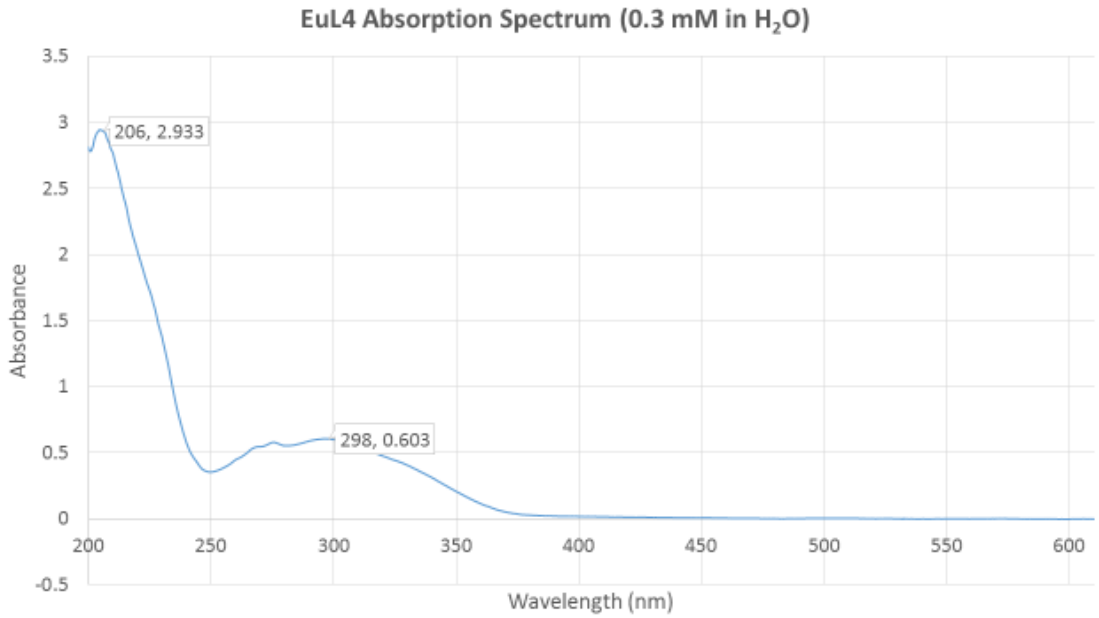

Figure 70. Absorption spectrum of **EuL4** (3 mL 0.3 mM in H_2O).

The characteristic Eu(III)-based luminescence was observed with **EuL4** following Eu(III) direct excitation at 397 nm. However, as expected, the five Eu(III) emissive bands (ΔJ = 0, ΔJ = 1, ΔJ = 2, ΔJ = 3 and ΔJ = 4) were low in intensity due to the Eu(III) low molar absorption coefficient. After recording the emission of **EuL4** by setting the excitation wavelength at 298 nm, which corresponded to longest wavelength absorption peak observed in **EuL4** absorption spectrum, an intense Eu(III) based luminescence was achieved (Figure 71).

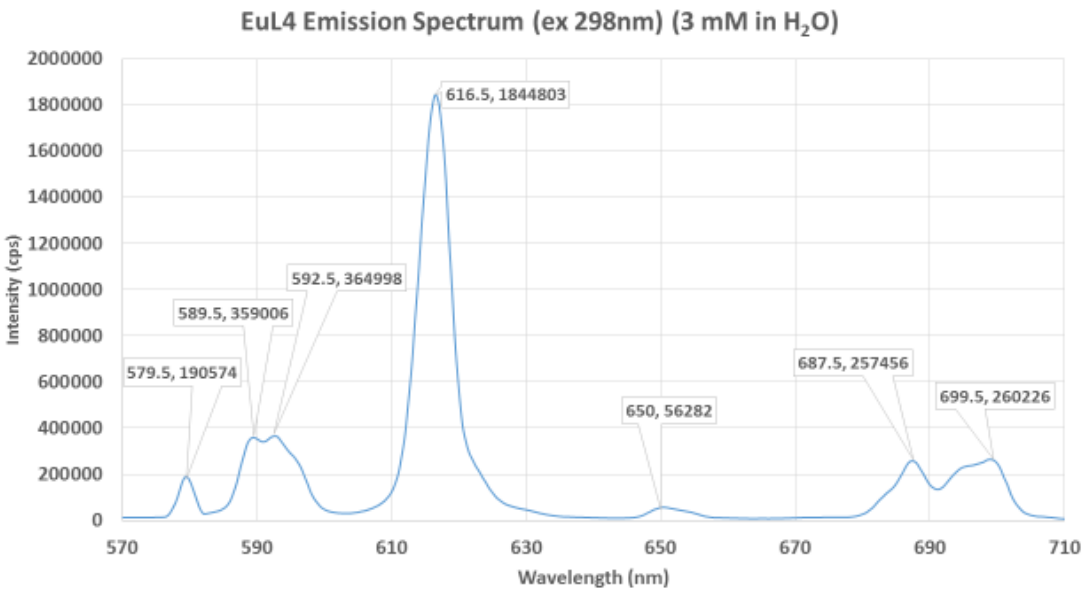

Figure 71. Emission spectrum of **EuL4** (3 mL 3 mM in H_2O) recorded upon excitation of the coumarin 3 carboxylic acid antenna at 298 nm. The *ΔJ* values are shown on the spectrum.

The increasing in the intensity of the five europium emissive bands was due to an antenna effect exerted by the coumarin 3 carboxylic acid towards Eu(III). The sensitization of the Eu(III) emission in **EuL4** achieved using the coumarin 3 carboxylic acid as Eu(III) sensitizer antenna confirmed that the triphenyl phosphonium derivatives as well as the linker spacer length separating the antenna from the lanthanide ion did not affect the lanthanide emission. The **EuL4** excitation spectrum was recorded by monitoring the europium emission at 616 nm (Figure 72).

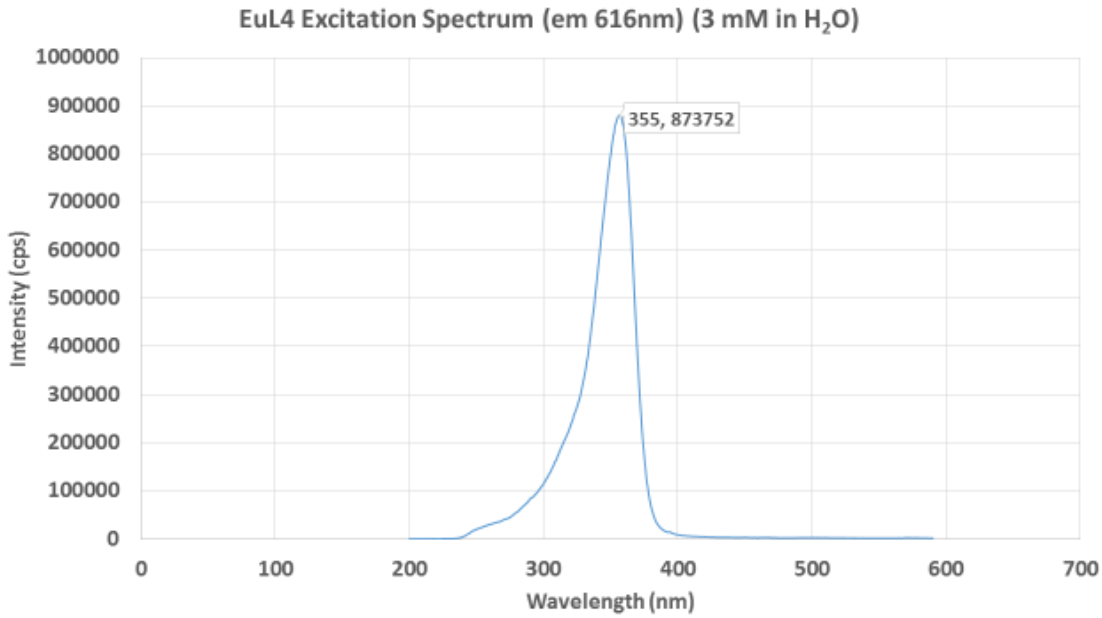

Figure 72. Excitation spectrum of **EuL4** (3 mL 3 mM in H_2O) recorded by monitoring the Eu(III) emission at 616 nm.

EuL4 excitation spectrum showed a maximum peak at 355 nm. The difference between **EuL4** absorption and excitation spectra was indicative of a partial energy transfer process from the coumarin 3 carboxylic acid to the Eu(III). This could be due to a partial absorption of the incident light by the phenyl rings present on the benzyl ester group and the triphenyl phosphonium moieties.

The photophysical properties of **TbL4** were not measured due to a very low amount of complex obtained that did not allowed to make enough concentrated solution to record its absorption, emission and excitation profiles.

4.4 Photophysical properties of EuL4 and EuL5 measured in the presence of H_2O_2 and Fe(II) perchlorate

As discussed so far, **EuL4** and **EuL5** were the only lanthanide complexes that, among those synthesized in this project, exhibited the characteristic Eu(III)-based luminescence. Therefore **EuL4** and **EuL5** were chosen among the complexes examined so far to be evaluated for their response to the presence of ROS species. In order to verify whether or not **EuL4** and **EuL5** were able to sense the presence of ROS, their photophysical properties were measured in the presence of H_2O_2 by using emission spectroscopy. The test was performed in a cuvette containing 500 µL of a **EuL4** and **EuL5** 3 mM aqueous solution. The europium emission of **EuL4** and **EuL5** were recorded in absence and presence of added H_2O_2 and Fe(II) perchlorate. The Fe(II) perchlorate should be able to catalyse the formation of hydroxyl radicals from H_2O_2, which are ROS species, as to mimic what happens within the cells during the Fenton reaction catalysed by Fe(II)-containing enzymes (see chapter 1, section 1.3.2). While the concentration of Fe(II) perchlorate was kept constant at 30 µM, the H_2O_2 was tested at 120 µM and 720 µM according to the protocol [85]. Figure 73 shows the **EuL4** emission recorded in the presence of increasing amount of H_2O_2 and upon excitation of the sensitizer antenna, the coumarin 3 carboxylic acid derivative, at 324 nm.

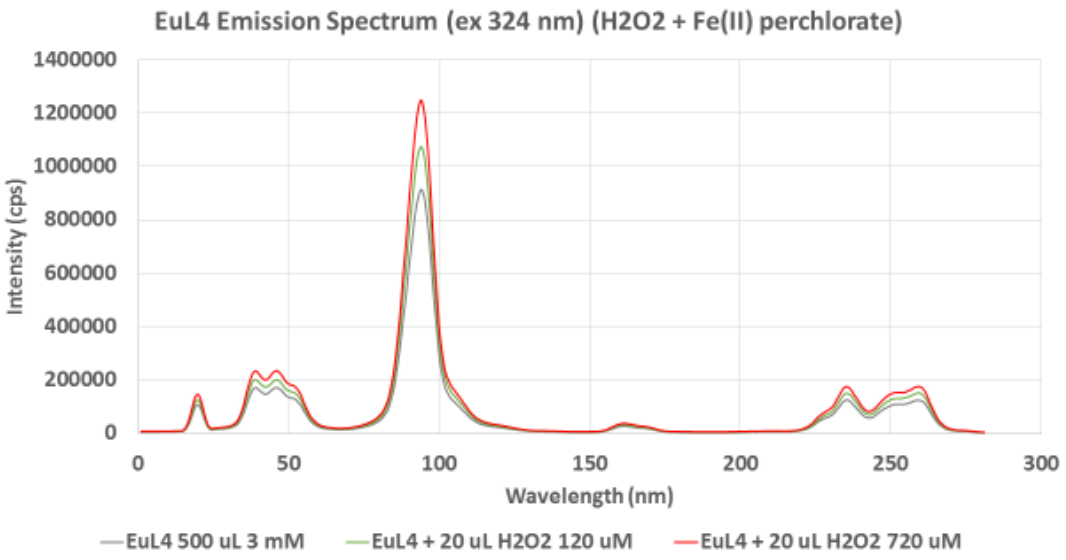

Figure 73. **EuL4** emission spectra recorded in absence athe presence of increasing concentration of H_2O_2 upon excitation at 324 nm.

As it is possible to see in Figure 73, a dose dependent increase of the Eu(III)-based emission intensity was observed upon the addition H_2O_2, while no changes in the Eu(III) emission profile form were observed, indicating that there were no changes of that the Eu(III) coordination environment. The intensity of the $\Delta J = 1$ transitions (around 588 nm) is known to be insensitive to changes in Eu(III) coordination environment, whilst the intensity of the $\Delta J = 2$ (around 618 nm) and $\Delta J = 4$ (around 702 nm) transitions changes considerably [86]. For example, changes in the $\Delta J = 2/\Delta J = 1$ could be indicative of changes in the Eu(III) coordination environment, such as those caused by the replacement of the solvent molecule involved in the coordination with another coordinating species, such as an anionic analyte [83]. The fact that no changes of the Eu(III) emission profile form were observed in **EuL4** upon H_2O_2 and Fe(II) perchlorate, suggested that no changes in the Eu(III) coordination took place, meaning that the solvent molecule involved in the coordination were not replaced by H_2O_2 or hydroxyl radicals generated in solution. The increase in the Eu(III) emission could be the consequence of changes in the photophysical properties of the Eu(III) sensitizer, namely

the coumarin 3 carboxylic acid, induced by the hydroxyl radicals generated in situ by Fe(II) perchlorate and H_2O_2. It is well known in fact that the coumarin 3 carboxylic acid could be hydroxylated in the presence of hydroxyl radicals generating compounds, with the position 7 of the coumarin ring representing the most favourable hydroxylation site. Opposite results were obtained with the Eu(III)-based complex **EuL5**, where a slight dose dependent decrease of the Eu(III)-based luminescence was observed upon the addition of H_2O_2, as it is possible to note in Figure 74. The **EuL5** emission was recorded in absence and presence of added Fe(II) perchlorate and H_2O_2 by exciting the chromophore antennae, namely the two coumarin 151 derivatives, at 339 nm.

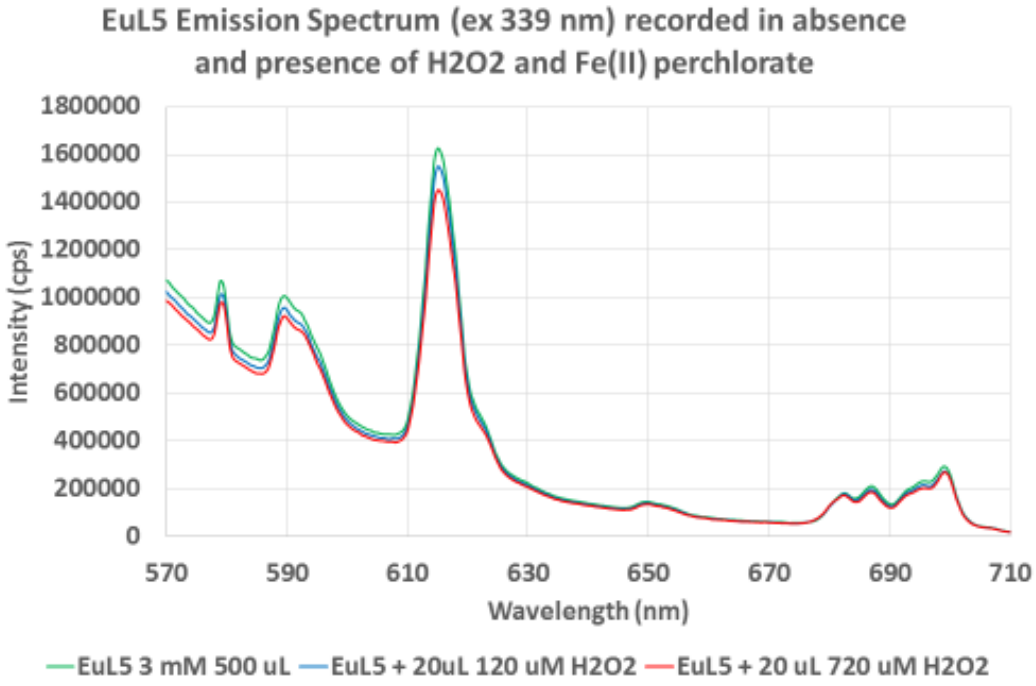

Figure 74. **EuL5** emission spectra recorded in absence and presence of H_2O_2 and Fe(II) perchlorate upon excitation at 339 nm.

Also in this case, no changes in the Eu(III) emission spectral form were observed suggesting that there were no changes in the Eu(III) coordination sphere. The slight dose dependent quenching of Eu(III) emission in **EuL5** could be attributable to changing in the

photophysycal properties of the two sensitizer antennae, namely the two coumarin 151 derivatives, caused by the hydroxyl radicals generated by Fe(II) perchlorate and H_2O_2. While the hypothesized hydroxylation of the coumarin 3 carboxylic acid derivative could improve the sensitization of the Eu(III) emission in **EuL4**, a probable hydroxylation of the coumarin 151 derivatives could be responsible indeed of reducing the efficiency of the Eu(III) sensitization in **EuL5**, explaining why in this case a slight decrease of the Eu(III)-based emission was observed. It was also hypothesized that the changes of the photophysical properties of the coumarin 151 derivatives could be due to the replacement of one or more fluorine atoms of the CF_3 function present on the coumarin 151 derivatives rather than the hydroxylation of the coumarin ring.

5. Results and Discussion: testing the lanthanide complexes on cells and isolated mitochondria.

This chapter describes three types of test that were performed on the lanthanide complexes synthesised in this project. The first two tests assess the impact of the lanthanide complexes on the functioning of the mitochondria as it is important to determine if the sensor is in itself toxic to cells. The first of these is mitochondrial stress test (MST) that was performed by measuring key parameters of mitochondrial function, by directly measuring the oxygen consumption rate (OCR) of cells, and of the glycolytic function by measuring the extracellular acidification rate (ECAR) of the medium surrounding the cells [87]. The second test, the calcium loading capacity assay, was performed on isolated mitochondria with the aim of investigating the effect of the lanthanide complexes synthesized in this project on the mitochondrial capability to uptake and internalize Ca^{2+}. The third and final test was a cellular ROS assay that evaluated the complexes ability to respond to changes in ROS in a cellular environment. This was performed on the lanthanide complexes **EuL4** and **EuL5** to evaluate whether or not these complexes were responsive to ROS species, such as H_2O_2 and $OH^{\cdot}$, in a cellular environment by measuring changes in their luminescence intensity eventually caused by increased ROS levels. The choice of testing **EuL4** and **EuL5** with the cellular ROS assay was made based on the results obtained with the photophysical studies discussed in the chapter 4, where it was evident that **EuL4** and **EuL5** were the only complexes among those synthesised in this project that exhibited the characteristic lanthanide-based luminescence. All the other complexes were not tested with the cellular ROS assay since, as discussed in the chapter 4, they did not show the typical lanthanide-based luminescence.

5.1 Mitochondrial Stress Test (MST)

The MST is a cell-based test used to predict the toxicity of a compound by measuring its effects on mitochondrial function. An important advantage of the MST is that it allows the simultaneous measurements of the oxygen consumption rate (OCR) and extracellular acidification rate (ECAR) of cells as indicators of mitochondrial respiration and glycolysis, respectively [87]. In the MST, the OCR and the ECAR of the cells are measured following the sequential addition of several compounds, each capable of modulating a specific component of the mitochondrial ETC (Figure 75), a detailed description has been provided in the chapter 1 (section 1.3.1).

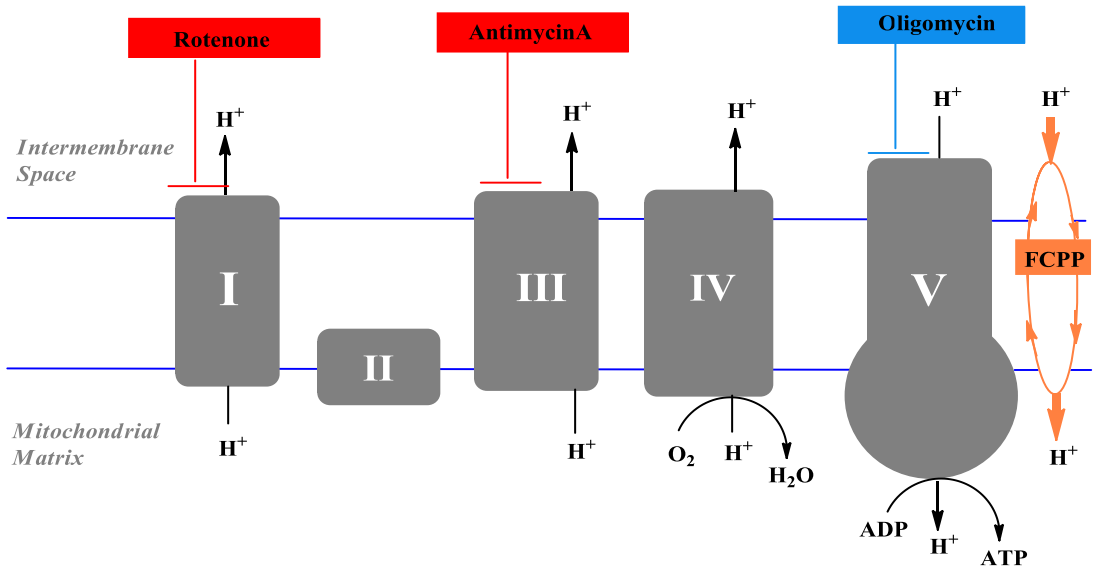

Figure 75. The picture illustrates the complexes of the ETC and the target of action of all of the compounds used in the Seahorse assay acting as modulators of the ETC.

The compounds that are sequentially injected into the wells containing the cells and the compounds to be tested for their toxicity are: oligomycin, carbonyl cyanide-4 (trifluoromethoxy) phenylhydrazone (FCCP) and a mixture of antimycin A, rotenone and glucose. Oligomycin inhibits ATP synthase (complex V) [88] and results in a decrease in OCR (Figure 75). FCCP is a protonophore (H^+ ionophore) that acts as mitochondria uncoupler since it causes an increase in proton (H^+) conductance through the inner

mitochondrial membrane, collapses the proton gradient and dissipates the mitochondrial membrane potential generated during the mitochondrial ETC [89]. As a consequence, the electron flow through the ETC increases in a futile attempt to restore the proton gradient and mitochondrial membrane potential across the inner mitochondrial membrane, and consequently oxygen is highly consumed by complex IV (Figure 75). Mitochondrial uncoupling is any process by which electron transport is not exploited to synthesize ATP or exert other important functions such as ion transport. All processes that allow protons to enter the matrix independently of ATP synthase are said to "uncouple" the substrate oxidation from ATP synthesis [90]. Rotenone is a complex I inhibitor [91] while antimycin A acts as complex III inhibitor [92] (Figure 75). The combination of rotenone and antimycin A blocks the mitochondrial ETC and allows the calculation of non-mitochondrial respiration, which is driven by any process outside the mitochondria [93] (Figure 70). In these experiments glucose was also included in the final injection. If cells switched to glycolysis following the rotenone and antimycin injection it could be inferred that there was no cytotoxicity and any effects seen in the traces were due to a direct effect on mitochondrial function. Figure 76 shows a typical cellular OCR profile measured with the MST.

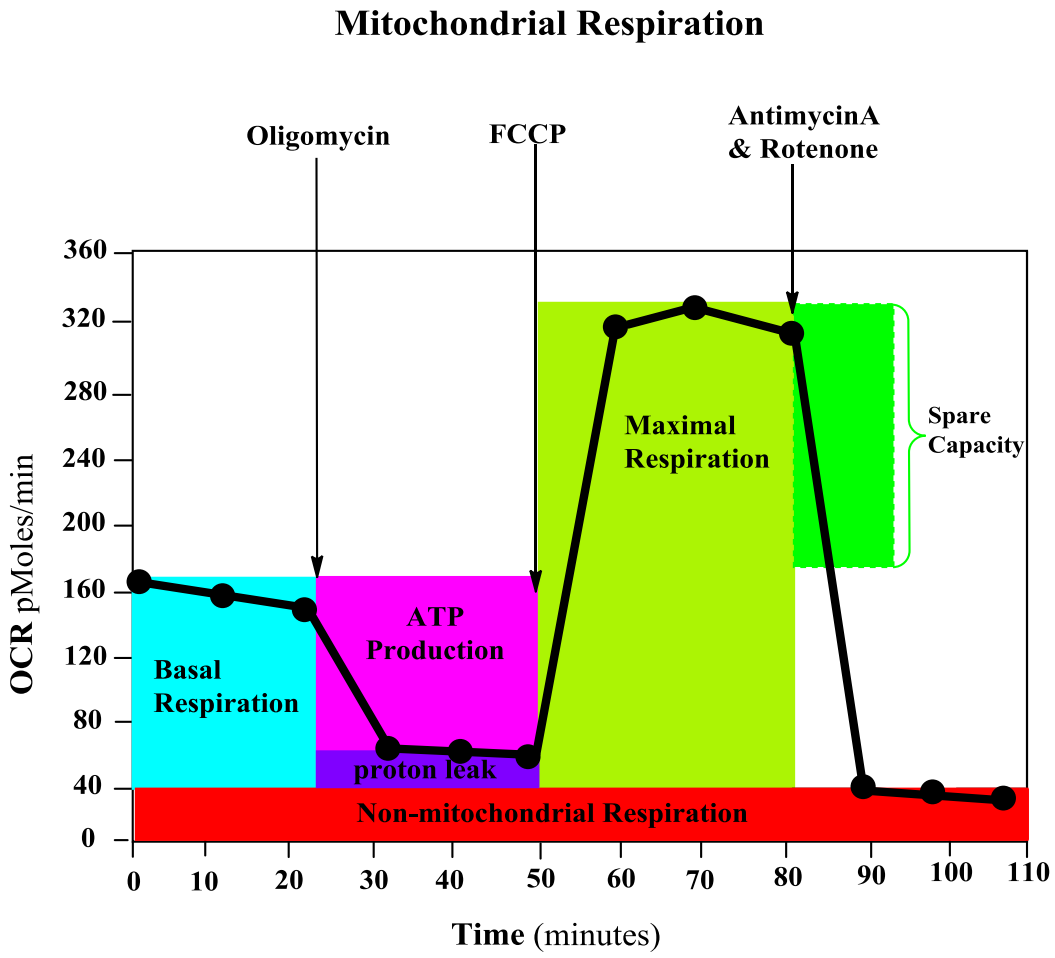

Figure 76. Profile of the key parameters of mitochondrial respiration.

5.1.1 Parameters of mitochondrial respiration measured with the MST

The OCR of cells measured during the first 60 minutes following injection of the lanthanide complexes of interest without addition of ETC modulators compounds, represents the basal respiration (Figure 76). Basal respiration represents the oxygen consumption used to meet cellular ATP demand under baseline conditions [93] and is due to two processes: ATP production and mitochondrial proton leak [94]. ATP production occurs in Complex V, as described above. Proton leak is the process by which protons (H^+) can return from the mitochondrial inner membrane space to the matrix independently of ATP synthase [95]. An increase in proton leak can occur when the integrity of the membrane has been disturbed and in general mitochondrial toxins tend

to increase proton leak. Although the precise mechanism of basal proton leak is not fully understood, it may be due to adenine nucleotide translocase (ANT), a transmembrane protein responsible for exchanging ADP for ATP across the mitochondrial inner membrane [96]. A decrease in the OCR is observed after the injection of oligomycin, an ATP synthase inhibitor. This enables the measurement of ATP- and proton leak-driven respiration [94].

5.1.1.1 Spare respiratory capacity: FCCP injection

The injection of FCCP causes a huge increase in the OCR (Figure 76). FCCP stimulates the respiratory chain to operate at its maximum capacity, which causes a rapid oxidation of substrates, such as sugars, fats and amino acids, to cope with this metabolic demand. The maximum level of OCR observed after FCCP injection represents the maximum rate of respiration that cells can achieve [93]. It is used to calculate the spare respiratory capacity, which is defined as the difference between maximal respiration and basal respiration. The spare respiratory capacity is a measure of the ability of the cell to respond to increased energy demand, indicating how closely the cell is working to its maximum limit. The cell's ability to respond to high energy demand can be an indicator of cell healthy, while the lack of spare capacity indicates a mitochondrial dysfunction [93].

5.1.1.2 Non-mitochondrial respiration: rotenone and antimycin A injection

The last injection, which is a mixture containing rotenone and antimycin A, causes a decrease in the OCR, due to the block of the ETC via inhibition of the complex I and III exerted respectively by rotenone and antimycin A (Figure 76). The oxygen consumption that persists after rotenone and antimycin A injection is due to cellular enzymes that continue to consume oxygen and is defined as “non-mitochondrial oxygen consumption”. The non-mitochondrial respiration is an important parameter since it enables an accurate measurement of mitochondrial respiration by subtracting the non-mitochondrial respiration from the total OCR [93].

5.1.1.3 Extracellular acidification rate: glycolytic activity of the cells

The ECAR measured simultaneously with the OCR gives important information about the glycolytic activity of the cells. Glycolysis is the metabolic pathway that converts glucose to pyruvate and occurs in most organisms in the cytosol of the cell. When the oxygen level is low, pyruvate is converted to lactate with the subsequent production of ATP and protons (H^+). The protons (H^+) are transported outside the cell to keep constant the intracellular pH and the accumulation of the protons (H^+) into the extracellular medium causes an extracellular acidification [94]. An advantage of the MST is that it allows the simultaneous calculation of the cellular OCR and ECAR. This is an important advantage since it allows identification of compounds that have effects on the mitochondrial functions via OCR, as well as compounds that have effects on the glycolytic function of the cells via ECAR [94]. In many cases the OCR and ECAR measurements are complimentary with inhibition of ATP production by oxidative phosphorylation causing a parallel increase in ATP production by glycolysis and vice versa. Concurrent drops in both OCR and ECAR may be indicative of compound cytotoxicity.

5.1.2 Understanding the effects of the lanthanide complexes on cellular and mitochondrial functions using the MST

A MST was performed on the lanthanide complexes **EuL1**, **TbL1**, **EuL2**, **TbL2**, **NdL3**, **YbL3**, **EuL4** and **TbL4** synthesised in this project in order to understand their effects on the cellular and mitochondrial functions. All the complexes were tested at concentrations of 200 µM, 50 µM, 12.5 µM, 3.1 µM and 0.8 µM and their related OCR and ECAR profiles were recorded in presence and absence of cells (HepG2 liver cancer cell line). The OCR (pmol/min) was recorded in real time upon the sequential injections described above. The ECAR profiles were recorded in order to measure the compounds' effect on the glycolytic activity of the cells. The ECAR profiles were recorded in real time upon the

same sequential injection of the compounds seen above for the OCR profiles recording with the difference that in the last injection (injection 4) the glucose was added together with rotenone and antimycin A to stimulate glycolysis. In all graphs injection 1 refers to the test compound injection, while injections 2, 3 and 4 correspond to the oligomycin, FCCP and rotenone/antimycin A/glucose injections respectively. All OCR and ECAR profiles recorded in the presence of cells were compared to the OCR profile related to the control, which contains just the cells and DMSO vehicle and appears in all diagrams as a bold blue line. The OCR and ECAR profiles were also recorded in absence of cells to see if there were any compounds' interference when the cells were not present, such as saturation of OCR and /or ECAR fluorophores.

5.1.2.1 MST results of the lanthanide complexes analysed with the MST test

Table 7 and 8 show a summary of the MTS data related to all lanthanide complexes analysed with this test and provide a direct comparison between the data of all complexes.

OCR RATE measured in presence of cells				
Compound	**OCR RATE after compound injection (injection 1): basal respiration**	**OCR RATE after oligomicyn injection (injection 2): proton leak**	**OCR RATE after FCCP injection (injection 3): spare respiratory capacity**	**OCR RATE after rotenone/antimycin A injection (injection 4): non-mitochondrial respiration**
EuL1 / TbL1	increase	increase	erosion	increase
EuL2 / TbL2	erosion	no effect	erosion	no effect
NdL3 / YbL4	increase	increase	erosion	increase
EuL4 / TbL4	no effect	no effect	no effect	no effect

Table 7. Summary of compounds effect on the parameters of mitochondrial respiration recorded in presence of cells.

Compound	OCR LEVEL in absence of cells: interference of compound on OCR fluorophore	ECAR LEVEL in absence of cells: interference of compound on the ECAR (pH) fluorophore	ECAR RATE in presence of cells: glycolysis recovery
EuL1 and TbL1	observed	observed	observed for 3.1 and 0.8 µM
EuL2 and TbL2	not observed	observed	observed for 3.1 and 0.8 µM
NdL3 and YbL4	observed	observed	observed from 12.5 to 0.8 µM
EuL4 and TbL4	not observed	slight effect observed for 200 and 50 µm	observed from 12.5 to 0.8 µM

Table 8. Summary of compounds effect on OCR and ECAR fluorophores and glycolysis recovery.

5.1.2.2 OCR profiles of EuL1

Figure 77 shows the OCR RATE profile related to **EuL1** recorded in presence of cells.

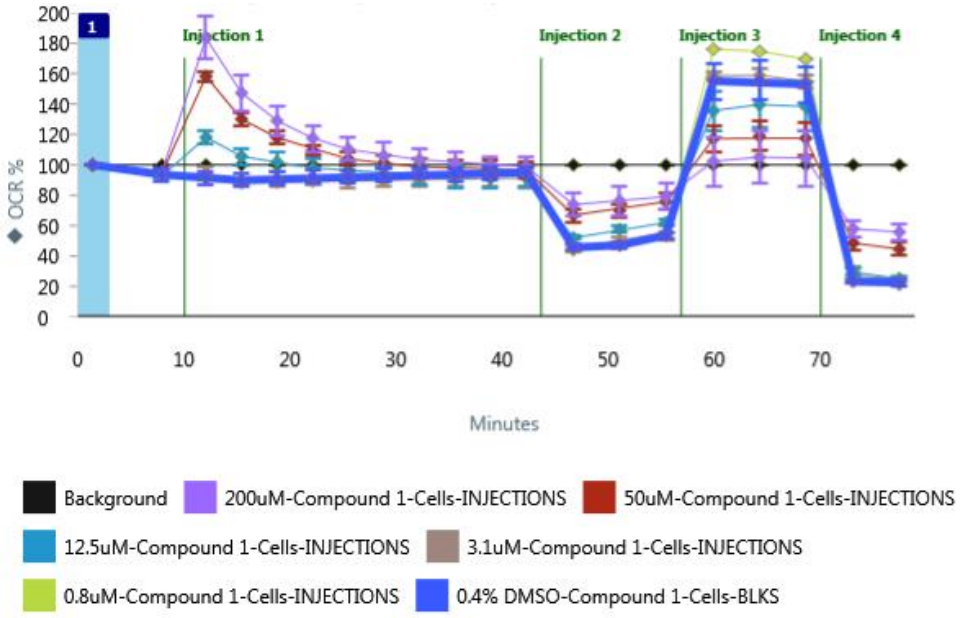

Figure 77. OCR RATE of cells measured during the MST performed on **EuL1** in presence of cells. **Injection 1** corresponds to **EuL1** injection, **injection 2** corresponds to oligomicyn injection, **injection 3** corresponds to FCCP injection and **injection 4** corresponds to rotenone/antimycin A injection.

Looking at the diagram shown in Figure 77 it seemed that **EuL1** injection (injection 1) had an uncoupling effect since an initial high dose dependent increase of OCR was observed. However the supposed uncoupling effect by **EuL1** cannot be confirmed looking at the **EuL1** OCR RATE profile recorded in absence of cells shown in Figure 78 since a large increase of oxygen consumption by **EuL1** down to 3.1 µM was observed even when cells were not present.

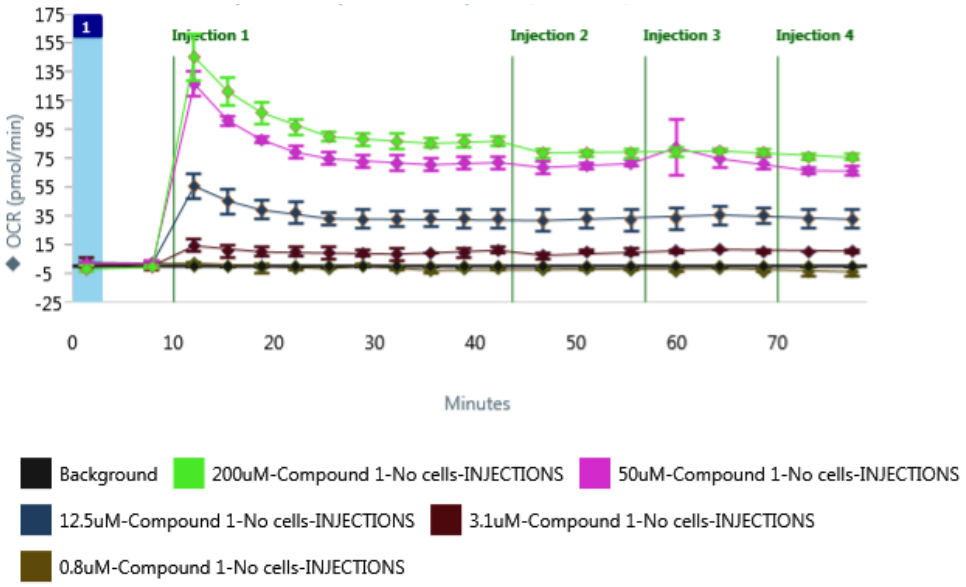

Figure 78. **EuL1** OCR RATE measured during the MST in absence of cells. **Injection 1** corresponds to **EuL1** injection, **injection 2** corresponds to oligomicyn injection, **injection 3** corresponds to FCCP injection and **injection 4** corresponds to rotenone/antimycin A injection.

The oxygen consumption observed for **EuL1** in absence of cells could be due to its ability to incorporate oxygen or a gradually accumulating effect on the OCR fluorophore. However there was no further evidence to support either of these hypothesis. The diagram in Figure 79 shows the **EuL1** OCR LEVEL recorded in absence of cells.

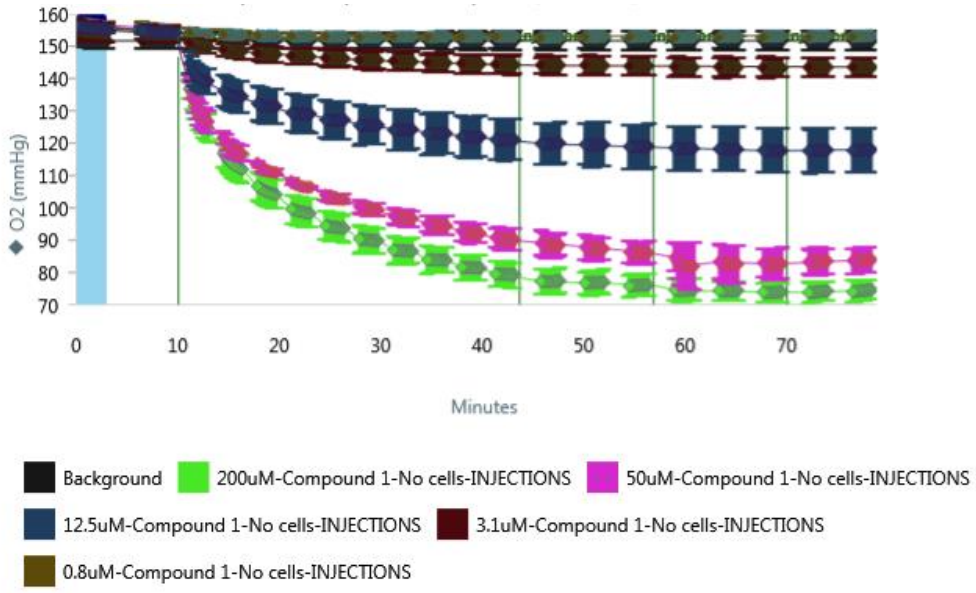

Figure 79. **EuL1** OCR LEVEL measured during the MST in absence of cells. **Injection 1** corresponds to **EuL1** injection, **injection 2** corresponds to oligomicyn injection, **injection 3** corresponds to FCCP injection and **injection 4** corresponds to rotenone/antimycin A injection.

Whilst there was not an instantaneous decrease in oxygen level, **EuL1** caused a dose dependant drop in oxygen levels in absence of cells. This was a further evidence that the huge increase in OCR RATE recorded in presence of cells (Figure 77) could not be interpreted as uncoupling effect as it was a systematic effect caused by **EuL1**. Looking back at **EuL1** OCR in presence of cells (Figure 77) it is possible to note that, despite the compound interference, it had a deleterious effect on maximal respiration, recorded upon FCCP injection (injection 3). In particular 200 µM, 50 µM and 12 µM of **EuL1** showed an erosion of the spare respiratory capacity (maximal respiration) indicating that **EuL1** had a toxic effect on cells from 200-12.5 µM. From figure 77 it is also possible to note that there was an increase in non-mitochondrial respiration following rotenone and antimycin A (injection 4) suggesting that **EuL1** was in some way consuming oxygen from the system as this was also seen in wells without cells. However it could not be ruled out that there was a gradual cumulative effect of **EuL1** on the OCR fluorophore with time that appeared to give the impression of oxygen removal from the system. 3.1 and 0.8

µM of **EuL1** however showed a trend similar to the controls so they can be considered 'non-toxic'.

5.1.2.3 ECAR profiles of EuL1

Looking at the ECAR LEVEL of **EuL1** recorded in absence of cells (Figure 80), it is clear that **EuL1** had an immediate effect on ECAR LEVEL without cells meaning that **EuL1** caused by an immediate interference with the absorbance of the ECAR fluorophore down to 0.8 µM.

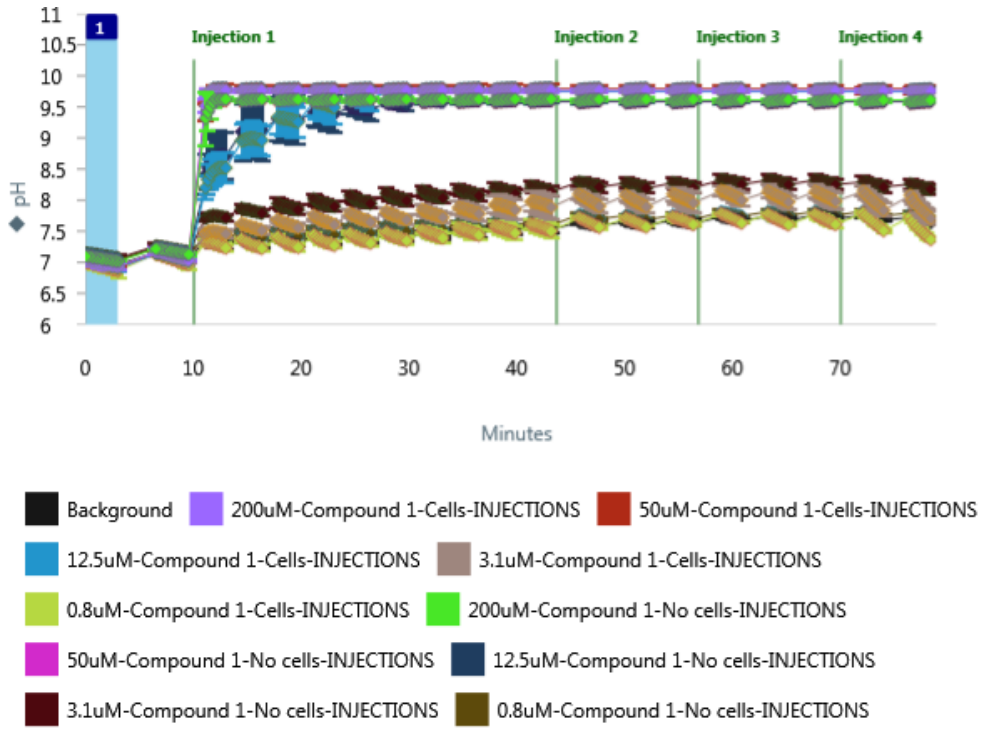

Figure 80. **EuL1** ECAR LEVEL measured during the MST in absence of cells. **Injection 1** corresponds to **EuL1** injection, **injection 2** corresponds to oligomicyn injection, **injection 3** corresponds to FCCP injection and **injection 4** corresponds to rotenone/antimycin A injection.

The **EuL1** interferece with the ECAR fluorophore made the interpretation of the ECAR RATE profile recorded in presence of cells (Figure 81) difficult with response flatling at almost all concentrations of **EuL1**.

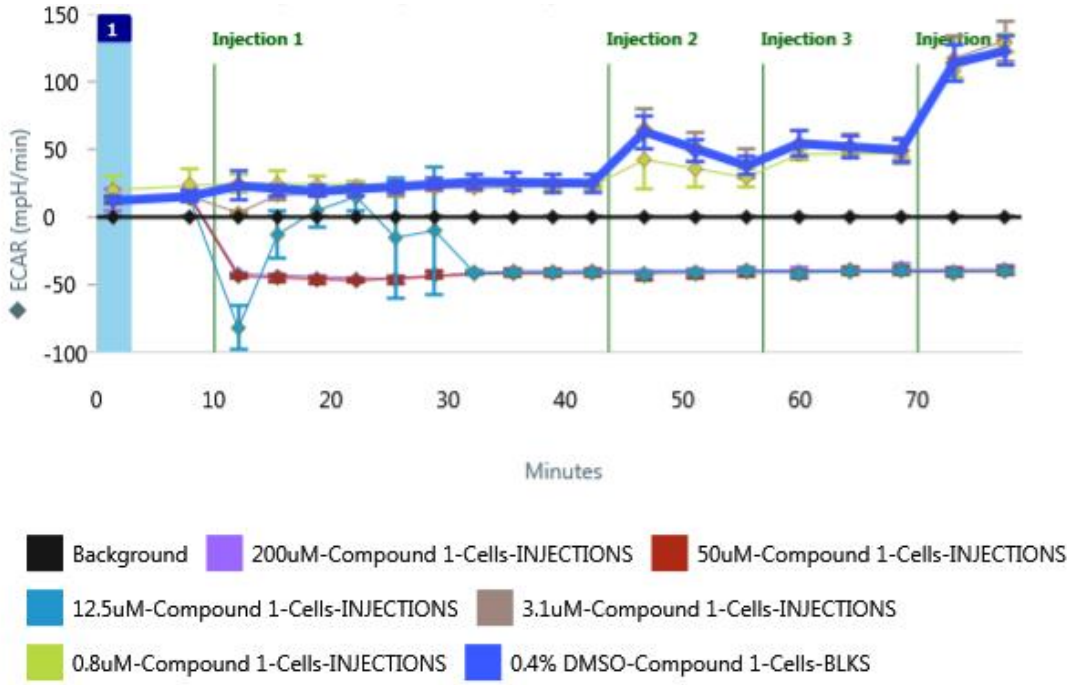

Figure 81. **EuL1** ECAR RATE measured during the MST in presence of cells. **Injection 1** corresponds to **EuL1** injection, **injection 2** corresponds to oligomicyn injection, **injection 3** corresponds to FCCP injection and **injection 4** corresponds to rotenone/antimycin A injection.

However for concentrations of 3.1 and 0.8 µM an elevation in ECAR was observed following injection of rotenone/antimycin A, which also included glucose to stimulate the glycolysis, indicating that the cells were still alive and switched to glycolysis. This means that **EuL1** two lower doses were not cytotoxic and this is consistent with the OCAR data. Since the **TbL1** MST results were the same seen for **EuL1**, they have not been discussed in this section. The similarity in the MST results obtained for **EuL1** and **TbL1** was due to the similar chemical structure of both compounds. However the MST data related to **TbL1** can be found in Appendix A.1.1 for a direct comparison. In the following sections, a summary of the MTS results of **EuL2**, **TbL2**, **NdL3**, **YbL3**, **EuL4** and **TbL4** is provided and their related OCR and ECAR profiles can be found in Appendix A.1.

5.1.2.4 MST results of the lanthanide complexes EuL2 and TbL2.

The highest two doses of **EuL2**, 200 and 50 μM, caused an impairment of oxidative phosphorylation since a decrease of the basal OCR and an erosion of the spare respiratory capacity were observed (see Figure 104 in Appendix A.1.2). All the other concentrations (from 12.5 - 0.8 μM), did not cause any effect on mitochondrial function, indicating that **EuL2** was not mitotoxic at the lowest three doses. The impairment of oxidative phosphorylation by **EuL2** at two top doses was confirmed by the results obtained with the OCR measured in absence of cells (see Figure 105 in Appendix A.1.2) as no significant effect on the OCR were shown by **EuL2** in absence of cells. This indicated that **EuL2** did not interfere with the OCR fluorophore and the results related to the OCR measured in presence of cells were actual rather than a consequence of compound interference. **EuL2** had an interference with the ECAR fluorophore (see Figure 106 in Appendix A.1.2). However, despite the interference with the ECAR fluorophore, a complete recovery of the glycolysis was observed for the **EuL2** lowest two doses (3.1 and 0.8 μM) upon injection of rotenone/antimycin A (see Figure 107 in Appendix A.1.2), indicating that **EuL2** was not cytotoxic at these concentrations. The **TbL2** MST results were the same seen for **EuL2** and can be found in Appendix A.1.2.

5.1.2.5 MST results of the lanthanide complexes NdL3 and YbL3.

NdL3 caused an increase of OCR after injection 1 and 2 (see Figure 112 in Appendix A.1.3) that could be interpreted as uncoupling effect. However, similarly to what was seen for **EuL1**, the supposed uncoupling effect was not confirmed by the OCR measured in absence of cells, since a large increase of oxygen consumption by **NdL3** down to 3.1 μM was observed even when cells were not present (see Figures 113 and 114 in Appendix A.1.3). This indicated that the increase of oxygen consumption observed in presence of cells could not be interpreted as uncoupling effect as it was due to compound interference with the OCR fluorophore. However, despite the compound interference,

NdL3 had a deleterious effect on maximal respiration recorded upon FCCP injection (injection 3) (see Figure 112 in Appendix A.1.3). In particular 200 µM, 50 µM and 12 µM of **NdL3** showed an erosion of the spare respiratory capacity (maximal respiration) indicating that **NdL3**, similarly to **EuL1**, had a toxic effect on cells from 200-12.5 µM. Similarly to **EuL1**, **NdL3** also had an interference with the ECAR fluorophore (see Figure 115 in Appendix A.1.3), which made the interpretation of the ECAR RATE profile recorded in presence of cells quite difficult. However there was some recovery of glycolysis exhibited even at 50 µM following rotenone/animycin A addition. All other concentrations (from 12.5-0.8 µM) demonstrated a better glycolysis recovery (see Figure 116 in Appendix A.1.3), but never quite reached control levels indicating a possible dose dependent cytotoxicity or a dose dependant effect of the compound on the pH fluorophore. The **YbL3** MST results were the same seen for **NdL3** and can be found in Appendix A.1.3.

5.1.2.6 MST results of the lanthanide complexes EuL4 and TbL4.

EuL4 did not exhibit any mitochondrial and cellular toxicity with the slight exception of 200 µM which showed a small erosion of oxygen consumption at basal and maximal respiration (see Figure 122 in Appendix A.1.4). The **TbL4** MST results were the same seen for **EuL4** and can be found in Appendix A.1.4.

The MST data for **EuL4** and **TbL4** demonstarted a far superior mitochondrial and cellular toxicty profile and therefore they represent the most promising compounds for future development. Whilst the interpretation of the other complexes was complicated by the various effects on the ECAR and OCR flurophores, it appeared clear that they all cause imapirment of mitochondrial and cellular function at lower levels than **EuL4** and **TbL4**.

5.2 Calcium Loading Capacity Assay

In order to further investigate the effect of the lanthanide complexes on mitochondrial function, a calcium loading assay was performed. The aim of this assay was to identify compounds with potential mitochondrial toxicity, through a decrease of the mitochondrial calcium loading capacity (CLC), as they are likely to cause mitochondrial dysfunction. Ligands that can bind lanthanide ions also show high affinity for calcium.

5.2.1 Mitochondrial calcium influx and efflux

Before introducing the calcium loading capacity assay, it is important to briefly introduce the mechanisms that regulate the calcium uptake and efflux within the mitochondria. Calcium enters the mitochondria manly through the mitochondrial calcium uniporter (MCU) [97], however other influx pathways are involved in the transport of the calcium from the inner membrane space to the matrix. These include, for example, the leucine zipper-EF-hand containing transmembrane protein 1 (LETM1), which is an H^+/Ca^{2+} exchanger [98], [99]. The driving force that allows the calcium to accumulate into the mitochondrial matrix through the MCU is the negative membrane potential across the inner mitochondrial membrane, which is generated by the proton flow from the matrix to the inner membrane space during the ETC [99]. This means that the mitochondria calcium uptake and the ETC are linked. Therefore, not only compounds that cause a direct MCU inhibition, but also compounds that interfere with the mitochondrial membrane potential, such as uncouplers and ETC inhibitors, could be responsible for compromising the mitochondrial calcium loading capacity and as consequence could cause mitochondrial dysfunction.

5.2.1.1 Mitochondrial calcium efflux mechanisms

Two mechanisms are involved in the calcium efflux: the Na^+-dependent (mNCX) and the Na^+-independent Ca^{2+} efflux [100]. In addition to these mechanisms, the calcium as well as other small ions and molecules may leave mitochondria through the mitochondria permeability transition pore (MPTP), which are proteinaceous pores located in both the

inner and outer mitochondrial membrane [100]. The MPTP opening occurs when large quantities of calcium accumulates into the mitochondrial matrix and interact with cyclophilin D [100], which is a protein located in the mitochondrial matrix that has a modulatory activity on the MPTP [101].

5.2.2 Calcium Loading Capacity Assay Background

Figure 82 shows the CLC profile of isolated mitochondria and the effect that cyclosporine A and antimycin A have on the mitochondrial CLC.

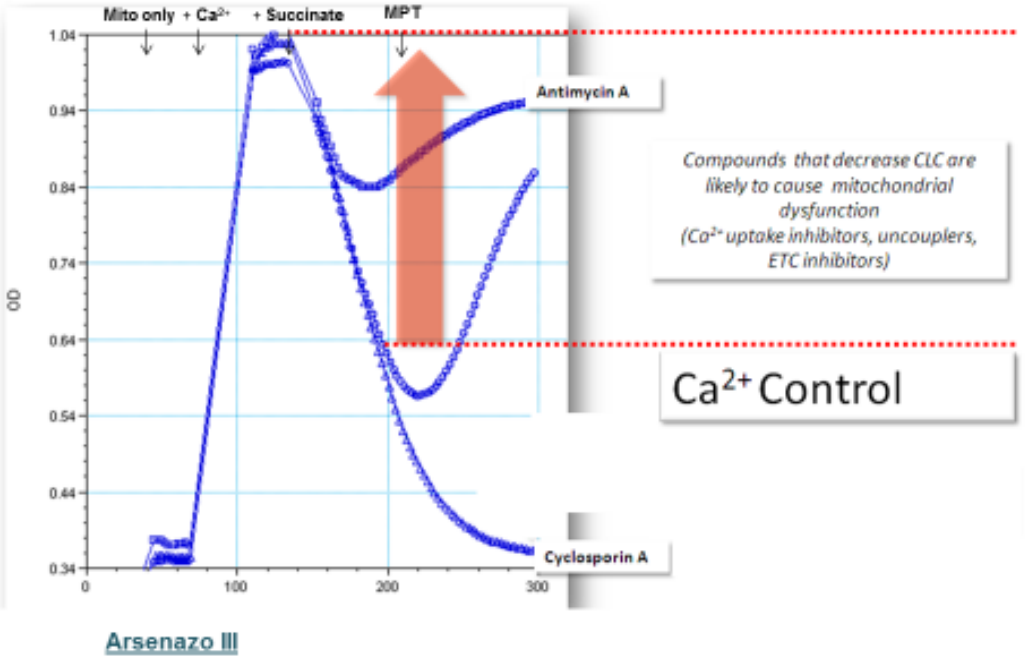

Figure 82. Mitochondrial Calcium Loading Capacity (CLC) assay profile related to the effect of the antimycin A and cyclosporin A on the mitochondrial CLC. This picture has been provided by GSK pharmaceutical company.

The CLC profile represents the variation of the calcium concentration in the extra mitochondrial medium. Variations in calcium concentrations were followed by measuring

changes in the absorbance spectrum of arsenazo III, a metallochromic dye used in the determination of calcium in biological samples [102], [103]. The free calcium (Ca^{2+}) concentration can be determined by directly measuring the absorbance of the Ca^{2+}-arsenazo III complex at 600-660 nm [102], [103]. As it is shown in Figure 82, upon the addition of calcium to the wells containing the isolated mitochondria and the medium, a strong absorption of the arsenazo III was observed. After the injection of calcium, succinate was added to the medium in order to provide a substrate for the mitochondrial ETC. Succinate is a substrate that stimulates the ETC at the level of complex II. Here the succinate is converted into fumarate by the catalytic activity of the succinate dehydrogenase, also called complex II (see the chapter 1 for more explanation). The increasing polarization of the mitochondrial membrane caused by the addition of succinate allows the calcium to enter the mitochondria through the MCU, and this was detected by a decrease of arsenazo III absorbance as consequence of lowered calcium medium concentration (Figure 82). When the calcium reaches a critical concentration within the mitochondria matrix, the MPTP opens and calcium is released back into the medium. This was indicated by an increase of the arsenazo III absorbance as consequence of the increased calcium concentration in the medium (Figure 82). Figure 82 shows the effect of the antimycin A and the cyclosporine A on the mitochondrial CLC. Antimycin A, which is a complex III inhibitor, caused a significant erosion of the mitochondrial CLC (Figure 82). This effect was due to the depolarization of the inner mitochondrial membrane generated by a slowdown of the proton pumping during the ETC as consequence of the complex III inhibition by antimycin A. This in turn prevented the opening of the calcium influx pathway through the MCU. Cyclosporin A inhibits the formation of the MPTP and thus does not stop mitochondria uptaking calcium but inhibits its release upon reaching concentration that would normally trigger the MPTP. In Figure 82 calcium uptake was observed upon the addition of the cyclosporin A, as indicated by a large decrease of arsenazo III absorbance. The increased calcium uptake by mitochondria induced by cyclosporine A is caused by the cyclosporine A ability to bind

the mitochondrial cyclophilin D, which in turn inhibits the MPTP [104]. As a consequence the calcium cannot exit the mitochondria upon its internalization into the matrix and is not returned to the media.

5.2.3 Lanthanide Complexes Calcium Loading Capacity Assay results

A calcium loading assay was performed on the same lanthanide complexes tested with the MST. All complexes were tested at concentration of 250 µM, 125 µM, 62.5 µM, 15.6 µM, 3.9 µM and 0.9 µM. Figure 83 shows the calcium loading capacity profile measured for **EuL1**. **EuL1** caused a significant erosion of the mitochondrial CLC down to 15.6 µM. In fact **EuL1** 15.6 µM, 3.9 µM and 0.9 µM showed a profile similar to the control, indicating that these concentrations did not affect the capacity of mitochondria to internalize the calcium.

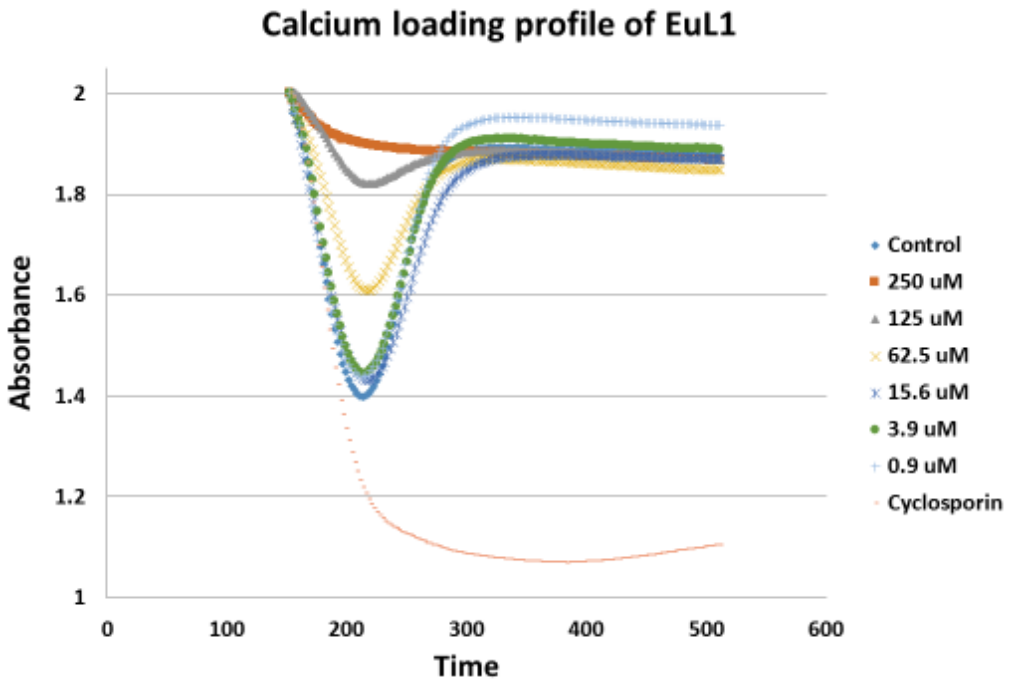

Figure 83. Calcium loading profile of **EuL1**.

The significant CLC erosion caused by **EuL1** could be due to several factors. However it was initially noted from the calcium loading traces that there was a calcium chelating

effect with all compounds (**EuL1**-**TbL4**) (see Figure 84 showing the calcium chelating effect of **EuL1**, the calcium chelating traces related to the other complexes can be found in Appendix A.3).

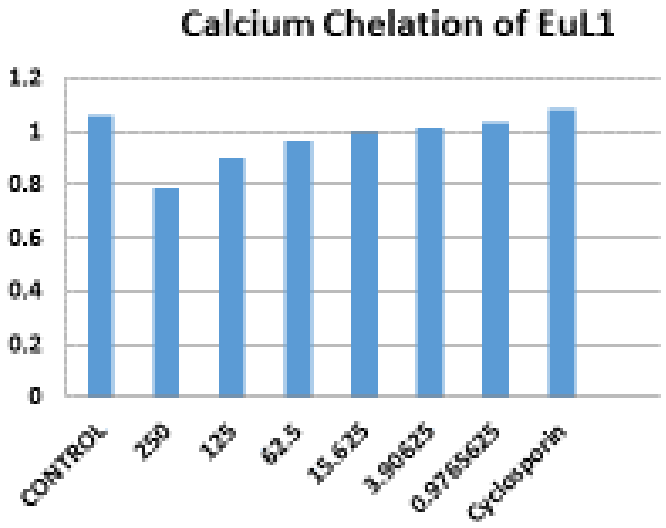

Figure 84. Calcium chelation of **EuL1**.

However the calcium loading traces performed with the uncomplexed generic ligand, shown in Figure 85, showed no reproduction of this trend which suggests this chelating effect is not arising from direct competition for the ligands between the Ca^{2+} and the Ln^{3+}.

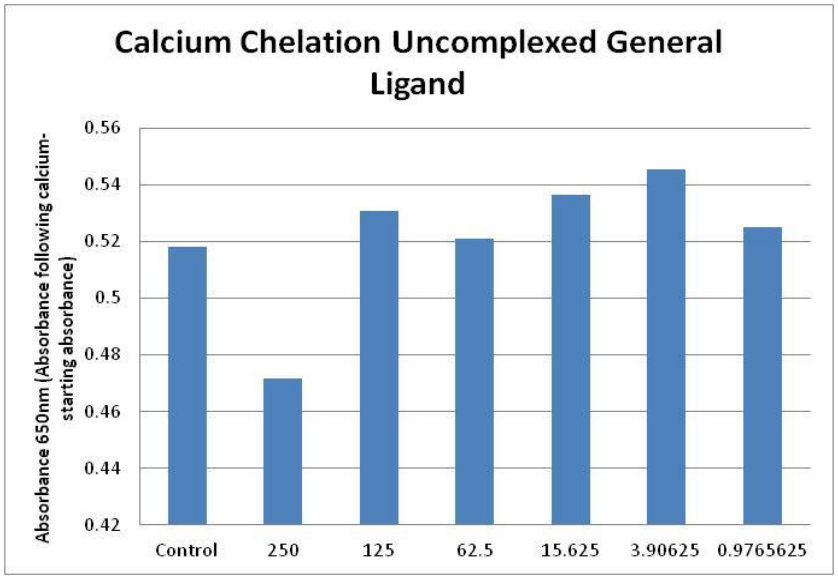

Figure 85. Calcium chelation of the uncomplexed generic ligand.

In Figure 83 it is important to note that, whilst the calcium chelation alters the calcium absorbance value of the CLC profile before succinate addition, all concentrations of **EuL1** still triggered the MPTP with the exception of 250 µM. Even in this instance for the 250 µM CLC trace to be caused by calcium chelation alone, almost all of the calcium would have to be removed from the system. This was clearly not the case as Figure 84 shows the calcium absorbance only dropped to approximately 80% of control so the majority of calcium remained. Therefore it could be inferred that the calcium was not chelated enough to become limiting in these experiments. This suggested that the effect seen at the 250 µM level could be due to mitochondrial toxicity or complete inhibition of mitochondrial calcium uptake. Whilst all compounds demonstrated inhibition of mitochondrial calcium loading (see Appendix A.2, where **TbL2**-**YbL3** CLC profiles are reported), it should be noted that even at 250 µM **EuL4** and **TbL4** still demonstrated a degree of calcium loading compared to the other 6 complexes (see Figures 86 and 87) and appeared to slightly less potent in their effects on calcium loading. This was in correlation with the MST data that suggested that **EuL4** and **TbL4** showed the lowest toxicity and are the most promising complexes for future development.

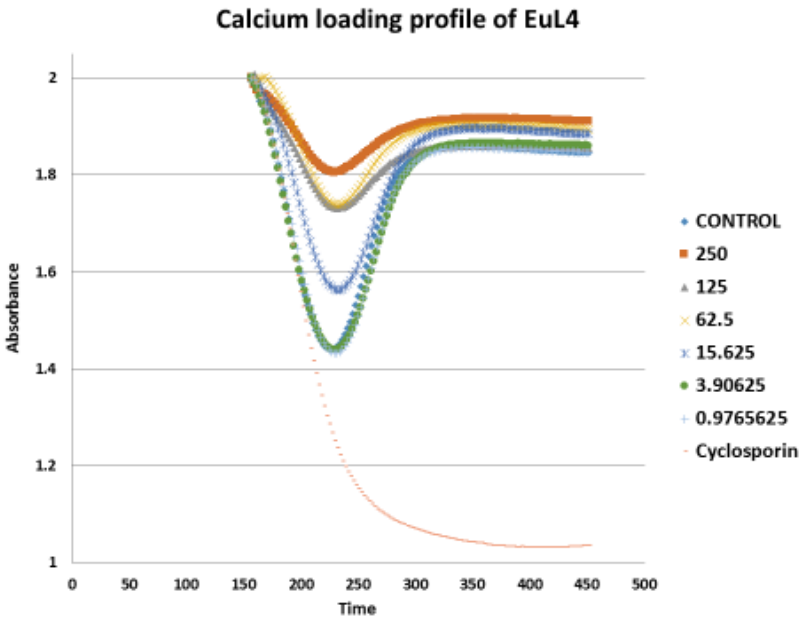

Figure 86. Calcium loading profile of **EuL4**.

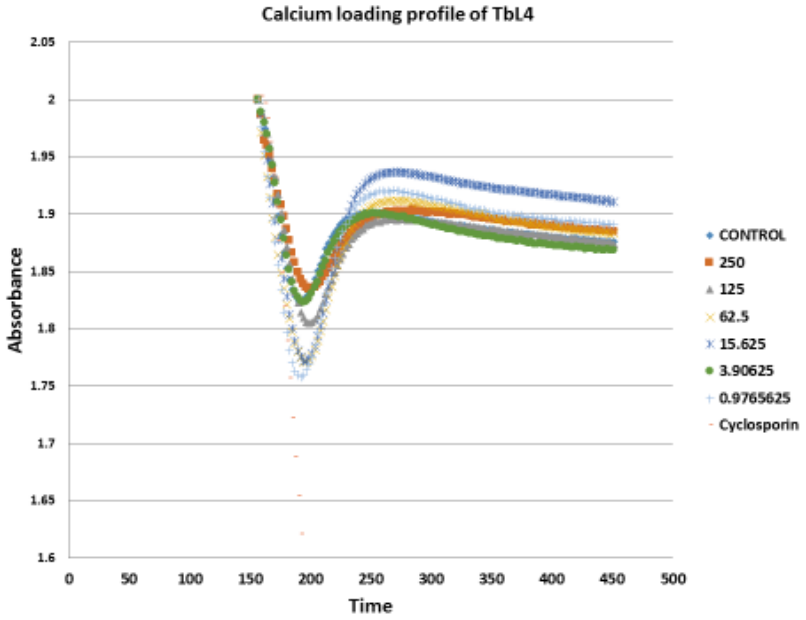

Figure 87. Calcium loading profile of **TbL4**.

5.3 Cell-based test to measure the photophysical properties of the lanthanide complexes in vitro

A cell-based test was performed on two europium complexes that were synthesized in this project, namely the **EuL5** and **EuL4** since, as discussed in the chapter 4, they were the only compounds among those synthesized that exhibited a strong europium-based luminescence. The aim of this test was to evaluate whether or not these complexes could sense high ROS levels in a cellular environment by measuring changes in their fluorescence intensity. Two pendant arms of coumarin 151 were attached to the cyclen ring to sensitize the Eu(III) emission in **EuL5**. The coumarin 151 moieties should also be able to interact with OH· or other ROS species, and this interaction should cause changes of the coumarin 151 photophysical properties and consequently changes in the Eu(III) emission. Whilst in **EuL4** the coumarin 3 carboxylic acid was used as sensitizer antenna of Eu(III) and receptor unit for ROS species. The coumarin 3 carboxylic acid should be able to react with ROS species, such as OH·, and changes in its photophysical properties caused by this interaction should induce changes in the Eu(III) emission [105]. In order to evaluate the response of **EuL5** and **EuL4** to high ROS levels, a cell-based test was performed on both complexes. The cell line used in this test was HSC-3 (human squamous cell carcinoma cell line). H_2O_2 and tBHP (tert-Butyl Hydroperoxide) were used as ROS generator compounds, since they are able to induce an oxidative stress within the cells by increasing the ROS production [106]. MitoSOX, which is a fluorogenic ROS-sensing dye that is targeted to mitochondria in live cells, was used as probe positive control. Oxidation of MitoSOX by superoxide produces red fluorescence [107]. The assay was performed on a 96 well plate containing HSC-3 cells at a density of 100000 cells/well (Figure 88).

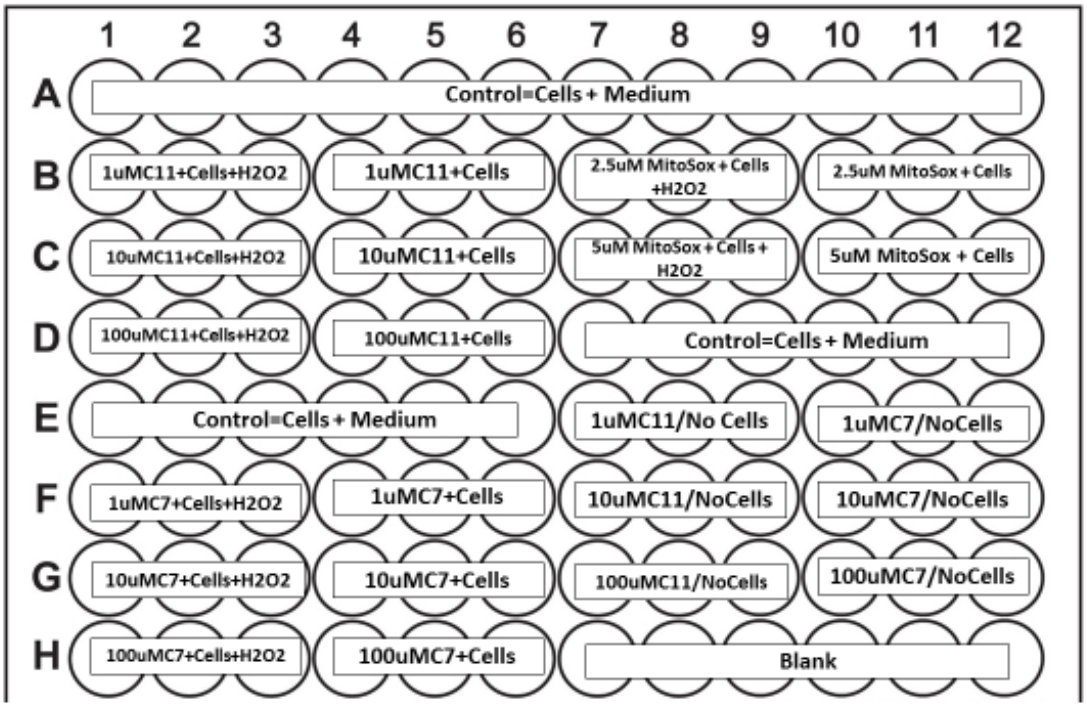

Figure 88. Example of a 96 well plate used to measure the fluorescence intensity of **EuL5** and **EuL4** in vitro.

Figure 88 shows how a 96 well plate was filled to measure the fluorescence intensity of **EuL5** and **EuL4** in vitro. Apart from the wells that were filled only with 100 µl of **EuL5** and **EuL4** dissolved in medium at concentration of 1 µM, 10 µM and 100 µM, all the other wells contained cells. The wells containing just the cells and medium were used as control, while the wells containing the cells and 1 µM, 10 µM and 100 µM of **EuL5** and **EuL4** were used to measure the fluorescence intensity of **EuL5** and **EuL4** within the cells in absence of ROS generator compounds. The wells containing the cells previously exposed to 50 µM of H_2O_2 and then incubated with **EuL5** and **EuL4** at concentration of 1 µM, 10 µM and 10 0µM, were used to measure the fluorescence intensity of **EuL5** and **EuL4** in the presence of high levels of ROS generated by H_2O_2 (Figure 88). In this assay another 96 well plate was filled as described above but replacing the H_2O_2 with 150 µM of tBHP. The fluorescence intensity of **EuL5** and **EuL4** was recorded using a microplate reader and each measurement was made in triplicate. The fluorescence intensity of

EuL5 and **EuL4** was recorded by monitoring the excitation at 390 nm and the emission at 645 nm. This choice was made taking into account the filters available with the microplate reader used for the measurements and by selecting among the available wavelengths the ones closest to the excitation and emission wavelengths of **EuL5** and **EuL4**. The excitation wavelengths of **EuL5** and **EuL4** were 340 nm and 300 nm respectively (see chapter 4 for more explanation), while the emission wavelength was 615 nm, which corresponds to the most emissive band $\Delta J = 2$ of the Eu(III) emission (see the chapter 4 for more explanation). The comparison between the fluorescence intensity of **EuL5** and **EuL4** recorded from the wells containing the cells previously incubated with H_2O_2 and tBHP and those containing the cells that were not incubated with H_2O_2 and tBHP allowed to evaluate whether or not **EuL5** and **EuL4** were able to detect the variation of ROS levels. The fluorescence intensity of **EuL5** and **EuL4** was measured before washing all the wells twice with the medium and after washing the wells, while the fluorescence intensity of the MitoSOX control was only recorded after washing according to the protocol. The fluorescence intensity recorded after washing the wells enabled the calculation of the fluorescence intensity of **EuL5** and **EuL4** that entered the cells and eliminate the interferences of **EuL5** and **EuL4** that were probably present in the extracellular medium before washing.

5.3.1 In vitro measurements of EuL5 and EuL4 fluorescence intensity obtained before washing the wells

The figures 89 and 90 show the fluorescence intensity of **EuL5** and **EuL4** respectively, recorded upon exposure of the cells to tBHP as ROS generator and before washing the wells. In both cases the control was represented by the cells and medium.

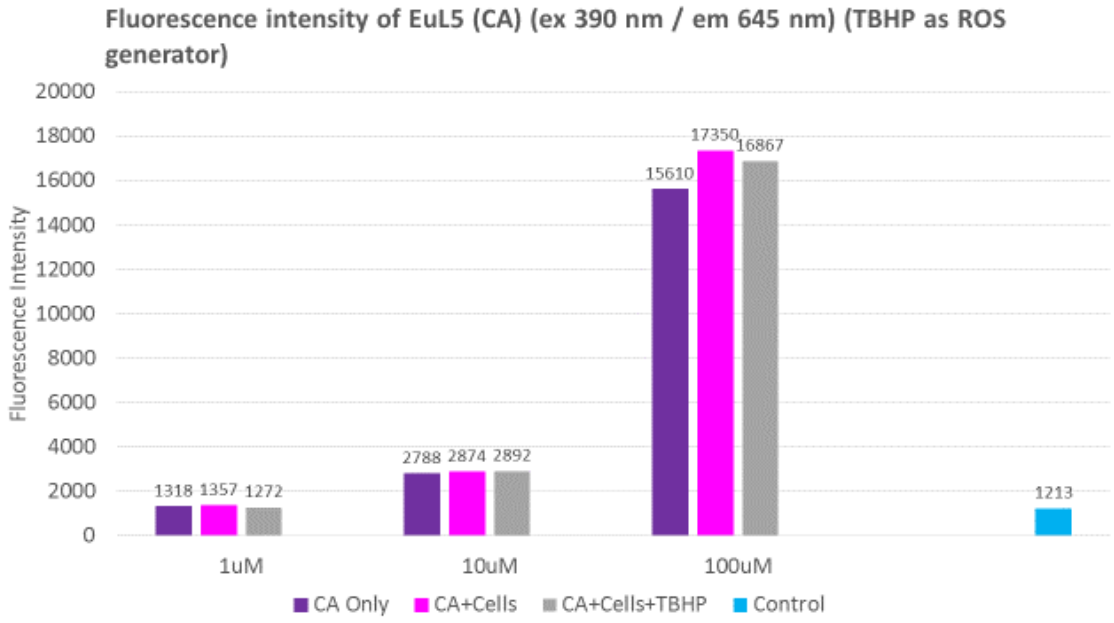

Figure 89. Fluorescence intensity of **EuL5** (CA) recorded upon exposure of cells to tBHP as ROS generator. The fluorescence intensity was recorded upon excitation at 390 nm and emission at 645 nm and before washing the wells.

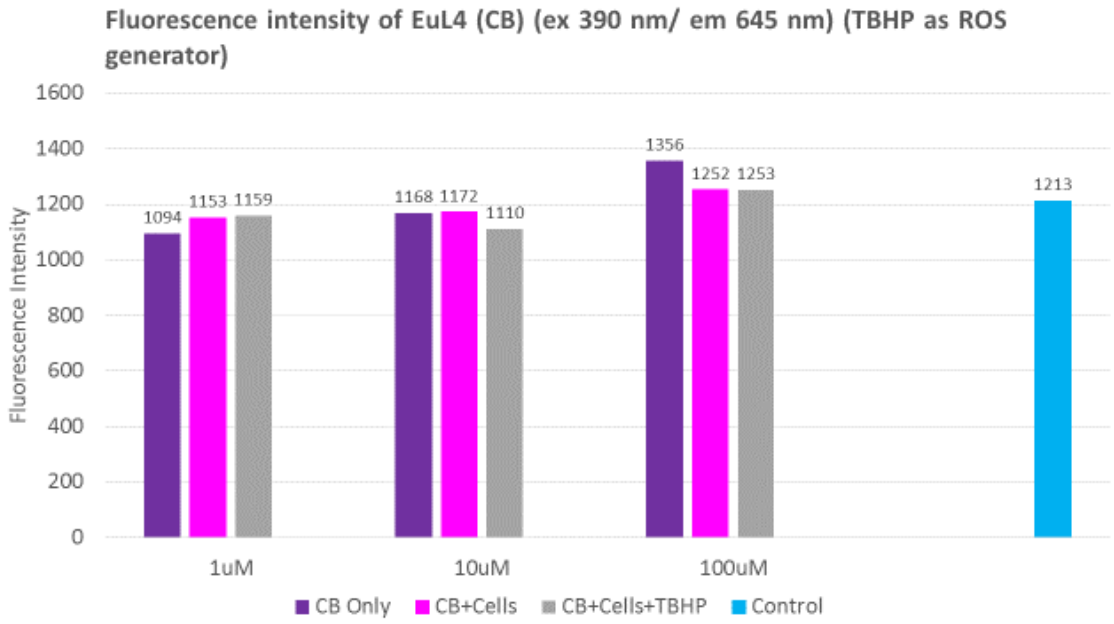

Figure 90. Fluorescence intensity of **EuL4** (CB) recorded upon exposure of cells to tBHP as ROS generator. The fluorescence intensity was recorded upon excitation at 390 nm and emission at 645 nm and before washing the wells.

As it is shown in the graphs of Figures 89 and 90, the fluorescence intensity of **EuL5** and **EuL4** recorded from the wells containing the cells previously exposed to tBHP and from those containing the cells incubated with **EuL5** and **EuL4** but not exposed to tBHP, were approximately the same. This was observed for all the concentrations of **EuL5** and **EuL4**, namely 1 μM, 10 μM and 100 μM. This indicated that no significant **EuL5** and **EuL4** fluorescence changes took place upon exposure of the cells to tBHP, meaning that **EuL5** and **EuL4** were not responsive to high ROS levels generated by tBHP. Figures 91 and 92 show the fluorescence intensity of **EuL5** and **EuL4** respectively, recorded upon exctitation at 390 nm and emission at 645 nm when H_2O_2 was employed as ROS generator. Again in these cases the control was represented by the cells and medium.

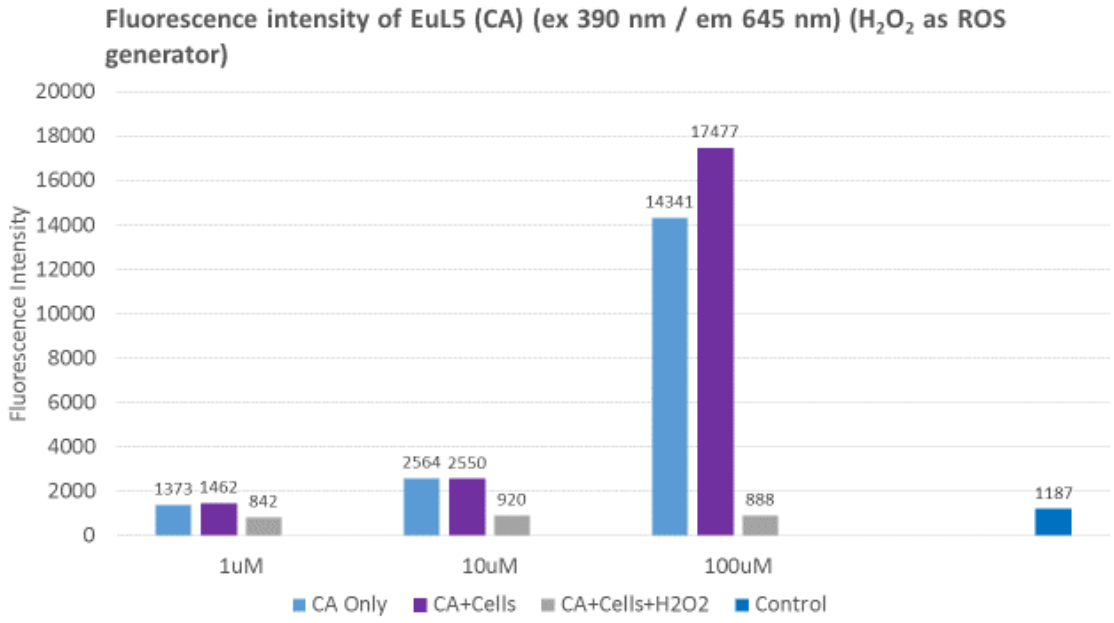

Figure 91. Fluorescence intensity of **EuL5** (CA) recorded upon exposure of cells to H_2O_2 as ROS generator. The fluorescence intensity was recorded upon excitation at 390 nm and emission at 645 nm and before washing the wells.

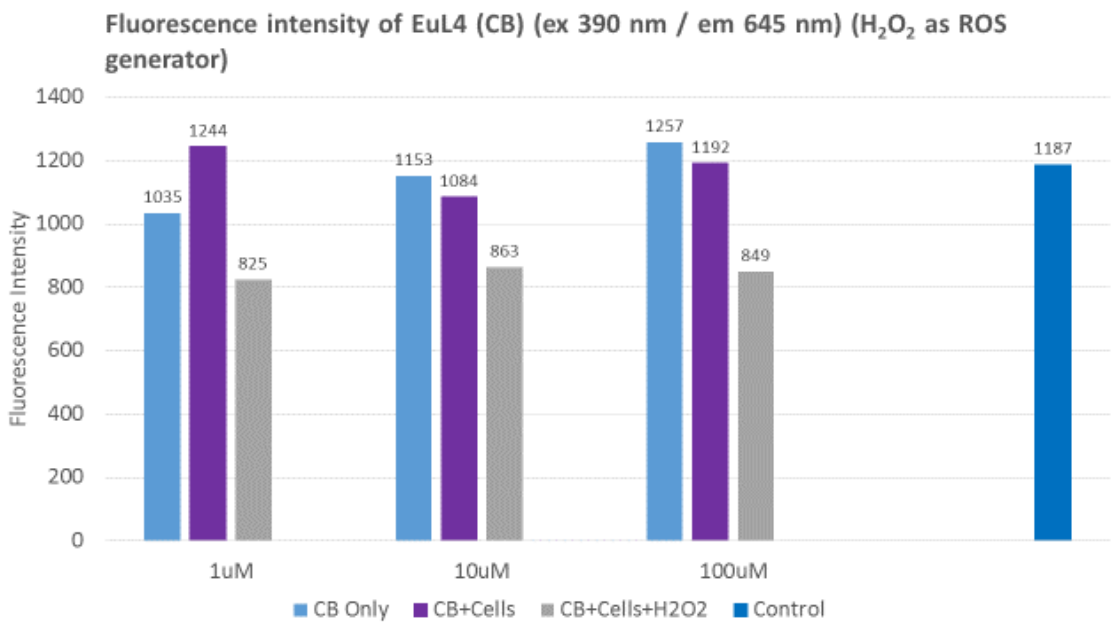

Figure 92. Fluorescence intensity of **EuL4** (CB) recorded upon exposure of cells to H_2O_2 as ROS generator. The fluorescence intensity was recorded upon excitation at 39 0nm and emission at 645 nm and before washing the wells.

A decrease in the fluorescence intensity of both **EuL5** and **EuL4** was observed upon exposure of the cells to H_2O_2. Although a decrease in fluorescence intesity was observed for **EuL5** and **EuL4** at all concentrations they were tested, namely 1 µM, 10 µM and 100 µM, this effect was particularly pronounced for 100 µM **EuL5** (Figure 91). This indicated that **EuL5** and **EuL4** were responsive to high ROS levels generated by H_2O_2 and 100 µM **EuL5** was the most responsive. It is interestingly to note how the fluorescence intensity of **EuL5** (Figure 91) and **EuL4** (Figure 92) measured upon exposure the cells to H_2O_2 were approximately the same independently from the concentration they were tested. This indicated that the fluorescence of **EuL5** and **EuL4** was completely quenched by H_2O_2 or by other ROS species, such as OH·.

5.3.1.1 ROS sensing ability of EuL5 in vitro and cuvette when H_2O_2 was used as ROS generator

The quenching of **EuL5** fluorescence observed in vitro could be due to a direct Eu(III) quenching caused H_2O_2, OH· or other ROS species or changes of the photophysical properties of the sensitizer antennae used in **EuL5**, namely the coumarin 151, as consequence of its interaction with ROS species generated by H_2O_2. The **EuL5** fluorescence quenching observed in vitro was consinstent with the results obtained with the photophysical test performed on **EuL5** in the presence of H_2O_2 and Fe(II) perchlorate (chapter 4, section 4.4), where a decrease of the Eu(III) luminescence was observed upon H_2O_2 and Fe(II) perchlorate addition. Therefore the **EuL5** quencing observed in vitro could support the hypothesis that the hydroxylation of the coumarin 151 by OH· could cause changes in its photophysical properties thus preventing it to act efficiently as sensitizer toward Eu(III), and as consequence no emission from the Eu(III) could be achieved. However it could not be excluded a direct quenching of Eu(III) and/or the sensitizer antenna by other ROS species present in the cells.

5.3.1.2 ROS sensing ability of EuL4 in vitro and cuvette when H_2O_2 was used as ROS generator

By contrast the quenching of the **EuL4** fluorescence observed in vitro was not consistent with the the results obtained with the photophysical test performed on **EuL4** in the presence of H_2O_2 and Fe(II) perchlorate, where an increase of the Eu(III) luminescence was indeed observed upon H_2O_2 and Fe(II) perchlorate addition. These inconsistent results could be due to the fact that, whilst the increase of the Eu(III) luminescence observed with **EuL4** in solution could be attributable to the hydroxylation of the coumarin 3 carboxylic acid by OH· generated in situ by H_2O_2 and Fe(II) perchlorate, the quenching of **EuL4** fluorescence in vitro could be due to a direct Eu(III) quenching exerted by, and/or to the reaction of coumarinn 3 carboxylic acid with other types of ROS species generated within the cells upon H_2O_2 exsposure.

5.3.1.3 Differences in EuL5 and EuL4 responses to high ROS levels generated by tBHP and H_2O_2

A plausible explanation to the absence of response by **EuL5** and **EuL4** to high ROS levels generated by tBHP while a response was observed when H_2O_2 was used as ROS generator could be that different sets of ROS are generated by H_2O_2 and tBHP. Exposure of cells to tBHP leads to an oxidative stress mainly caused by the production of peroxyl and alkoxyl radicals via cytochrome P450 [106], [108]. On the other hand, the oxidative stress generated within the cells treated with H_2O_2 is mainly attributable to the formation of $OH^{\bullet}$ as consequence of the Haber-Weiss reaction [9]. Therefore it may be that the absence of response by **EuL5** and **EuL4** to high ROS levels generated by tBHP could be attributable to the fact that the products of tBHP transformation, namely the peroxyl and alkoxyl radicals, were not able to react with the antennae used in **EuL5** and **EuL4**, so that to affect their ability to act as Eu(III) sensitizers, or were not able to cause a direct quenching of Eu(III) emission. Although the results related to the **EuL5** and **EuL4** fluorescence intensity measurements discussed so far provide important information about their photophysical properties in vitro, they cannot be considered fully representative of their photophysical behaviour in a cellular environment. That is because the fluorescence intensity measured for **EuL5** and **EuL4** could be affected by the presence of **EuL5** and **EuL4** that did not enter the cells and remained into the extracellular medium. In order to measure the fluorescence intensity of **EuL5** and **EuL4** without having any interference form by the amount that did not enter the cells, all the wells were washed twice with medium in order to eliminate traces of **EuL5** and **EuL4** that remained in the extracellular medium. In the next section, the fluorescence intensity of **EuL5** and **EuL4** recorded after washing the wells are described together with the fluorescence intensity of the MitoSOX ROS positive control.

5.3.2 In vitro measurements of EuL5 and EuL4 fluorescence intensity obtained after washing the wells

Figures 93 and 94 show the fluorescence intensity of **EuL5** and **EuL4** respectively recorded upon excitation at 390 nm and emission at 645 nm and upon washing all the wells twice with HBSS (balanced salt solution) medium. The control consisted of the cells just incubated with medium.

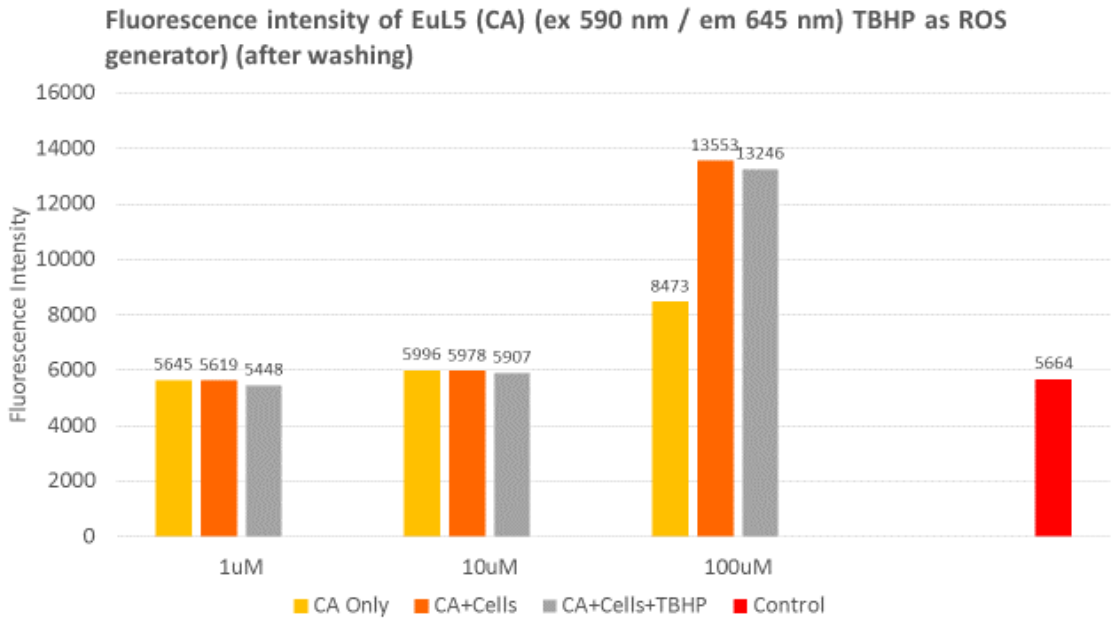

Figure 93. Fluorescence intensity of **EuL5** (CA) recorded upon exposure of cells to tBHP as ROS generator. The fluorescence intensity was recorded upon excitation at 390 nm and emission at 645 nm and after washing the wells.

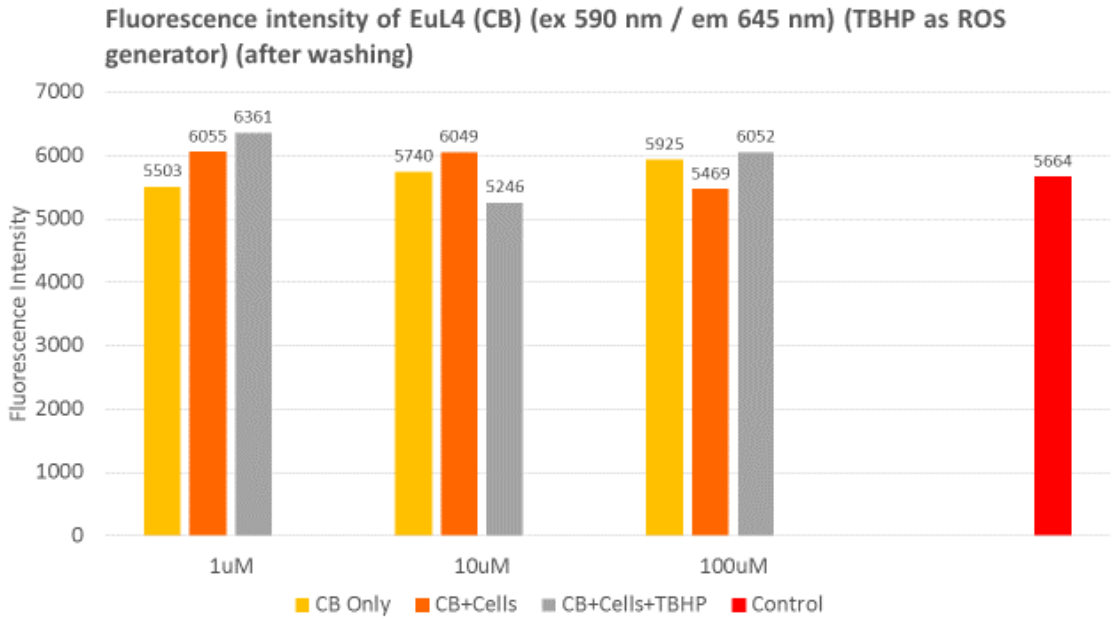

Figure 94. Fluorescence intensity of **EuL4** (CB) recorded upon exposure of cells to tBHP as ROS generator. The fluorescence intensity was recorded upon excitation at 390 nm and emission at 645 nm and after washing the wells.

As shown in Figures 93 and 94, no changes of **EuL5** and **EuL4** photophysical properties were observed when they were incubated in the cells previously exposed to tBHP, indicating that these compounds were not responsive to high ROS levels generated by tBHP. The absence of response by **EuL5** and **EuL4** to high ROS levels generated by tBHP was observed for all concentrations at which these compounds were tested, namely 1 µM, 10 µM and 100 µM. These results were aligned with the results related to the fluorescence intensity measurements obtained with **EuL5** and **EuL4** before washing all wells. Figures 95 and 96 show the fluorescence intensity measurements of **EuL5** and **EuL4** respectively recorded upon excitation at 390 nm and emission at 645 nm and upon exposure of cells to H_2O_2.

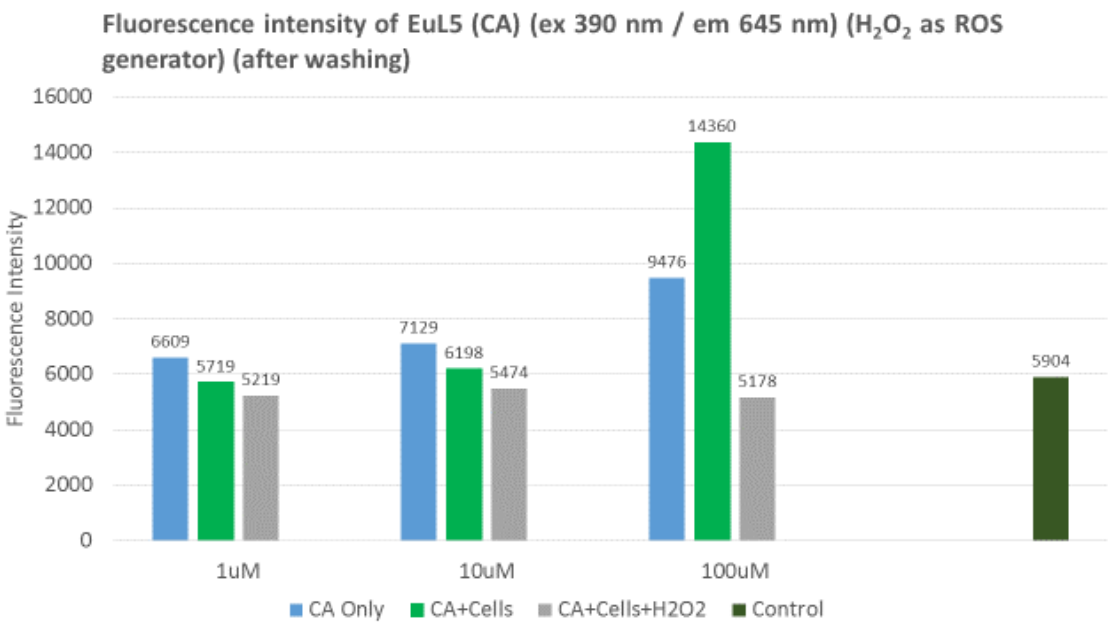

Figure 95. Fluorescence intensity of **EuL5** (CA) recorded upon exposure of cells to H_2O_2 as ROS generator. The fluorescence intensity was recorded upon excitation at 390 nm and emission at 645 nm and after washing the wells.

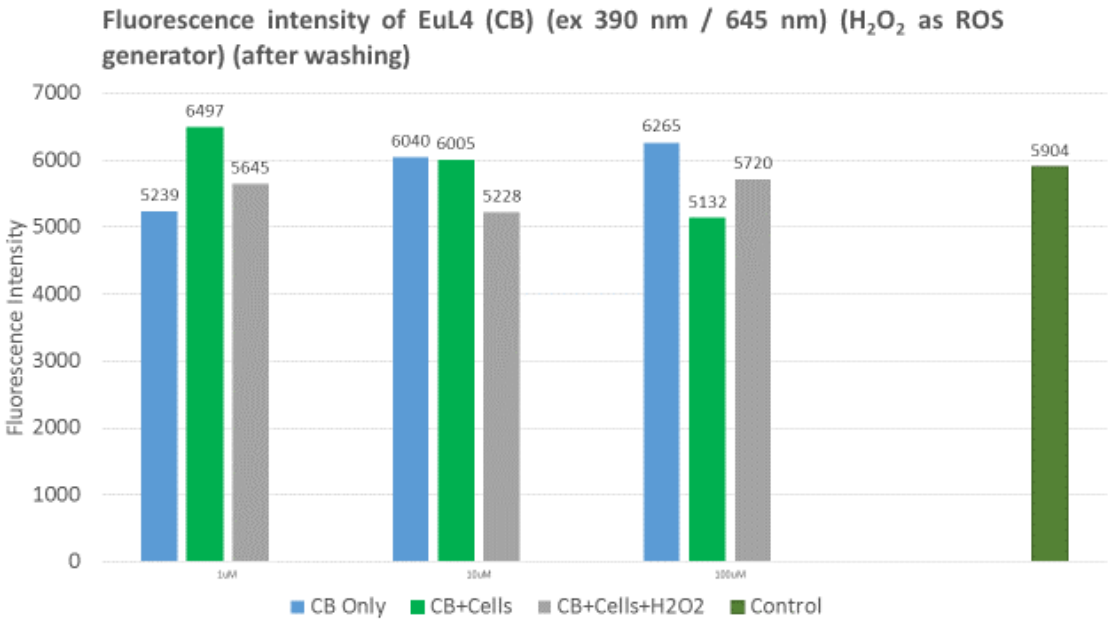

Figure 96. Fluorescence intensity of **EuL4** (CB) recorded upon exposure of cells to H_2O_2 as ROS generator. The fluorescence intensity was recorded upon excitation at 390 nm and emission at 645 nm and after washing the wells.

As it is possible to note in Figure 95, while no significant decrease of 1 µM **EuL5** and 10 µM **EuL5** fluorescence intensity were observed when **EuL5** was injected into the cells that were previously exposed to H_2O_2, a significant decrease at 100 µM **EuL5** was indeed observed. These results were only partially aligned with the results related to the fluorescence intensity measurements of **EuL5** recorded before washing all the wells. In fact, although a strong decrease of the fluorescence intensity of 100 µM **EuL5** was measured both before and after washing the wells, the decrease of fluorescence intensity of 1 µM **EuL5** and 10 µM **EuL5** was more significant before washing the wells compared to after washing the wells. This could be explained by the fact that the fluorescence intensity of **EuL5** recorded before washing the wells were affected by the presence of **EuL5** in the extracellular medium that was removed after washing. Similarly to **EuL5**, also **EuL4** showed a similar behaviour as some differences between the fluorescence intensity recorded before and after washing the wells were observed. A lower decrease of 1 µM **EuL4** and 10 µM **EuL4** fluorescence intensity was observed after washing the wells compared to the decrease of 1 µM **EuL4** and 10 µM **EuL4** observed before washing the wells. In addition, inconsistent results were observed for 100 µM **EuL4** before and after washing. While a decrease of 100 µM **EuL4** fluorescence intensity was observed before washing the wells (Figure 92), a slight increase of 100 µM **EuL4** fluorescence intensity was observed after washing the wells (Figure 96). If the fluorescence intensity of 1µM, 10 µM and 100 µM of **EuL4** recorded in the wells containing the cells incubated with **EuL4** are considered (Figure 96), an increase in the fluorescence intensity was expected as the **EuL4** concentration increased. However, a decrease of the **EuL4** fluorescence intensity was observed as the concentration increased implying the washing process may adversely affect the concentration of the complex in the cells. This hypothesis can be supported by the results obtained with the MitoSOX positive control fluorescence intensity measurements. According to the protocol, the MitoSOX

fluorescence intensity was only recorded after washing and upon excitation at 544 nm at and emission at 590 nm. Figures 97 and 98 show the fluorescence intensity related to MitoSOX recorded upon exposure of the cells to H_2O_2 and tBHP respectively.

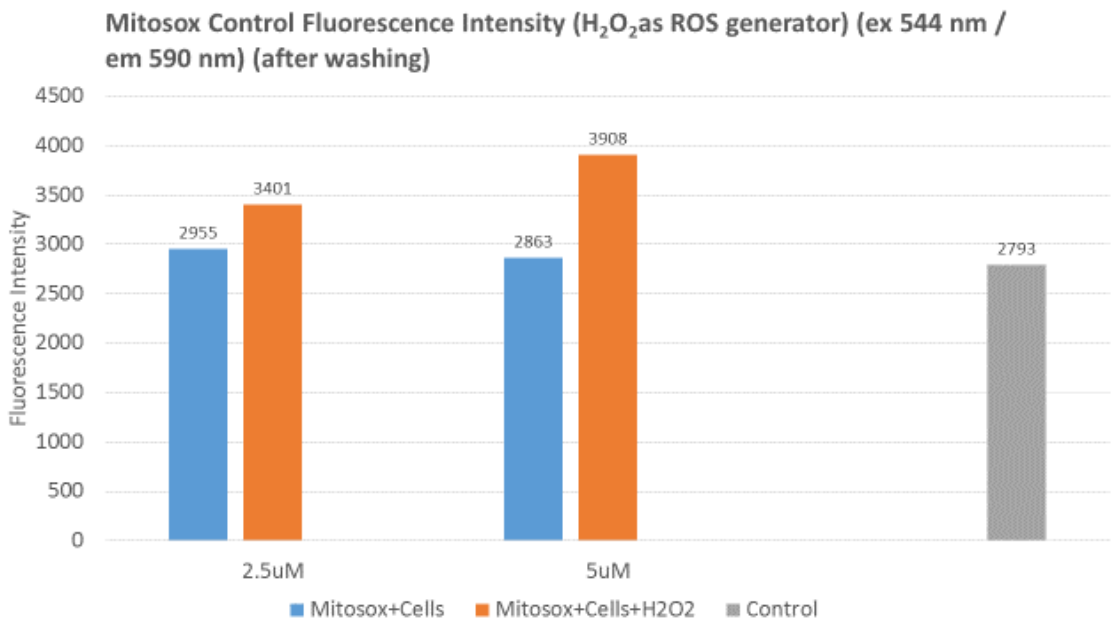

Figure 97. Fluorescence intensity of MitoSOX recorded upon exposure of cells to H_2O_2. The fluorescence intensity was recorded upon excitation at 544 nm and emission at 590 nm and after washing the wells.

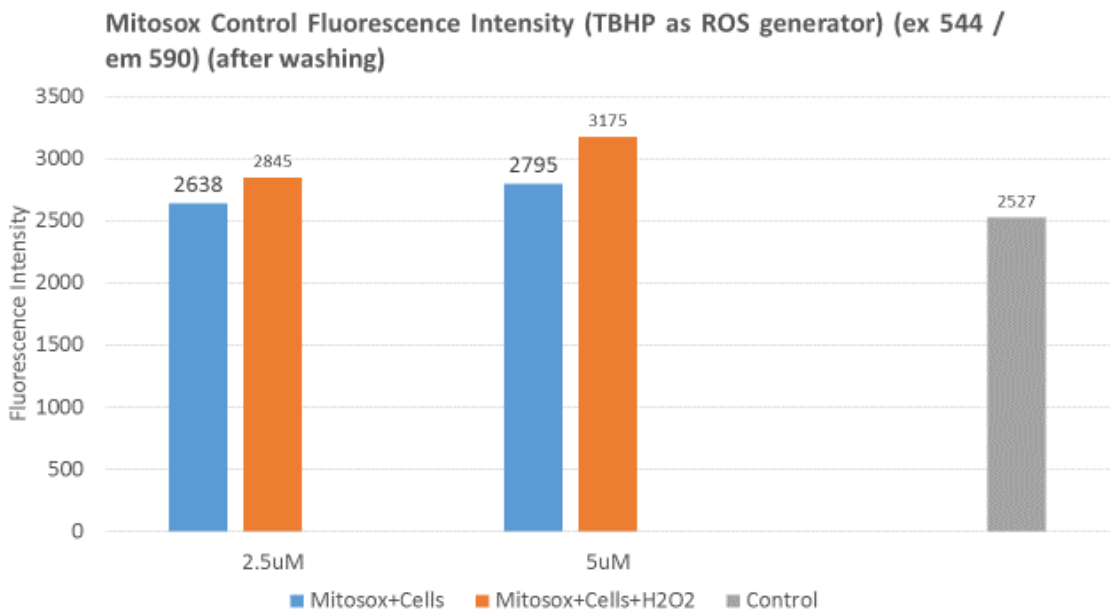

Figure 98. Fluorescence intensity of MitoSOX recorded upon exposure of cells to tBHP. The fluorescence intensity was recorded upon excitation at 544 nm and emission at 590 nm and after washing the wells.

Although an increase of MitoSOX fluorescence intensity was observed both when H_2O_2 and tBHP were used as ROS generators, the magnitude of this increase was not so huge as expected from a compound known for its ability to detect variation of ROS levels within the cells. This could be due to that fact that washing all wells twice with the medium affected in some way the fluorescence intensity measurement. It may be that washing all wells one time may improve the fluorescence intensity measurements thus avoiding inconsistent results.

The two tests assessing the impact on the mitochondrial function showed the complexes **EuL4** and **TbL4** to have moderate to no effect on the cells suggesting they are potentially useful as sensors for mitochondrial function. The two complexes that showed useful Ln(III) based emission (**EuL5** and **EuL4**) were tested in cell cultures and the cells tolerated these complexes allowing Eu(III) emission and responses to ROS to be recorded. Qualitatively **EuL5** and **EuL4** showed a response to ROS however there was a potential impact on washing the cells.

6. Conclusion and Future Work

The aim of this project was to synthesise lanthanide complexes based on asymmetrically substituted cyclen ligands in order to produce luminescent molecular sensors able to signal the presence of ROS species. A series of lanthanide complexes based on asymmetrically substituted cyclen ligands were designed. This was achieved by the asymmetrical functionalisation of the cyclen ring with four pendant arms. Two arms, each containing a triphenylphosphonium derivative, were incorporated on the cyclen ring in order to target the complexes to mitochondria as they are the main source of ROS. The other two arms of the cyclen ring contained an organic chromophore and a carboxylic function protected with a benzyl ester group respectively. The chromophore antenna was used to sensitize the Ln(III) emission via an antenna effect and in the meantime to react with ROS species. Changes in the photophysical properties of the chromophore antenna caused by ROS were responsible for changes in the Ln(III) emission. The carbonyl function present on the arm containing the benzyl ester group, together with the four nitrogen atoms of the cyclen ring and two carbonyl functions present on the triphenylphosphonium containing moieties, were involved in the Ln(III) coordination.

6.1 The synthesis

The first unsuccessful synthetic strategy was based on the direct and selective N-alkylation of four pendant arms on the cyclen ring. This synthetic approach required that the pendant arms had to be synthesised separately and then could be used for the direct N-alkylation. Two arms containing an N-methyl-L-glucamine derivative were chosen in order to increase the hydrophilicity of the ligand due to the presence of ten hydroxyl functions that would have made the ligand an amphiphilic molecule thus providing it with similar properties of plasma and mitochondria membranes and facilitating its diffusion through these systems of membranes.

Although the pendant arms that had to be incorporated on the cyclen ring by direct N-alkylation reaction were successfully synthesised and two of them were successfully incorporated on the cyclen ring to obtain the 1-N-Boc-ethylmine-4-coumarin 2 acetamide-1,4,7,10-tetraazacyclododecane **(24)**, it was not possible to introduce the two arms containing the N-methyl-L-glucamine derivatives via direct N-alkylation reaction. This could be due to the instability of N-methyl-L-glucamine pentaactetate bromoacetate **(26)** under the reflux conditions used for the direct N-alkylation, or to their steric hindrance, which could in some way prevent the N-alkylation reaction of the 1-4 disubstituted cyclen **(24)** from taking place, or to a combination of both. Based on the hypothesis that the N-methyl-L-glucamine pentaactetate bromoacetate **(26)** was not stable under the reflux conditions used for the direct N-alkylation, it was replaced by another moiety, which was thought to be stable under reflux conditions. In particular, two moieties, each containing a lipophilic triphenylphosphonium cation, were used as mitochondria-targeted molecules to replace the two molecules of N-methyl-L-glucamine pentaactetate bromoacetate **(26)**. The net positive charge present on the triphenylphosphonium cation was expected to target the compound to the negatively charged mitochondria.

Based on the hypothesis that the steric hindrance of the two N-methyl-L-glucamine pentaactetate bromoacetate **(26)** moieties could be responsible for the failure of the direct N-alkylation reaction, a second, successful synthetic approach for the synthesis of the asymmetrically substituted cyclen-based ligands was used. It involved the synthesis of an intermediate ligand, the 1-N-Boc ethylamine-4,7-diallyl acetate-10-benzyl acetate-1,4,7,10-tetraazacyclododecane (DABBC) **(36)**, which was called “the generic ligand” since it possesses a generic chemical structure that could be modified in many ways in order to produce different types of ligands. The generic ligand was designed and synthesised by exploiting an orthogonal protection strategy. The generic ligand was designed in a way that it contained three different protecting groups, used for masking the reactivity of carboxyl and amino functions. These protecting groups could be

selectively and sequentially removed allowing inserting different pendant arms on the cyclen ring. The sequential attachment of different pendant arms to the cyclen ring, after that each protecting group was removed, could allow to obtain an asymmetrically substituted cyclen-based ligand and could be achieved using a peptide coupling reaction. Three protecting groups were chosen for the synthesis of the general ligand: one Boc group to protect the primary amino function, two allyl ester groups and one benzyl ester group to protect three carboxylic functions. The synthetic route involving the orthogonal deprotection strategy allowed the issues encountered with the direct N-alkylation strategy to be overcome and the synthesis of different types of ligands, based on asymmetrically substituted cyclen. In fact, starting from the generic ligand and selectively removing the protecting groups attached to it, it was possible to successfully synthesise different types of asymmetrically substituted cyclen based ligands, which were complexed with Ln(III) ions.

6.2 Future work: the synthesis

As discussed in the section 3.2.3, four ligands (**L1**, **L2**, **L3** and **L4**), based on symmetrically substituted cyclen and bearing two pendant arms containing a triphenylphosphonium cation as mitochondria targeting moiety and one pendant arm containing a sensitizer antenna that in the meantime could react with ROS species, were successfully synthesized in this project. However it was not possible to introduce a further antenna that would have generated a reversible system of antennae described in the section 3.1. This was due to the fact that one step of the multistep orthogonal deprotection strategy, which starting from the DABBC **(36)** led to the synthesis of **L1**, **L2**, **L3** and **L4**, was unsuccessful after various reaction conditions. In future work, the introduction of a second antenna replacing the benzyl ester group could be achieved in two ways:

1. By changing the order by which the protecting groups are removed from the generic ligand. The allyl ester groups' cleavage can be followed by the Boc group

removal rather than the benzyl ester group removal. Then the benzyl ester group can be removed under strong acidic conditions, using for example hydrogen bromide, rather than reduction conditions via catalytic hydrogenation. However this procedure can be applied only if the pendant arms to be incorporated on the cyclen ring after each deprotection are stable not only under mild acidic conditions used for the Boc group removal but also under the strong acidic conditions used for the benzyl ester group removal.

2. By optimising the reactions conditions used for the benzyl ester group removal via catalytic hydrogenation. The catalytic hydrogenation can be performed under high H_2 pressure by using an autoclave rather than a glass round bottom flask. The autoclave may improve the efficiency of the catalytic hydrogenation as a higher concentration of H_2 in solution can be achieved in such a hermetically closed and pressurised system.

The orthogonal deprotection strategy involving the synthesis of the intermediate generic ligand proved to be a very versatile synthetic route since starting from the same molecule, the generic ligand, it was possible to obtain different types of asymmetrically substituted cyclen base-ligands. The versatility of the new synthetic route can be exploited in future works to produce other types of Ln^{3+} complexes based on asymmetrically substituted cyclen-based ligands targeted to different cellular organelles. This can be achieved by replacing the two arms containing the mitochondria targeting molecules, namely the triphenylphosphonium derivatives, with two arms containing different types of targeting molecules, such as peptide sequences, carbohydrates or antibodies.

6.3 Photophysical studies

All ligands synthesised in this project were complexed with trivalent lanthanide ions, giving rise to eleven lanthanide complexes of Eu(III), Tb(III), Nd(III) and Yb(III). Since

NdL3 and **YbL3** were complexed with the near infrared emitting Nd(III) and Yb(III), it was not possible to measure their photophysical properties using the fluorimeter available at the Open University due to the inability of the instrument to record the emission profiles falling in the near infrared region. The photophysical studies performed on **EuL2**, **TbL2** and **EuL6**, where the coumarin 343 was used as sensitizer antenna towards Eu(III) and Tb(III), demonstrated that it was not possible to achieve the Ln^{3+} sensitization using the coumarin 343 as sensitizer antenna since the characteristic L^{3+}-based luminescence was not observed upon exciting the coumarin 343 antenna. The absorption properties studies performed on **EuL1**, **TbL1** and **EuL7**, where the dihydrofluorescein diacetate was used as Eu(III) and Tb(III) sensitizer antenna, revealed that the dihydrofluorecein diacetate lost the acetate groups, as it was shown by the presence of a peak between 490 and 500 nm on the absorption spectra of **EuL1**, **TbL1** and **EuL7**. The emission studies performed on **EuL1**, **TbL1** and **EuL7** demonstrated that the dihydrofluorescein sensitizer antenna, formed upon acetate groups' cleavage, was not able to sensitize the Eu(III) and Tb(III) emission since the characteristic Ln^{3+}-based emission was not observed upon excitation of the dihydrofluorescein antenna at around 500 nm. On the other hand, according to the data reported in literature by Steemers et al. [83], the dihydrofluorescein diacetate can be a suitable Eu(III) and Tb(III) sensitizer if the acetate groups are not cleaved off during the complexation reaction, as its longest-wavelength absorption peak falls at 280 nm.

The photophysical studies performed on **EuL4** and **EuL5** demonstrated that the sensitisation of the Eu(III) emission could be achieved using the coumarin 3 carboxylic and coumarin 151 respectively as sensitizer antennae since the characteristic Eu(III) emission profile was observed upon excitation of the coumarin 3 carboxylic acid and the coumarin 151. The difference between **EuL4** and **EuL5** absorption and excitation spectra was indicative of a partial energy transfer process from the coumarin 3 carboxylic acid and coumarin 151 antennae to the Eu(III). In conclusion, **EuL4** and **EuL5** were the only complexes among those synthesised in this project to exhibit the characteristic Eu(III)

based luminescence. For this reason they were selected among all complexes to be evaluated for their response to the presence of ROS species. **EuL4** and **EuL5** photophysical properties were measured in the presence of H_2O_2 and Fe(II) perchlorate by using emission spectroscopy. A dose dependent increase of the Eu(III)-based emission intensity in **EuL4** was observed upon the addition H_2O_2, while no changes in the Eu(III) emission profile form were observed, indicating that there were no changes of that the Eu(III) coordination environment. A slight dose dependent decrease of the Eu(III)-based emission intensity in **EuL5** was observed upon the addition H_2O_2, while no changes in the Eu(III) emission profile form were observed, indicating that, similarly to **EuL4**, there were no changes of that the Eu(III) coordination environment.

6.4 Future work: photophysical studies

Future works based on the photophysical studies include:

1. Testing the lanthanide complexes containing the coumarin 343 as sensitizer antenna, namely **EuL2**, **TbL2** and **EuL6**, in order to assess if they would be able to sense the presence of ROS species. In particular the emission of **EuL2**, **TbL2** and **EuL6** will be recorded in absence and presence of hydroxyl radicals in order to see if the hydroxylation of the coumarin 343 by hydroxyl radicals generated in situ in the Fenton reaction catalysed by Fe(II) perchlorate could cause changes in its photophysical properties such that a switching on of the Ln^{3+} emission can be achieved.
2. Optimise the reactions conditions related to the complexation reaction of the ligands containing the dihydrofluorescein as Eu(III) and Tb(III) sensitizer with the Ln^{3+} in order to prevent the acetate group's cleavage. This would allow the synthesis of luminescent Eu(III) and Tb(III) complexes based on switch on/off mechanism. In this systems the sensitisation of the Eu(III) or Tb(III) luminescence

achieved using the dihydrofluorescein diacetate as sensitizer antenna should be switched off upon antenna oxidation by ROS species.

6.5 Biological studies

A mitochondrial stress test (MST) was performed on **EuL1**, **TbL1**, **EuL2**, **TbL2**, **NdL3**, **YbL3**, **EuL4** and **TbL4** to assess how test compounds affect various components of the mitochondrial electron transport chain with the aim to identify compounds that exhibit a potential mitochondrial and/or cellular toxicity [87]. A calcium loading capacity assay was performed on the same lanthanide complexes tested with the MST with the aim of investigating their effect on the mitochondrial capability to uptake and internalize Ca^{2+}.
A cellular ROS assay, was performed on the lanthanide complexes **EuL4** and **EuL5** to evaluate whether or not these complexes were responsive to ROS species, such as H_2O_2 and OH·, in a cellular environment by measuring changes in their luminescence intensity eventually caused by increased ROS levels. **EuL4** and **EuL5** were tested with the cellular ROS since they were the only complexes among those synthesised in this project that exhibited the characteristic lanthanide-based luminescence.

6.5.1 Mitochondrial Stress Test

A mitochondrial stress test (MST) was performed on the lanthanide complexes to verify if these complexes exhibit a potential mitochondrial and/or cellular toxicity. All complexes were tested at concentrations of 200 µM, 50 µM, 12.5 µM, 3.1 µM and 0.8 µM and their related OCR and ECAR profiles were recorded in presence and absence of cells (HepG2 liver cancer cell line). The OCR (pmol/min) was recorded in real time upon the sequential injection of oligomycin (ATP synthase inhibitor), FCCP (mitochondrial uncoupler), and rotenone/antimycin A/gluocose (complex I and III inhibitors), whilst the The ECAR

profiles were recorded in order to measure the compounds' effect on the glycolytic activity of the cells. When considering the MST data for each complex in its entirety it can be concluded that:

- **EuL1** and **TbL1** had a gradual effect on the oxygen fluorophore or could remove oxygen from the system on its own.
- **EuL1** and **TbL1** had an immediate and dose dependent effect on the pH fluorophore.
- **EuL1** and **TbL1** appeared to be non-toxic to cells at the two lowest doses of 3.1 and 0.8 µM, however exact interpretation of an effect/no effect level was difficult.
- **EuL2** and **TbL2** had a negative effect on basal and maximal respiration at the top two doses.
- **EuL2** and **TbL2** appeared to have no effect on oxygen consumption or mitochondrial function at 12.5, 3.1 and 0.8 µM and, whilst the pH fluorophore saturation rendered interpretation difficult, cells recovered glycolysis at 3.1 and 0.8 µM.
- 200, 50 and 12.5 µM of **NdL3** and **YbL3** had a deleterious effect on maximal respiration following FCCP injection.
- **NdL3** and **YbL3** showed a recovery of glycolysis up to 50 µM suggesting that **NdL3** and **YbL3** are not overtly cytotoxic and whilst a possible dose response remained it could be due to a dose related response of the compound on the pH fluorophore.
- The ECAR and OCR results obtained with **EuL4** and **TbL4** demonstrated that they did not exhibit any mitochondrial and cellular toxicity with the slight exception of 200 µM, which showed a small erosion of oxygen consumption at basal and maximal respiration.
- The MST data for **EuL4** and **TbL4** demonstarted a far superior mitochondrial and cellular toxicty profile and represent the most promising compounds for future development. Whilst the interpretation of the other complexes was complicated by the various effects on the pH and oxygen flurophores, it appeared clear that they all

caused imapirment of mitochondrial and cellular function at lower levels than **EuL4** and **TbL4**.

6.5.2 Calcium Loading Capacity Test

The calcium loading capacity profiles related to **EuL1**, **TbL1**, **EuL2**, **TbL2**, **NdL3**, **YbL3,** **EuL4** and **TbL4,** showed that these complexes were responsible for a significant erosion of the mitochondrial CLC. The significant CLC erosion caused by these complexes could be due to several factors. The significant erosion of the CLC caused by **EuL1-TbL4** could be due to mitochondrial toxicity or complete inhibition of mitochondrial calcium uptake. Whilst all compounds demonstrated inhibition of mitochondrial calcium loading, **EuL4** and **TbL4** demonstrated a degree of calcium loading compared to the other 6 complexes even at 250 µM and appeared to slightly less potent in their effects on calcium loading. This was in correlation with the MST data that suggested that **EuL4** and **TbL4** showed the lowest toxicity and are the most promising complexes for future development.

6.5.3 Cellular ROS assay

The aim of this test was to evaluate whether or not these complexes could sense high ROS levels in a cellular environment by measuring changes in their fluorescence intensity. **EuL4** and **EuL5** were tested at concentration of 1 µM, 10 µM and 100 µM. H_2O_2 (tested at concentration of 50 µM) and tBHP (tested at concentration of 150 µM) were used as ROS generator compounds, since they are able to induce an oxidative stress within the cells by increasing the ROS production [103]. MitoSOX, which is a fluorogenic ROS-sensing dye that is targeted to mitochondria in live cells, was used as probe positive control. The comparison between the fluorescence intensity of **EuL4** and **EuL5** recorded from the wells containing the cells previously incubated with H_2O_2 and tBHP and those containing the cells that were not incubated with H_2O_2 and tBHP allowed to evaluate

whether or not **EuL4** and **EuL5** were able to detect the variation of ROS levels. The results of the Cellular ROS assay can be summarised as follows:

- The fluorescence intensity of **EuL4** and **EuL5** recorded from the wells containing the cells previously exposed to tBHP and from those containing the cells incubated with **EuL4** and **EuL5** but not exposed to tBHP, were approximately the same. This indicated that **EuL4** and **EuL5** were not responsive to high ROS levels generated by tBHP.
- A complete quenching of **EuL4** and **EuL5** fluorescence was observed upon exposure of the cells to H_2O_2 indicating that **EuL4** and **EuL5** were responsive to high ROS levels generated by H_2O_2.
- The quenching of **EuL5** fluorescence observed in vitro was consistent with photophysical test performed on **EuL5** in the presence of H_2O_2 and Fe(II) perchlorate, where a decrease of the Eu(III) luminescence was observed upon H_2O_2 and Fe(II) perchlorate addition. By contrast the quenching of the **EuL4** fluorescence observed in vitro was not consistent with the the results obtained with the photophysical test performed on **EuL4** in the presence of H_2O_2 and Fe(II) perchlorate, where an increase of the Eu(III) luminescence was indeed observed upon H_2O_2 and Fe(II) perchlorate addition.
- In order to measure the fluorescence intensity of **EuL4** and **EuL5** without having any interference form by the amount that did not enter the cells, all the wells were washed twice with medium in order to eliminate traces of **EuL4** and **EuL5** that remained in the extracellular medium.
- Although a strong decrease of the fluorescence intensity of 100 µM **EuL5** was measured both before and after washing the wells, the decrease of fluorescence intensity of 1 µM and 10 µM **EuL5** was more significant before washing the wells compared to the one observed after washing the wells.
- A lower decrease of 1 µM **EuL4** and 10 µM **EuL4** fluorescence intensity was observed after washing the wells compared to the decrease of 1 µM **EuL4** and

10 µM **EuL4** observed before washing the wells. In addition, while a decrease of 100 µM **EuL4** fluorescence intensity was observed before washing the wells, a slight increase of 100 µM **EuL4** fluorescence intensity was observed after washing the wells. This inconsistent result could be due to the fact that probably wells' washing twice caused the release of a certain amount of compound that had previously entered the cells thus reducing its concentration within the cells.

- This hypothesis can be supported by the results obtained with the MitoSOX positive control fluorescence intensity measurements. According to the protocol, the MitoSOX fluorescence intensity was only recorded after washing. Although an increase of MitoSOX fluorescence intensity was observed both when H_2O_2 and tBHP were used as ROS generators and for, the magnitude of this increase was not so huge as expected from a compound known for its ability to detect variation of ROS levels within the cells.

6.6 Future work: biological studies

Although the lanthanide complexes **EuL4** and **EuL5** demonstrated to be able to act as ROS sensors, the small variation of the signal generated by them when tested in presence of ROS species makes these complexes not applicable to further in vitro and in vivo studies. However, taking advantages from the feasibility and versatility of the synthetic route developed in this project it will be possible to synthesise other types of Ln^{3+} complexes, based on asymmetrically substituted cyclen ligands, more responsive to the presence of ROS species by using different types of sensitizer antennae that allow a better sensitization and control of the Ln^{3+} luminescence, and in the meantime a major selectivity and reactivity towards ROS species.

Although a working ROS sensor was not successfully developed, this work has shown it is achievable. The synthetic strategy is broadly adaptable to a wide variety of ligands

that should produce more response in complexes and the protocol for the ROS assay can be modified to develop a quantifiable response.

References:

[1] Bernard Valeur and Mário N. Berberan-Santos. *Molecular Fluorescence. Principles and Applications.* John Wiley & Sons, Incorporated, 2013.

[2] Xijuan Tan and Zhenghua Song. *Human Saliva-Based Quantitative Monitoring of Clarithromycin by Flow Injection Chemiluminescence Analysis: A Pharmacokinetic Study.* Appl Biochem Biotechnol, 2014, 172, 1320-1331.

[3] Ramon Martinez-Manez. *Virtual Issue: Molecular Sensors*. ChemistryOpen 2014, 3, 232.

[4] Zhi-Qiang Hu, Ying-Ying Gu, Wen-Zhou Hu, Lei-Li Sun, Jiang-Hua Zhu, and Yi Jiang. *A Highly Selective and Sensitive Turn-On Fluorescent Chemosensor Based on Rhodamine 6G for Iron(III)*. ChemistryOpen, 2014, 3, 264-268.

[5] Gilles Muller. *Luminescent chiral lanthanide (III) complexes as potential molecular probes.* Dalton Trans., 2009, 44, 9692-9707.

[6] D. Parker. *Excitement in f block: structure, dynamics and function of nine-coordinate chiral lanthanide complexes in aqueous media.* Chem. Soc. Rev., 2004, 33, 156.

[7] Stephen Faulkner, Simon J. A. Pope and Benjamin P. Burton-Pye. *Lanthanide Complexes for Luminescence Imaging Applications.* Applied Spectroscopy Reviews, 2005, 40, 1-31.

[8] Turrens JF. *Mitochondrial formation of reactive oxygen species.* J. Physiol., 2003, 552.2, 335-344.

[9] Assim A. Alfadda and ReemM. Sallam. *Reactive Oxygen Species in Health and Disease.* Journal of Biomedicine and Biotechnology, 2012.

[10] Aashiq Hussain Bhat, Khalid Bashir Dar, Suhail Anees, Mohammad Afzal Zargar, Akbar Masood, Manzoor Ahmad Sofi, Showkat Ahmad Ganie. *Oxidative stress, mitochondrial dysfunction and neurodegenerative diseases; a mechanistic insight.* Biomedicine & Pharmacotherapy, 2015, 74, 101-110.

[11] Marian Valko, Dieter Leibfritz, Jan Moncola, Mark T.D. Cronin, Milan Mazura, Joshua Telser. *Free radicals and antioxidants in normal physiological functions and human disease.* The International Journal of Biochemistry & Cell Biology, 2007, 39, 44-84.

[12] Andreas N. Kavazis and Scott K. Powers. *Impact of Exercise, Reactive Oxygen and Reactive Nitrogen Species on Tumor Growth.*

[13] Seon-Young Kim, Sang-Jin Kim, Byoung-Joo Kim, So-Young Rah, Sung Mo Chung, Mie-Jae Im and Uh-Hyun Kim. *Doxorubicin-induced reactive oxygen species generation and intracellular Ca2+ increase are reciprocally modulated in rat cardiomyocytes*. Experimental and Molecular Medicine, 2006, 38, 535-545.

[14] Xiaoqiang Chen, Fang Wang, Ji Young Hyun, Tingwen Wei, Jian Qiang, Xintong Ren, Injae Shin and Juyoung Yoon. *Recent progress in the development of fluorescent, luminescent and colorimetric probes for detection of reactive oxygen and nitrogen species*. Chem. Soc. Rev., 2016, 45, 2976-3016**.**

[15] Damian G. Deavall, Elizabeth A.Martin, Judith M. Horner, and Ruth Roberts. *Drug-Induced Oxidative Stress and Toxicity.* Journal of Toxicology, 2012, 1-13.

[16] Jihad Rene Albani. *Principles and Applications of Fluorescence Spectroscopy*. John Wiley & Sons, Incorporated 2008.

[17] J.-C.G. Bünzli and V.K. Pecharsky. *Handbook on the Physics and Chemistry of Rare Earths: including Actinides.* North-Holland, 2016, 50, 9-25.

[18] S. V. Eliseeva and J.-C. G. Bünzli. *Lanthanide luminescence for functional materials and bio-sciences*. Chem. Soc. Rev., 2010, 39,189-227.

[19] Jean-Claude G. Bünzli and Claude Piguet. *Taking advantage of luminescent lanthanide ions.* Chem. Soc. Rev., 2005, 34, 1048-1077.

[20] David Parker and J. A. Gareth Williams. *Getting excited about lanthanide complexation chemistry.* J. Chem. SOC. Dalton Trans., 1996, 3613-3628.

[21] David Parker. *Luminescent lanthanide sensors for pH, pO2 and selected anions.* Coordination Chemistry Reviews, 2000, 205,109-130

[22] Anders Døssing. *Luminescence from Lanthanide (3^+) Ions in Solution*. Eur. J. Inorg. Chem., 2005, 1425-1434.

[23] Zheming Wang, Gregory R. Choppin, Plinio Di Bernardo, Pier-Luigi Zanonato, Roberto Portanova and Marilena Tolazzi. *Luminescence Spectroscopic Study of Europium(iii) and Terbium(iii) with Ethylenediamine in Dimethyl Sulfoxide.* J. Chem. Soc., Dalton Trans., 1993, 2791-2796.

[24] David Parker and J. A. Gareth Williams. *Luminescence behaviour of cadmium, lead, zinc, copper, nickel and lanthanide complexes of octadentate macrocyclic ligands bearing naphthyl chromophores.* J. Chem. Soc. Perkin Trans., 1995, 2, 1305-1314.

[25] Chang, C.J., Gunnlaugsson, T., James, T.D. *Imaging agents*. Chem. Soc. Rev., 2015, 44, 4484-4486.

[26] Brian K. McMahon, Robert Pal and David Parker. *A bright and responsive europium probe for determination of pH change within the endoplasmic reticulum of living cells.* Chem. Commun., 2013, 49, 5363-5365.

[27] Marco Giardiello, Mauro Botta, and Mark P. Lowe. *pH-Responsive Lanthanide Complexes Based on Reversible Ligation of a Diphenylphosphinamide*. Inorg. Chem., 2013, 52, 14264-14269.

[28] Ian M. Clarkson, Andrew Beeby, James I. Bruce, Linda J. Govenlock, Mark P. Lowe, E. Celine Mathieu, David Parker and Kanthi Senanayake. *Experimental assessment of the efficacy of sensitised emission in water from a europium ion, following intramolecular excitation by a phenanthridinyl group*. New J. Chem., 2000, 24, 377-386.

[29] Evan A. Weitz and Valerie C. Pierre. *A ratiometric probe for the selective time-gated luminescence detection of potassium in water*. Chem. Commun., 2011, 47, 541-543.

[30] Oxana Kotova, Steve Comby and Thorfinnur Gunnlaugsson. *Sensing of biologically relevant d-metal ions using a Eu(III)-cyclen based luminescent displacement assay in aqueous pH 7.4 buffered solution*. Chem. Commun., 2011, 47, 6810-6812.

[31] Elias Pershagen, Johan Nordholm, and K. Eszter Borbas. *Luminescent Lanthanide Complexes with Analyte-Triggered Antenna Formation*. J. Am. Chem. Soc., 2012, 134, 9832-9835.

[32] James I. Bruce, Rachel S. Dickins, Linda J. Govenlock, Thorfinnur Gunnlaugsson, Stefan Lopinski, Mark P. Lowe, David Parker, Robert D. Peacock, Justin J. B. Perry, Silvio Aime, and Mauro Botta. *The Selectivity of Reversible Oxy-Anion Binding in Aqueous Solution at a Chiral Europium and Terbium Center: Signaling of Carbonate Chelation by Changes in the Form and Circular Polarization of Luminescence Emission.* J. Am. Chem. Soc., 2000, 122, 9674-9684.

[33] David G Smith, Robert Pal, and David Parker. *Measuring Equilibrium Bicarbonate Concentrations Directly in Cellular Mitochondria and in Human Serum Using Europium/Terbium Emission Intensity Ratios.* Chem. Eur. J., 2012, 18, 11604-11613.

[34] Rebeca Acin-Perez, Eric Salazar, Margarita Kamenetsky, Jochen Buck, Lonny R. Levin, and Giovanni Manfredi. *Cyclic AMP produced inside mitochondria regulates oxidative phosphorylation.* Cell Metab., 2009, 9, 265-276.

[35] Jack D. Routledge, Xuejian Zhang, Michael Connolly, Manuel Tropiano, Octavia A. Blackburn, Alan M. Kenwright, Paul D. Beer, Simon Aldridge, and Stephen Faulkner. *Lanthanide Complexes that Respond to Changes in Cyanide Concentration in Water.* Angew. Chem., 2017, 56, 7783-7786.

[36] Emily R. Neil, Mark A. Fox, Robert Pal and David Parker. *Induced europium CPL for the selective signalling of phosphorylated amino-acids and O-phosphorylated hexapeptides.* Dalton Trans., 2016, 45, 8355-8366.

[37] K. Eszter Borbas, James I. Bruce. *Synthesis of asymmetrically substituted cyclen-based ligands for the controlled sensitisation of lanthanides.* Org. Biomol. Chem., 2007, 5, 2274-2282.

[38] Andras Bodi, K. Eszter Borbas and James I. Bruce. *Near IR-emitting DNA-probes exploiting stepwise energy transfer processes.* Dalton Trans., 2007, 4352-4358.

[39] Petr KlÃ¡n and Jakob Wirz. *Photochemistry of Organic Compounds: From Concepts to Practice.* 2009.

[40] Christine C Winterbourn. *Reconciling the chemistry and biology of reactive oxygen species.* Nature Chemical Biology, 2008, 4, 278-286.

[41] Barry Halliwell. *Oxidative stress and neurodegeneration: where are we now?* Journal of Neurochemistry, 2006, 97, 1634-1658.

[42] Katerina Krumova and Gonzalo Cosa. *Chapter 1: Overview of Reactive Oxygen Species*. From the book *Singlet Oxygen: Applications in Biosciences and Nanosciences*, Santi Nonell and Cristina Flors, European Society for Photobiology, 2016, 1.

[43] Stefan I. Liochev and Irwin Fridovich. *Superoxide and Iron: Partners in Crime.* Iumb Life, 1999, 48, 157-161.

[44] Hiroshi Kasai. *Chemistry-based studies on oxidative DNA damage: formation, repair, and mutagenesis*. Free Radical Biology & Medicine, 2002, 33, 450-456.

[45] Mark D. Evans, Miral Dizdaroglu, Marcus S. Cooke. *Oxidative DNA damage and disease: induction, repair and significance.* Mutation Research, 2004, 567, 1-61.

[46] Harvey Lodish, Arnold Berk, S Lawrence Zipursky, Paul Matsudaira, David Baltimore, and James Darnell. *Electron Transport and Oxidative Phosphorylation*. Molecular Cell Biology, 2000.

[47] Lubert Stryer. *Biochemistry.* W.H. Freeman and Company, 1995.

[48] Bruce Alberts, Alexander Johnson, Julian Lewis, Martin Raff, Keith Roberts, and Peter Walter. *Molecular Biology of the Cell*. New York: Garland Science, 2002.

[49] Volodymyr I. Lushchak. *Free radicals, reactive oxygen species, oxidative stress and its classification.* Chemico-Biological Interactions, 2014, 224, 164-175.

[50] Vladimir P. Skulachev. *Mitochondria-Targeted Antioxidants as Promising Drugs for Treatment of Age-Related Brain Diseases.* Journal of Alzheimer's Disease 2012, 28, 283-289.

[51] Michael P. Murphy. *How mitochondria produce reactive oxygen species*. Biochem. J., 2009, 417, 2009, 1-13.

[52] Barry Halliwell and John M.C. Gutteridge. *Biologically relevant metal ion-dependent hydroxyl radical generation.* FEBS Letters, 1992, 307, 108-112.

[53] Jayasri Nanduri, Damodara Reddy Vaddi, Shakil A. Khan, Ning Wang, Vladislav Makerenko, Nanduri R. Prabhakar. *Xanthine Oxidase Mediates Hypoxia-Inducible Factor-2α Degradation by Intermittent Hypoxia.* Plos One., 2013, 8 (10), e75838.

[54] Teruhide Yamaguchi, Katsuko Kakinuma, Mizuho Kaneda, and Kokichi Shimada. *Comparative Studies on Alveolar Macrophages and Polymorphonuclear Leukocytes: I. H_2O_2 and O_2^- Generation by Rabbit Alveolar Macrophages.* J. Biochein., 1980, 87, 1449-1455.

[55] Joshua W. Miller, Jacob Selhub, James A. Joseph. *Oxidative damage caused by free radicals produced during catecholamine autoxidation: Protective effects of O-methylation and melatonin.* Free Radical Biology and Medicine, 1996, 21, 241-249.

[56] L. Zuo, T. Zhou, B. K. Pannell, A. C. Ziegler and T. M. Best. *Biological and physiological role of reactive oxygen species – the good, the bad and the ugly.* Acta Physiol, 2015, 214, 329-348.

[57] J. T. Hancock, R. Desikan and S. J. Neil. *Role of reactive oxygen species in cell signalling pathways.* Biochemical Society Transactions, 2001, 29, 345-349.

[58] Yochai Basel and Alfred Hassner. *Di-tert-butyl Dicarbonate and 4-(Dimethylamino) pyridine Revisited*. *Their Reactions with Amines and Alcohols.* J. Org. Chem. 2000**,** *65,* 6368-6380.

[59] Stephen Hanessian, Roberto Margarita, Adrian Hall, Shawn Johnstone, Martin Tremblay, and Luca Parlanti. *Total Synthesis and Structural Confirmation of the Marine*

Natural Product Dysinosin A: A Novel Inhibitor of Thrombin and Factor VIIa. J. Am. Chem. Soc., 2002, 124, 13342-13343.

[60] Julien Massue, Sally E. Plush, Celia S. Bonnet, Doireann A. Moore and Thorfinnur Gunnlaugsson. *Selective mono N-alkylations of cyclen in one step syntheses.* Tetrahedron Letters, 2007, 48, 8052-8055.

[61] Christian A. G. N. Montalbetti and Virginie Falque. *Amide bond formation and peptide coupling.* Tetrahedron, 2005, 61, 10827-10852.

[62] Cong Li and Wing-Tak Wong. *A Simple, Regioselective Synthesis of 1, 4-Bis(tert-butoxycarbonylmethyl)-tetraazacyclododecane.* J. Org. Chem., 2003, 68, 2956-2959.

[63] Jerry Isaacson and Yoshihisa Kobayashi. *An Ugi Reaction in the Total Synthesis of (-)-Dysibetaine.* Angew. Chem. Int. Ed. 2009, 48, 1845-1848.

[64] Peter G., M. Wuts. *Greene's Protective Groups in Organic Synthesis.* John Wiley & Sons, Inc*,* 2014.

[65] Sieglinde Friedrich-Bochnitschek, Herbert Waldmann, and Horst Kunz. *Allyl Esters as Carboxy Protecting Groups in the Synthesis of O-Glycopeptides.* J. Org. Chem., 1989, 54, 751-756.

[66] Alan R. Katritzky, Ekaterina Todadze, Parul Angrish , and Bogdan Draghici. *Efficient Peptide Coupling Involving Sterically Hindered Amino Acids***.** J. Org. Chem.*,* 2007, *72*, 5794-5801.

[67] Christophe Bongars, Peter Bougeard, Adrian Bury, Christopher J. Cooksey, Michael D. Johnson, Stewart Mitchell, Paul A. Owens, Famida Rajah. *Homolytic displacement at carbon: XI. Intramolecular homolytic displacement as a route to cyclopentane and tetrahydrofuran derivatives from hex-5-enyl- andhex-3-oxo-5-enylcobaloximes.* Journal of Organometallic Chemistry, 1985, 289, 163-171.

[68] C. Wängler, B. Wängler, M. Eisenhut,U. Haberkorn and W. Mier. *Improved syntheses and applicability of different DOTA building blocks for multiply derivatized scaffolds.* Bioorganic & Medicinal Chemistry, 2008, 16, 2606-2616.

[69] François Guibè. *Allylic Protecting Groups and Their Use in a Complex Environment. Part II: Allylic Protecting Groups and their Removal through Catalytic Palladium π-Ally Methodology.* Tetrahedron, 1998, 54, 2967-3042.

[70] Sieglinde Friedrich-Bochnitschek, Herbert Waldmann, and Horst Kunz. *Allyl Esters as Carboxy Protecting Groups in the Synthesis of O-Glycopeptides.* J. Org. Chem. 1989, 54, 751-756.

[71] Sandrine Lemaire-Audoire, Monique Savignac, Guy Pourcelot, Jean-Pierre Genêt, Jean-Marie Bernard. *Chemoselective removal of allylic protecting groups using water-soluble $Pd(OAc)_2$/TPPTS catalyst.* Journal of Molecular Catalysis, 1997, 116 247-258.

[72] Detcho A. Stoyanovsky, Jianfei Jiang, Michael P. Murphy, Michael Epperly, Xiaolan Zhang, Song Li, Joel Greenberger, Valerian Kagan, and Hülya Bayır. *Design and Synthesis of a Mitochondria-Targeted Mimic of Glutathione Peroxidase, MitoEbselen-2, as a Radiation Mitigator.* Med. Chem. Lett. 2014, 5, 1304-1307.

[73] Nu Xiaoa, Zhong-Xing Jianga, and Y. Bruce Yua. *Enantioselective Synthesis of (2R, 3S)- and (2S, 3R)-4,4,4-trifluoro-N-Fmoc-O-tert-butyl-threonine and their Racemization-free Incorporation into Oligopeptides via Solid-phase Synthesis.* Biopolymers, 2007, 88, 6,781-796.

[74] Pijus K. Mandal and John S. McMurray. *Pd-C-Induced Catalytic Transfer Hydrogenation with Triethylsilane.* J. Org. Chem. 2007, 72, 6599-660.

[75] Luís M. P. Lima, Alexandre Lecointre, Jean-Francçis Morfin, Andrés de Blas, Dimitris Visvikis, Loïc J. Charbonnière, Carlos Platas-Iglesias, and Raphaël Tripier. *Positively Charged Lanthanide Complexes with Cyclen-Based Ligands: Synthesis, Solid-State and Solution Structure, and Fluoride Interaction.* Inorg. Chem. 2011, 50, 12508-12521.

[76] David Parker and J. A. Gareth Williams. *Modest effectiveness of carbostyrill24 as a sensitising chromophore in europium and terbium amide complexes based on 1,4,7,10-tetraazacyclododecane.* J. Chem. Soc. Perkin Trans., 1996, 2, 1586-1581.

[77] R. B. Woodward, Franz Sondheimer, David Taub, Karl Heusler, W. M. McLamore. *The Total Synthesis of Steroids.* J. Am. Chem. *Soc.*, 1952, *74*, 4223-4251.

[78] Stephen L. Hempel, Garry R. Buettner, Yunxia Q. O'Malley, Duane A. Wessels, and Dawn M. Flaherty. *Dihydrofluorescein diacetate is superior for detecting intracellular oxidants: comparison with 2',7'dichlorodihydrofluorescein diacetate, 5(and 6)-carboxy-2',7'dichlorodihydrofluorescein diacetate, and dihydrorhodamine 123.* Free Radical Biology and Medicine, 1999, 27, 146-159.

[79] John P. Crow. *Dichlorodihydrofluorescein and Dihydrorhodamine 123 Are Sensitive Indicators of Peroxynitrite in Vitro: Implications for Intracellular Measurement of Reactive Nitrogen and Oxygen Species.* Nitric Oxide: Biology and Chemistry, 1997, 1, 145-157.

[80] Binghe Wang, Eric V. Anslyn. *Chemosensors: Principles, Strategies, and Applications*. John Wiley & Sons, 2011.

[81] Thomas Just Sørensen, Alan M. Kenwright and Stephen Faulkner. *Bimetallic lanthanide complexes that display a ratiometric response to oxygen concentrations.* Chem. Sci., 2015, 6, 2054-2059.

[82] Jeong-a Yu. *An observation of back energy transfer in complex Tb(III) with 2-naphthoate in methanol.* Journal of Luminescence, 1998, 78, 265-270.

[83] Frank J. Steemers, Willem Verboom, David N. Reinhoudt, J Erik B. Van Der Tal, and Jan W. Verhoeven. *New Sensitizer-Modified Calix[4]arenes Enabling Near-UV Excitation of Complexed Luminescent Lanthanide Ions.* J. Am. Chem. Soc., 1995, 117, 9408-9414.

[84] Zheming Wang, Gregory R. Choppin, Plinio Di Bernardo, Pier-Luigi Zanonato, Roberto Portanova and Marilena Tolazzi. *Luminescence Spectroscopic Study of Europium(iii) and Terbium(iii) with Ethylenediamine in Dimethyl Sulfoxide.* J. Chem. Soc. Dalton Trans., 1993, 2791-2796.

[85] Masaki Misawa and Junko Takahashi. *Generation of reactive oxygen species induced by gold nanoparticles under x-ray and UV Irradiations.* Nanomedicine: Nanotechnology, Biology and Medicine, 2011, 7, 604-614.

[86] Stephen J. Butler and David Parker. *Anion binding in water at lanthanide centres: from structure and selectivity to signalling and sensing.* Chem. Soc. Rev., 2013, 42, 1652-1666.

[87] Ruolan Wang, Steven J. Novick, James B. Mangum, Kennedy Queen, David A. Ferrick, George W. Rogers, and Julie B. Stimmel. *The Acute Extracellular Flux (XF) Assay to Assess Compound Effects on Mitochondrial Function.* Journal of Biomolecular Screening 2015, 20, 422-429.

[88] Arthur R. Salomon, David W. Voehringer, Leonard A. Herzenberg, and Chaitan Khosla. *Understanding and exploiting the mechanistic basis for selectivity of polyketide inhibitors of F0F1-ATPase.* Proc. Natl. Acad. Sci. USA, 2000, 97, 14766-14771.

[89] Minh-Son To, Edoardo C. Aromataris, Joel Castro, Michael L. Roberts, Greg J. Barritt, Grigori Y. Rychkov. *Mitochondrial uncoupler FCCP activates proton conductance but does not block store-operated Ca^{2+} current in liver cells.* Archives of Biochemistry and Biophysics, 2010, 495, 152-158.

[90] Shona A. Mookerjee, Ajit S. Divakaruni, Martin Jastroch, and Martin D. Brand. *Mitochondrial uncoupling and lifespan.* Mech Ageing Dev., 2010, 131, 463-472.

[91] Nianyu Li, Kathy Ragheb, Gretchen Lawler, Jennie Sturgis, Bartek Rajwa, J. Andres Melendez, and J. Paul Robinson. *Mitochondrial Complex I Inhibitor Rotenone Induces Apoptosis through Enhancing Mitochondrial Reactive Oxygen Species Production.* The Journal of Biological Chemistry, 2003, 278, 8516-8525.

[92] Xiuquan Ma, Mingzhi Jin, Yu Cai, Hongguang Xia, Kai Long, Junli Liu, Qiang Yu, and Junying Yuan. *Mitochondrial Electron Transport Chain Complex III Is Required for Antimycin A to Inhibit Autophagy.* Chem Biol. 2011, 18, 1474-1481.

[93] Martin D. Brand and David G. Nicholls. *Assessing mitochondrial dysfunction in cells.* Biochem. J., 2011, 435, 297-312.

[94] Lisa S. Pike Winer, Min Wu. *Rapid Analysis of Glycolytic and Oxidative Substrate Flux of Cancer Cells in a Microplate.* Plos One, 2014, 9 (10), e109916.

[95] Martin Jastroch, Ajit S. Divakaruni, Shona Mookerjee, Jason R. Treberg, and Martin D. Brand. *Mitochondrial proton and electron leaks.* Essays Biochem., 2010, 47, 53-67.

[96] Ajit S. Divakaruni and Martin D. Brand. *The Regulation and Physiology of Mitochondrial Proton Leak.* Physiology, 2011, 26, 192-205.

[97] Toren Finkel, Sara Menazza, Kira M. Holmström, Randi J. Parks, Julia Liu, Junhui Sun, Jie Liu, Xin Pan, Elizabeth Murphy. *The Ins and Outs of Mitochondrial Calcium.* Circulation Research, 2015, 1810-1819.

[98] Karin Nowikovsky and Paolo Bernardi. *LETM1 in mitochondrial cation transport.* Front Physiol., 2014, 5, 1-3.

[99] Jaime Santo-Domingo, Nicolas Demaurex. *Calcium uptake mechanisms of mitochondria.* Biochimica et Biophysica Acta, 2010, 1797, 907-912.

[100] Uta C. Hoppe. *Mitochondrial calcium channels*. Febs Letters, 2010, 584, 1975-1981.

[101] Judit Doczi, Lilla Turiak, Szilvia Vajda, Miklos Mandi, Beata Torocsik, Akos A. Gerencser, Gergely Kiss, Csaba Konrad, Vera Adam-Vizi, and Christos Chinopoulos. *Complex Contribution of Cyclophilin D to Ca^{2+}-induced Permeability Transition in Brain Mitochondria, with Relation to the Bioenergetic State.* The Journal of Biological Chemistry, 2011, 286, 6345-6353.

[102] Anibal E. Vercesi, Silvia N. J. Moreno and Roberto Docampo. *Ca^{2+}/H^{+} exchange in acidic vacuoles of Trypanosoma*. Biochem. J., 1994, 304, 227-233.

[103] N. O. Leary, A. Pembroke, and P. F. Duggan. *Single Stable Reagent (Arsenazo Ill) for Optically Robust Measurement of Calcium in Serum and Plasma.* Clin.Chem., 1992, 38, 904-908.

[104] A.P. Halestrap, C.P. Connern, E.J. Griffiths and P.M. Kerr. *Cyclosporin A binding to mitochondrial cyclophilin inhibits the permeability transition pore and protects hearts*

from ischaemia/reperfusion injury. Molecular and Cellular Biochemistry, 1997, 174, 167-172.

[105] Yefim Manevich, Kathryn D. Heldt and John E. Biaglow. *Coumarin-3-Carboxyl Acid as a Detector for Hydroxyl Radicals Generated Chemically and by Gamma Radiation.* Radiation Research, 1997, 148, 580-591.

[106] Otto Kulera, René Endlicher, Tomáš Roušar, Halka Lotková, Tomáš Garnol, Zdenjk Drahota, and Zuzana Hervinková. *The Effect of tert-Butyl Hydroperoxide-Induced Oxidative Stress on Lean and Steatotic Rat Hepatocytes In Vitro.* Hindawi Publishing Corporation Oxidative Medicine and Cellular Longevity Volume 2014.

[107] *MitoSOX Red mitochondrial superoxide indicator for live-cell imaging (M36008).* Molecular probes Invitrogen detection technologies-product information.

[108] Michael J. DAVIES. *Detection of peroxyl and alkoxyl radicals produced by reaction of hydroperoxides with rat liver microsomal fractions*. Biochem. J., 1989, 257, 603-606.

Appendix

Appendix A.1 - MST data of TbL1, EuL2, TbL2, NdL3, YbL3, EuL4 and TbL4.

Appendix A.1.1 - TbL1 MST data

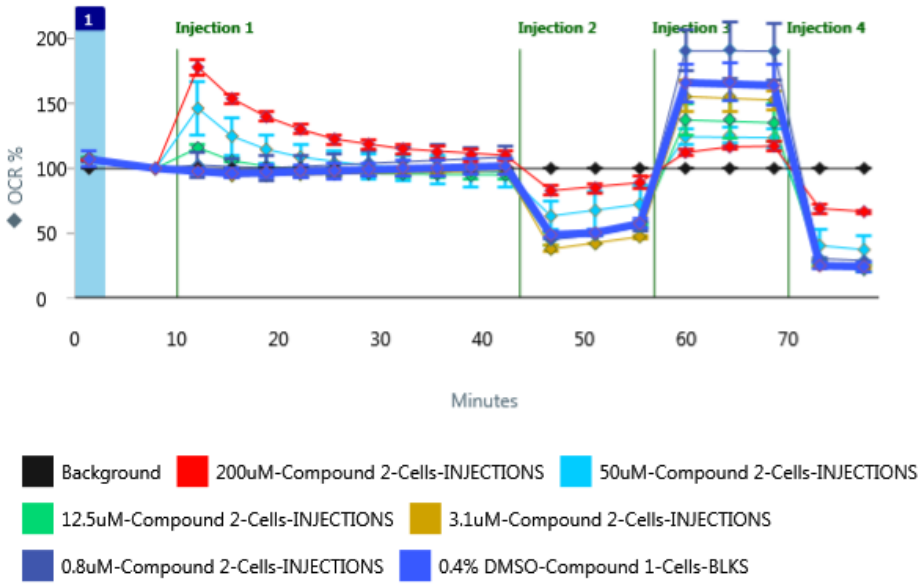

Figure 99. OCR RATE of cells measured during the MST performed on **TbL1**. **Injection 1** corresponds to **TbL1** injection, **injection 2** corresponds to oligomicyn injection, **injection 3** corresponds to FCCP injection and **injection 4** corresponds to rotenone/antimycin A injection.

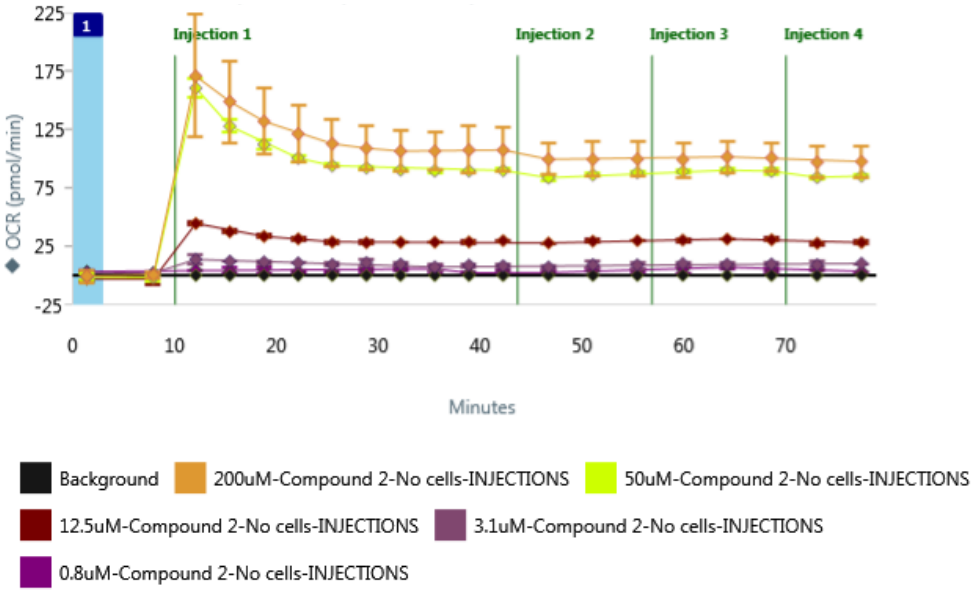

Figure 100. **TbL1** OCR rate measured during the MST in absence of cells. **Injection 1** corresponds to **TbL1** injection, **injection 2** corresponds to oligomicyn injection, **injection 3** corresponds to FCCP injection and **injection 4** corresponds to rotenone/antimycin A injection.

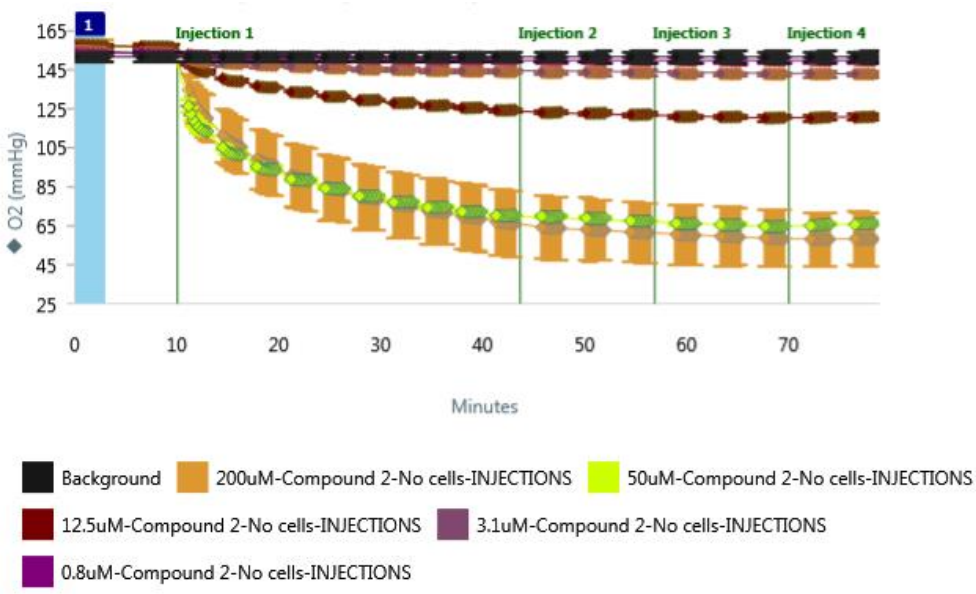

Figure 101. **TbL1** OCR LEVEL measured during the MST in absence of cells. **Injection 1** corresponds to **TbL1** injection, **injection 2** corresponds to oligomicyn injection, **injection 3** corresponds to FCCP injection and **injection 4** corresponds to rotenone/antimycin A injection.

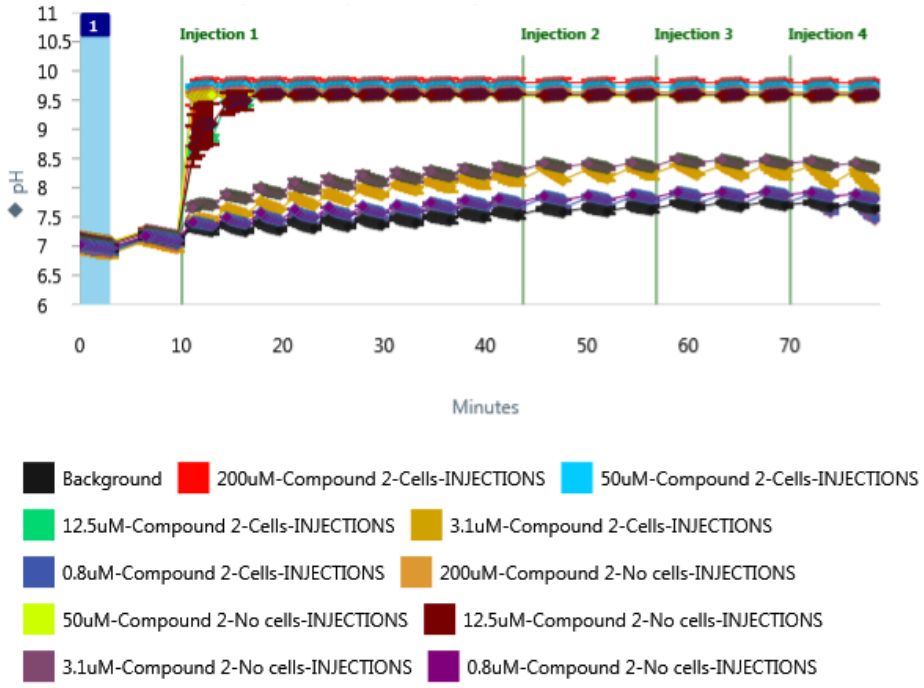

Figure 102. **TbL1** ECAR LEVEL measured during the MST in absence and presence of cells. **Injection 1** corresponds to **TbL1** injection, **injection 2** corresponds to oligomicyn injection, **injection 3** corresponds to FCCP injection and **injection 4** corresponds to rotenone/antimycin A injection.

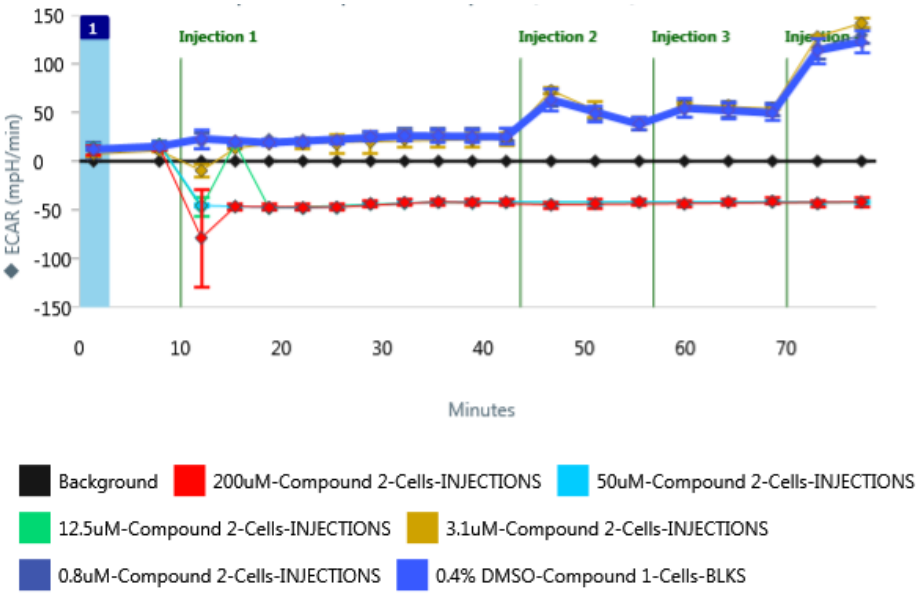

Figure 103. C2 ECAR RATE measured during the MST in presence of cells. **Injection 1** corresponds to **TbL1** injection, **injection 2** corresponds to oligomicyn injection, **injection 3** corresponds to FCCP injection and **injection 4** corresponds to rotenone/antimycin A injection.

Appendix A.1.2 – EuL2 and TbL2 MST data

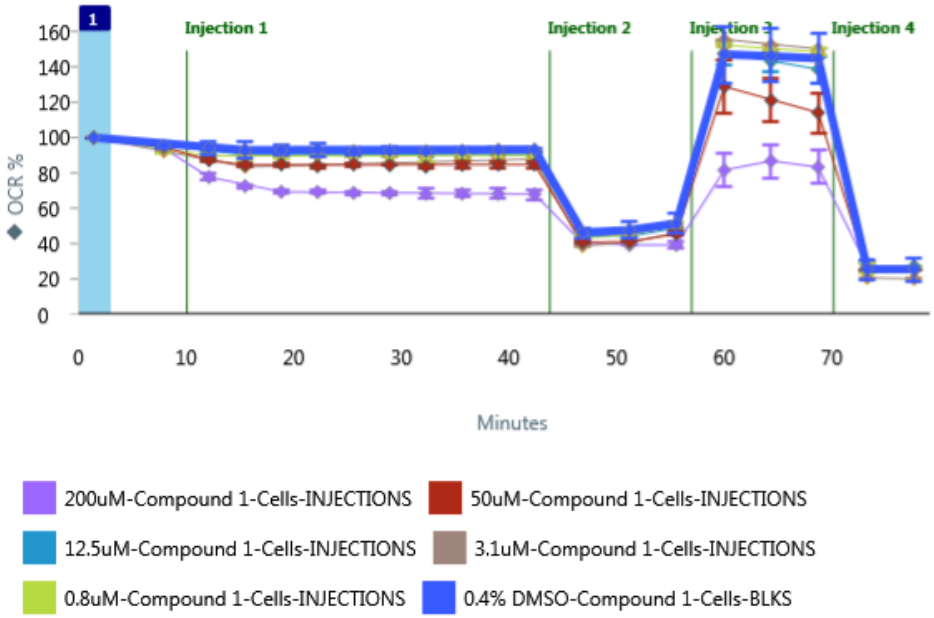

Figure 104. OCR RATE of cells measured during the MST performed on **EuL2**. **Injection 1** corresponds to **EuL2** injection, **injection 2** corresponds to oligomicyn injection, **injection 3** corresponds to FCCP injection and **injection 4** corresponds to rotenone/antimycin A injection.

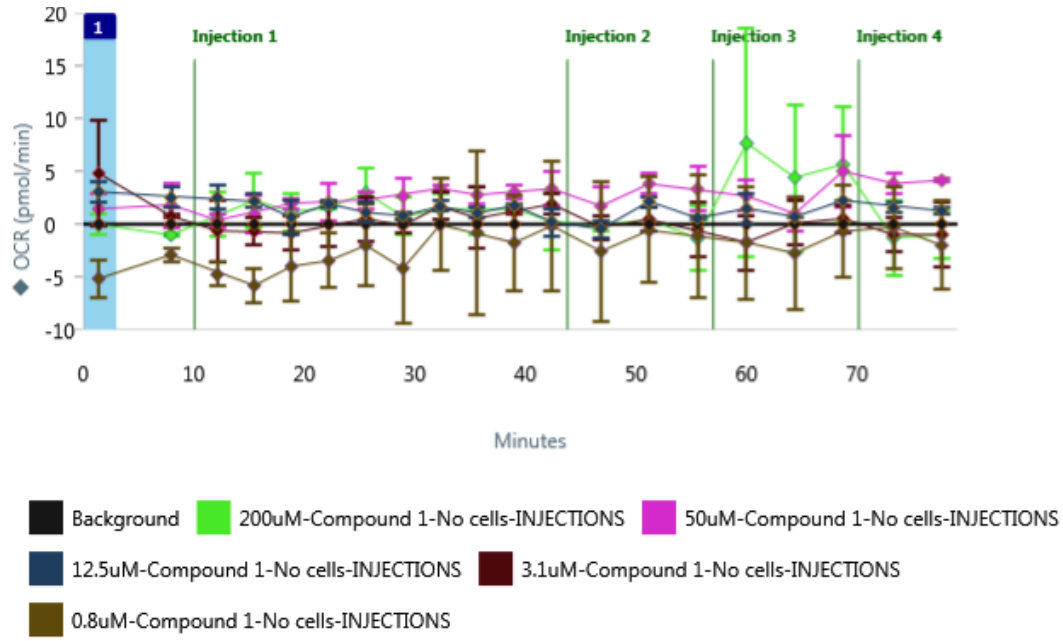

Figure 105. **EuL2** OCR RATE measured during the MST in absence of cells. **Injection 1** corresponds to **EuL2** injection, **injection 2** corresponds to oligomicyn injection, **injection 3** corresponds to FCCP injection and **injection 4** corresponds to rotenone/antimycin A injection.

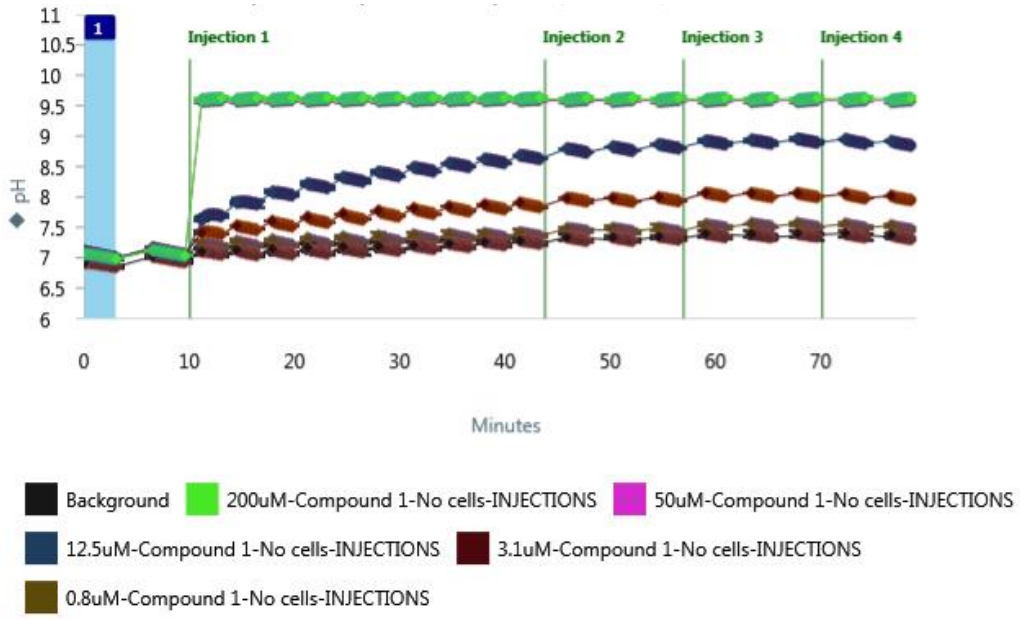

Figure 106. **EuL2** ECAR LEVEL measured during the MST in absence of cells. **Injection 1** corresponds to **EuL2** injection, **injection 2** corresponds to oligomicyn injection, **injection 3** corresponds to FCCP injection and **injection 4** corresponds to rotenone/antimycin A injection.

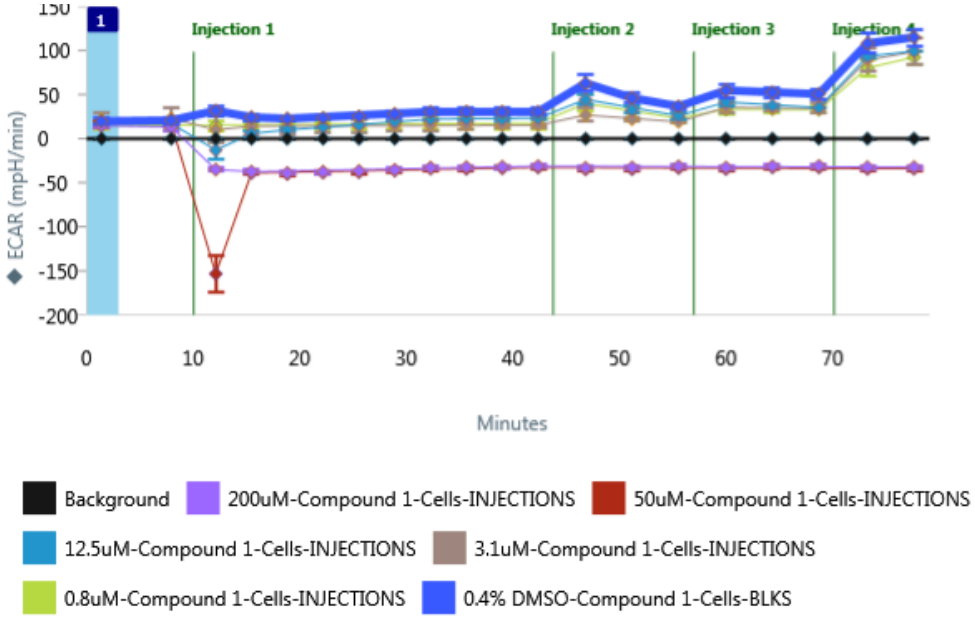

Figure 107. **EuL2** ECAR RATE measured during the MST in presence of cells. **Injection 1** corresponds to **EuL2** injection, **injection 2** corresponds to oligomicyn injection, **injection 3** corresponds to FCCP injection and **injection 4** corresponds to rotenone/antimycin A injection.

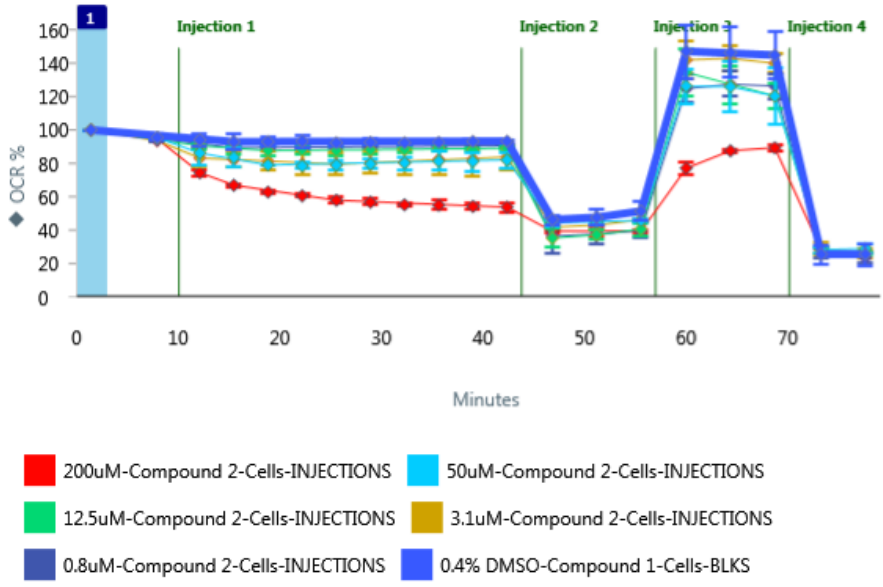

Figure 108. OCR RATE of cells measured during the MST performed on **TbL2**. **Injection 1** corresponds to **TbL2** injection, **injection 2** corresponds to oligomicyn injection, **injection 3** corresponds to FCCP injection and **injection 4** corresponds to rotenone/antimycin A injection.

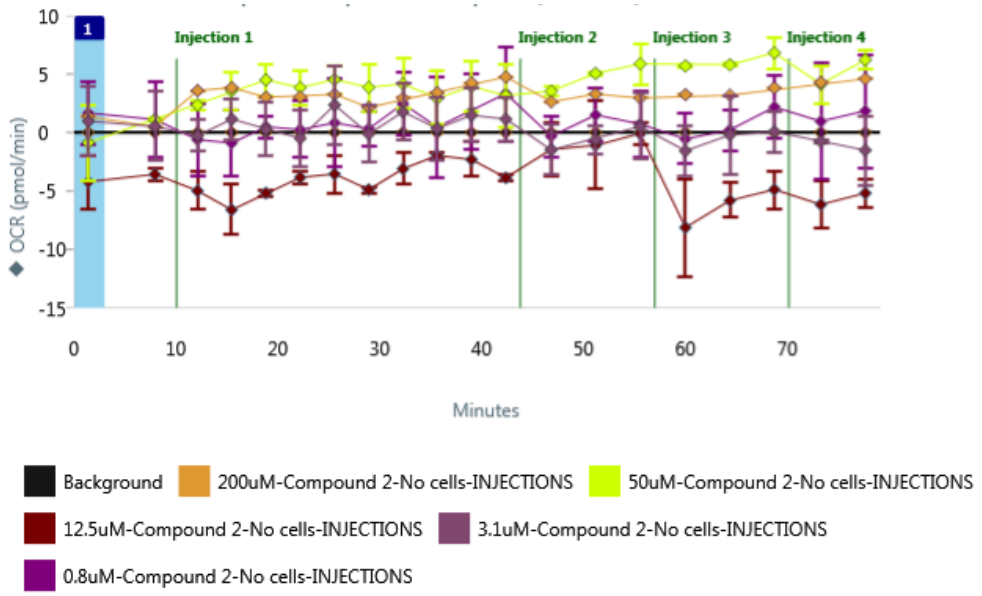

Figure 109. **TbL2** OCR RATE measured during the MST in absence of cells. **Injection 1** corresponds to **TbL2** injection, **injection 2** corresponds to oligomicyn injection, **injection 3** corresponds to FCCP injection and **injection 4** corresponds to rotenone/antimycin A injection.

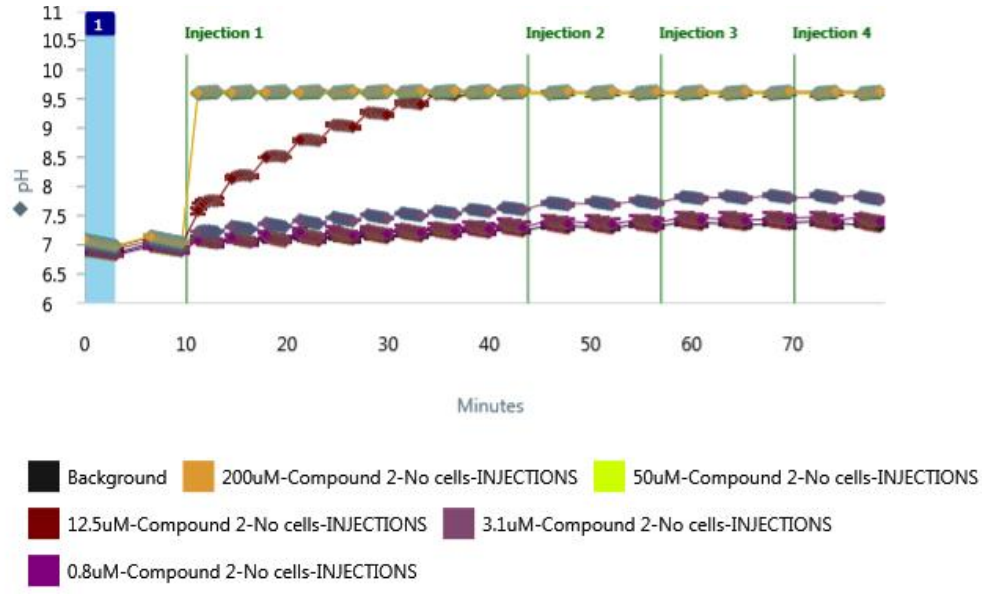

Figure 110. **TbL2** ECAR LEVEL measured during the MST in absence of cells. **Injection 1** corresponds to **TbL2** injection, **injection 2** corresponds to oligomicyn injection, **injection 3** corresponds to FCCP injection and **injection 4** corresponds to rotenone/antimycin A injection.

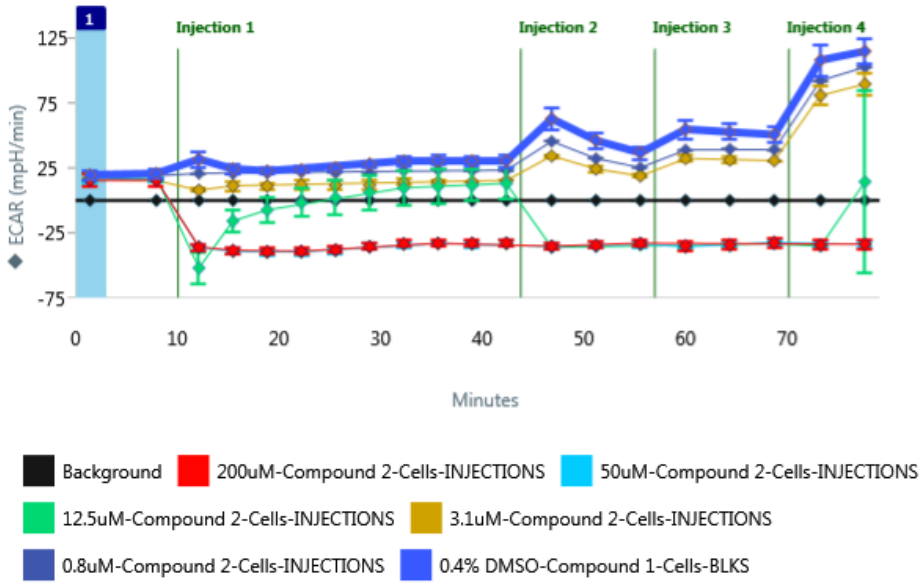

Figure 111. **TbL2** ECAR RATE measured during the MST in presence of cells. **Injection 1** corresponds to **TbL2** injection, **injection 2** corresponds to oligomicyn injection, **injection 3** corresponds to FCCP injection and **injection 4** corresponds to rotenone/antimycin A injection.

Appendix A.1.3 – NdL3 and YbL3 MST data

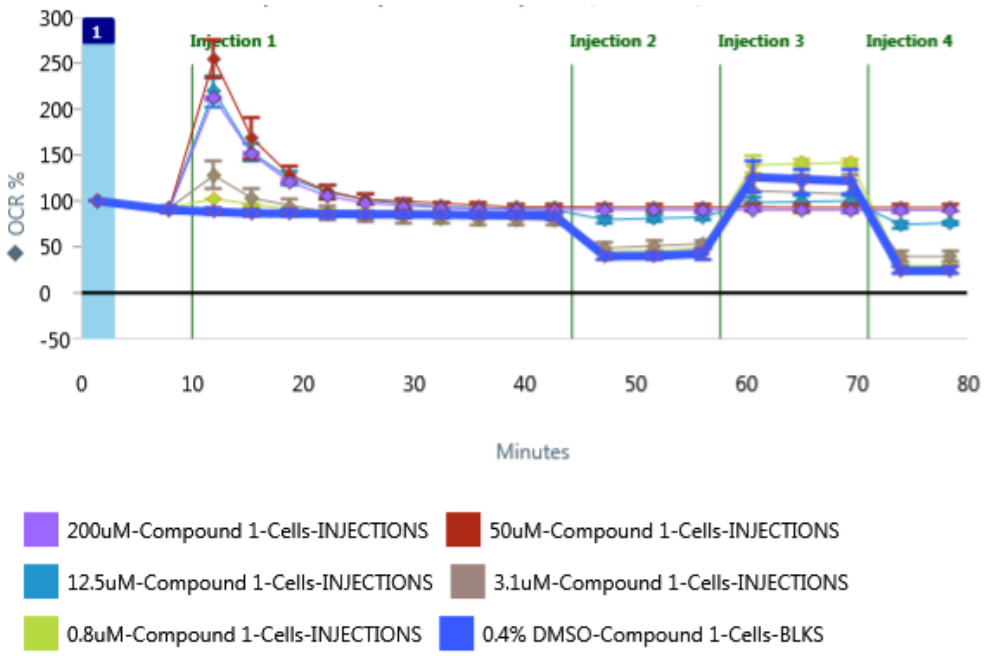

Figure 112. OCR RATE of cells measured during the MST performed on **NdL3**. **Injection 1** corresponds to **NdL3** injection, **injection 2** corresponds to oligomicyn injection, **injection 3** corresponds to FCCP injection and **injection 4** corresponds to rotenone/antimycin A injection.

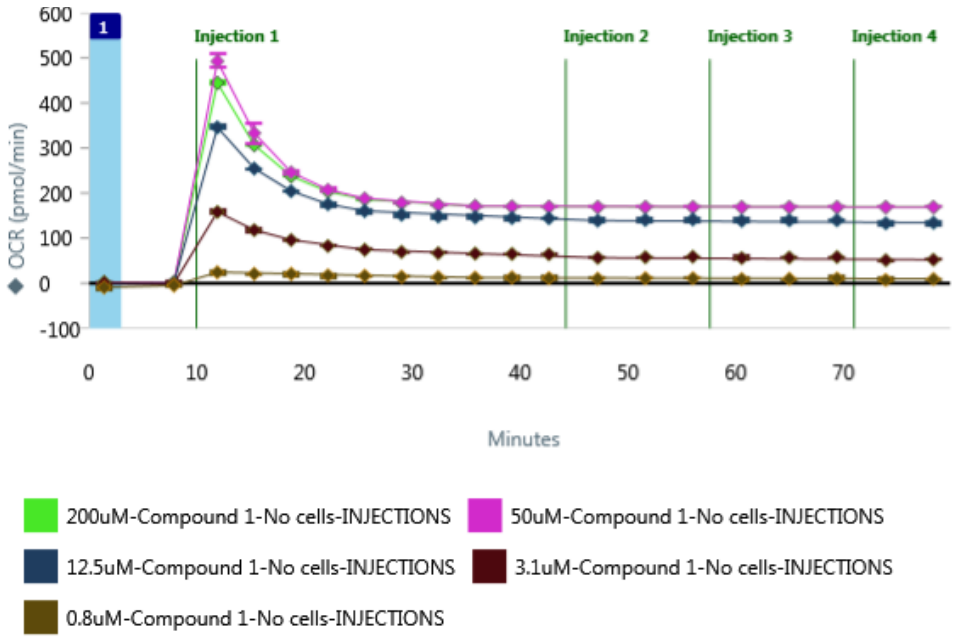

Figure 113. **NdL3** OCR RATE measured during the MST in absence of cells. **Injection 1** corresponds to **NdL3** injection, **injection 2** corresponds to oligomicyn injection, **injection 3** corresponds to FCCP injection and **injection 4** corresponds to rotenone/antimycin A injection.

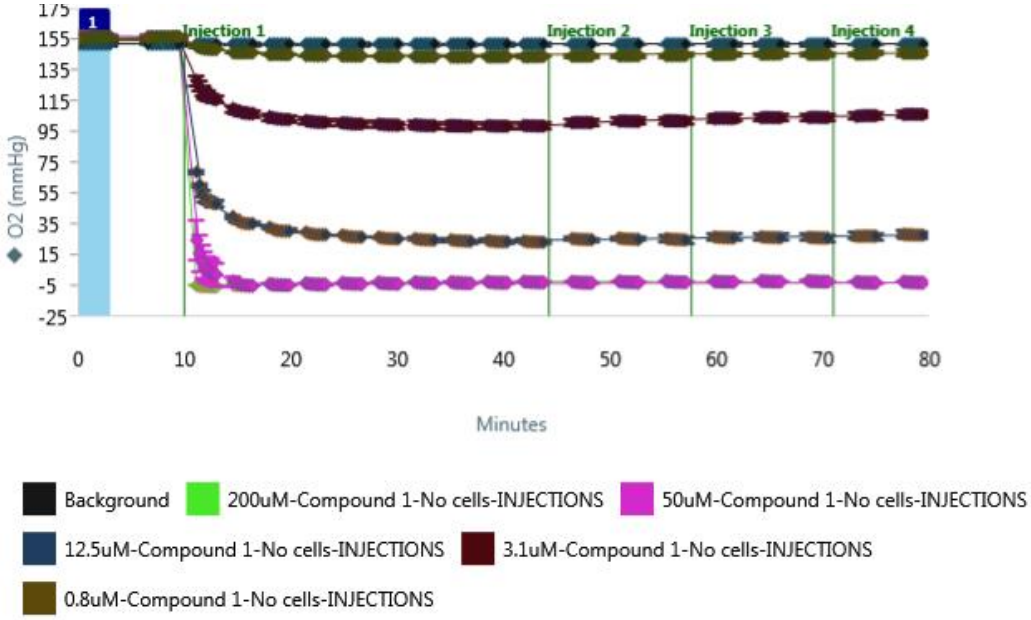

Figure 114. **NdL3** OCR LEVEL measured during the MST in absence of cells. **Injection 1** corresponds to **NdL3** injection, **injection 2** corresponds to oligomicyn injection, **injection 3** corresponds to FCCP injection and **injection 4** corresponds to rotenone/antimycin A injection.

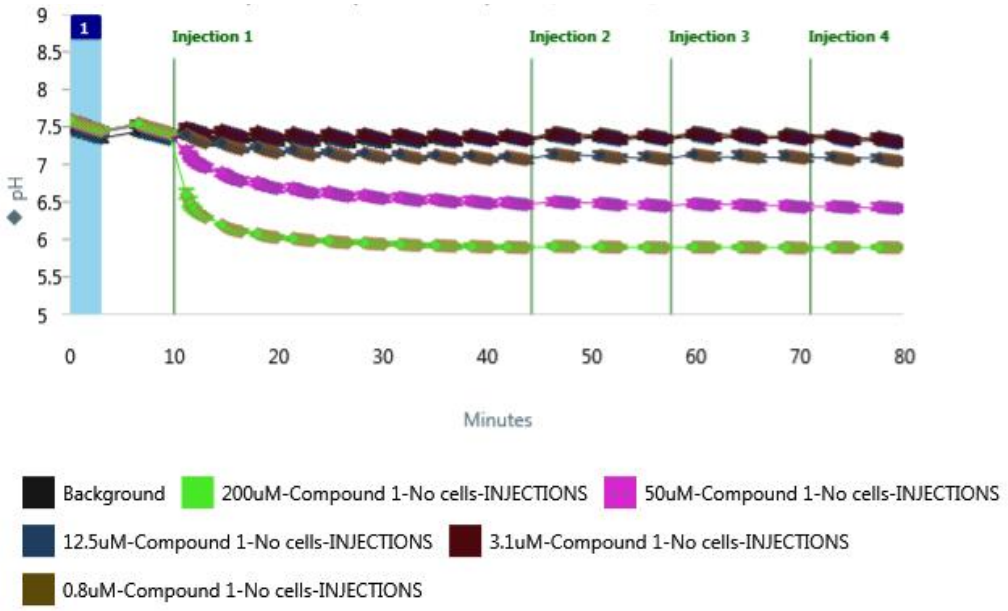

Figure 115. **NdL3** ECAR LEVEL measured during the MST in absence of cells. **Injection 1** corresponds to **NdL3** injection, **injection 2** corresponds to oligomicyn injection, **injection 3** corresponds to FCCP injection and **injection 4** corresponds to rotenone/antimycin A injection.

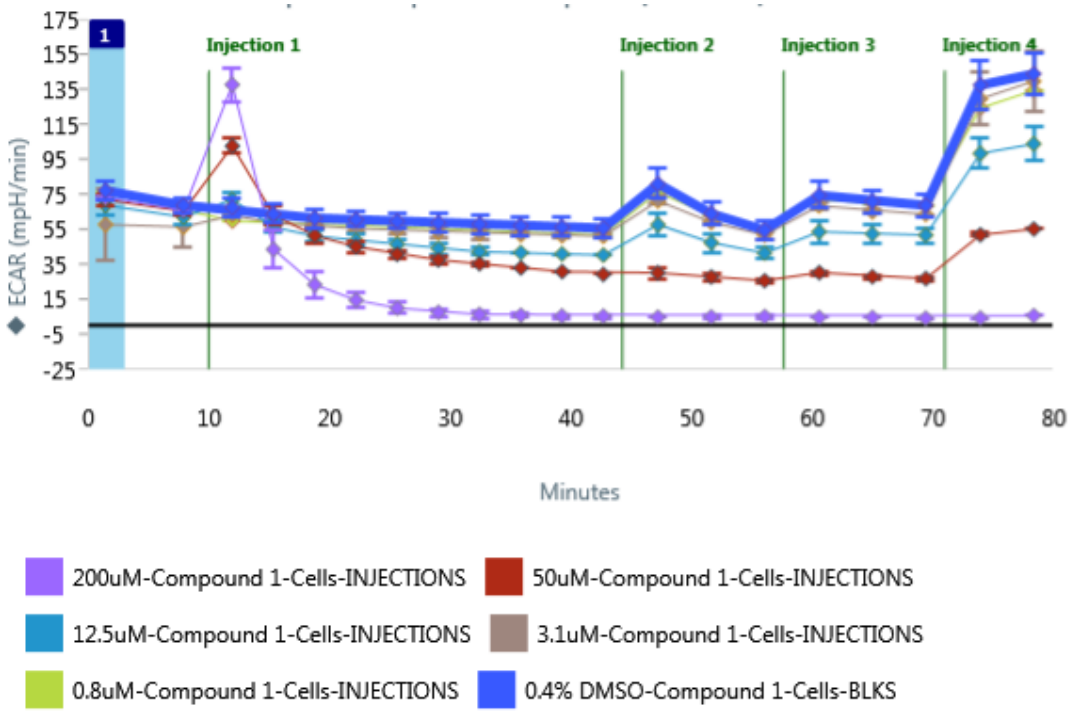

Figure116. **NdL3** ECAR RATE measured during the MST in presence of cells. **Injection 1** corresponds to **NdL3** injection, **injection 2** corresponds to oligomicyn injection, **injection 3** corresponds to FCCP injection and **injection 4** corresponds to rotenone/antimycin A injection.

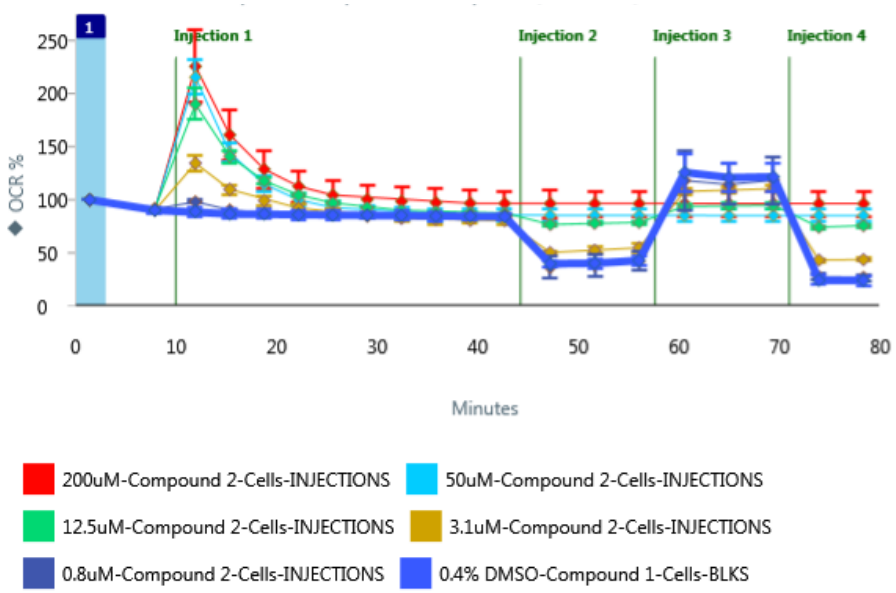

Figure 117. OCR RATE of cells measured during the MST performed on **YbL3**. **Injection 1** corresponds to **YbL3** njection, **injection 2** corresponds to oligomicyn injection, **injection 3** corresponds to FCCP injection and **injection 4** corresponds to rotenone/antimycin A injection.

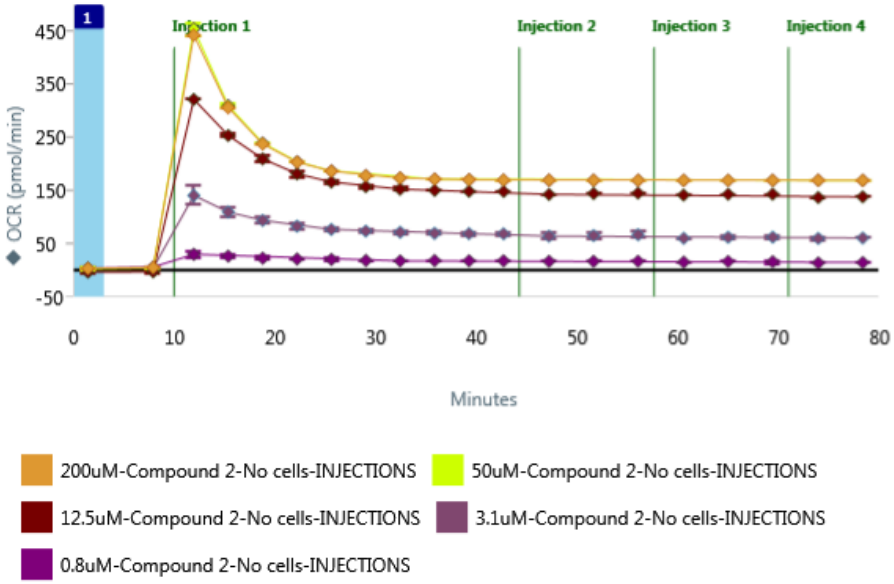

Figure 118. **YbL3** OCR RATE measured during the MST in absence of cells. **Injection 1** corresponds to **YbL3** injection, **injection 2** corresponds to oligomicyn injection, **injection 3** corresponds to FCCP injection and **injection 4** corresponds to rotenone/antimycin A injection.

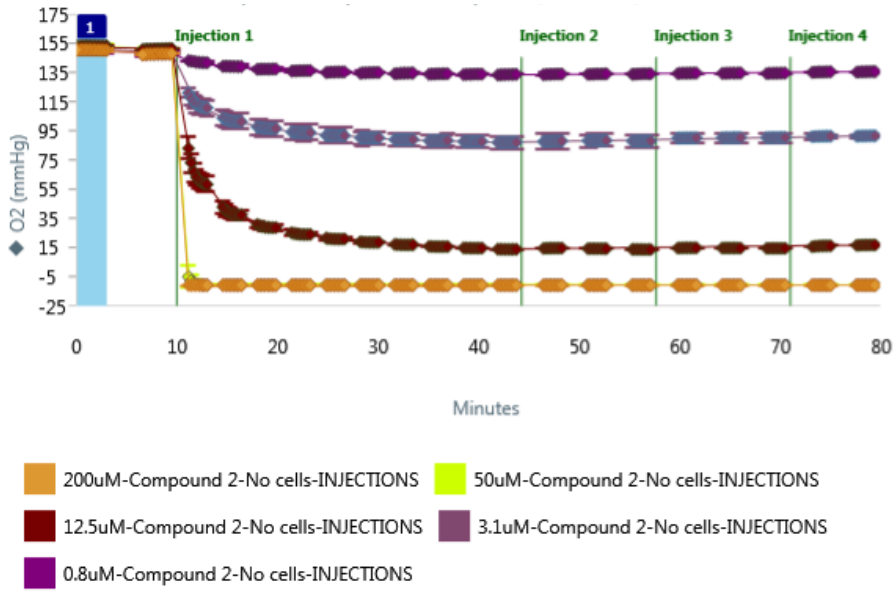

Figure 119. **YbL3** OCR LEVEL measured during the MST in absence of cells. **Injection 1** corresponds to **YbL3** injection, **injection 2** corresponds to oligomicyn injection, **injection 3** corresponds to FCCP injection and **injection 4** corresponds to rotenone/antimycin A injection.

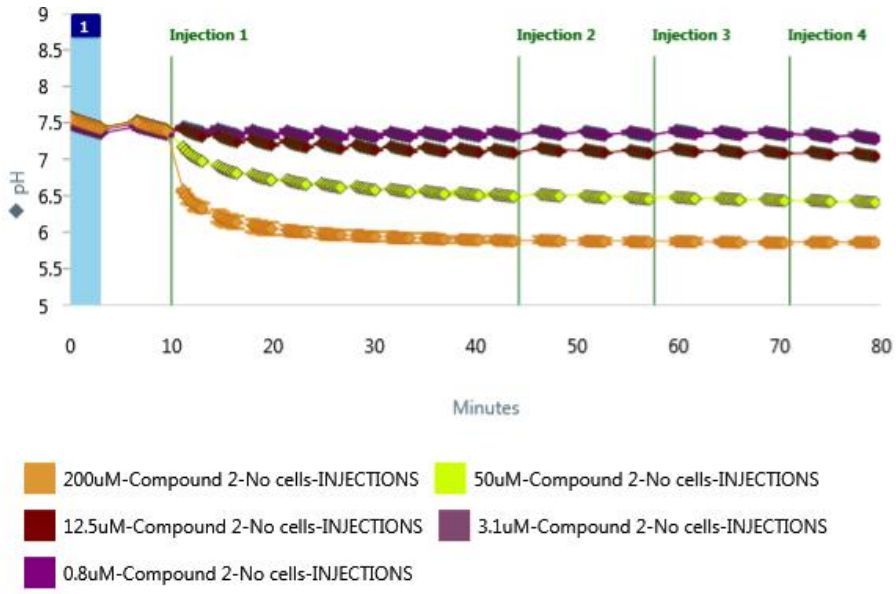

Figure 120. **YbL3** ECAR LEVEL measured during the MST in absence of cells. **Injection 1** corresponds to **YbL3** injection, **injection 2** corresponds to oligomicyn injection, **injection 3** corresponds to FCCP injection and **injection 4** corresponds to rotenone/antimycin A injection.

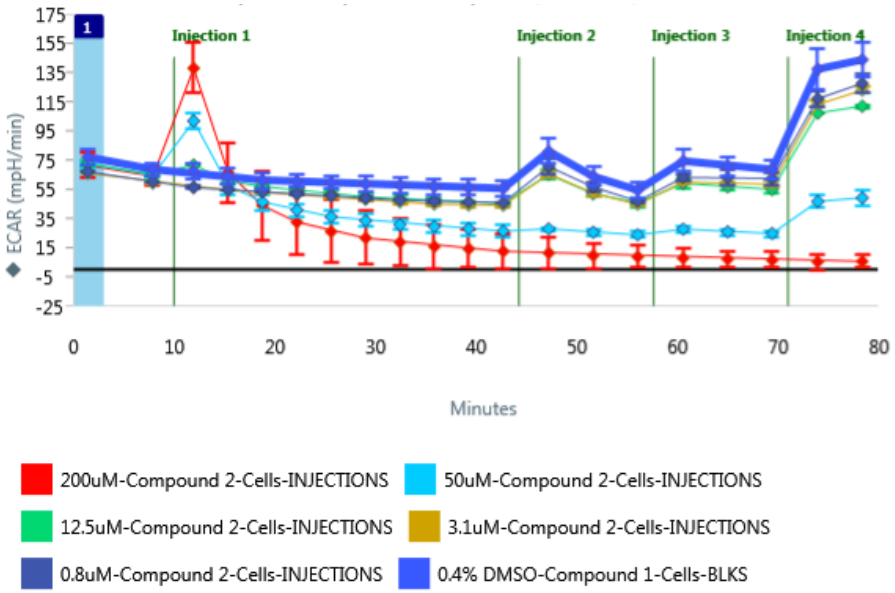

Figure 121. **YbL3** ECAR RATE measured during the MST in presence of cells. **Injection 1** corresponds to **YbL3** injection, **injection 2** corresponds to oligomicyn injection, **injection 3** corresponds to FCCP injection and **injection 4** corresponds to rotenone/antimycin A injection.

Appendix A.1.4 – EuL4 and TbL4 MST data

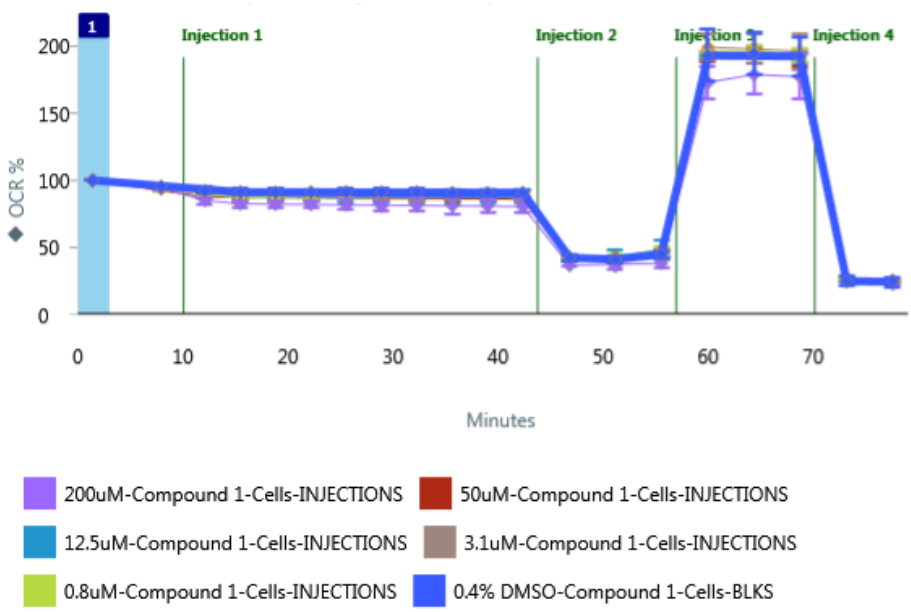

Figure 122. OCR RATE of cells measured during the MST performed on **EuL4**. **Injection 1** corresponds to **EuL4** injection, **injection 2** corresponds to oligomicyn injection, **injection 3** corresponds to FCCP injection and **injection 4** corresponds to rotenone/antimycin A injection.

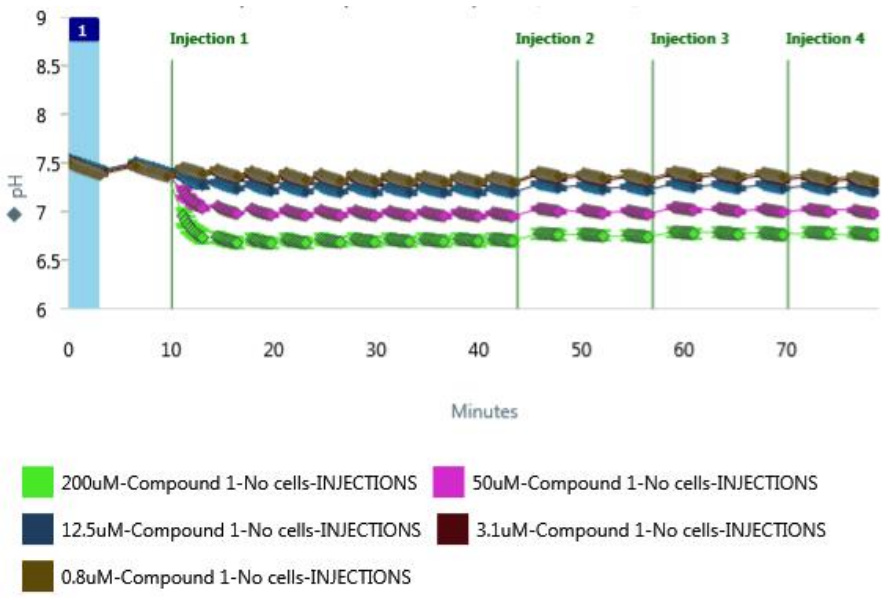

Figure 123. **EuL4** ECAR LEVEL measured during the MST in absence of cells. **Injection 1** corresponds to **EuL4** injection, **injection 2** corresponds to oligomicyn injection, **injection 3** corresponds to FCCP injection and **injection 4** corresponds to rotenone/antimycin A injection.

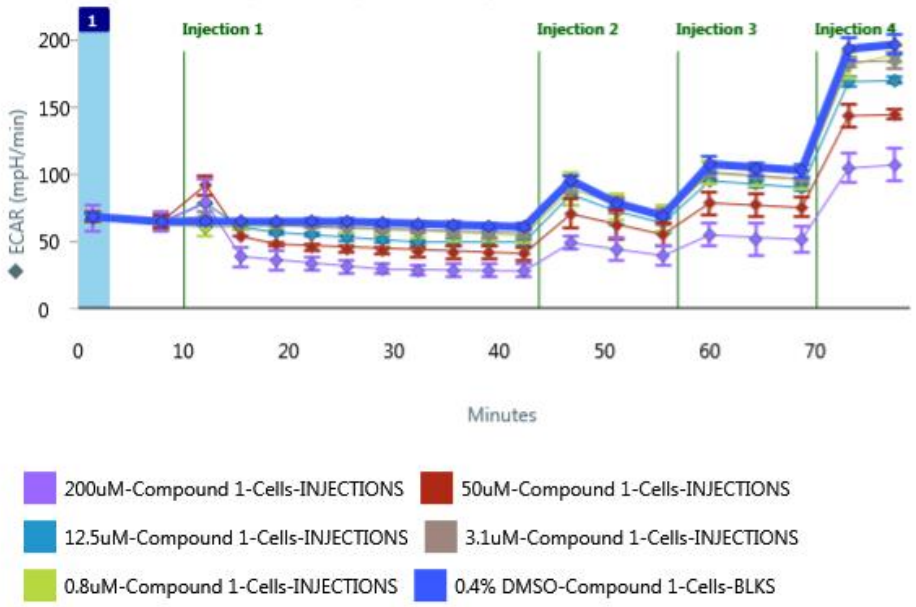

Figure 124. **EuL4** ECAR RATE measured during the MST in presence of cells. **Injection 1** corresponds to **EuL4** injection, **injection 2** corresponds to oligomicyn injection, **injection 3** corresponds to FCCP injection and **injection 4** corresponds to rotenone/antimycin A injection.

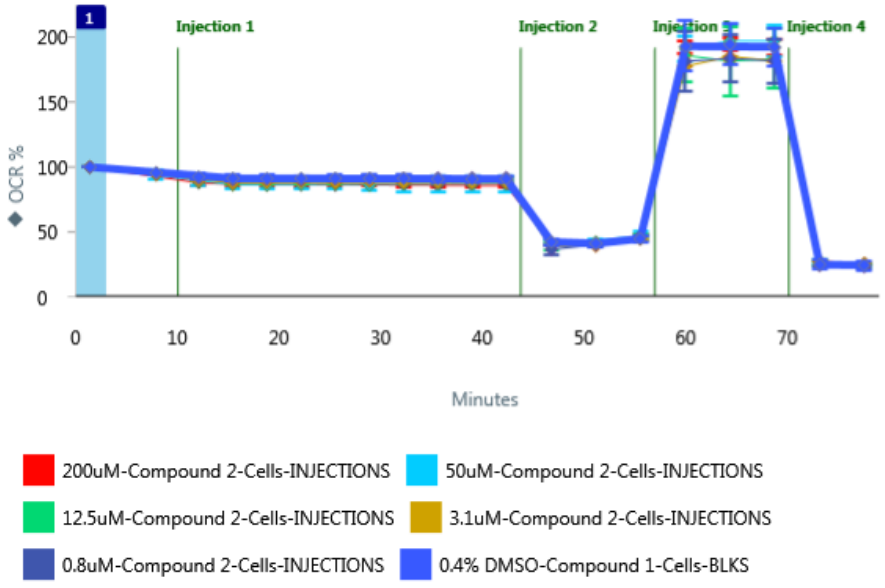

Figure 125. OCR RATE of cells measured during the MST performed on **TbL4**. **Injection 1** corresponds to **TbL4** injection, **injection 2** corresponds to oligomicyn injection, **injection 3** corresponds to FCCP injection and **injection 4** corresponds to rotenone/antimycin A injection.

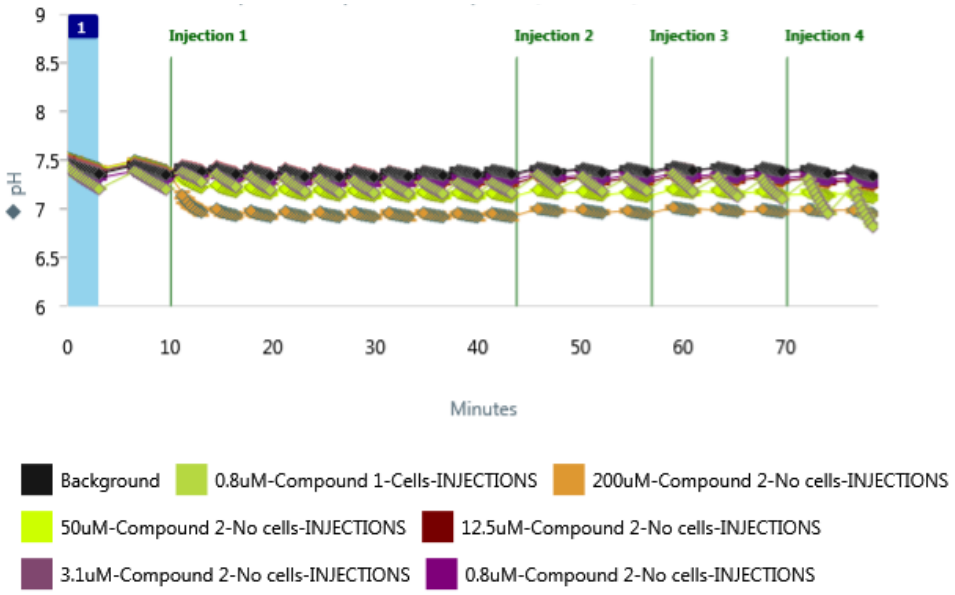

Figure 126. **TbL4** ECAR LEVEL measured during the MST in absence of cells. **Injection 1** corresponds to **TbL4** injection, **injection 2** corresponds to oligomicyn injection, **injection 3** corresponds to FCCP injection and **injection 4** corresponds to rotenone/antimycin A injection.

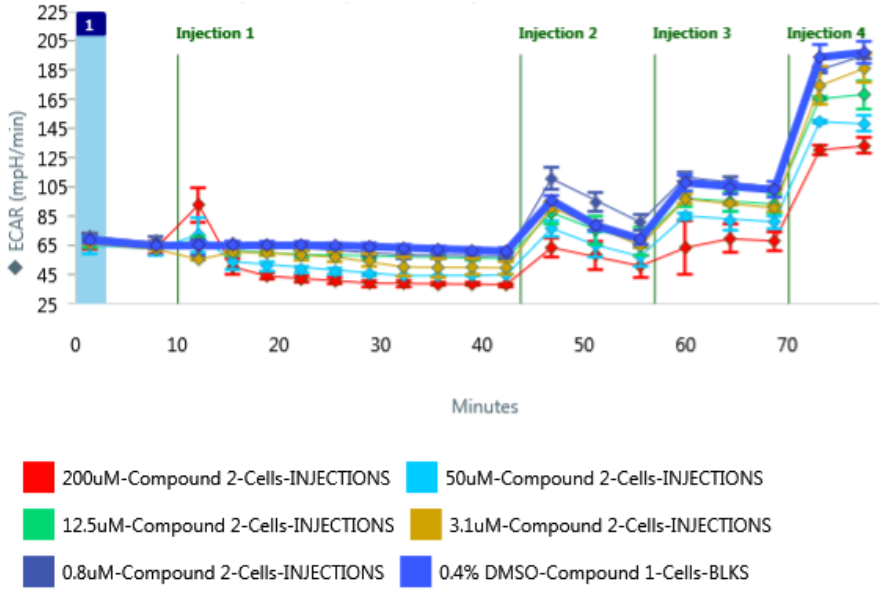

Figure 127. **TbL4** ECAR RATE measured during the MST in presence of cells. **Injection 1** corresponds to **TbL4** injection, **injection 2** corresponds to oligomicyn injection, **injection 3** corresponds to FCCP injection and **injection 4** corresponds to rotenone/antimycin A injection.

Appendix A.2 - Calcium loading capacity profiles of TbL1, EuL2, TbL2, NdL3 and YbL3.

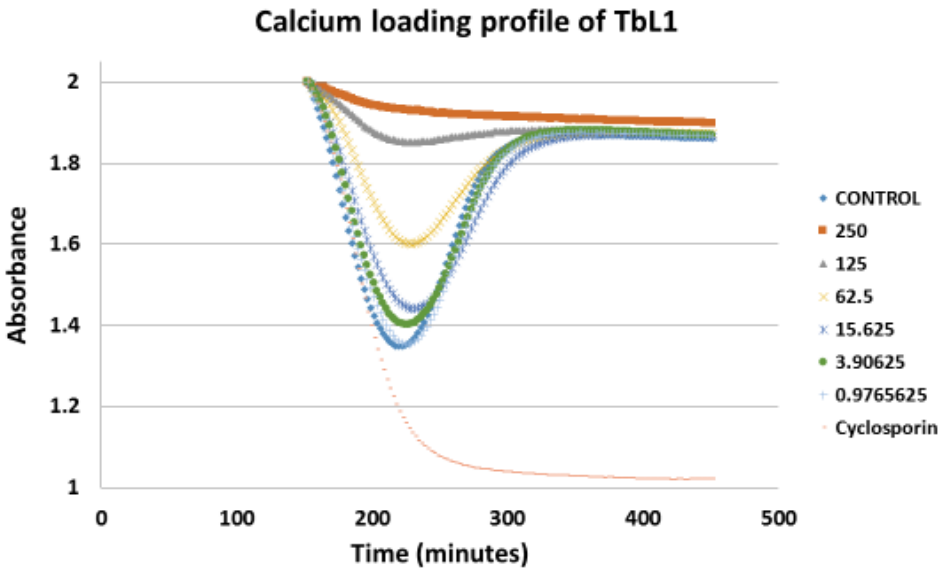

Figure 128. Calcium loading capacity profile of **TbL1**.

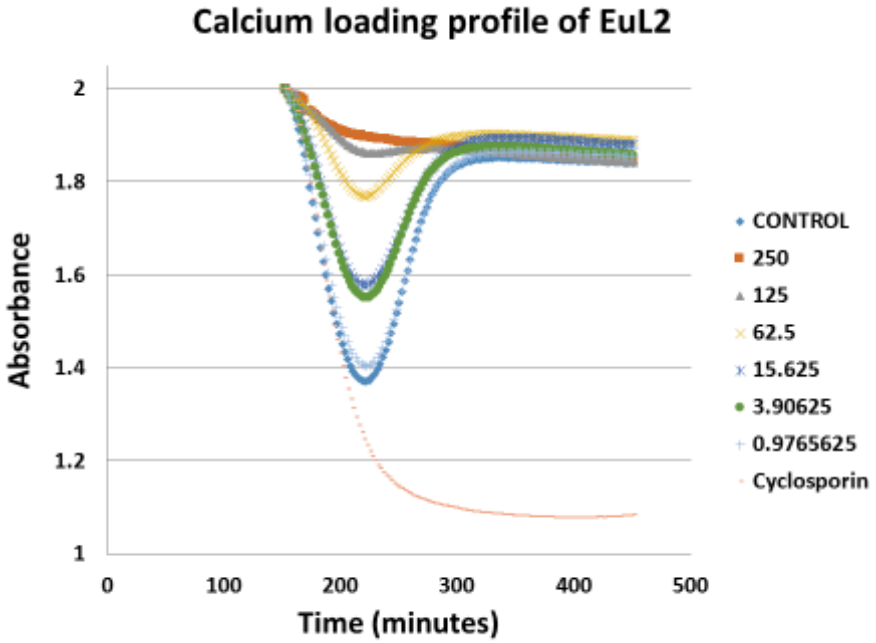

Figure 129. Calcium loading capacity profile of **EuL2**.

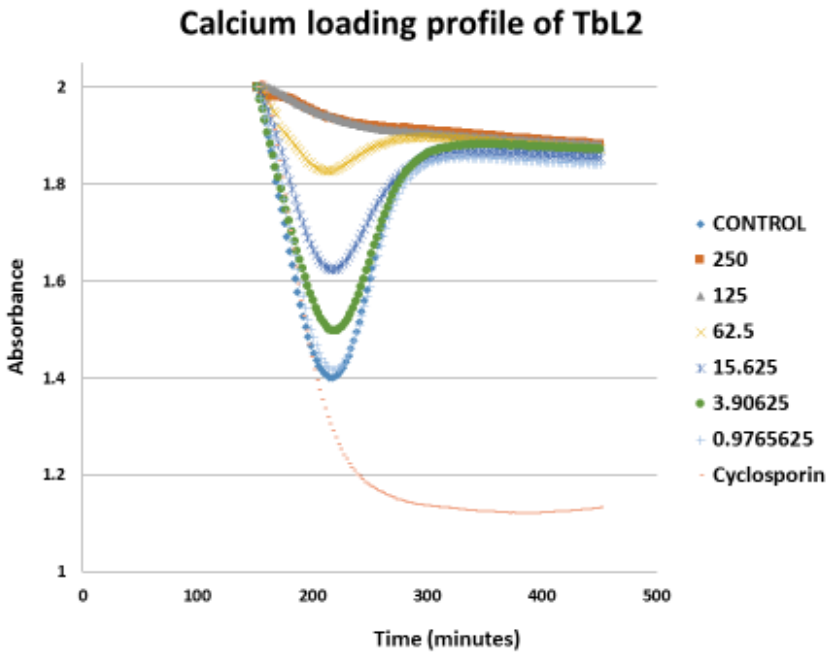

Figure 130. Calcium loading capacity profile of **TbL2**.

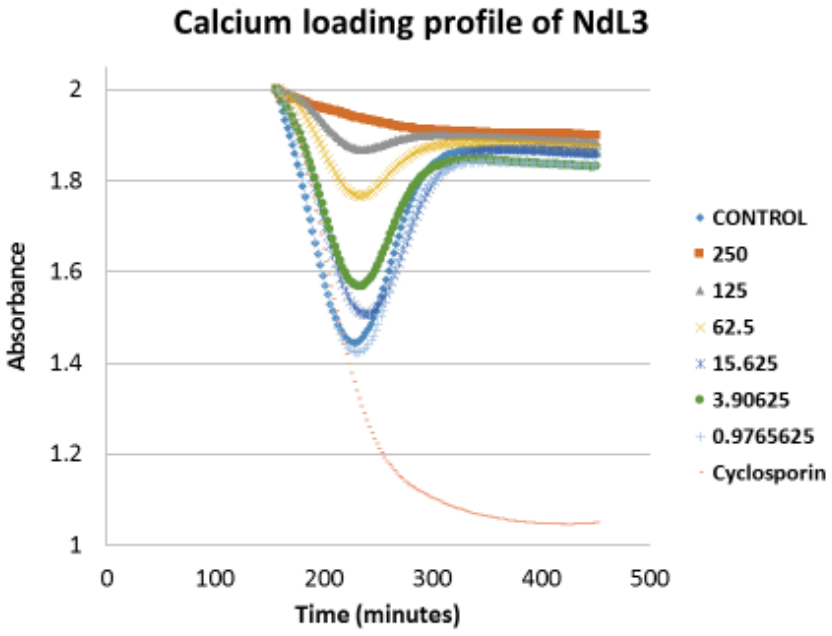

Figure 131. Calcium loading capacity profile of **NdL3**.

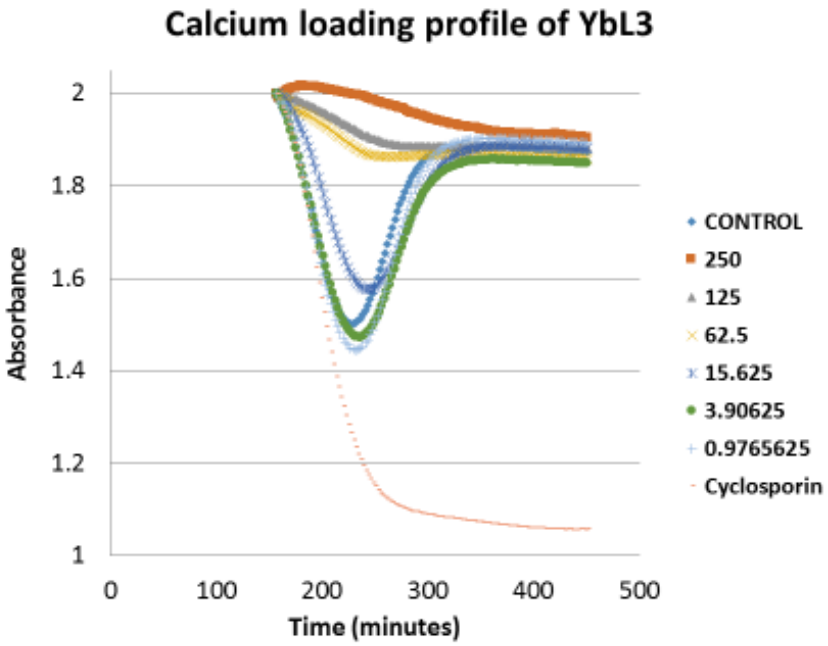

Figure 132. Calcium loading capacity profile of **YbL3**.

Appendix A.3 - Calcium chelation of TbL1, EuL2, TbL2, NdL3, YbL3, EuL4 and TbL4.

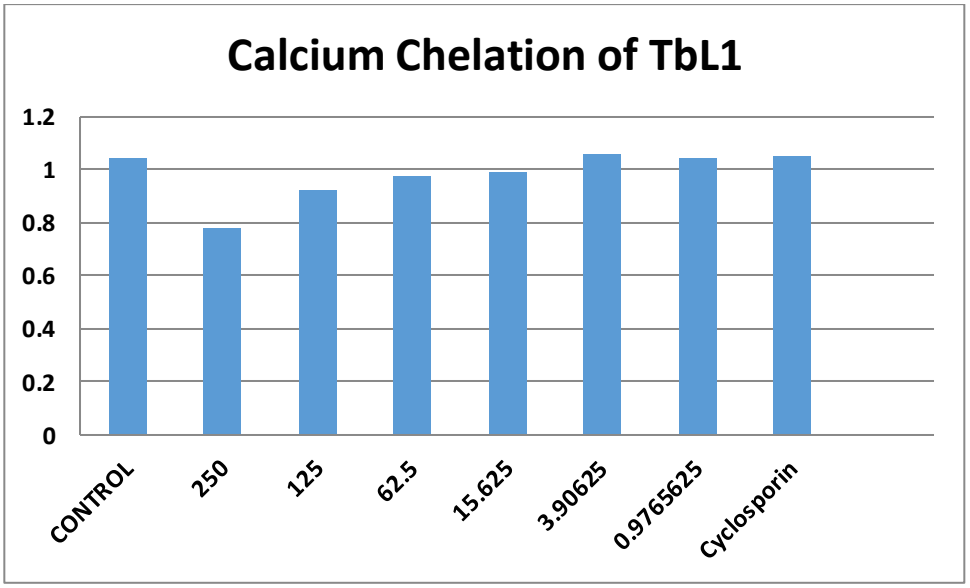

Figure 133. Calcium chelation of **TbL1**.

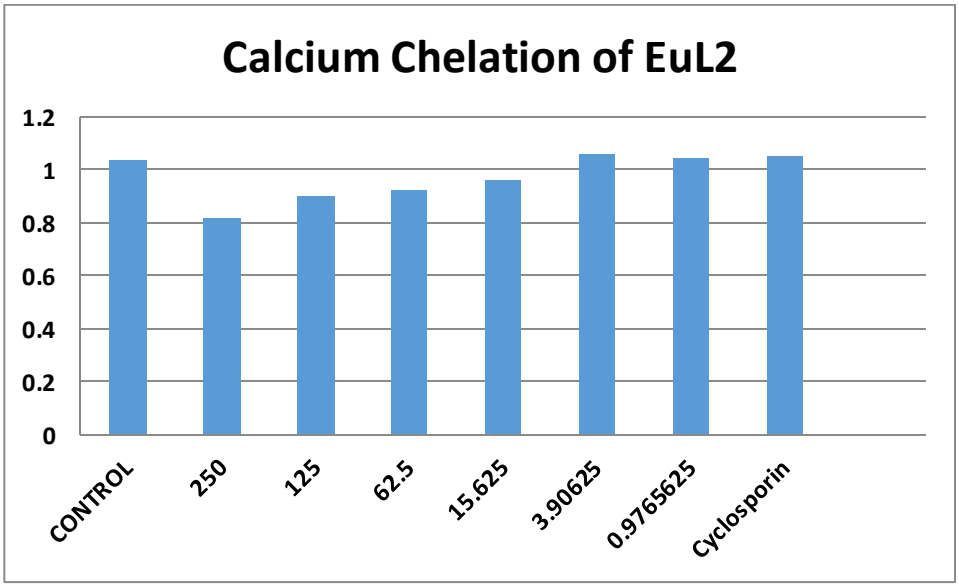

Figure 134. Calcium chelation of **EuL2**.

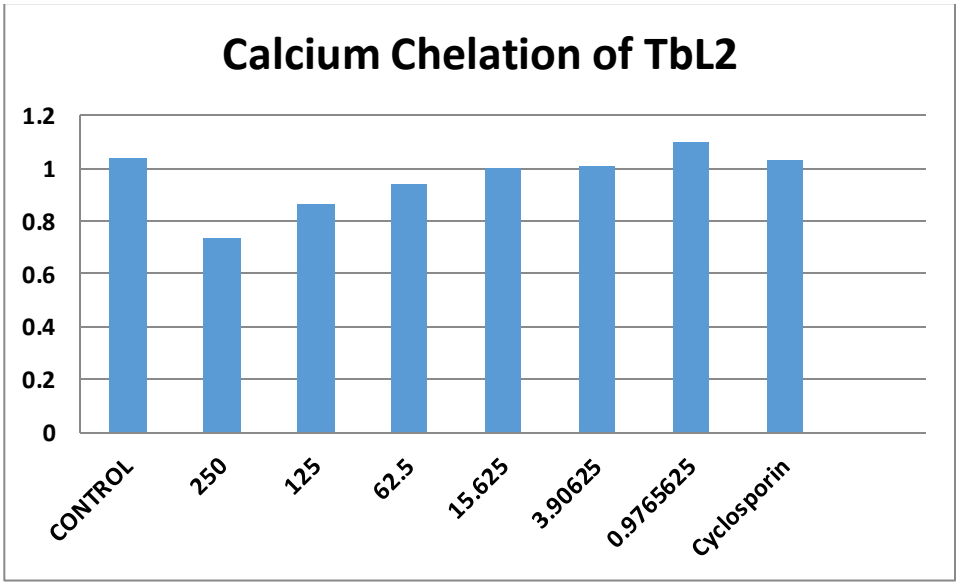

Figure 135. Calcium chelation of **TbL2**.

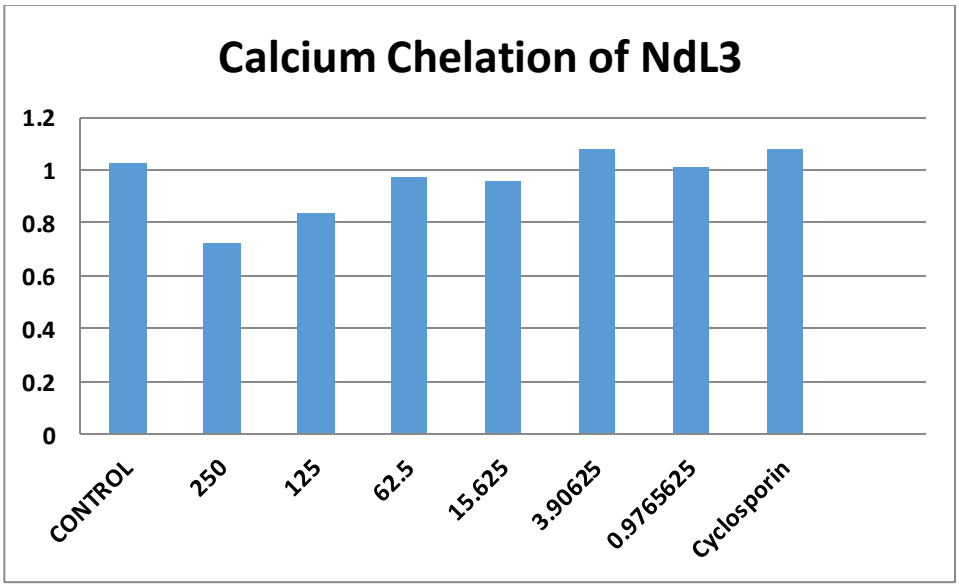

Figure 136. Calcium chelation of **NdL3**.

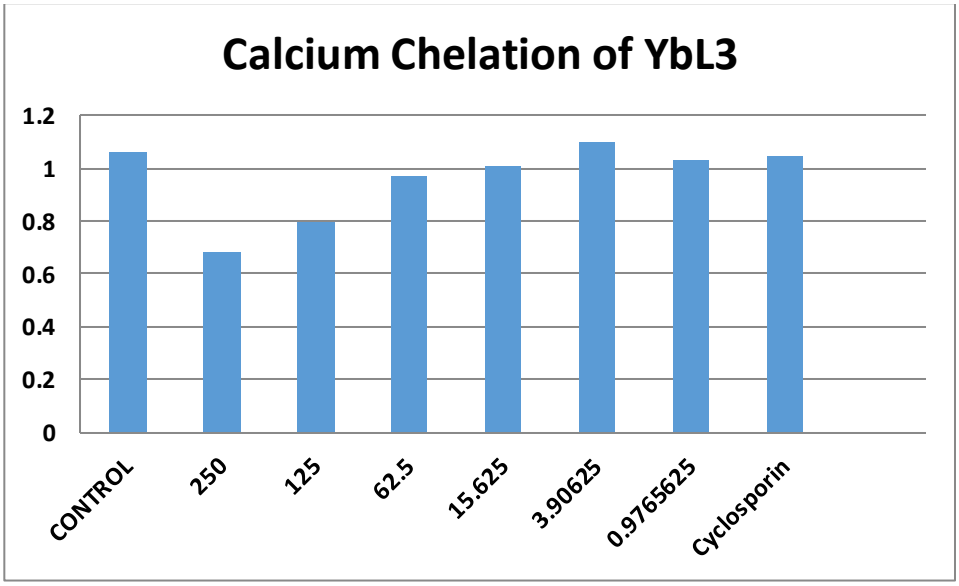

Figure 137. Calcium chelation of **YbL3**.

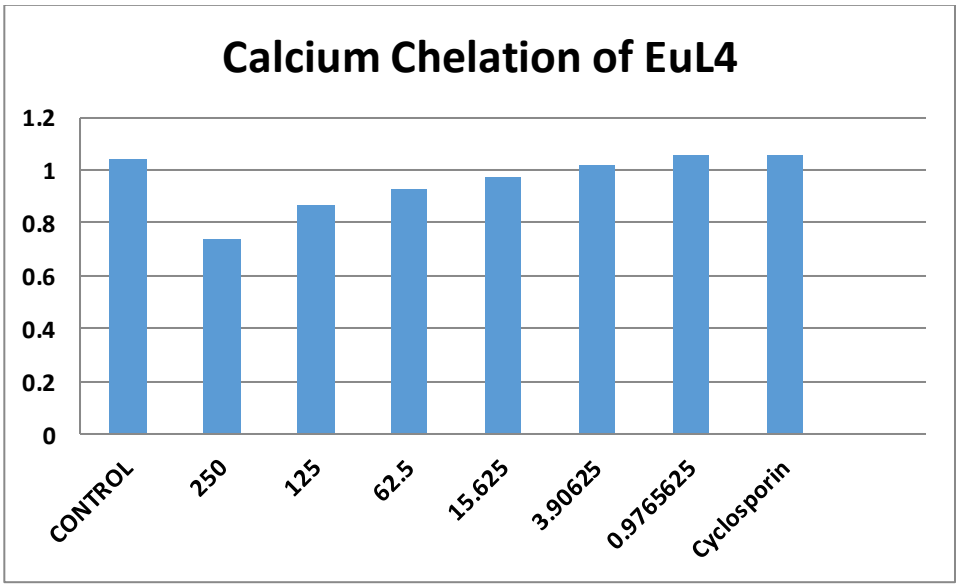

Figure 138. Calcium chelation of **EuL4**.

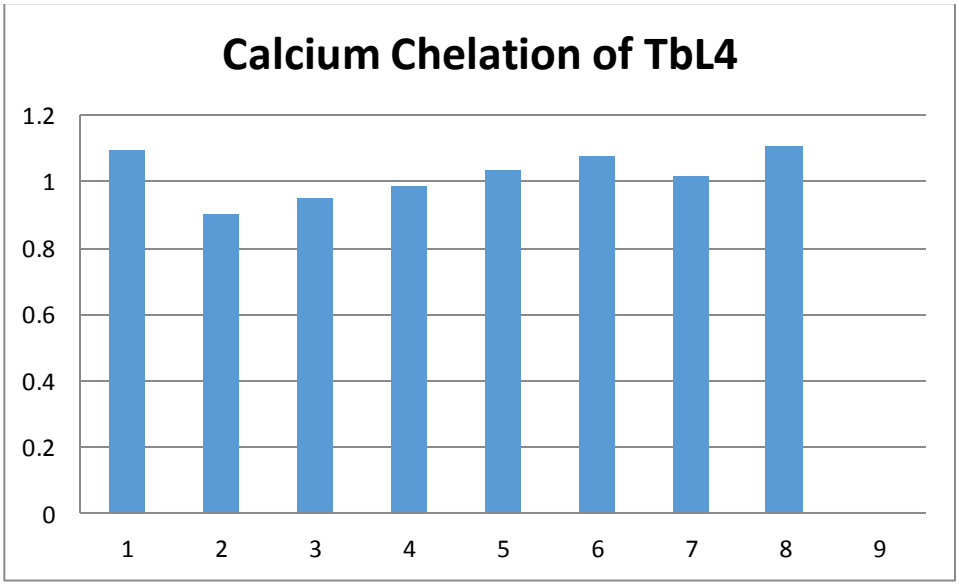

Figure 139. Calcium chelation of **TbL4**.